University of Bielefeld

Department of Cell Biology

– AG Molecular Neurobiology –

Analysis of the NF-κB Signal Transduction Pathway

in Neurological Disorders and Cancer

Cumulative Dissertation

Submitted for the fulfilment of the requirements

for the doctoral degree of natural science

Doctor rerum naturalis (Dr. rer. nat.)

by Carsten Slotta

2017

supervised by Prof. Dr. Barbara Kaltschmidt

Publications

Parts of this dissertation are published, submitted or in preparation for publication:

"Plekhg5-regulated autophagy of synaptic vesicles reveals a pathogenic mechanism in motoneuron disease".
Lüningschrör P, Binotti B, Dombert B, Heimann P, Perez-Lara A, **Slotta C**, Thau-Habermann N, Rüdt von Collenberg C, Karl F, Damme M, Horowitz A, Maystadt I, Füchtbauer A, Füchtbauer EM, Jablonka S, Blum R, Üçeyler N, Petri S, Kaltschmidt B, Jahn R, Kaltschmidt C & Sendtner M. Nat Commun. 2017 Oct 30;8(1):678 – will be referred to as *Lüningschrör et al. 2017*

"Plekhg5 mediates myelin breakdown by regulating the immune response in peripheral nerves".
Slotta C, Lüningschrör P, Weikert UM, Briese M, Appenzeller S, Heimann P, Sendtner M, Kaltschmidt C & Kaltschmidt B. *in submission* – will be referred to as *Slotta et al. a*

"Impaired clearance of autolysosomes in *PLEKHG5*-deficient human glioma cells".
Slotta C, Friedrich KE, Kitke A, Greiner JFW, Kaltschmidt C & Kaltschmidt B. *in preparation* – will be referred to as *Slotta et al. b*

"CRISPR/Cas9-mediated knockout of c-*REL* in HeLa cells results in profound defects of the cell cycle".
Slotta C, Schlüter T, Ruiz-Perera LM, Kadhim HM, Tertel T, Henkel E, Hübner W, Greiner JFW, Huser T, Kaltschmidt B & Kaltschmidt C. PLoS One. 2017 Aug 2;12(8):e0182373 – will be referred to as *Slotta et al. 2017*

"CRISPR/Cas9-mediated deficiency of human *IKBK1*/*IKBK2* leads to TNFα-induced programmed cell death in an NF-κB-independent manner".
Slotta C, Storm J, Kleinwächter S, Pfisterer N, Pieper M, Ruiz-Perera LM, Henkel E, Greiner JFW, Kaltschmidt B & Kaltschmidt C. *under review – will be referred to as Slotta et al. c*

The following studies are published or in preparation for publication but not referred to in this dissertation:

"An investigation of the specificity of research antibodies against NF-κB-subunit p65"
Slotta C, Müller J, Tran L, Hauser S, Widera D, Kaltschmidt B & Kaltschmidt C. J Histochem Cytochem. 2014 Feb;62(2):157-61.

"Direct counting of NF-κB p65 is sufficient for the simulation of NF-κB dynamics"
Slotta C, Mothes J, Mönkemöller V, Hübner W, Essfeld F, Seidel T, Huser T, Kaltschmidt B, Wolf J & Kaltschmidt C. *in preparation*

Table of contents

1. Abbreviations

Abbreviation	Acceptation
ALS	Amyotrophic lateral sclerosis
AMBRA1	BECN1‑regulated autophagy protein 1
ATG	Autophagy-related genes
BAFFR	B-cell activating factor belonging to TNF-family receptor
Cas9	CRISPR-associated protein 9
CD40	Cluster of differentiation 40
cIAP1/2	Cellular inhibitors of apoptosis 1 and 2
CMT	Charcot Marie Tooth disease
CRISPR	Clustered Regularly Interspaced Short Palindromic Repeats
CSC	Cancer stem cells
DSMA IV	Distal spinal muscular atrophy type IV
FADD	Fas-associated protein with death domain
FIP200	Focal adhesion kinase family integrating protein 200
GBM	Glioblastoma multiforme
GEF	Guanine nucleotide exchange factor
IKK1/2	Inhibitor of nuclear factor kappa-B kinase subunit alpha/beta
IκBα	Inhibitor of nuclear factor kappa-B alpha
LTβR	Lymphotoxin beta receptor
LUBAC	Linear ubiquitin assembly complex
MLKL	Pseudokinase mixed lineage kinase like
mTOR	Mammalian target of rapamycin
mTORC1	mTOR complex 1
NEMO	NF-kappa-B essential modulator
NF-κB	Nuclear factor kappa-light-chain-enhancer of activated B-cells
NMJ	Neuromuscular junction
PI(P)3	Phosphatidylinositol 3-phosphate
Plekhg5	Pleckstrin homology domain containing, family G member 5

Rab26	Ras-related protein Rab26
RhoA	Ras homolog gene family, member A
RIPK1	Receptor-interacting serine/threonine-protein kinase 1
TAB2/3	TAK1-binding proteins 2 and 3
TAK1	TGF-beta activated kinase 1
TNFR1/2	TNF receptors 1 and 2
TNFα	Tumor necrosis factor alpha
TRADD	TNFR1 associated death domain protein
TRAF2	TNF receptor associated factor 2
ULK	Unc-51 like autophagy activating kinase
VEGF	Vascular epidermal growth factor

2. List of Figures

3. Abstract

The transcription factor NF-κB is an essential regulator in a broad range of cellular processes. Due to its importance, it is tightly associated with numerous diseases. The thesis presented deals with the roles of NF-κB in the context of a motoneuron disease and cancer.

One part focused on the analysis of *Plekhg5*-deficient mice as a new mouse model for motoneuron disease. Plekhg5 is a known activator of NF-κB signaling and previously, mutations found within the human *PLEKHG5* gene were associated with different motoneuron diseases. Mutant mice developed a pathology with late onset. With Plekhg5 being expressed in both, neurons and Schwann cells, research focused on both cell types. Most prominently on the neuronal site, a direct function of Plekhg5 as a GEF for Rab26 could be demonstrated. Previously, Rab26 was described as a regulator of the autophagy-mediated clearance of synaptic vesicles. Consequently, lack of Plekhg5 resulted in the accumulations of synaptic vesicles within neuromuscular junctions impeding proper muscle innervation. Besides this motoneuron-specific function, deficiency of Plekhg5 in Schwann cells additionally contributed to the disease observed in mutant mice, becoming evident as an altered myelination within peripheral nerves. Causative for these effects are impaired autophagy in Schwann cells and reduced chemokine expression resulting in reduced T-lymphocyte recruitment.

Part two of the thesis presented focused on the generation and analysis of CRISPR/Cas9-mediated gene knockouts in human cells. These included the NF-κB activator Plekhg5 and several members of the canonical NF-κB signaling pathway. Genetic depletion of Plekhg5 in human glioma cells extended the findings of Plekhg5 as a regulator of autophagy from the nervous system to human cancer cells. Notably, in this different cellular context, Plekhg5 was shown to be involved at a different stage of autophagy. Deficiency of members of the NF-κB family being involved in canonical NF-kB signaling resulted in different results. Knockout of the NF-κB subunit c-Rel resulted in profound defects of the cell cycle. However most prominently, a double knockout of the upstream kinases IKK1 and IKK2 vastly increased the sensitivity of human cells to TNF-induced cell death in

an NF-κB-independent manner. This strongly indicates that the IKK complex might be a promising target with regard to cancer therapy.
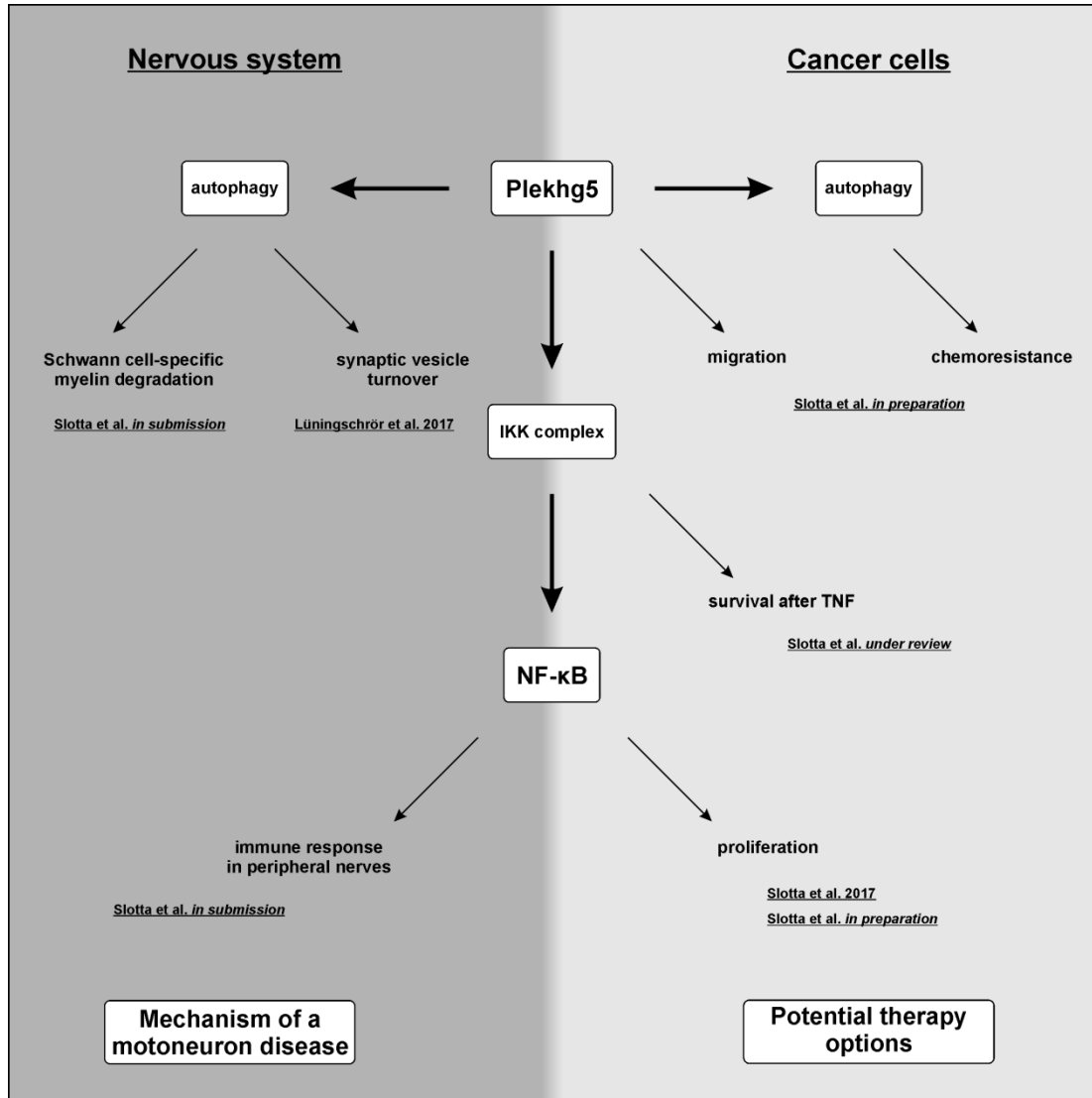

Figure 1. Schematic overview of the major findings in the thesis presented. In the nervous system, new mechanistic insights of a motoneuron disease were obtained. In cancer cells, several loss-of-function approaches were performed culminating in potential new therapeutic approaches.

4. Zusammenfassung

Der Transkriptionsfaktor NF-κB ist an der Regulation verschiedenster, zellulärer Prozesse beteiligt. Fehlregulierte Aktivierung von NF-κB ist aufgrund dessen mit einer Vielzahl verschiedener Krankheiten assoziiert. In der vorgelegten Dissertation wurde die Beteiligung von NF-κB im Rahmen einer Motorneuronerkrankung als auch im Zusammenhang mit Krebserkrankungen untersucht.

Im ersten Teil dieser Arbeit erfolgte die Analyse eines Mausmodells, in welchem das Gen *Plekhg5* entfernt worden war. Bereits in früheren Arbeiten konnte gezeigt werden, dass Plekhg5 NF-κB aktivieren kann. Darüber hinaus waren Mutationen im humanen *PLEKHG5* Gen als Ursache verschiedener motorneuronaler Erkrankungen beschrieben worden. *Plekhg5*-defiziente Mäuse zeigten im fortgeschrittenen Alter Symptome einer motorneuronalen Erkrankung. Aufgrund der Tatsache, dass Plekhg5 sowohl in Motorneuronen, als auch in Schwann Zellen exprimiert wird, wurden anschließend Zell-spezifische Effekte untersucht. In Motorneuronen konnte eine direkte Funktion von Plekhg5 als GEF für Rab26 im Rahmen des Autophagie-vermittelten Abbaus synaptischer Vesikel gezeigt werden. Verlust von Plekhg5 führte zu einer Anstauung synaptischer Vesikel, welche eine funktionelle Innervation der Muskelzellen massiv beeinträchtigte. Abseits dieser motorneuronspezifischen Funktion trug der Verlust von Plekhg5 in Schwann Zellen ebenfalls zum beobachteten Krankheitsbild der Tiere bei. Hier konnten insbesondere Veränderungen der Myelinscheide in peripheren Nerven detektiert werden. Als ursächlich dafür konnte eine gestörte Autophagie in Schwann Zellen, sowie eine verminderte Ausschüttung von Botenstoffen für die Rekrutierung von T-Lymphozyten ausgemacht werden.

Im zweiten Teil der hier vorgelegten Dissertation lag der Fokus auf der Erschaffung und Charakterisierung mehrerer genetischer Verlustmutanten in kultivierten menschlichen Zellen mittels des CRISPR/Cas9 Systems. Unter anderem wurden Mutanten für den NF-κB Aktivator Plekhg5 und mehrerer Mitglieder des kanonischen NF-κB Signalwegs erstellt. Mit dem Verlust von Plekhg5 in menschlichen Glioblastomzellen konnten die Erkenntnisse von Plekhg5 als Regulator der Autophagie vom Nervensystem auf menschliche

Krebszellen erweitert werden. Interessanterweise war Plekhg5 hier an einer anderen Stelle innerhalb des autophagischen Prozesses beteiligt als zuvor im Nervensystem beschrieben.

Die Verlustmutanten verschiedener Mitglieder der NF-κB Familie führten zu unterschiedlichen Effekten. Verlust der NF-κB Untereinheit c-Rel resultierte in einer erheblichen Störung des Zellzyklus. Die dramatischste Auswirkung zeigte sich hingegen in einem massiv gesteigerten Zelltod nach Zugabe von TNF-α in einer Doppelverlustmutante der NF-κB aktivierenden Kinasen IKK1 und IKK2. Dieser Effekt konnte als NF-κB unabhängig identifiziert werden und zeigt, dass der IKK Komplex ein äußerst vielversprechendes Ziel für die Krebstherapie sein könnte.

5. Introduction

5.1 The Nuclear Factor kappa B

The inducible transcription factor nuclear factor kappa-light-chain enhancer of activated B-cells (NF-κB) plays a pivotal role in a broad range of cellular processes and therefore is in the center of active research. Identified more than thirty years ago (Sen and Baltimore, 1986), it was first described to play important roles within the immune system (reviewed in (Vallabhapurapu and Karin, 2009)). Nowadays, a large amount of studies have described NF-κB as a major regulator of numerous cellular processes within different cellular systems such as cell growth, differentiation, apoptosis, inflammation, learning and memory (Kaltschmidt and Kaltschmidt, 2015, Perkins, 2007).

5.1.1 The NF-κB family

In mammals, NF-κB is comprised of five subunits: RelA (p65), RelB, c-Rel, p50 (NF-κB1) and p52 (NF-κB2), which form either homo- or heterodimers. All subunits share the so-called Rel-homology domain (RHD) at their N-terminus (Baeuerle and Baltimore, 1996). The RHD is necessary for dimerization of the subunits and DNA-binding. In contrast, only members of the Rel family (RelA, RelB and c-Rel) additionally contain a transactivation domain (Fig. 2). Consequently, only dimers containing at least one of the Rel proteins are able to activate transcription, whereas e.g. a p50:50 homodimer acts as transcriptional repressor (Hayden and Ghosh, 2012). The subunits p50 and p52 are being expressed as the precursor proteins p105 and p100. During signaling, they are processed by partial proteasomal degradation to the final and active subunits.

In addition to the NF-κB subunits, several inhibitor proteins have been described. They are all defined by the presence of multiple ankyrin repeat domains (Fig. 2). Among these, the inhibitor of κB alpha (IκBα) is characterized as the key regulator in canonical NF-κB signaling (Hayden and Ghosh, 2014). By masking the nuclear localization sequence of NF-κB, IκBα restrains the transcription factor within the cytosol. Notably, IκBα also contains a nuclear import sequence within the second ankyrin repeat
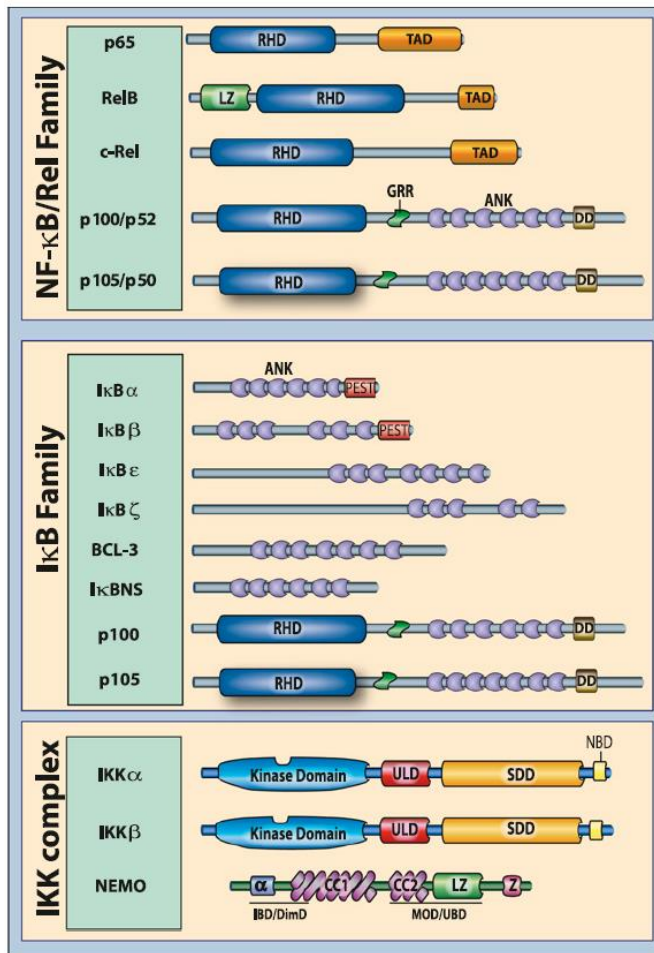
Figure 2. The NF-κB family. It can be divided into NF-κB subunits, the inhibitory IκB proteins and the IKK complex. RHD, rel homology domain; TAD, transactivation domain; LZ, Leucin zipper domain; DD, death domain; ANK, Ankyrin repeat domain; SDD, scaffolding and dimerization domain; ULD, ubiquitin-like domain; Z, zinc finger domain. Taken from (Hayden and Ghosh, 2012).

allowing unbound IκBα to enter the nucleus. Here it is able to interact with DNA-bound NF-κB resulting in its dissociation from the DNA and translocation to the cytosol (Sachdev et al., 1998). Of note, in their precursor form p105 and p100, p50 and p52 can also act as inhibitor proteins as they prevent NF-κB from translocating into the nucleus (Savinova et al., 2009).

5.1.2 NF-κB signaling pathways

NF-κB signaling has been described to be mediated via two distinct pathways. Each of them can be activated by a variety of stimuli. In the most common and best characterized canonical (classical) pathway, cytokines like TNFα or IL-1β bind to their respective receptor (e.g. TNF receptor 1) at the plasma membrane. A first step in this signaling cascade is the activation of the TGFβ-activated kinase 1 (TAK1). TAK1 will activate the IκB kinase (IKK) complex, a major regulatory factor in canonical NF-κB signaling. It is comprised of the catalytic subunits IKK1 (IKKα) and IKK2 (IKKβ) and the

regulatory subunit NF-κB essential modulator (NEMO/IKKγ) (Fig. 2). The activated IKK complex will phosphorylate IκBα at Ser32/36, which in turn will lead to its polyubiquitination mediated by SCF$^{β\text{-TrCP}}$ E3 ubiquitin ligases and its degradation by the 26S proteasome (Ben-Neriah, 2002).
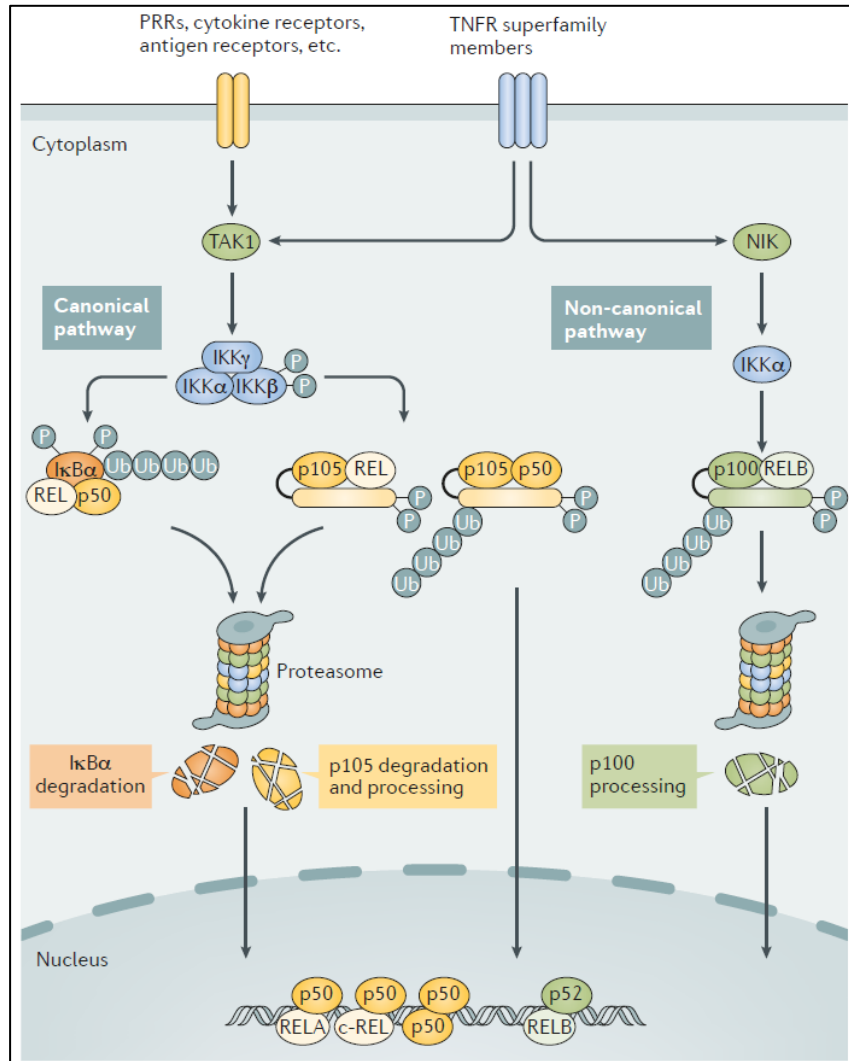
Figure 2. Schematic overview of the canonical (left) and non-canonical (right) NF-κB signaling pathway. Taken from (Sun, 2017).

Notably, IKK2 is generally believed to be responsible for the phosphorylation of IκBα since e.g. *Ikk1*-deficient mice do not display impairments in canonical signaling (Hu et al., 1999). However, CRISPR/Cas9-mediated knockouts of IKK1 and IKK2 in HEK293 cells resulted in comparable impairments of canonical NF-κB signaling (Fig. 4) questioning the universality of this dogma (Slotta et al. c). By degradation of IκBα, the NLS of NF-κB is unmasked so that NF-κB is no longer retained within the cytoplasm but translocates into the nucleus resulting in the expression of target genes (Perkins, 2007,

Hayden and Ghosh, 2008).
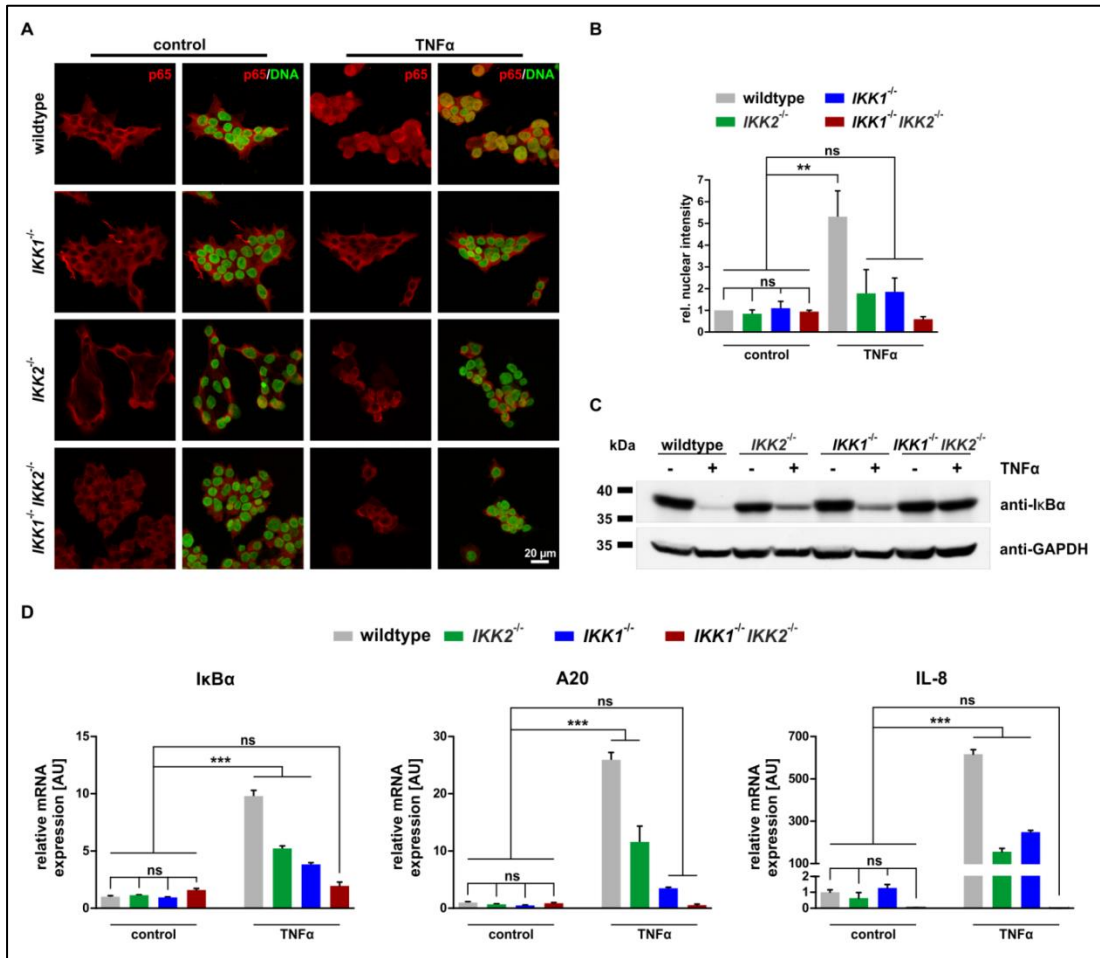
Figure 4. Activation of canonical NF-κB signaling is strongly reduced in *IKK1*-, *IKK2*- and *IKK1/2*-deficient cells. (A,B) Nuclear translocation of NF-κB p65 after 30 min of TNF stimulation is significantly impaired in all mutant cells compared to wildtype cells. **(C)** TNF-induced degradation of IκBα is reduced in IKK1- and IKK2-deficient cells compared to wildtype and not-existent in IKK1/2-double-deficient cells. **(D)** qPCR analysis of the NF-κB target genes IκBα, A20 and IL-8 display reduced NF-κB activity after 6 h of TNF-treatment in all mutant cells compared to wildtype cells. Taken from (Slotta et al. c).

In the alternative, non-canonical pathway NF-κB is predominantly comprised of RelB and p52 (Sun, 2012). Signaling is triggered upon activation of several members of the TNFR superfamily, including but not restricted to B-cell activating factor belonging to TNF-family receptor (BAFFR) (Claudio et al., 2002), lymphotoxin b receptor (LTβR) (Dejardin et al., 2002) and cluster of differentiation 40 (CD40) (Coope et al., 2002).

Binding to their specific receptors results in the activation of IKK1 by the NF-κB-inducing kinase (NIK) (Fig. 3). IKK1 phosphorylates the precursor protein p100, which leads to processing to the NF-κB subunit p52. During

processing, the NLS will be unmasked allowing NF-κB to enter the nucleus.

5.1.3 NF-κB within the nervous system

Next to the immune system, NF-κB is extensively researched within the nervous system. Here, it is strongly involved in neurogenesis, learning and memory as well as neuroprotection (reviewed in (Kaltschmidt and Kaltschmidt, 2009)).

Constitutively active NF-κB has been found in cortical and hippocampal neurons (Kaltschmidt et al., 1994b). Moreover, inducible forms of NF-κB have been found in synapses suggesting it to be a regulator in response to synaptic transmission (Kaltschmidt et al., 1993, Meberg et al., 1996, Meffert et al., 2003). Indeed, upon stimulation NF-κB was found to be transported retrogradely from the synapse to the soma (Mikenberg et al., 2007, Wellmann et al., 2001, Widera et al., 2016). Forebrain neuron-specific inhibition of NF-κB activity resulted in loss of neuroprotection and severe structural and cognitive deficits in mice (Fridmacher et al., 2003, Imielski et al., 2012). In an inducible transgenic mouse model this could be rescued even in adult mice additionally indicating a role of NF-κB in adult neurogenesis (Imielski et al., 2012). This is in line with observations of NF-κB being present in neural stem cells and neuronal progenitor cells contributing to proliferation and differentiation (Widera et al., 2006, Koo et al., 2010).

Due to its involvement in numerous processes, aberrant regulation of NF-κB is associated with several neurological disorders and neurodegenerative diseases, such as Alzheimer's disease, Parkinson's disease and Huntington's disease (Kaltschmidt et al., 1999b, Hunot et al., 1997, Mogi et al., 2007, Ghosh et al., 2007, Marcora and Kennedy, 2010).

5.1.4 Immune response in neurological disorders and its effect on myelination

Many neurodegenerative diseases comprise immunological features. Neuroinflammation is a key feature shared by many neurodegenerative diseases, such as Alzheimer's and Parkinson's disease and amyotrophic

lateral sclerosis (Heneka et al., 2015, Wang et al., 2015, Philips and Robberecht, 2011). Often inflammation and immune response activation develop early during disease and precede e.g. neuronal loss (Doty et al., 2015). In almost every disorder of the central nervous system (CNS), activated microglia – the CNS macrophages – can be found (Long-Smith et al., 2009, Prokop et al., 2013, Sargsyan et al., 2005). In addition to this microgliosis, reactive astrocytes and also lymphocytes can be found, e.g. in multiple sclerosis (MS) (Pender and Greer, 2007).

One process that can be triggered by the neuroinflammatory environment is degradation of the myelin sheath (demyelination). The myelin sheath is an essential component for axonal integrity and function. In the CNS it is generated and maintained by oligodendrocytes and in the peripheral nervous system (PNS) by Schwann cells (Nave and Werner, 2014). Suppressing the immune response in demyelinating neuropathies is a promising approach for therapy. In mouse models for demyelinating CNS and PNS disorders, impairments in the immune response resulted in improved myelin maintenance (Ip et al., 2006, Schmid et al., 2000).

NF-κB is a central regulator of inflammatory processes and as such in the center of research in the context of neurological disorders with inflammatory features. In reactive microglia a strong activation of NF-κB was demonstrated indicating NF-κB to be a key regulator in neuroinflammation (Kaltschmidt et al., 1994a, Bethea et al., 1998). In MS, a well-characterized demyelinating disease, neuroinflammation is a key feature. The blood-brain barrier becomes permeable, followed by strong infiltration of T-lymphocytes into the brain (Pender and Greer, 2007). Notably, in oligodendrocytes and activated microglia elevated activation of NF-κB was observed in MS patients linking NF-κB to demyelination (Bonetti et al., 1999). In fact, NF-κB modulating substances such as Fingolimod are already being used in MS therapy to reduce demyelination (Sanford, 2014).

5.1.5 NF-κB in cancer

Besides involvement in neurological disorders, deregulation of NF-κB signaling is also particularly associated with tumor formation and progression

(Xia et al., 2014, Li et al., 2005, Ben-Neriah and Karin, 2011). As a key regulator of inflammation, it cross-links cancer and inflammation (Xia et al., 2014). A chronic inflammatory environment results in cellular stress, the recruitment of inflammatory factors and DNA damage, which in turn favors tumor formation. Therefore, "tumor-promoting inflammation" has been described as one of the hallmarks of cancer (Hanahan and Weinberg, 2011). However, besides contributing to a pro-inflammatory environment, deregulated NF-κB signaling promotes tumor formation and progression also by other means. For different types of cancer cells, it was shown that elevated NF-κB activity is tightly connected with proliferation of tumor cells. Consequently, by inhibition of NF-κB proliferation could be reduced, as was e.g. shown in an Ikk2-depleted mouse model for lung carcinoma (Xia et al., 2012). Inhibiting NF-κB activation by the expression of a mutated form of IκBα (IκBAA1), which cannot be degraded, also resulted in reduced proliferation of murine tumor cells (Meylan et al., 2009) and human HeLa cells (Kaltschmidt et al., 1999a), a broadly used model for cervical cancers.

Inhibition of NF-κB activity is a prominently researched approach for anticancer therapy. By inhibition of the IKK complex using chemicals such as thalidomide or BAY11-7082, the severity of lymphomas could markedly be reduced (Mitsiades et al., 2002, Keifer et al., 2001, Garcia et al., 2005). Already used for the treatment of multiple myelomas is the proteasome inhibitor bortezomib that prevents the degradation of IκBα (Mulligan et al., 2007). However, global inhibition of NF-κB activity can result in severe adverse effects, such as systemic inflammation (Greten et al., 2007). Therefore, subunit-specific inhibition of NF-κB holds a great potential in therapy.
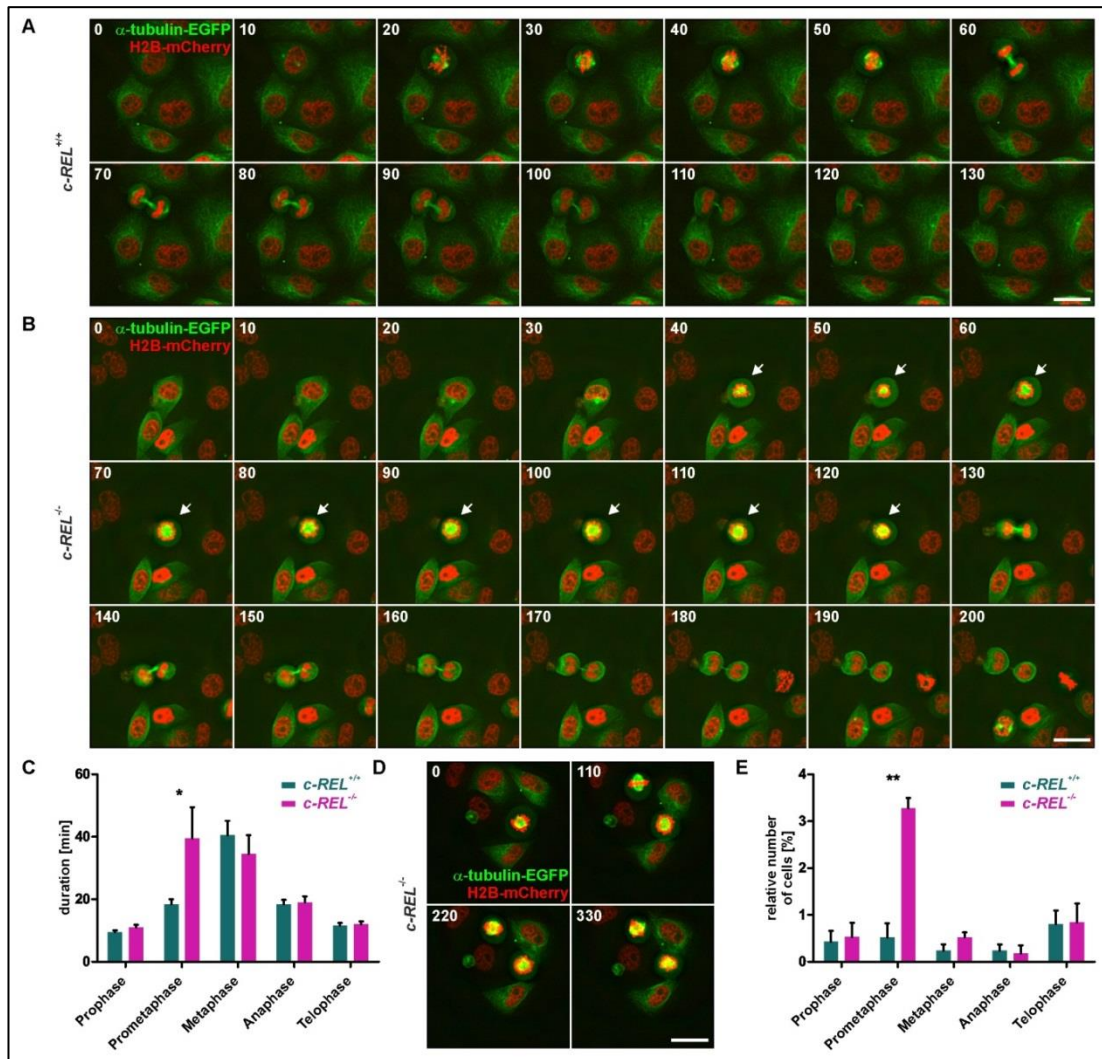
5.1.5.1 The role of c-Rel in cancer

Among the NF-κB subunits, particularly c-Rel is in the focus of cancer research. Originally, it was identified as the homologue of the avian retroviral oncoprotein v-REL, which induces lymphoma formation in birds (Gilmore and Gerondakis, 2011).

A broad range of studies has described the involvement of c-Rel in lymphoid

cancers (reviewed in (Hunter et al., 2016)). In primary mediastinal B-cell lymphoma (PMBL), an amplification of the REL locus was observed resulting in increased NF-κB activity (Weniger et al., 2007). Moreover, in adult T-cell leukemia/lymphoma (ATLL) increased expression of c-Rel was linked with resistance to therapy (Ramos et al., 2007). Recently, c-Rel was shown to be crucial for the generation and maintenance of activated regulatory T cells (aTregs) (Grinberg-Bleyer et al., 2017). These cells play an important role in the inhibition of anti-tumor immune responses helping the tumors to evade recognition by the immune system. Treg-specific ablation of c-Rel, but not of p65, resulted in drastically reduced melanoma growth in mice and additionally increased the effect of immunotherapy (Grinberg-Bleyer et al., 2017).

Besides B- and T-cell lymphomas, an increasing number of reports describe the functions of c-Rel in solid tumors. Here it was reported that c-Rel does not necessarily promote tumors and can also act as a tumor-suppressor. In 35 primary breast cancers, c-Rel expression was vastly increased and in a mouse model with forced expression of c-Rel in breast tissue, more than 30 % of the animals developed tumors (Cogswell et al., 2000, Romieu-Mourez et al., 2003). In HeLa cells, c-Rel-deficiency resulted in profound defects of the cell cycle. In particular, the prometaphase in c-Rel-deficient cells was markedly prolonged and a significant subset of cells even arrested at this mitotic stage without entering the G2 phase of the cell cycle (Fig. 5) (Slotta et al., 2017). These observations indicate a more tumor-promoting role of c-Rel. However, in a model for colitis-associated colon adenocarcinoma, c-Rel-deficiency resulted in a more severe phenotype (Burkitt et al., 2015).

In summary, this stresses the importance of the analysis of particular NF-κB subunit functions resulting in potentially more specific therapeutic approaches with less adverse effects.

Figure 5. Significantly delayed prometaphase in *c-REL*-deficient HeLa cells. (A,B) Live-cell imaging of wildtype (A) and mutant (B) cells displayed prolonged prometaphase in c-REL-deficient cells (arrows). **(C)** Quantification revealed a significance delay of the prometaphase (39.50 ± 9.96 min) of mutant cells compared to wildtype cells (18.42 ± 1.58 min). **(D)** Exemplary images of c-REL knockout cells arresting during mitosis. **(E)** Fluorescence imaging of fixed cells showed a significant subset of mutant cells within prometaphase compared to wildtype. Taken from (Slotta et al., 2017).

5.1.6 TNF signaling and its association with cell death

The tumor necrosis factor alpha (TNFα) is a pro-inflammatory cytokine and one of the best characterized activators of the canonical NF-κB signaling pathway. TNF signaling is associated with cell death and on a broader scale with tissue homeostasis and inflammation (reviewed in (Kondylis et al., 2017)). Therefore, targeting of TNF signaling provides a promising approach in the context of several diseases, especially of those that include inflammatory features (Peyrin-Biroulet, 2010). In particular, TNF signaling

20

has been associated with cancer formation and progression (reviewed in (Wang and Lin, 2008)). In a broad range of tumorigenic tissues and tumor cells, expression of TNF is highly elevated (Ferrajoli et al., 2002, Szlosarek et al., 2006). Conversely, many tumor cells are particularly resistant to TNF-induced cell death (Wang and Lin, 2008). Holding great anticancer potential, research focuses on the applicability of TNF in anticancer therapy. This includes the generation of mutated forms of TNF to increase its cytotoxicity, receptor affinity and half-life and to decrease its otherwise severe side-effects including systemic shock and widespread inflammation (Shibata et al., 2004, Lucas et al., 2001, Yan et al., 2006).
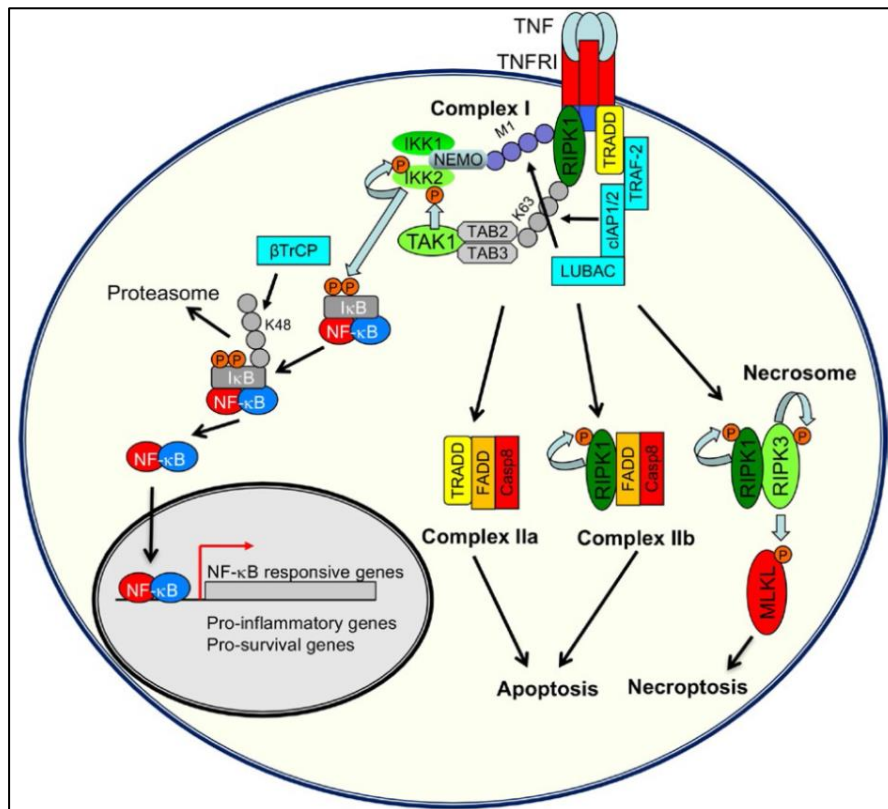
Figure 6. TNFR1 signaling pathway. Upon binding of TNF, complex I is assembled, which can result in the activation of the NF-κB signaling pathway but also lead to cell death mediated via complex IIa, IIb or the necrosome. Taken from (Kondylis et al., 2017).

Signaling by TNF is mediated by the two specific TNF receptors (TNFR) 1 and 2, whereby signaling primarily acts via TNFR1, which in contrast to TNFR2 is expressed ubiquitously (Walczak, 2011). Binding of trimeric TNFα causes trimerization of TNFR1, which induces the formation of the so-called

complex I (Fig. 6). This complex consists of the receptor-interacting serine/threonine-protein kinase 1 (RIPK1) and TNFR1 associated death domain protein (TRADD), which rapidly bind to the activated TNFR1, followed by TRADD-mediated recruitment of TNF receptor associated factor 2 (TRAF2) (Ermolaeva et al., 2008, Haas et al., 2009). This results in the binding of the E3 ubiquitin ligases cellular inhibitors of apoptosis (cIAP) 1 and 2, which add K63-linked ubiquitin chains to RIPK1. Following this ubiquitination two additional complexes are recruited. The IKK complex directly binds to the K63-linked ubiquitination chain. Additionally, the linear ubiquitin assembly complex (LUBAC) is recruited, adding M1-linked ubiquitin chains to RIPK1 (Peltzer et al., 2016). This second ubiquitination provides a signal for a complex consisting of TAK1 and the TAK1-binding proteins (TAB) 2 and 3 (Varfolomeev and Vucic, 2016). When this complex comes into close proximity to the IKK complex, TAK1 phosphorylates IKK2 and by this triggers its autophosphorylation, which is required for downstream signaling (Zhang et al., 2014a).

Two checkpoints have been described to regulate cell death upon TNF signaling (O'Donnell and Ting, 2011). The first one is well characterized and dependent on the activation of canonical NF-κB signaling, which results in the expression of pro-survival target genes, such as cFLIP (Van Antwerp et al., 1996, Micheau et al., 2001, Wang et al., 1998, Panayotova-Dimitrova et al., 2013). By this, formation of the so-called complex IIa is inhibited (Micheau and Tschopp, 2003). In this complex, Fas-associated protein with death domain (FADD) and caspase 8 are activated dependent on TRADD (Fig. 6), which induces apoptosis (Ofengeim and Yuan, 2013). The second checkpoint in comparison is far less well understood and just gained attention in recent years. It regulates cell death upstream of and by this independent on NF-κB activation (Legarda-Addison et al., 2009, Wang et al., 2008, Dondelinger et al., 2013, O'Donnell et al., 2007). This checkpoint is believed to act in dependence on RIPK1, either by prevention of its integration in the apoptosis complex IIb, in which it is required for activation of FADD and caspase 8, or by its integration into the necrosome (Fig. 6). Formation of the necrosome consisting of RIPK1/3 and the RIPK3 substrate pseudokinase

mixed lineage kinase like (MLKL) results in necroptotic cell death, a more recently described programmed cell death, which is independent on caspase 8 (He et al., 2009, Sun et al., 2012, Cho et al., 2009, Vanlangenakker et al., 2010). Recently, the IKK complex was reported to be a major regulator in TNF-induced cell death. While originally believed that the IKK complex was only mandatory for initiating canonical NF-κB signaling, Dondelinger and colleagues demonstrated the complex also to act directly on RIPK1 (Dondelinger et al., 2015). The IKK complex phosphorylates and thereby inhibits RIPK1 preventing its incorporation into complex IIb or the necrosome. By this, the IKK complex also acts as a regulator in TNF-induced cell death in an NF-κB-independent manner (Dondelinger et al., 2015). The study by Dondelinger was conducted by analyzing several knockout mouse models. Notably, only in mice deficient for both, Ikk1 and Ikk2, TNF-induced cell death was vastly elevated. Deficiency of either Ikk1 or Ikk2 was not sufficient to impair IKK-mediated prevention of TNF-induced cell death significantly (Dondelinger et al., 2015). These findings suggest the IKK complex to be a promising target to sensitize cells to TNF-induced cell death, which as described above is a highly researched approach for potential TNF applications in anticancer therapy. However, differences between humans and mice in TNF signaling have been reported in the past. Mice deficient for RelA, Ikk2 or NEMO die during embryonic development due to TNF-induced cell death of hepatocytes resulting in liver degeneration (Beg et al., 1995, Li et al., 1999, Tanaka et al., 1999, Rudolph et al., 2000). In contrast, Panicke and colleagues reported a frameshift mutation within the human *IKBKB* gene (encoding for IKK2) to be causative for severe combined immunodeficiency (SCID). None of the patients analyzed showed any signs of liver degeneration (Pannicke et al., 2013). These reported differences stress the necessity to analyze the role of the IKK complex in human cells in addition to mice.
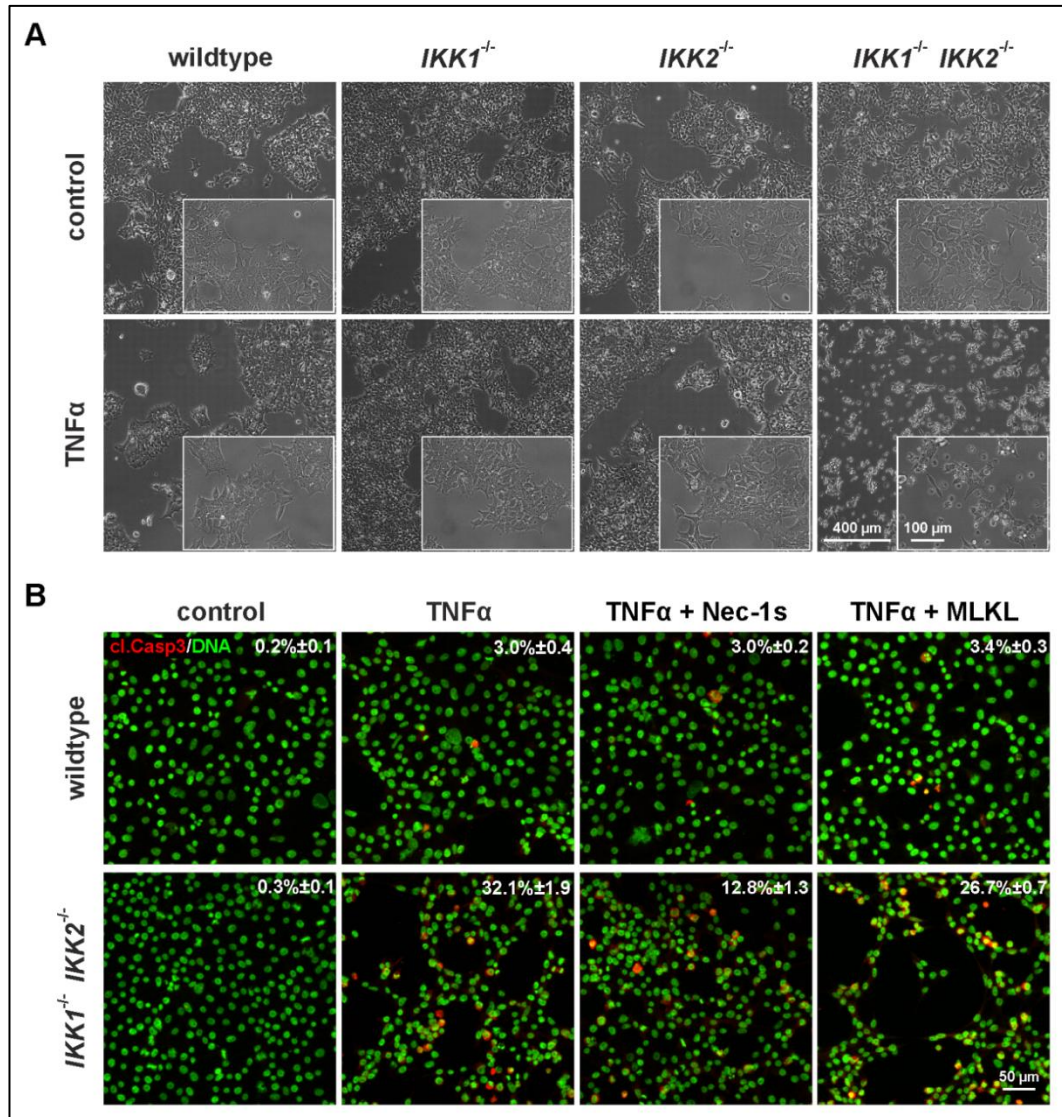
Figure 7. Cell death is increased after TNFα treatment in *IKK1/2*-deficient cells. (A) Light microscopic analysis of cells after 24 h stimulation with TNFα. A high number of dead cells was observed only in cells deficient for both IKK1 and IKK2. **(B)** Immunocytochemical stainings for activated caspase-3. A strong increase in caspase-3-positive cells in TNFa-treated double-deficient cells was detectable, which could partially be prevented using the RIPK1 inhibitor Necrostatin-1s (Nec-1s). Application of the MLKL inhibitor Necrosulfonamide only slightly lowered the amount of caspase-3-positive cells. Modified from (Slotta et al. c).

To initially investigate this, IKK1 and IKK2 were genetically depleted in human cells using CRISPR/Cas9 (Slotta et al. c). While also IKK1 and IKK2 single knockouts showed severe impairments in the activation of canonical NF-κB signaling (Fig. 4), only in cells deficient for both, IKK1 and IKK2, a vastly increased cell death after TNFα treatment was observed (Fig. 7). In line with the results obtained in mice by Dondelinger and colleagues, cell death was mediated in dependence of RIPK1 and independent on NF-κB

(Dondelinger et al., 2015, Slotta et al. c). This strongly indicates a similar role of the IKK complex as a major checkpoint in regulating TNF-induced cell death in human cells making it a promising target for future therapeutic approaches.

5.2 Autophagy

Autophagy (ancient greek: autóphagos; self-devouring) is a catabolic process, in which damaged or non-used cellular substances are being degraded and subsequently recycled. By this, autophagy serves as a regulatory mechanism to maintain homeostasis within cells, tissues and organisms. Three different autophagic pathways have been described, macroautophagy, microautophagy and chaperone-mediated autophagy (CMA) (Boya et al., 2013). Here, the mechanisms of macroautophagy (hereafter referred to as autophagy) will be addressed. While originally thought to be a non-specific cellular degradation process, today numerous specialized forms of autophagy have been described that selectively degrade e.g. organelles such as mitochondria (mitophagy) or ribosomes (ribophagy) (Kiel, 2010), synaptic vesicles (Shen et al., 2015) or even intracellular pathogens (xenophagy) (Levine et al., 2011).

As an essential cellular process, deregulation of autophagy is closely connected to diseases such as neurological disorders and cancer (Levy et al., 2017, Menzies et al., 2015).

5.2.1 Basic principles of autophagy

Today's understanding of the importance of autophagy as well as its mechanisms is largely based on the discovery of the autophagy-related (Atg) genes in yeast (Tsukada and Ohsumi, 1993, Harding et al., 1995, Thumm et al., 1994). Many of these genes are conserved in humans.

A major and well characterized regulatory factor of autophagy is the mammalian target of rapamycin (mTOR). Upon e.g. starving conditions, the mTOR complex 1 (mTORC1) – usually suppressing autophagy induction – is inhibited and by this initiates autophagy (Jung et al., 2010).

The autophagic degradation process can be divided into five different stages: initiation, nucleation of the autophagosome (forming of the phagophore), expansion and elongation of the autophagosome membrane, fusion with the lysosome and finally the degradation of the intravesicular components (Fig. 8) (reviewed in (Levy et al., 2017)). In the initiating phase, the ULK1 complex consisting of the unc-51 like autophagy activating kinases (ULK) 1 and 2, the

26

focal adhesion kinase family integrating protein 200 (FIP200), ATG13 and ATG101 complex is activated (Fig. 8). This in turn results in the activation of a complex, which comprises the class III phosphoinositide 3-kinase (PI3K) VPS34, which together with Beclin 1, ATG14, VPS15, UV radiation resistance-associated gene protein (UVRAG) and the BECN1‑regulated autophagy protein 1 (AMBRA1) forms phosphatidylinositol 3-phosphate (PI(P)3), an essential part of the autophagosome membrane. By this the phagophore is assembled.
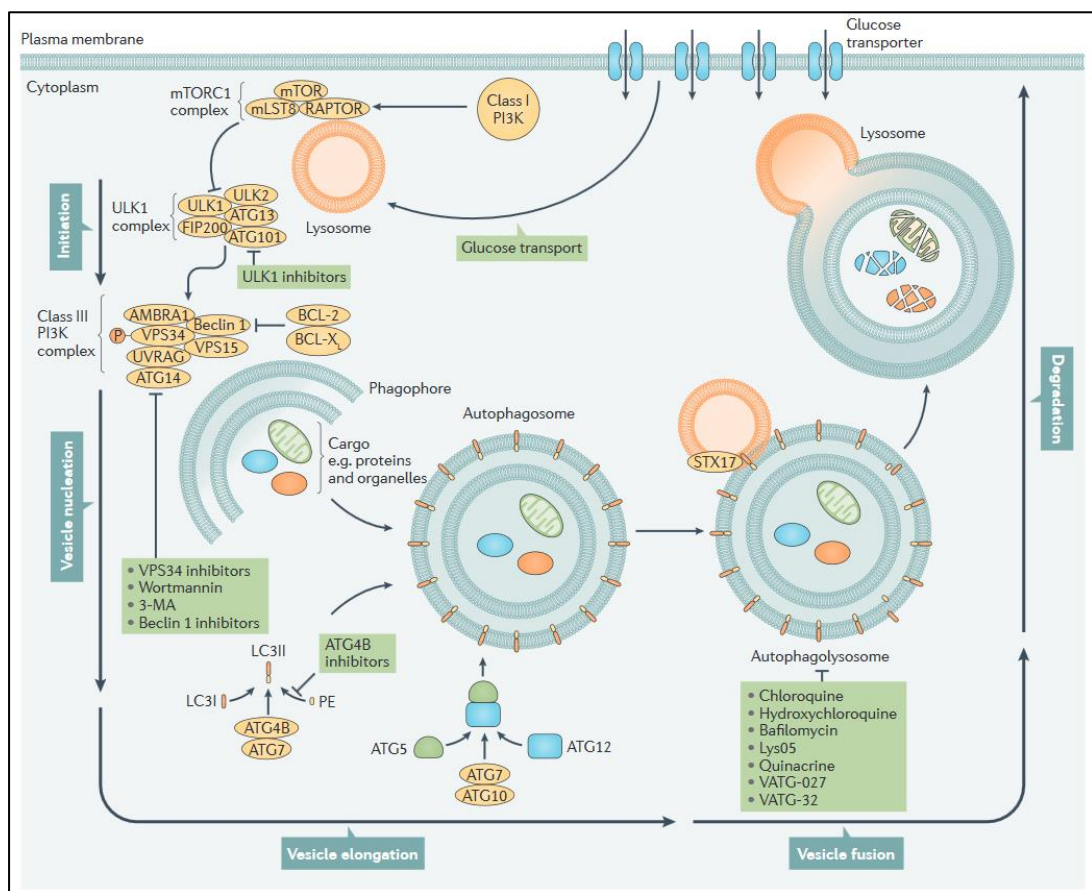
Figure 8. The autophagy degradation pathway and pharmacological inhibitors targeting at different stages of autophagy. Taken from (Levy et al., 2017).

Elongation of the membrane, mediated by the ATG5-ATG12 complex conjugated to ATG16, results in the autophagosome (Geng and Klionsky, 2008) having now engulfed the cargo that is to be degraded. ATG4B and ATG7 conjugate the microtubule associated protein 1 light chain 3 alpha (MAP1LC3A, also known as LC3I) to the lipid phosphatidylethanolamine (PE). The now termed LC3II protein is recruited to the membrane of the

autophagosome and serves as the most commonly used autophagosome marker (Klionsky et al., 2016). Mediated by the SNARE protein syntaxin17 (STX17), the autophagosome now fuses with the lysosome resulting in the autolysosome (often also referred to as autophagolysosome). Finally, the engulfed cargo will be degraded.

5.2.2 Autophagy in cancer – a double-edged sword

Autophagy is strongly within the focus of cancer research. However, things are complicated in this context and usually autophagy is described as a "double-edged sword" (White and DiPaola, 2009, Hippert et al., 2006, Kimmelman, 2011, Kenific et al., 2010). Originally, suppression of autophagy was associated with the formation of tumors. The autophagy relevant gene *BECN1* (encoding for Beclin 1) is highly suspected to be a tumor suppressor (Liang et al., 1999). It is monoallelically deleted in 40 % of all prostate cancers, 50 % of breast cancers and up to 75 % of ovarian cancers (Aita et al., 1999). Moreover, in heterozygous Beclin 1- deficient mice spontaneous malignant tumor formation was highly elevated (Yue et al., 2003, Qu et al., 2003). However, the role of Beclin 1 as a tumor suppressor is now strongly being questioned. The *BECN1* locus is adjacent to *BRCA1* (breast cancer 1), a known breast and ovarian tumor suppressor (Laddha et al., 2014). Mutations in *BRCA1* are known to cause the formation of breast and ovarian cancer. Monoallelic loss of *BRCA1* therefore might be the driving force in tumor formation and not *BECN1*. In line with that, in mouse models with a monoallelic loss of *Becn1* (but still carrying both copies of *Brca1*) tumorigenesis was not elevated but even reduced (Huo et al., 2013). Moreover, in large-scale genomic analyses no recurrent mutations within *BECN1* or other essential autophagy genes were found (Vogelstein et al., 2013, Lawrence et al., 2014).

In contrast to the questionable role of autophagy in tumor formation, once a tumor is formed the general view is that inhibition of autophagy is beneficial within anticancer therapy (Amaravadi et al., 2007, Levy and Thorburn, 2011). In fact, many substances that inhibit autophagy at different stages are being used in clinical trials for anticancer therapies (for an overview see (Levy et

al., 2017)). Cancer cells are particularly dependent on autophagy, potentially due to higher metabolism caused by deregulated proliferation (Rabinowitz and White, 2010). Moreover, upregulated autophagy was shown in hypoxic tumor regions to be essential for cell survival (Degenhardt et al., 2006). Additionally, it was shown that especially cancer stem cells (CSCs) rely on autophagy (Lei et al., 2017). CSCs are a small subpopulation within a tumor, which have the capacity to self-renewal and differentiation (Gupta et al., 2009). Due to this they have the ability to induce tumor formation. Being especially resistant to conventional anticancer therapy, CSCs are often responsible for tumor recurrence (Suresh et al., 2016). Inhibition of autophagy in combination with anticancer therapy therefore is now extensively being investigated to increase effectiveness of therapy and lower recurrence rates (Lei et al., 2017).

5.2.3 Role of autophagy in neurodegenerative diseases

Accumulation and aggregation of misfolded proteins is a feature of many neurodegenerative diseases, especially in those with a late onset, which e.g. includes Alzheimer's disease (AD) and Parkinson's disease (PD) (Zare-Shahabadi et al., 2015, Lynch-Day et al., 2012). Many genes associated with neurodegenerative diseases – either as causative or as risk factor – also play a role in the autophagy pathway. Among the 27 major genes known to be implicated in amyotrophic lateral sclerosis (ALS), 7 genes are being associated with autophagy (reviewed in (Hardiman et al., 2017)). In a mouse model for a late onset motoneuron disease comprising features of ALS and Charcot-Marie-Tooth (CMT) disease, impaired formation of autophagosomes in motoneurons was described, strongly contributing to disease progression (Fig. 9) (Lüningschrör et al., 2017).
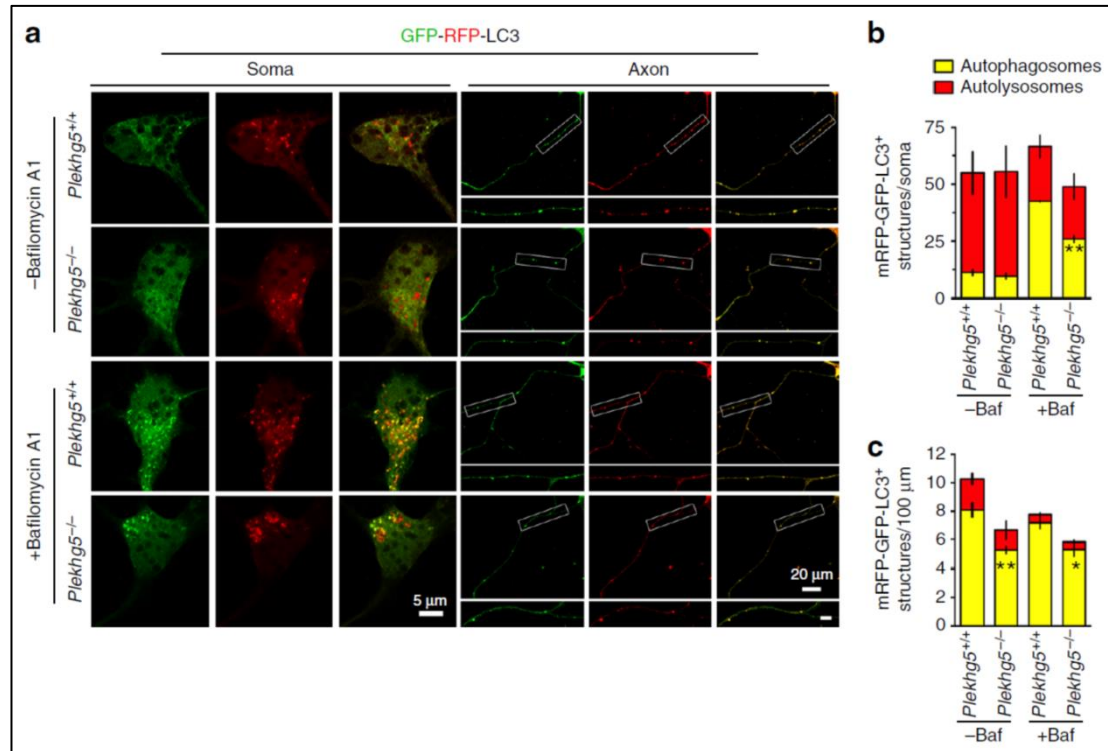
Figure 9. Formation of autophagosomes is impaired in motoneurons from *Plekhg5*-deficient mice. (a) Motoneurons were transduced with GFP-RFP-LC3 reporter and the fluorescent structures were quantified in the soma **(b)** and within the axon **(c)**. Modified from (Lüningschrör et al., 2017).

While most research focusses on autophagy in neuronal cells, many neurological disorders have a "glia component", meaning that also defects in glia cells contribute to the disease. Recent studies suggest that autophagy in glia cells may be equally important in the pathogenesis of the diseases, especially those with inflammatory features. In reactive astrocytes, autophagy was shown to be essential for cell survival (Motori et al., 2013). Moreover, autophagy was demonstrated to be protective for oligodendrocytes in a model of a demyelinating disease (Smith et al., 2013). However, more work is required to show the contributions of glial autophagy to the respective pathology in neurodegenerative diseases.

With impaired autophagy being causative for the formation of neurodegenerative diseases, potential therapeutic approaches deal with the upregulation of this process (Harris and Rubinsztein, 2011).

As described earlier, formation of the autophagy-initiating ULK1 complex is inhibited by mTOR. One of the first inducers of autophagy discovered is the

mTOR inhibitor rapamycin, which has been studied extensively in regard to its therapeutic potential (Ravikumar et al., 2004, Rodriguez-Muela et al., 2012, Spilman et al., 2010, Jiang et al., 2014). Recently, research however concentrated on upregulating autophagy independent of mTOR, because mTOR also has other functions besides autophagy regulation. Though the mechanism is not known yet, the disaccharide trehalose can act as an activator of autophagy and as such was able to enhance lifespan in ALS mouse models (Castillo et al., 2013, Zhang et al., 2014b).

5.3 Plekhg5

The Pleckstrin homology domain containing, family G member 5 (Plekhg5) is a guanine exchange factor (GEF), highly expressed within the nervous system, endothelial cells and tumor cells (Marx et al., 2005, Azzedine et al., 2013, Liu and Horowitz, 2006, Dachsel et al., 2013). It consists of 1083 amino acids (human transcript variant 2; NCBI refseq: NM_198681.3) and contains multiple functional domains for GTP/GDP exchange and membrane association (Fig. 10). While early publications defined Plekhg5 as a GEF specific for RhoA, direct interaction with a member of the Rab-family, Rab26, could be demonstrated recently (Lüningschrör et al., 2017). Furthermore, Plekhg5 is known to activate NF-κB although the exact mechanisms are not understood yet (Maystadt et al., 2007, Matsuda et al., 2003).
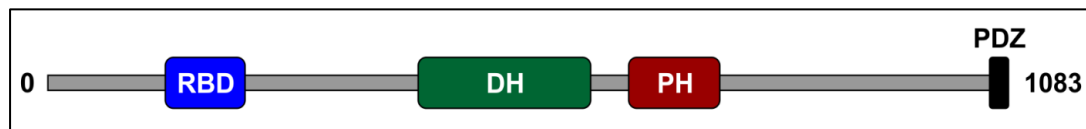
Figure 10. Schematic overview of the functional domains of Plekhg5. RBD, Rnd3 binding domain; DH, Dbl homology domain; PH, Pleckstrin homology domain; PDZ, PDZ binding motif.

5.3.1 Involvement of Plekhg5 in peripheral neuropathies

Several mutations found within the human *PLEKHG5* gene have been associated with different motoneuron diseases. While one point mutation within the pleckstrin homology (PH) domain (F647S) was associated with distal spinal muscular atrophy (DSMA IV) (Maystadt et al., 2007), another one (P630H) was found in a screening approach of patients suffering from ALS (Ozoguz et al., 2015). Moreover, *PLEKHG5* mutations have been described as one cause for an intermediate form of CMT (Azzedine et al., 2013, Kim et al., 2013). Based on measurements of the nerve conduction velocities (NCV), CMT diseases – the most common inherited neuropathy with a prevalence of 1 in 2500 (Reilly et al., 2011) – are classified into two major groups (Thomas and Calne, 1974, Keller and Chance, 1999, Nelis et al., 1999). In type I (CMT1), the NCV is lower than 38 m/s, which is caused by defects of the Schwann cells resulting in abnormal myelination (e.g.

demyelination). CMT2 on the contrary is characterized by rather normal NCVs higher than 40 m/s, but reduced motor action potentials. Histologically, axonopathy – mostly a loss of large caliber axons – can be detected. While in CMT1 the Schwann cells and in CMT2 the neurons are affected, a third intermediate form has been described, showing characteristics of both forms (Rossi et al., 1985, Saporta et al., 2011). Since Plekhg5 was shown to be expressed in both, neurons and Schwann cells, it is not surprising that it is associated with the intermediate form of CMT (Kim et al., 2013, Azzedine et al., 2013, Lüningschrör et al., 2017).

To date, two different mouse models were generated to analyze the role of Plekhg5 in the context of motoneuron disease. In 2013, Azzedine and co-workers presented data based on a *Plekhg5*-deficient mouse generated earlier by Garnaas and colleagues (Azzedine et al., 2013, Garnaas et al., 2008). In their study they demonstrated a slight decrease in the NCV resembling a mild intermediate CMT. However, no loss of motoneurons was demonstrated concluding that the phenotype of these mice did not resemble a lower motoneuron disease as described in humans by Maystadt and colleagues (Azzedine et al., 2013, Maystadt et al., 2007). Recently, a novel *Plekhg5*-deficient mouse line was characterized by Lüningschrör and co-workers, in which significant loss of motoneurons was demonstrated, while the NCV was only very mildly and not significantly affected (Fig. 11c, g) (Lüningschrör et al., 2017). In contrast to the mouse analyzed by Azzedine and colleagues, these mice also developed a clear motoneuron disease pathology as could be demonstrated by hindlimb clasping, reduced grip strengths and reduced performance on the rotarod (Fig. 11b, d-f) (Lüningschrör et al., 2017). Two potential reasons might be the cause for the different observations in these mouse models. First, as described by Lüningschrör and co-workers, symptoms did not start before 12 months of age and in the study by Azzedine *et al.* no mice older than 12 months were analyzed. A potential pathology therefore might not have been detected. The second potential reason lies within the generation of the mouse model. The mice used by Azzedine were generated using the Cre-lox system, by which a region including the exons 9 to 13 was excised. This resulted in the

expression of a truncated protein lacking the RhoGEF domain but still containing most of the PH domain (Azzedine et al., 2013). In contrast, the gene-trap approach used by Lüningschrör and colleagues resulted in the expression of a protein lacking both functional domains (Lüningschrör et al., 2017).
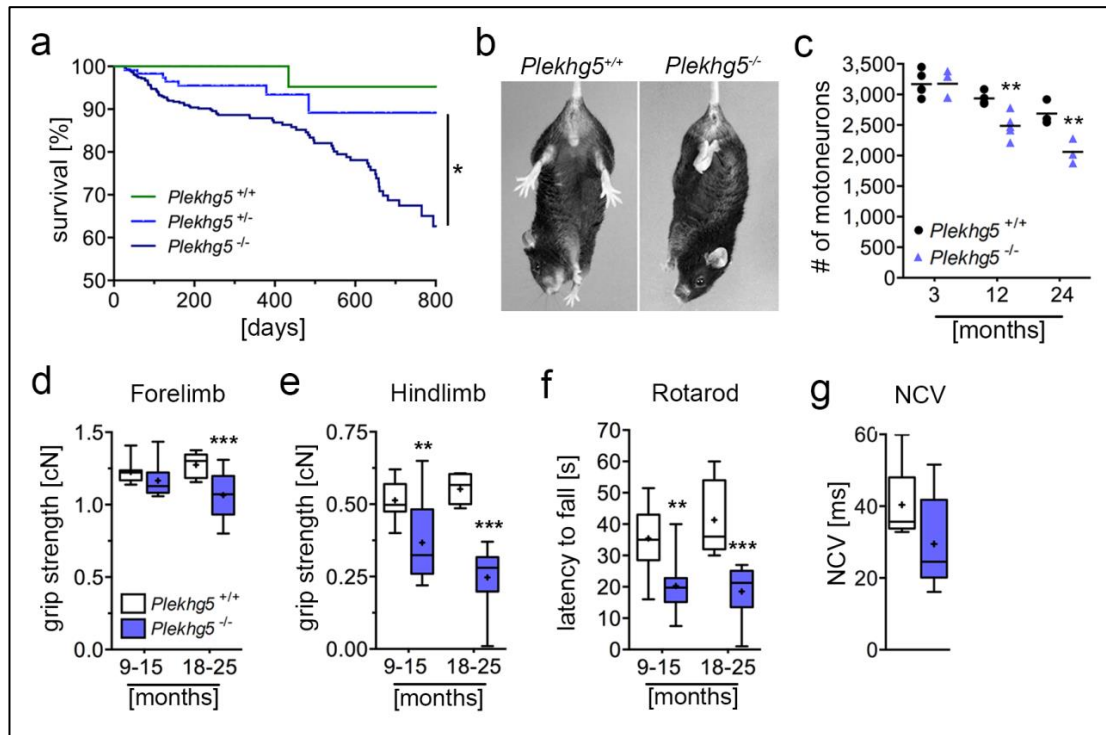
Figure 11. *Plekhg5*-deficient mice develop a late onset motoneuron disease. (a) Reduced life-span of *Plekhg5* mutant mice. **(b)** Hind-limp clasping in 15-month-old mutant mice. **(c)** Progressive loss of motoneurons within the spinal cord. **(d, e)** Decreased grip strengths of forelimbs **(d)** and hindlimbs **(e)**. **(f)** Reduced performance of *Plekhg5*-deficient mice on the accelerating rotarod. **(g)** Slightly decreased sciatic nerve conduction velocity in mutant mice. Modified from (Lüningschrör et al., 2017).

In the following, the roles of Plekhg5 in motoneurons and Schwann cells will be discussed.

5.3.1.1 The role of Plekhg5 in motoneurons

Motoneurons are the efferent neurons that innervate all cross-striated muscles throughout the body. While also cells residing in the motor cortex of the brain are classified as (upper) motoneurons, they do not directly act on muscle cells but are interneurons that activate the lower motoneurons

34

residing in the spinal cord, which in turn directly innervate muscles. Thus, the term motoneuron is often restricted to lower motoneurons. As stated above, several genes in humans known to be involved in autophagy are associated with motoneuron diseases, such as ALS (Hardiman et al., 2017). In mice deficient for the autophagy-related genes *Atg5* or *Atg7* progressive motoneuron loss could be observed (Hara et al., 2006, Komatsu et al., 2006). Besides shared autophagic pathways and functions compared to other cells, there is an additional need for autophagy-mediated degradation of synaptic vesicles in neurons. Synapses are highly dynamic structures and there is a persistent turnover of synaptic vesicles, which requests for controlled degradation (Caroni et al., 2012, Chung and Barres, 2012). Cell-autonomous degradation of synaptic vesicles was long thought to be mediated via the classical endosomal-lysosomal pathway (Raiborg and Stenmark, 2009). Still, not many evidences for this were reported, e.g. only sparse information is available, whether synaptic vesicle proteins are ubiquitinated – the initial step in the classical endosomal-lysosomal pathway (Katzmann et al., 2002, Na et al., 2012). In 2015, Binotti and colleagues reported autophagy-mediated degradation of synaptic vesicles, which was controlled by the GTPase Rab26 (Binotti et al., 2015). Extending these findings, Plekhg5 could be demonstrated to directly act as a GEF for Rab26 in regulating this process (Lüningschrör et al., 2017). Hence, the autophagic impairments in Plekhg5-depleted motoneurons presented above (Fig. 9) could be explained by reduced activation of Rab26. As a consequence of impaired autophagy-mediated clearance of synaptic vesicles, large accumulations of synaptic vesicles were present in neuromuscular junctions (NMJs) of *Plekhg5*-deficient mice (Fig. 12). By this, proper innervation of muscle cells was impeded resulting in the motoneuron disease phenotype described above.
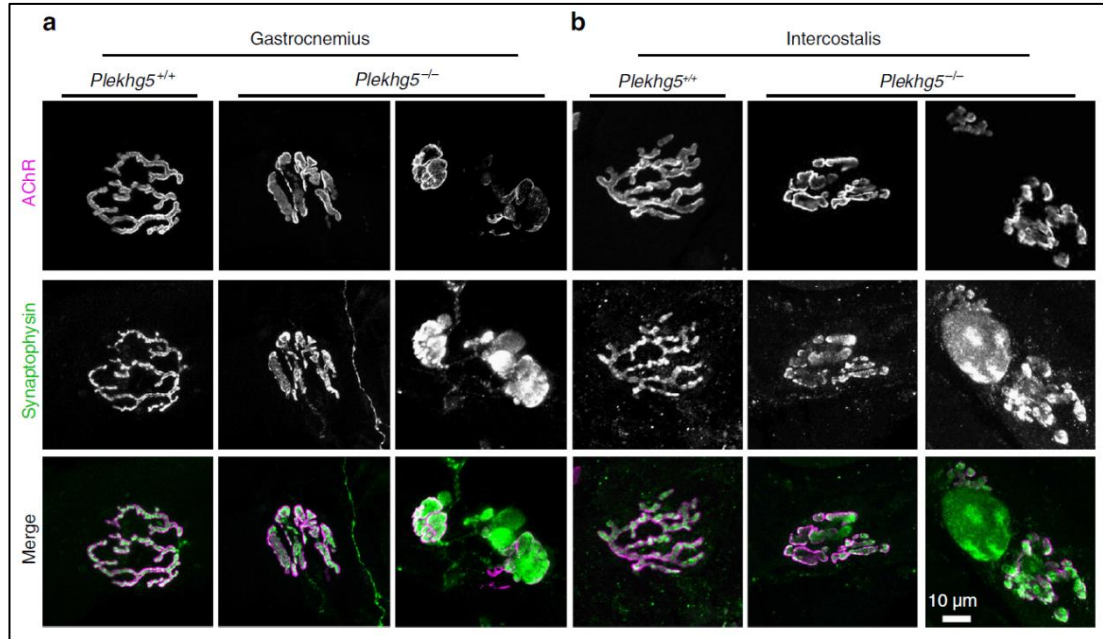
Figure 12. The presynaptic region of neuromuscular junctions is strongly impaired in *Plekhg5***-deficient mice.** Gastrocnemius **(a)** and intercostal **(b)** muscles were stained for the acetylcholine receptor (AChR) marking the postsynapse and for synaptophysin marking the presynapse. Modified from (Lüningschrör et al., 2017).

5.3.1.2 The function of Plekhg5 in Schwann cells

As stated above, Plekhg5 expression is not restricted to neurons within the nervous system. Particularly in Schwann cells, high expression of Plekhg5 was demonstrated (Azzedine et al., 2013).

Schwann cells are the myelinating glial cells in the PNS. Their main task under physiological conditions is the establishment and maintenance of the myelin sheath wrapped around the axons, which is essential for fast action potential propagation (Nave and Werner, 2014). However, under pathological conditions, Schwann cells display a great plasticity. Upon axonal lesions or in PNS disorders, Schwann cells are able to undergo huge differentiation processes. Originally, this was described as de-differentiation to a more immature Schwann cell type (Chen et al., 2007). However, there is now evidence that Schwann cells in fact differentiate to a distinct repair-cell type termed Bungner cell (Arthur-Farraj et al., 2012). Therefore, trans-differentiation or reprogramming appears to be a more fitting term to describe these cellular changes (Jessen and Mirsky, 2016). This great plasticity of Schwann cells is thought to be one of the main reasons for the high

36

regenerative capacity of the PNS in contrast to the CNS since oligodendrocytes – the myelinating glia of the CNS – do not display this grade of plasticity (Vargas and Barres, 2007).

Recently, a novel function of Schwann cells upon acute injury and potentially within PNS disorders has been described. Recovery of peripheral nerves after injury heavily relies on the clearance of axonal and myelin debris in a process called Wallerian degeneration (Vargas and Barres, 2007, Conforti et al., 2014). Gomez-Sanchez and co-workers demonstrated that initial myelin breakdown after sciatic nerve injury was performed directly by Schwann cells in an autophagy-dependent manner – a process termed myelinophagy (Gomez-Sanchez et al., 2015). In line with that, autophagy of myelin was also observed during axonal degeneration in the dental pulp (Suzuki et al., 2015). It was suggested that this process might not only play a role after acute injury but also in the context of inherited peripheral neuropathies. Extending these initial findings of autophagy-mediated myelin degradation, Slotta and colleagues reported impairments in the formation of autophagosomes in Schwann cells lacking Plekhg5 (Fig. 13), which resulted in demyelination deficits within peripheral nerves (Slotta et al. a).
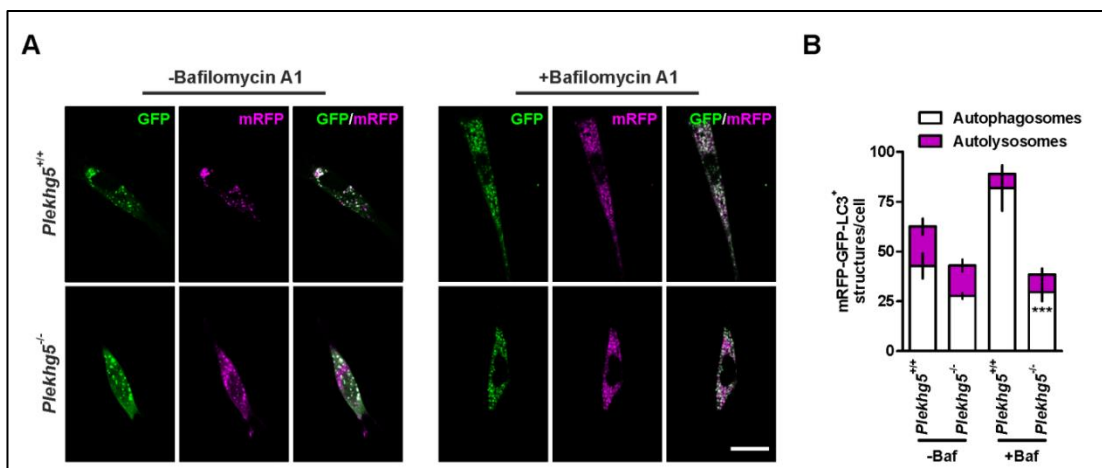
Figure 13. Biogenesis of autophagosomes is impaired in Plekhg5-depleted Schwann cells. (A) Primary Schwann cells were transduced with a GFP-RFP-LC3 reporter, which allows to selectively mark autophagosomes and autolysosomes based on the fluorescence. **(B)** Significantly decreased numbers of autophagosomes in mutant mice. Scale bar: 20 µm. Modified from (Slotta et al. a).

Plekhg5-deficient mice displayed an increased number of axons with myelin

infoldings (Fig. 14) and an overall modest hypermyelination within the sciatic nerve (Slotta et al. a). These forms of myelin alterations were previously reported in demyelinating disorders preceding myelin breakdown (Quattrone et al., 1996, Fabrizi et al., 2000, Chung et al., 2011). However, no signs of demyelination were observable even in old mice (Slotta et al. a). As myelinophagy was described only as the initial process of myelin degradation (Gomez-Sanchez et al., 2015), impairments due to *Plekhg5*-deficiency could not be the single cause for the alterations observed.
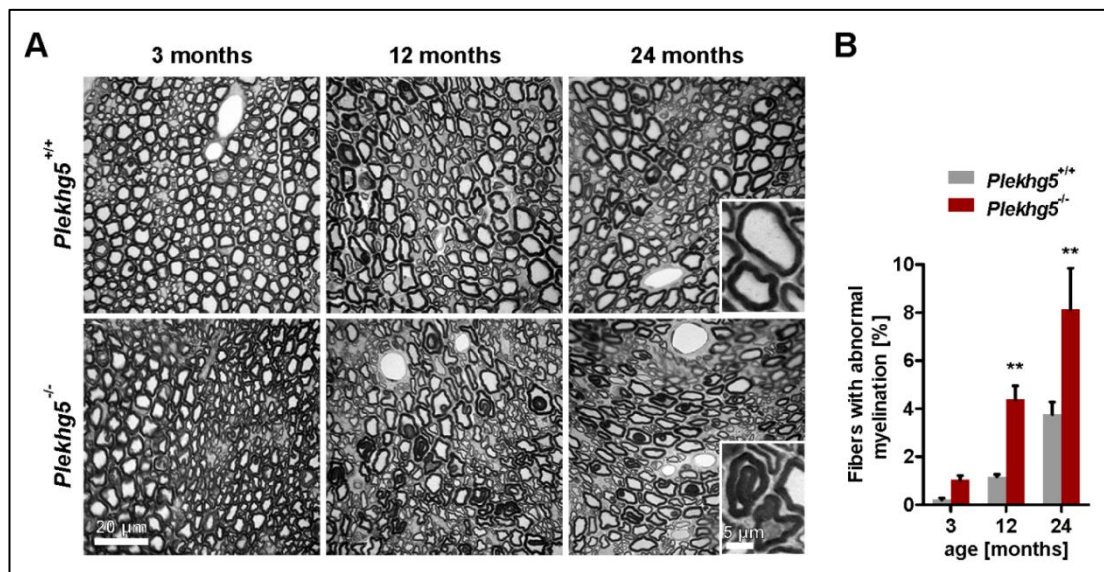
Figure 14. Altered myelination within the sciatic nerve of Plekhg5-deficient mice. (A) Histological analysis of semi-thin sections of mutant mice displaying severe myelin alterations. Most prominently infoldings of the myelin sheath were observed (blowups). **(B)** Progressive increase of fibers with abnormal myelination in *Plekhg5*-deficient mice. Modified from (Slotta et al. a).

Besides this initial autophagy-mediated myelin breakdown, an increasing number of reports describe the immunocompetence of Schwann cells in pathological situations. Here Schwann cells contribute to both, the innate and the adaptive immune response (reviewed in (Ydens et al., 2013)). During the innate immune response, Schwann cells produce and secrete cytokines, such as TNF and IL-1β and chemokines such as monocyte chemoattractant protein 1 (MCP1) (Shamash et al., 2002, Tofaris et al., 2002). To a large extent this is regulated by NF-κB. Despite the axonal pathology in *Plekhg5*-deficient mice (Lüningschrör et al., 2017), using RNAseq no increase in the

expression of NF-κB-regulated cytokines or chemokines was detected within the sciatic nerve (Slotta et al. a). As Plekhg5 is a known activator of NF-κB, this observation suggests an impaired activation of NF-κB in Schwann cells due to lack of Plekhg5 and by this the lack of inflammation within the sciatic nerve. Furthermore, *Plekhg5*-deficient mice displayed a reduced number of CD4- and CD8-positive T-lymphocytes within the sciatic nerve indicating also the adaptive immune response to be affected (Slotta et al. a).

In summary, *Plekhg5*-defiency in Schwann cells culminates in an immunosuppression within peripheral nerves despite an axonal pathology. Therefore, Plekhg5 might be a promising target for the treatment of PNS disorders with inflammatory and/or demyelinating features.

5.3.2 Plekhg5 in tumor cells

In addition to its expression in endothelial cells and within the nervous system, Plekhg5 was reported to be highly expressed in different tumorigenic tissues and cancer cell lines. In skin cancer cells Plekhg5 was shown to be involved in increased proliferation in response to vascular epidermal growth factor (VEGF) A (Yoshida et al., 2015). In U251-MG cells, a broadly used cellular model of GBM (Westermark et al., 1973), Dachsel and colleagues demonstrated Plekhg5 to regulate polarity-oriented migration (Dachsel et al., 2013). In both studies, the role of Plekhg5 as a GEF for RhoA was described. However, as mentioned above, Plekhg5 was also reported to directly act as a GEF for a member of the Rab protein family in regulating synaptic autophagy in motoneurons (Lüningschrör et al., 2017). Extending the findings of Plekhg5 as regulator of autophagy from motoneurons to cancer cells, U251-MG cells were genetically depleted of Plekhg5 using CRISPR/Cas9 (Slotta et al. b). Deficiency of Plekhg5 resulted in morphological changes from typically bipolar cells to a more apolar cell type, similar to observations by Dachsel and co-workers upon shRNA-mediated knockdown of Plekhg5 (Dachsel et al., 2013, Slotta et al. b). Moreover, cells lacking Plekhg5 displayed a significantly reduced proliferation (Slotta et al. b).
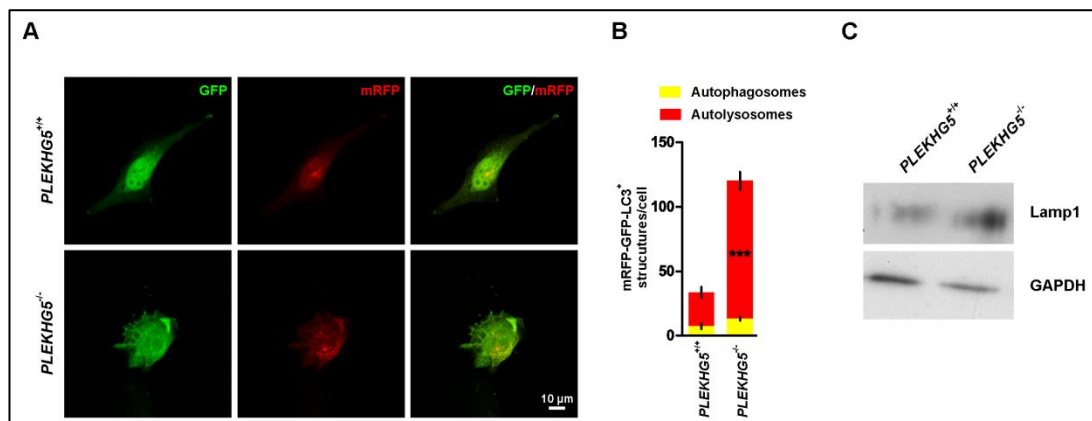

Figure 15. Clearance of autolysosomes is compromised in *PLEKHG5*-deficient U251-MG cells. (A, B) U251-MG cells were transduced with a GFP-RFP-LC3 reporter and the fluorescent structures were quantified. A strongly elevated number of autolysosomes was observed **(C)** Increased amount of the lysosomal marker Lamp1 in *PLEKHG5*-deficient cells. Modified from (Slotta et al. b).

Regarding changes in the autophagic process, Plekhg5-depleted cells showed a significant increase in the number of autolysosomes (Fig. 15). Upon application of Bafilomycin A1, levels were normalized to wildtype cells (Slotta et al. b). This indicated an impaired or delayed clearance of autolysosomes. Notably, *Plekhg5*-deficiency in murine motoneurons and Schwann cells resulted in an impaired formation of autophagosomes (Lüningschrör et al., 2017, Slotta et al. a), demonstrating Plekhg5 to regulate autophagy at different stages depending on the cellular or environmental context. U251-MG cells, as described earlier, are a model system broadly used to study GBMs. GBMs are among the most aggressive tumors and survival rate, even with maximum treatment, is no longer than 14 months (Koshy et al., 2012). Glioblastoma cells are particularly resistant to chemotherapy. Upon treatment with Temozolomide (TMZ), a standard chemotherapeutic agent, glioblastoma cells upregulate autophagic processes helping them to survive (Wurstle et al., 2017, Knizhnik et al., 2013). Targeting autophagy in GBMs next to chemotherapy therefore appears to be particularly promising to increase efficiency of chemotherapy. Future studies will have to address, whether Plekhg5 might serve as an additional target to impair autophagy during chemotherapy.

In summary, Plekhg5 appears to be a promising genetic target for anticancer therapy, since it is involved in cancer cell proliferation and migration (i.e. cancer invasion) but also in regulating autophagy.

6. Outlook

In part one of this thesis the different roles of Plekhg5 in motoneurons and Schwann cells have been analyzed. Deficiency in neurons and Schwann cells both contributed to the pathology observed in *Plekhg5*-deficient mice. Further extending these promising findings, cell-type-specific rescue of Plekhg5 could be performed. The gene-trap cassette within the *Plekhg5* locus additionally contains LoxP sites (Lüningschrör et al., 2017) allowing re-establishment of the original genomic locus using the Cre-Lox system.

In regard to the reduced immune response in peripheral nerves of *Plekhg5*-deficient mice, it is tempting to speculate whether a Schwann cell-specific depletion of Plekhg5 would improve the phenotype in mouse models with a peripheral neuropathy that includes neuroinflammatory features, e.g. the classical ALS mouse model SOD1^{G93A}. Moreover, since a significant subset of the downregulated genes for T-lymphocyte recruitment were target genes for NF-κB, Schwann cell-specific inhibition of NF-κB activity also might be a promising approach.

Part two of the thesis presented focused on the analysis of several CRISPR/Cas9-mediated knockouts in human cells. Since all findings aimed to provide new mechanistic insights for future anticancer therapeutic approaches, they should be reproduced in primary human tumor cells in the next step.

With regard to the *PLEKHG5*-deficient human glioma cells generated in this thesis, potential consequences of the altered autophagy in the context of chemotherapy should be investigated. Since the application of chemotherapeutics is known to elevate autophagy, alterations in the autophagic process potentially would sensitize cells to chemotherapy.

As the simultaneous depletion of IKK1 and IKK2 greatly sensitized cells to TNF-induced cell death, future studies should take on this promising finding to analyze its applicability in the context of anticancer therapy. This in particular involves the delivery methods to ensure both efficient and specific genetic modifications, so that effectively only tumor cells are affected. Moreover, methods for local TNF application have to be validated.

7. References

AITA, V. M., LIANG, X. H., MURTY, V. V., PINCUS, D. L., YU, W., CAYANIS, E., KALACHIKOV, S., GILLIAM, T. C. & LEVINE, B. 1999. Cloning and genomic organization of beclin 1, a candidate tumor suppressor gene on chromosome 17q21. *Genomics,* 59**,** 59-65.

AMARAVADI, R. K., YU, D., LUM, J. J., BUI, T., CHRISTOPHOROU, M. A., EVAN, G. I., THOMAS-TIKHONENKO, A. & THOMPSON, C. B. 2007. Autophagy inhibition enhances therapy-induced apoptosis in a Myc-induced model of lymphoma. *J Clin Invest,* 117**,** 326-36.

ARTHUR-FARRAJ, P. J., LATOUCHE, M., WILTON, D. K., QUINTES, S., CHABROL, E., BANERJEE, A., WOODHOO, A., JENKINS, B., RAHMAN, M., TURMAINE, M., WICHER, G. K., MITTER, R., GREENSMITH, L., BEHRENS, A., RAIVICH, G., MIRSKY, R. & JESSEN, K. R. 2012. c-Jun reprograms Schwann cells of injured nerves to generate a repair cell essential for regeneration. *Neuron,* 75**,** 633-47.

AZZEDINE, H., ZAVADAKOVA, P., PLANTE-BORDENEUVE, V., VAZ PATO, M., PINTO, N., BARTESAGHI, L., ZENKER, J., POIROT, O., BERNARD-MARISSAL, N., ARNAUD GOUTTENOIRE, E., CARTONI, R., TITLE, A., VENTURINI, G., MEDARD, J. J., MAKOWSKI, E., SCHOLS, L., CLAEYS, K. G., STENDEL, C., ROOS, A., WEIS, J., DUBOURG, O., LEAL LOUREIRO, J., STEVANIN, G., SAID, G., AMATO, A., BARABAN, J., LEGUERN, E., SENDEREK, J., RIVOLTA, C. & CHRAST, R. 2013. PLEKHG5 deficiency leads to an intermediate form of autosomal-recessive Charcot-Marie-Tooth disease. *Hum Mol Genet,* 22**,** 4224-32.

BAEUERLE, P. A. & BALTIMORE, D. 1996. NF-kappa B: ten years after. *Cell,* 87**,** 13-20.

BEG, A. A., SHA, W. C., BRONSON, R. T., GHOSH, S. & BALTIMORE, D. 1995. Embryonic lethality and liver degeneration in mice lacking the RelA component of NF-kappa B. *Nature,* 376**,** 167-70.

BEN-NERIAH, Y. 2002. Regulatory functions of ubiquitination in the immune system. *Nat Immunol,* 3**,** 20-6.

BEN-NERIAH, Y. & KARIN, M. 2011. Inflammation meets cancer, with NF-kappaB as the matchmaker. *Nat Immunol,* 12**,** 715-23.

BETHEA, J. R., CASTRO, M., KEANE, R. W., LEE, T. T., DIETRICH, W. D. & YEZIERSKI, R. P. 1998. Traumatic spinal cord injury induces nuclear factor-kappaB activation. *J Neurosci,* 18**,** 3251-60.

BINOTTI, B., PAVLOS, N. J., RIEDEL, D., WENZEL, D., VORBRUGGEN, G., SCHALK, A. M., KUHNEL, K., BOYKEN, J., ERCK, C., MARTENS, H., CHUA, J. J. & JAHN, R. 2015. The GTPase Rab26 links synaptic vesicles to the autophagy pathway. *Elife,* 4**,** e05597.

BONETTI, B., STEGAGNO, C., CANNELLA, B., RIZZUTO, N., MORETTO,

G. & RAINE, C. S. 1999. Activation of NF-kappaB and c-jun transcription factors in multiple sclerosis lesions. Implications for oligodendrocyte pathology. *Am J Pathol,* 155**,** 1433-8.

BOYA, P., REGGIORI, F. & CODOGNO, P. 2013. Emerging regulation and functions of autophagy. *Nat Cell Biol,* 15**,** 713-20.

BURKITT, M. D., HANEDI, A. F., DUCKWORTH, C. A., WILLIAMS, J. M., TANG, J. M., O'REILLY, L. A., PUTOCZKI, T. L., GERONDAKIS, S., DIMALINE, R., CAAMANO, J. H. & PRITCHARD, D. M. 2015. NF-kappaB1, NF-kappaB2 and c-Rel differentially regulate susceptibility to colitis-associated adenoma development in C57BL/6 mice. *J Pathol,* 236**,** 326-36.

CARONI, P., DONATO, F. & MULLER, D. 2012. Structural plasticity upon learning: regulation and functions. *Nat Rev Neurosci,* 13**,** 478-90.

CASTILLO, K., NASSIF, M., VALENZUELA, V., ROJAS, F., MATUS, S., MERCADO, G., COURT, F. A., VAN ZUNDERT, B. & HETZ, C. 2013. Trehalose delays the progression of amyotrophic lateral sclerosis by enhancing autophagy in motoneurons. *Autophagy,* 9**,** 1308-20.

CHEN, Z. L., YU, W. M. & STRICKLAND, S. 2007. Peripheral regeneration. *Annu Rev Neurosci,* 30**,** 209-33.

CHO, Y., CHALLA, S., MOQUIN, D., GENGA, R., RAY, T. D., GUILDFORD, M. & CHAN, F. K.-M. 2009. Phosphorylation-Driven Assembly of the RIP1-RIP3 Complex Regulates Programmed Necrosis and Virus-Induced Inflammation. *Cell,* 137**,** 1112-1123.

CHUNG, K. W., HYUN, Y. S., LEE, H. J., JUNG, H. K., KOO, H., YOO, J. H., KIM, S. B., PARK, C. I., KIM, H. N. & CHOI, B. O. 2011. Two recessive intermediate Charcot-Marie-Tooth patients with GDAP1 mutations. *J Peripher Nerv Syst,* 16**,** 143-6.

CHUNG, W. S. & BARRES, B. A. 2012. The role of glial cells in synapse elimination. *Curr Opin Neurobiol,* 22**,** 438-45.

CLAUDIO, E., BROWN, K., PARK, S., WANG, H. & SIEBENLIST, U. 2002. BAFF-induced NEMO-independent processing of NF-kappa B2 in maturing B cells. *Nat Immunol,* 3**,** 958-65.

COGSWELL, P. C., GUTTRIDGE, D. C., FUNKHOUSER, W. K. & BALDWIN, A. S., JR. 2000. Selective activation of NF-kappa B subunits in human breast cancer: potential roles for NF-kappa B2/p52 and for Bcl-3. *Oncogene,* 19**,** 1123-31.

CONFORTI, L., GILLEY, J. & COLEMAN, M. P. 2014. Wallerian degeneration: an emerging axon death pathway linking injury and disease. *Nat Rev Neurosci,* 15**,** 394-409.

COOPE, H. J., ATKINSON, P. G., HUHSE, B., BELICH, M., JANZEN, J., HOLMAN, M. J., KLAUS, G. G., JOHNSTON, L. H. & LEY, S. C. 2002. CD40 regulates the processing of NF-kappaB2 p100 to p52. *EMBO J,* 21**,** 5375-85.

DACHSEL, J. C., NGOK, S. P., LEWIS-TUFFIN, L. J., KOURTIDIS, A., GEYER, R., JOHNSTON, L., FEATHERS, R. & ANASTASIADIS, P. Z. 2013. The Rho guanine nucleotide exchange factor Syx regulates the balance of dia and ROCK activities to promote polarized-cancer-cell migration. *Mol Cell Biol,* 33**,** 4909-18.

DEGENHARDT, K., MATHEW, R., BEAUDOIN, B., BRAY, K., ANDERSON, D., CHEN, G., MUKHERJEE, C., SHI, Y., GELINAS, C., FAN, Y., NELSON, D. A., JIN, S. & WHITE, E. 2006. Autophagy promotes tumor cell survival and restricts necrosis, inflammation, and tumorigenesis. *Cancer Cell,* 10**,** 51-64.

DEJARDIN, E., DROIN, N. M., DELHASE, M., HAAS, E., CAO, Y., MAKRIS, C., LI, Z. W., KARIN, M., WARE, C. F. & GREEN, D. R. 2002. The lymphotoxin-beta receptor induces different patterns of gene expression via two NF-kappaB pathways. *Immunity,* 17**,** 525-35.

DONDELINGER, Y., AGUILETA, M. A., GOOSSENS, V., DUBUISSON, C., GROOTJANS, S., DEJARDIN, E., VANDENABEELE, P. & BERTRAND, M. J. 2013. RIPK3 contributes to TNFR1-mediated RIPK1 kinase-dependent apoptosis in conditions of cIAP1/2 depletion or TAK1 kinase inhibition. *Cell Death Differ,* 20**,** 1381-92.

DONDELINGER, Y., JOUAN-LANHOUET, S., DIVERT, T., THEATRE, E., BERTIN, J., GOUGH, P. J., GIANSANTI, P., HECK, A. J., DEJARDIN, E., VANDENABEELE, P. & BERTRAND, M. J. 2015. NF-kappaB-Independent Role of IKKalpha/IKKbeta in Preventing RIPK1 Kinase-Dependent Apoptotic and Necroptotic Cell Death during TNF Signaling. *Mol Cell,* 60**,** 63-76.

DOTY, K. R., GUILLOT-SESTIER, M. V. & TOWN, T. 2015. The role of the immune system in neurodegenerative disorders: Adaptive or maladaptive? *Brain Res,* 1617**,** 155-73.

ERMOLAEVA, M. A., MICHALLET, M. C., PAPADOPOULOU, N., UTERMOHLEN, O., KRANIDIOTI, K., KOLLIAS, G., TSCHOPP, J. & PASPARAKIS, M. 2008. Function of TRADD in tumor necrosis factor receptor 1 signaling and in TRIF-dependent inflammatory responses. *Nat Immunol,* 9**,** 1037-46.

FABRIZI, G. M., TAIOLI, F., CAVALLARO, T., RIGATELLI, F., SIMONATI, A., MARIANI, G., PERRONE, P. & RIZZUTO, N. 2000. Focally folded myelin in Charcot-Marie-Tooth neuropathy type 1B with Ser49Leu in the myelin protein zero. *Acta Neuropathol,* 100**,** 299-304.

FERRAJOLI, A., KEATING, M. J., MANSHOURI, T., GILES, F. J., DEY, A., ESTROV, Z., KOLLER, C. A., KURZROCK, R., THOMAS, D. A., FADERL, S., LERNER, S., O'BRIEN, S. & ALBITAR, M. 2002. The clinical significance of tumor necrosis factor-alpha plasma level in patients having chronic lymphocytic leukemia. *Blood,* 100**,** 1215-9.

FRIDMACHER, V., KALTSCHMIDT, B., GOUDEAU, B., NDIAYE, D., ROSSI,

F. M., PFEIFFER, J., KALTSCHMIDT, C., ISRAEL, A. & MEMET, S. 2003. Forebrain-specific neuronal inhibition of nuclear factor-kappaB activity leads to loss of neuroprotection. *J Neurosci,* 23**,** 9403-8.

GARCIA, M. G., ALANIZ, L., LOPES, E. C., BLANCO, G., HAJOS, S. E. & ALVAREZ, E. 2005. Inhibition of NF-kappaB activity by BAY 11-7082 increases apoptosis in multidrug resistant leukemic T-cell lines. *Leuk Res,* 29**,** 1425-34.

GARNAAS, M. K., MOODIE, K. L., LIU, M. L., SAMANT, G. V., LI, K., MARX, R., BARABAN, J. M., HOROWITZ, A. & RAMCHANDRAN, R. 2008. Syx, a RhoA guanine exchange factor, is essential for angiogenesis in Vivo. *Circ Res,* 103**,** 710-6.

GENG, J. & KLIONSKY, D. J. 2008. The Atg8 and Atg12 ubiquitin-like conjugation systems in macroautophagy. 'Protein modifications: beyond the usual suspects' review series. *EMBO Rep,* 9**,** 859-64.

GHOSH, A., ROY, A., LIU, X., KORDOWER, J. H., MUFSON, E. J., HARTLEY, D. M., GHOSH, S., MOSLEY, R. L., GENDELMAN, H. E. & PAHAN, K. 2007. Selective inhibition of NF-kappaB activation prevents dopaminergic neuronal loss in a mouse model of Parkinson's disease. *Proc Natl Acad Sci U S A,* 104**,** 18754-9.

GILMORE, T. D. & GERONDAKIS, S. 2011. The c-Rel Transcription Factor in Development and Disease. *Genes Cancer,* 2**,** 695-711.

GOMEZ-SANCHEZ, J. A., CARTY, L., IRUARRIZAGA-LEJARRETA, M., PALOMO-IRIGOYEN, M., VARELA-REY, M., GRIFFITH, M., HANTKE, J., MACIAS-CAMARA, N., AZKARGORTA, M., AURREKOETXEA, I., DE JUAN, V. G., JEFFERIES, H. B., ASPICHUETA, P., ELORTZA, F., ARANSAY, A. M., MARTINEZ-CHANTAR, M. L., BAAS, F., MATO, J. M., MIRSKY, R., WOODHOO, A. & JESSEN, K. R. 2015. Schwann cell autophagy, myelinophagy, initiates myelin clearance from injured nerves. *J Cell Biol,* 210**,** 153-68.

GRETEN, F. R., ARKAN, M. C., BOLLRATH, J., HSU, L. C., GOODE, J., MIETHING, C., GOKTUNA, S. I., NEUENHAHN, M., FIERER, J., PAXIAN, S., VAN ROOIJEN, N., XU, Y., O'CAIN, T., JAFFEE, B. B., BUSCH, D. H., DUYSTER, J., SCHMID, R. M., ECKMANN, L. & KARIN, M. 2007. NF-kappaB is a negative regulator of IL-1beta secretion as revealed by genetic and pharmacological inhibition of IKKbeta. *Cell,* 130**,** 918-31.

GRINBERG-BLEYER, Y., OH, H., DESRICHARD, A., BHATT, D. M., CARON, R., CHAN, T. A., SCHMID, R. M., KLEIN, U., HAYDEN, M. S. & GHOSH, S. 2017. NF-kappaB c-Rel Is Crucial for the Regulatory T Cell Immune Checkpoint in Cancer. *Cell,* 170**,** 1096-1108 e13.

GUPTA, P. B., CHAFFER, C. L. & WEINBERG, R. A. 2009. Cancer stem cells: mirage or reality? *Nat Med,* 15**,** 1010-2.

HAAS, T. L., EMMERICH, C. H., GERLACH, B., SCHMUKLE, A. C.,

CORDIER, S. M., RIESER, E., FELTHAM, R., VINCE, J., WARNKEN, U., WENGER, T., KOSCHNY, R., KOMANDER, D., SILKE, J. & WALCZAK, H. 2009. Recruitment of the linear ubiquitin chain assembly complex stabilizes the TNF-R1 signaling complex and is required for TNF-mediated gene induction. *Mol Cell,* 36**,** 831-44.

HANAHAN, D. & WEINBERG, R. A. 2011. Hallmarks of cancer: the next generation. *Cell,* 144**,** 646-74.

HARA, T., NAKAMURA, K., MATSUI, M., YAMAMOTO, A., NAKAHARA, Y., SUZUKI-MIGISHIMA, R., YOKOYAMA, M., MISHIMA, K., SAITO, I., OKANO, H. & MIZUSHIMA, N. 2006. Suppression of basal autophagy in neural cells causes neurodegenerative disease in mice. *Nature,* 441**,** 885-9.

HARDIMAN, O., AL-CHALABI, A., CHIO, A., CORR, E. M., LOGROSCINO, G., ROBBERECHT, W., SHAW, P. J., SIMMONS, Z. & VAN DEN BERG, L. H. 2017. Amyotrophic lateral sclerosis. *Nature Reviews Disease Primers,* 3**,** 17071.

HARDING, T. M., MORANO, K. A., SCOTT, S. V. & KLIONSKY, D. J. 1995. Isolation and characterization of yeast mutants in the cytoplasm to vacuole protein targeting pathway. *J Cell Biol,* 131**,** 591-602.

HARRIS, H. & RUBINSZTEIN, D. C. 2011. Control of autophagy as a therapy for neurodegenerative disease. *Nat Rev Neurol,* 8**,** 108-17.

HAYDEN, M. S. & GHOSH, S. 2008. Shared principles in NF-kappaB signaling. *Cell,* 132**,** 344-62.

HAYDEN, M. S. & GHOSH, S. 2012. NF-kappaB, the first quarter-century: remarkable progress and outstanding questions. *Genes Dev,* 26**,** 203-34.

HAYDEN, M. S. & GHOSH, S. 2014. Regulation of NF-kappaB by TNF family cytokines. *Semin Immunol,* 26**,** 253-66.

HE, S., WANG, L., MIAO, L., WANG, T., DU, F., ZHAO, L. & WANG, X. 2009. Receptor Interacting Protein Kinase-3 Determines Cellular Necrotic Response to TNF-α. *Cell,* 137**,** 1100-1111.

HENEKA, M. T., CARSON, M. J., EL KHOURY, J., LANDRETH, G. E., BROSSERON, F., FEINSTEIN, D. L., JACOBS, A. H., WYSS-CORAY, T., VITORICA, J., RANSOHOFF, R. M., HERRUP, K., FRAUTSCHY, S. A., FINSEN, B., BROWN, G. C., VERKHRATSKY, A., YAMANAKA, K., KOISTINAHO, J., LATZ, E., HALLE, A., PETZOLD, G. C., TOWN, T., MORGAN, D., SHINOHARA, M. L., PERRY, V. H., HOLMES, C., BAZAN, N. G., BROOKS, D. J., HUNOT, S., JOSEPH, B., DEIGENDESCH, N., GARASCHUK, O., BODDEKE, E., DINARELLO, C. A., BREITNER, J. C., COLE, G. M., GOLENBOCK, D. T. & KUMMER, M. P. 2015. Neuroinflammation in Alzheimer's disease. *Lancet Neurol,* 14**,** 388-405.

HIPPERT, M. M., O'TOOLE, P. S. & THORBURN, A. 2006. Autophagy in

cancer: good, bad, or both? *Cancer Res,* 66**,** 9349-51.

HU, Y., BAUD, V., DELHASE, M., ZHANG, P., DEERINCK, T., ELLISMAN, M., JOHNSON, R. & KARIN, M. 1999. Abnormal morphogenesis but intact IKK activation in mice lacking the IKKalpha subunit of IkappaB kinase. *Science,* 284**,** 316-20.

HUNOT, S., BRUGG, B., RICARD, D., MICHEL, P. P., MURIEL, M. P., RUBERG, M., FAUCHEUX, B. A., AGID, Y. & HIRSCH, E. C. 1997. Nuclear translocation of NF-kappaB is increased in dopaminergic neurons of patients with parkinson disease. *Proc Natl Acad Sci U S A,* 94**,** 7531-6.

HUNTER, J. E., LESLIE, J. & PERKINS, N. D. 2016. c-Rel and its many roles in cancer: an old story with new twists. *Br J Cancer,* 114**,** 1-6.

HUO, Y., CAI, H., TEPLOVA, I., BOWMAN-COLIN, C., CHEN, G., PRICE, S., BARNARD, N., GANESAN, S., KARANTZA, V., WHITE, E. & XIA, B. 2013. Autophagy opposes p53-mediated tumor barrier to facilitate tumorigenesis in a model of PALB2-associated hereditary breast cancer. *Cancer Discov,* 3**,** 894-907.

IMIELSKI, Y., SCHWAMBORN, J. C., LUNINGSCHROR, P., HEIMANN, P., HOLZBERG, M., WERNER, H., LESKE, O., PUSCHEL, A. W., MEMET, S., HEUMANN, R., ISRAEL, A., KALTSCHMIDT, C. & KALTSCHMIDT, B. 2012. Regrowing the adult brain: NF-kappaB controls functional circuit formation and tissue homeostasis in the dentate gyrus. *PLoS One,* 7**,** e30838.

IP, C. W., KRONER, A., BENDSZUS, M., LEDER, C., KOBSAR, I., FISCHER, S., WIENDL, H., NAVE, K. A. & MARTINI, R. 2006. Immune cells contribute to myelin degeneration and axonopathic changes in mice overexpressing proteolipid protein in oligodendrocytes. *J Neurosci,* 26**,** 8206-16.

JESSEN, K. R. & MIRSKY, R. 2016. The repair Schwann cell and its function in regenerating nerves. *J Physiol,* 594**,** 3521-31.

JIANG, T., YU, J. T., ZHU, X. C., TAN, M. S., WANG, H. F., CAO, L., ZHANG, Q. Q., SHI, J. Q., GAO, L., QIN, H., ZHANG, Y. D. & TAN, L. 2014. Temsirolimus promotes autophagic clearance of amyloid-beta and provides protective effects in cellular and animal models of Alzheimer's disease. *Pharmacol Res,* 81**,** 54-63.

JUNG, C. H., RO, S. H., CAO, J., OTTO, N. M. & KIM, D. H. 2010. mTOR regulation of autophagy. *FEBS Lett,* 584**,** 1287-95.

KALTSCHMIDT, B. & KALTSCHMIDT, C. 2009. NF-kappaB in the nervous system. *Cold Spring Harb Perspect Biol,* 1**,** a001271.

KALTSCHMIDT, B. & KALTSCHMIDT, C. 2015. NF-KappaB in Long-Term Memory and Structural Plasticity in the Adult Mammalian Brain. *Front Mol Neurosci,* 8**,** 69.

KALTSCHMIDT, B., KALTSCHMIDT, C., HEHNER, S. P., DROGE, W. &

SCHMITZ, M. L. 1999a. Repression of NF-kappaB impairs HeLa cell proliferation by functional interference with cell cycle checkpoint regulators. *Oncogene,* 18**,** 3213-25.

KALTSCHMIDT, B., UHEREK, M., WELLMANN, H., VOLK, B. & KALTSCHMIDT, C. 1999b. Inhibition of NF-kappaB potentiates amyloid beta-mediated neuronal apoptosis. *Proc Natl Acad Sci U S A,* 96**,** 9409-14.

KALTSCHMIDT, C., KALTSCHMIDT, B. & BAEUERLE, P. A. 1993. Brain synapses contain inducible forms of the transcription factor NF-kappa B. *Mech Dev,* 43**,** 135-47.

KALTSCHMIDT, C., KALTSCHMIDT, B., LANNES-VIEIRA, J., KREUTZBERG, G. W., WEKERLE, H., BAEUERLE, P. A. & GEHRMANN, J. 1994a. Transcription factor NF-kappa B is activated in microglia during experimental autoimmune encephalomyelitis. *J Neuroimmunol,* 55**,** 99-106.

KALTSCHMIDT, C., KALTSCHMIDT, B., NEUMANN, H., WEKERLE, H. & BAEUERLE, P. A. 1994b. Constitutive NF-kappa B activity in neurons. *Mol Cell Biol,* 14**,** 3981-92.

KATZMANN, D. J., ODORIZZI, G. & EMR, S. D. 2002. Receptor downregulation and multivesicular-body sorting. *Nat Rev Mol Cell Biol,* 3**,** 893-905.

KEIFER, J. A., GUTTRIDGE, D. C., ASHBURNER, B. P. & BALDWIN, A. S., JR. 2001. Inhibition of NF-kappa B activity by thalidomide through suppression of IkappaB kinase activity. *J Biol Chem,* 276**,** 22382-7.

KELLER, M. P. & CHANCE, P. F. 1999. Inherited neuropathies: from gene to disease. *Brain Pathol,* 9**,** 327-41.

KENIFIC, C. M., THORBURN, A. & DEBNATH, J. 2010. Autophagy and metastasis: another double-edged sword. *Curr Opin Cell Biol,* 22**,** 241-5.

KIEL, J. A. 2010. Autophagy in unicellular eukaryotes. *Philos Trans R Soc Lond B Biol Sci,* 365**,** 819-30.

KIM, H. J., HONG, Y. B., PARK, J. M., CHOI, Y. R., KIM, Y. J., YOON, B. R., KOO, H., YOO, J. H., KIM, S. B., PARK, M., CHUNG, K. W. & CHOI, B. O. 2013. Mutations in the PLEKHG5 gene is relevant with autosomal recessive intermediate Charcot-Marie-Tooth disease. *Orphanet J Rare Dis,* 8**,** 104.

KIMMELMAN, A. C. 2011. The dynamic nature of autophagy in cancer. *Genes Dev,* 25**,** 1999-2010.

KLIONSKY, D. J., ABDELMOHSEN, K., ABE, A., ABEDIN, M. J., ABELIOVICH, H., ACEVEDO AROZENA, A., ADACHI, H., ADAMS, C. M., ADAMS, P. D., ADELI, K., ADHIHETTY, P. J., ADLER, S. G., AGAM, G., AGARWAL, R., AGHI, M. K., AGNELLO, M., AGOSTINIS, P., AGUILAR, P. V., AGUIRRE-GHISO, J., AIROLDI, E. M., AIT-SI-

ALI, S., AKEMATSU, T., AKPORIAYE, E. T., AL-RUBEAI, M., ALBAICETA, G. M., ALBANESE, C., ALBANI, D., ALBERT, M. L., ALDUDO, J., ALGUL, H., ALIREZAEI, M., ALLOZA, I., ALMASAN, A., ALMONTE-BECERIL, M., ALNEMRI, E. S., ALONSO, C., ALTAN-BONNET, N., ALTIERI, D. C., ALVAREZ, S., ALVAREZ-ERVITI, L., ALVES, S., AMADORO, G., AMANO, A., AMANTINI, C., AMBROSIO, S., AMELIO, I., AMER, A. O., AMESSOU, M., AMON, A., AN, Z., ANANIA, F. A., ANDERSEN, S. U., ANDLEY, U. P., ANDREADI, C. K., ANDRIEU-ABADIE, N., ANEL, A., ANN, D. K., ANOOPKUMAR-DUKIE, S., ANTONIOLI, M., AOKI, H., APOSTOLOVA, N., AQUILA, S., AQUILANO, K., ARAKI, K., ARAMA, E., ARANDA, A., ARAYA, J., ARCARO, A., ARIAS, E., ARIMOTO, H., ARIOSA, A. R., ARMSTRONG, J. L., ARNOULD, T., ARSOV, I., ASANUMA, K., ASKANAS, V., ASSELIN, E., ATARASHI, R., ATHERTON, S. S., ATKIN, J. D., ATTARDI, L. D., AUBERGER, P., AUBURGER, G., AURELIAN, L., AUTELLI, R., AVAGLIANO, L., AVANTAGGIATI, M. L., AVRAHAMI, L., AWALE, S., AZAD, N., BACHETTI, T., BACKER, J. M., BAE, D. H., BAE, J. S., BAE, O. N., BAE, S. H., BAEHRECKE, E. H., BAEK, S. H., BAGHDIGUIAN, S., BAGNIEWSKA-ZADWORNA, A., et al. 2016. Guidelines for the use and interpretation of assays for monitoring autophagy (3rd edition). *Autophagy,* 12**,** 1-222.

KNIZHNIK, A. V., ROOS, W. P., NIKOLOVA, T., QUIROS, S., TOMASZOWSKI, K. H., CHRISTMANN, M. & KAINA, B. 2013. Survival and death strategies in glioma cells: autophagy, senescence and apoptosis triggered by a single type of temozolomide-induced DNA damage. *PLoS One,* 8**,** e55665.

KOMATSU, M., WAGURI, S., CHIBA, T., MURATA, S., IWATA, J., TANIDA, I., UENO, T., KOIKE, M., UCHIYAMA, Y., KOMINAMI, E. & TANAKA, K. 2006. Loss of autophagy in the central nervous system causes neurodegeneration in mice. *Nature,* 441**,** 880-4.

KONDYLIS, V., KUMARI, S., VLANTIS, K. & PASPARAKIS, M. 2017. The interplay of IKK, NF-kappaB and RIPK1 signaling in the regulation of cell death, tissue homeostasis and inflammation. *Immunol Rev,* 277**,** 113-127.

KOO, J. W., RUSSO, S. J., FERGUSON, D., NESTLER, E. J. & DUMAN, R. S. 2010. Nuclear factor-kappaB is a critical mediator of stress-impaired neurogenesis and depressive behavior. *Proc Natl Acad Sci U S A,* 107**,** 2669-74.

KOSHY, M., VILLANO, J. L., DOLECEK, T. A., HOWARD, A., MAHMOOD, U., CHMURA, S. J., WEICHSELBAUM, R. R. & MCCARTHY, B. J. 2012. Improved survival time trends for glioblastoma using the SEER 17 population-based registries. *J Neurooncol,* 107**,** 207-12.

LADDHA, S. V., GANESAN, S., CHAN, C. S. & WHITE, E. 2014. Mutational

landscape of the essential autophagy gene BECN1 in human cancers. *Mol Cancer Res,* 12**,** 485-90.

LAWRENCE, M. S., STOJANOV, P., MERMEL, C. H., ROBINSON, J. T., GARRAWAY, L. A., GOLUB, T. R., MEYERSON, M., GABRIEL, S. B., LANDER, E. S. & GETZ, G. 2014. Discovery and saturation analysis of cancer genes across 21 tumour types. *Nature,* 505**,** 495-501.

LEGARDA-ADDISON, D., HASE, H., O'DONNELL, M. A. & TING, A. T. 2009. NEMO/IKKgamma regulates an early NF-kappaB-independent cell-death checkpoint during TNF signaling. *Cell Death Differ,* 16**,** 1279-88.

LEI, Y., ZHANG, D., YU, J., DONG, H., ZHANG, J. & YANG, S. 2017. Targeting autophagy in cancer stem cells as an anticancer therapy. *Cancer Lett,* 393**,** 33-39.

LEVINE, B., MIZUSHIMA, N. & VIRGIN, H. W. 2011. Autophagy in immunity and inflammation. *Nature,* 469**,** 323-35.

LEVY, J. M. & THORBURN, A. 2011. Targeting autophagy during cancer therapy to improve clinical outcomes. *Pharmacol Ther,* 131**,** 130-41.

LEVY, J. M. M., TOWERS, C. G. & THORBURN, A. 2017. Targeting autophagy in cancer. *Nat Rev Cancer,* 17**,** 528-542.

LI, Q., VAN ANTWERP, D., MERCURIO, F., LEE, K. F. & VERMA, I. M. 1999. Severe liver degeneration in mice lacking the IkappaB kinase 2 gene. *Science,* 284**,** 321-5.

LI, Q., WITHOFF, S. & VERMA, I. M. 2005. Inflammation-associated cancer: NF-kappaB is the lynchpin. *Trends Immunol,* 26**,** 318-25.

LIANG, X. H., JACKSON, S., SEAMAN, M., BROWN, K., KEMPKES, B., HIBSHOOSH, H. & LEVINE, B. 1999. Induction of autophagy and inhibition of tumorigenesis by beclin 1. *Nature,* 402**,** 672-6.

LIU, M. & HOROWITZ, A. 2006. A PDZ-binding motif as a critical determinant of Rho guanine exchange factor function and cell phenotype. *Mol Biol Cell,* 17**,** 1880-7.

LONG-SMITH, C. M., SULLIVAN, A. M. & NOLAN, Y. M. 2009. The influence of microglia on the pathogenesis of Parkinson's disease. *Prog Neurobiol,* 89**,** 277-87.

LUCAS, R., MONTESANO, R., PEPPER, M. S., HAFNER, M., SABLON, E., DUNANT, Y., GRAU, G. E., DE BAETSELIER, P., MANNEL, D. & FRANSEN, L. 2001. Lectin-deficient TNF mutants display comparable anti-tumour but reduced pro-metastatic potential as compared to the wild-type molecule. *Int J Cancer,* 91**,** 543-9.

LÜNINGSCHRÖR, P., BINOTTI, B., DOMBERT, B., HEIMANN, P., PEREZ-LARA, A., SLOTTA, C., THAU-HABERMANN, N., C, R. V. C., KARL, F., DAMME, M., HOROWITZ, A., MAYSTADT, I., FUCHTBAUER, A., FUCHTBAUER, E. M., JABLONKA, S., BLUM, R., UCEYLER, N., PETRI, S., KALTSCHMIDT, B., JAHN, R., KALTSCHMIDT, C. &

SENDTNER, M. 2017. Plekhg5-regulated autophagy of synaptic vesicles reveals a pathogenic mechanism in motoneuron disease. *Nat Commun,* 8**,** 678.

LYNCH-DAY, M. A., MAO, K., WANG, K., ZHAO, M. & KLIONSKY, D. J. 2012. The role of autophagy in Parkinson's disease. *Cold Spring Harb Perspect Med,* 2**,** a009357.

MARCORA, E. & KENNEDY, M. B. 2010. The Huntington's disease mutation impairs Huntingtin's role in the transport of NF-kappaB from the synapse to the nucleus. *Hum Mol Genet,* 19**,** 4373-84.

MARX, R., HENDERSON, J., WANG, J. & BARABAN, J. M. 2005. Tech: a RhoA GEF selectively expressed in hippocampal and cortical neurons. *J Neurochem,* 92**,** 850-8.

MATSUDA, A., SUZUKI, Y., HONDA, G., MURAMATSU, S., MATSUZAKI, O., NAGANO, Y., DOI, T., SHIMOTOHNO, K., HARADA, T., NISHIDA, E., HAYASHI, H. & SUGANO, S. 2003. Large-scale identification and characterization of human genes that activate NF-kappaB and MAPK signaling pathways. *Oncogene,* 22**,** 3307-18.

MAYSTADT, I., REZSOHAZY, R., BARKATS, M., DUQUE, S., VANNUFFEL, P., REMACLE, S., LAMBERT, B., NAJIMI, M., SOKAL, E., MUNNICH, A., VIOLLET, L. & VERELLEN-DUMOULIN, C. 2007. The nuclear factor kappaB-activator gene PLEKHG5 is mutated in a form of autosomal recessive lower motor neuron disease with childhood onset. *Am J Hum Genet,* 81**,** 67-76.

MEBERG, P. J., KINNEY, W. R., VALCOURT, E. G. & ROUTTENBERG, A. 1996. Gene expression of the transcription factor NF-kappa B in hippocampus: regulation by synaptic activity. *Brain Res Mol Brain Res,* 38**,** 179-90.

MEFFERT, M. K., CHANG, J. M., WILTGEN, B. J., FANSELOW, M. S. & BALTIMORE, D. 2003. NF-kappa B functions in synaptic signaling and behavior. *Nat Neurosci,* 6**,** 1072-8.

MENZIES, F. M., FLEMING, A. & RUBINSZTEIN, D. C. 2015. Compromised autophagy and neurodegenerative diseases. *Nat Rev Neurosci,* 16**,** 345-57.

MEYLAN, E., DOOLEY, A. L., FELDSER, D. M., SHEN, L., TURK, E., OUYANG, C. & JACKS, T. 2009. Requirement for NF-kappaB signalling in a mouse model of lung adenocarcinoma. *Nature,* 462**,** 104-7.

MICHEAU, O., LENS, S., GAIDE, O., ALEVIZOPOULOS, K. & TSCHOPP, J. 2001. NF-kappaB signals induce the expression of c-FLIP. *Mol Cell Biol,* 21**,** 5299-305.

MICHEAU, O. & TSCHOPP, J. 2003. Induction of TNF receptor I-mediated apoptosis via two sequential signaling complexes. *Cell,* 114**,** 181-90.

MIKENBERG, I., WIDERA, D., KAUS, A., KALTSCHMIDT, B. &

KALTSCHMIDT, C. 2007. Transcription factor NF-kappaB is transported to the nucleus via cytoplasmic dynein/dynactin motor complex in hippocampal neurons. *PLoS One,* 2**,** e589.

MITSIADES, N., MITSIADES, C. S., POULAKI, V., CHAUHAN, D., RICHARDSON, P. G., HIDESHIMA, T., MUNSHI, N. C., TREON, S. P. & ANDERSON, K. C. 2002. Apoptotic signaling induced by immunomodulatory thalidomide analogs in human multiple myeloma cells: therapeutic implications. *Blood,* 99**,** 4525-30.

MOGI, M., KONDO, T., MIZUNO, Y. & NAGATSU, T. 2007. p53 protein, interferon-gamma, and NF-kappaB levels are elevated in the parkinsonian brain. *Neurosci Lett,* 414**,** 94-7.

MOTORI, E., PUYAL, J., TONI, N., GHANEM, A., ANGELONI, C., MALAGUTI, M., CANTELLI-FORTI, G., BERNINGER, B., CONZELMANN, K. K., GOTZ, M., WINKLHOFER, K. F., HRELIA, S. & BERGAMI, M. 2013. Inflammation-induced alteration of astrocyte mitochondrial dynamics requires autophagy for mitochondrial network maintenance. *Cell Metab,* 18**,** 844-59.

MULLIGAN, G., MITSIADES, C., BRYANT, B., ZHAN, F., CHNG, W. J., ROELS, S., KOENIG, E., FERGUS, A., HUANG, Y., RICHARDSON, P., TREPICCHIO, W. L., BROYL, A., SONNEVELD, P., SHAUGHNESSY, J. D., JR., BERGSAGEL, P. L., SCHENKEIN, D., ESSELTINE, D. L., BORAL, A. & ANDERSON, K. C. 2007. Gene expression profiling and correlation with outcome in clinical trials of the proteasome inhibitor bortezomib. *Blood,* 109**,** 3177-88.

NA, C. H., JONES, D. R., YANG, Y., WANG, X., XU, Y. & PENG, J. 2012. Synaptic protein ubiquitination in rat brain revealed by antibody-based ubiquitome analysis. *J Proteome Res,* 11**,** 4722-32.

NAVE, K. A. & WERNER, H. B. 2014. Myelination of the nervous system: mechanisms and functions. *Annu Rev Cell Dev Biol,* 30**,** 503-33.

NELIS, E., TIMMERMAN, V., DE JONGHE, P., VAN BROECKHOVEN, C. & RAUTENSTRAUSS, B. 1999. Molecular genetics and biology of inherited peripheral neuropathies: a fast-moving field. *Neurogenetics,* 2**,** 137-48.

O'DONNELL, M. A., LEGARDA-ADDISON, D., SKOUNTZOS, P., YEH, W. C. & TING, A. T. 2007. Ubiquitination of RIP1 regulates an NF-kappaB-independent cell-death switch in TNF signaling. *Curr Biol,* 17**,** 418-24.

O'DONNELL, M. A. & TING, A. T. 2011. RIP1 comes back to life as a cell death regulator in TNFR1 signaling. *FEBS J,* 278**,** 877-87.

OFENGEIM, D. & YUAN, J. 2013. Regulation of RIP1 kinase signalling at the crossroads of inflammation and cell death. *Nature Reviews Molecular Cell Biology,* 14**,** 727.

OZOGUZ, A., UYAN, O., BIRDAL, G., ISKENDER, C., KARTAL, E., LAHUT,

S., OMUR, O., AGIM, Z. S., EKEN, A. G., SEN, N. E., KAVAK, P., SAYGI, C., SAPP, P. C., KEAGLE, P., PARMAN, Y., TAN, E., KOC, F., DEYMEER, F., OFLAZER, P., HANAGASI, H., GURVIT, H., BILGIC, B., DURMUS, H., ERTAS, M., KOTAN, D., AKALIN, M. A., GULLUOGLU, H., ZARIFOGLU, M., AYSAL, F., DOSOGLU, N., BILGUVAR, K., GUNEL, M., KESKIN, O., AKGUN, T., OZCELIK, H., LANDERS, J. E., BROWN, R. H. & BASAK, A. N. 2015. The distinct genetic pattern of ALS in Turkey and novel mutations. *Neurobiol Aging,* 36**,** 1764 e9-1764 e18.

PANAYOTOVA-DIMITROVA, D., FEOKTISTOVA, M., PLOESSER, M., KELLERT, B., HUPE, M., HORN, S., MAKAROV, R., JENSEN, F., PORUBSKY, S., SCHMIEDER, A., ZENCLUSSEN, A. C., MARX, A., KERSTAN, A., GESERICK, P., HE, Y. W. & LEVERKUS, M. 2013. cFLIP regulates skin homeostasis and protects against TNF-induced keratinocyte apoptosis. *Cell Rep,* 5**,** 397-408.

PANNICKE, U., BAUMANN, B., FUCHS, S., HENNEKE, P., RENSING-EHL, A., RIZZI, M., JANDA, A., HESE, K., SCHLESIER, M., HOLZMANN, K., BORTE, S., LAUX, C., RUMP, E. M., ROSENBERG, A., ZELINSKI, T., SCHREZENMEIER, H., WIRTH, T., EHL, S., SCHROEDER, M. L. & SCHWARZ, K. 2013. Deficiency of innate and acquired immunity caused by an IKBKB mutation. *N Engl J Med,* 369**,** 2504-14.

PELTZER, N., DARDING, M. & WALCZAK, H. 2016. Holding RIPK1 on the Ubiquitin Leash in TNFR1 Signaling. *Trends Cell Biol,* 26**,** 445-61.

PENDER, M. P. & GREER, J. M. 2007. Immunology of multiple sclerosis. *Curr Allergy Asthma Rep,* 7**,** 285-92.

PERKINS, N. D. 2007. Integrating cell-signalling pathways with NF-kappaB and IKK function. *Nat Rev Mol Cell Biol,* 8**,** 49-62.

PEYRIN-BIROULET, L. 2010. Anti-TNF therapy in inflammatory bowel diseases: a huge review. *Minerva Gastroenterol Dietol,* 56**,** 233-43.

PHILIPS, T. & ROBBERECHT, W. 2011. Neuroinflammation in amyotrophic lateral sclerosis: role of glial activation in motor neuron disease. *Lancet Neurol,* 10**,** 253-63.

PROKOP, S., MILLER, K. R. & HEPPNER, F. L. 2013. Microglia actions in Alzheimer's disease. *Acta Neuropathol,* 126**,** 461-77.

QU, X., YU, J., BHAGAT, G., FURUYA, N., HIBSHOOSH, H., TROXEL, A., ROSEN, J., ESKELINEN, E. L., MIZUSHIMA, N., OHSUMI, Y., CATTORETTI, G. & LEVINE, B. 2003. Promotion of tumorigenesis by heterozygous disruption of the beclin 1 autophagy gene. *J Clin Invest,* 112**,** 1809-20.

QUATTRONE, A., GAMBARDELLA, A., BONO, F., AGUGLIA, U., BOLINO, A., BRUNI, A. C., MONTESI, M. P., OLIVERI, R. L., SABATELLI, M., TAMBURRINI, O., VALENTINO, P., VAN BROECKHOVEN, C. &

ZAPPIA, M. 1996. Autosomal recessive hereditary motor and sensory neuropathy with focally folded myelin sheaths: clinical, electrophysiologic, and genetic aspects of a large family. *Neurology,* 46**,** 1318-24.

RABINOWITZ, J. D. & WHITE, E. 2010. Autophagy and metabolism. *Science,* 330**,** 1344-8.

RAIBORG, C. & STENMARK, H. 2009. The ESCRT machinery in endosomal sorting of ubiquitylated membrane proteins. *Nature,* 458**,** 445-52.

RAMOS, J. C., RUIZ, P., JR., RATNER, L., REIS, I. M., BRITES, C., PEDROSO, C., BYRNE, G. E., JR., TOOMEY, N. L., ANDELA, V., HARHAJ, E. W., LOSSOS, I. S. & HARRINGTON, W. J., JR. 2007. IRF-4 and c-Rel expression in antiviral-resistant adult T-cell leukemia/lymphoma. *Blood,* 109**,** 3060-8.

RAVIKUMAR, B., VACHER, C., BERGER, Z., DAVIES, J. E., LUO, S., OROZ, L. G., SCARAVILLI, F., EASTON, D. F., DUDEN, R., O'KANE, C. J. & RUBINSZTEIN, D. C. 2004. Inhibition of mTOR induces autophagy and reduces toxicity of polyglutamine expansions in fly and mouse models of Huntington disease. *Nat Genet,* 36**,** 585-95.

REILLY, M. M., MURPHY, S. M. & LAURA, M. 2011. Charcot-Marie-Tooth disease. *J Peripher Nerv Syst,* 16**,** 1-14.

RODRIGUEZ-MUELA, N., GERMAIN, F., MARINO, G., FITZE, P. S. & BOYA, P. 2012. Autophagy promotes survival of retinal ganglion cells after optic nerve axotomy in mice. *Cell Death Differ,* 19**,** 162-9.

ROMIEU-MOUREZ, R., KIM, D. W., SHIN, S. M., DEMICCO, E. G., LANDESMAN-BOLLAG, E., SELDIN, D. C., CARDIFF, R. D. & SONENSHEIN, G. E. 2003. Mouse mammary tumor virus c-rel transgenic mice develop mammary tumors. *Mol Cell Biol,* 23**,** 5738-54.

ROSSI, A., PARADISO, C., CIONI, R., RIZZUTO, N. & GUAZZI, G. 1985. Charcot-Marie-Tooth disease: study of a large kinship with an intermediate form. *J Neurol,* 232**,** 91-8.

RUDOLPH, D., YEH, W. C., WAKEHAM, A., RUDOLPH, B., NALLAINATHAN, D., POTTER, J., ELIA, A. J. & MAK, T. W. 2000. Severe liver degeneration and lack of NF-kappaB activation in NEMO/IKKgamma-deficient mice. *Genes Dev,* 14**,** 854-62.

SACHDEV, S., HOFFMANN, A. & HANNINK, M. 1998. Nuclear localization of IkappaB alpha is mediated by the second ankyrin repeat: the IkappaB alpha ankyrin repeats define a novel class of cis-acting nuclear import sequences. *Mol Cell Biol,* 18**,** 2524-34.

SANFORD, M. 2014. Fingolimod: a review of its use in relapsing-remitting multiple sclerosis. *Drugs,* 74**,** 1411-33.

SAPORTA, A. S., SOTTILE, S. L., MILLER, L. J., FEELY, S. M., SISKIND, C. E. & SHY, M. E. 2011. Charcot-Marie-Tooth disease subtypes and genetic testing strategies. *Ann Neurol,* 69**,** 22-33.

SARGSYAN, S. A., MONK, P. N. & SHAW, P. J. 2005. Microglia as potential contributors to motor neuron injury in amyotrophic lateral sclerosis. *Glia,* 51**,** 241-53.

SAVINOVA, O. V., HOFFMANN, A. & GHOSH, G. 2009. The Nfkb1 and Nfkb2 proteins p105 and p100 function as the core of high-molecular-weight heterogeneous complexes. *Mol Cell,* 34**,** 591-602.

SCHMID, C. D., STIENEKEMEIER, M., OEHEN, S., BOOTZ, F., ZIELASEK, J., GOLD, R., TOYKA, K. V., SCHACHNER, M. & MARTINI, R. 2000. Immune deficiency in mouse models for inherited peripheral neuropathies leads to improved myelin maintenance. *J Neurosci,* 20**,** 729-35.

SEN, R. & BALTIMORE, D. 1986. Multiple nuclear factors interact with the immunoglobulin enhancer sequences. *Cell,* 46**,** 705-16.

SHAMASH, S., REICHERT, F. & ROTSHENKER, S. 2002. The cytokine network of Wallerian degeneration: tumor necrosis factor-alpha, interleukin-1alpha, and interleukin-1beta. *J Neurosci,* 22**,** 3052-60.

SHEN, D. N., ZHANG, L. H., WEI, E. Q. & YANG, Y. 2015. Autophagy in synaptic development, function, and pathology. *Neurosci Bull,* 31**,** 416-26.

SHIBATA, H., YOSHIOKA, Y., IKEMIZU, S., KOBAYASHI, K., YAMAMOTO, Y., MUKAI, Y., OKAMOTO, T., TANIAI, M., KAWAMURA, M., ABE, Y., NAKAGAWA, S., HAYAKAWA, T., NAGATA, S., YAMAGATA, Y., MAYUMI, T., KAMADA, H. & TSUTSUMI, Y. 2004. Functionalization of tumor necrosis factor-alpha using phage display technique and PEGylation improves its antitumor therapeutic window. *Clin Cancer Res,* 10**,** 8293-300.

SLOTTA, C., FRIEDRICH, K. E., KITKE, A., KALTSCHMIDT, B. & KALTSCHMIDT, C. Impaired clearance of autolysosomes in *PLEKHG5*-deficient human glioma cells. *in preparation.*

SLOTTA, C., LÜNINGSCHRÖR, P., HEIMANN, P., BRIESE, M., WEIKERT, U. M., APPENZELLER, S., SENDTNER, M., KALTSCHMIDT, B. & KALTSCHMIDT, C. *Plekhg5*-deficiency results in immunosuppression in peripheral nerves during motoneuron disease. *submitted.*

SLOTTA, C., SCHLUTER, T., RUIZ-PERERA, L. M., KADHIM, H. M., TERTEL, T., HENKEL, E., HUBNER, W., GREINER, J. F. W., HUSER, T., KALTSCHMIDT, B. & KALTSCHMIDT, C. 2017. CRISPR/Cas9-mediated knockout of c-REL in HeLa cells results in profound defects of the cell cycle. *PLoS One,* 12**,** e0182373.

SLOTTA, C., STORM, J., PFISTERER, N., KLEINWÄCHTER, S., PIEPER, M., RUIZ-PERERA, L. M., HENKEL, E., GREINER, J. F. W., KALTSCHMIDT, B. & KALTSCHMIDT, C. CRISPR/Cas9-mediated deficiency of human *IKBK1*/*IKBK2* leads to TNFα-induced programmed cell death in an NF-κB-independent manner. *under*

review.

SMITH, C. M., MAYER, J. A. & DUNCAN, I. D. 2013. Autophagy promotes oligodendrocyte survival and function following dysmyelination in a long-lived myelin mutant. *J Neurosci,* 33**,** 8088-100.

SPILMAN, P., PODLUTSKAYA, N., HART, M. J., DEBNATH, J., GOROSTIZA, O., BREDESEN, D., RICHARDSON, A., STRONG, R. & GALVAN, V. 2010. Inhibition of mTOR by rapamycin abolishes cognitive deficits and reduces amyloid-beta levels in a mouse model of Alzheimer's disease. *PLoS One,* 5**,** e9979.

SUN, L., WANG, H., WANG, Z., HE, S., CHEN, S., LIAO, D., WANG, L., YAN, J., LIU, W., LEI, X. & WANG, X. 2012. Mixed Lineage Kinase Domain-like Protein Mediates Necrosis Signaling Downstream of RIP3 Kinase. *Cell,* 148**,** 213-227.

SUN, S. C. 2012. The noncanonical NF-kappaB pathway. *Immunol Rev,* 246**,** 125-40.

SUN, S. C. 2017. The non-canonical NF-kappaB pathway in immunity and inflammation. *Nat Rev Immunol,* 17**,** 545-558.

SURESH, R., ALI, S., AHMAD, A., PHILIP, P. A. & SARKAR, F. H. 2016. The Role of Cancer Stem Cells in Recurrent and Drug-Resistant Lung Cancer. *Adv Exp Med Biol,* 890**,** 57-74.

SUZUKI, K., LOVERA, M., SCHMACHTENBERG, O. & COUVE, E. 2015. Axonal Degeneration in Dental Pulp Precedes Human Primary Teeth Exfoliation. *J Dent Res,* 94**,** 1446-53.

SZLOSAREK, P. W., GRIMSHAW, M. J., KULBE, H., WILSON, J. L., WILBANKS, G. D., BURKE, F. & BALKWILL, F. R. 2006. Expression and regulation of tumor necrosis factor alpha in normal and malignant ovarian epithelium. *Mol Cancer Ther,* 5**,** 382-90.

TANAKA, M., FUENTES, M. E., YAMAGUCHI, K., DURNIN, M. H., DALRYMPLE, S. A., HARDY, K. L. & GOEDDEL, D. V. 1999. Embryonic lethality, liver degeneration, and impaired NF-kappa B activation in IKK-beta-deficient mice. *Immunity,* 10**,** 421-9.

THOMAS, P. K. & CALNE, D. B. 1974. Motor nerve conduction velocity in peroneal muscular atrophy: evidence for genetic heterogeneity. *J Neurol Neurosurg Psychiatry,* 37**,** 68-75.

THUMM, M., EGNER, R., KOCH, B., SCHLUMPBERGER, M., STRAUB, M., VEENHUIS, M. & WOLF, D. H. 1994. Isolation of autophagocytosis mutants of Saccharomyces cerevisiae. *FEBS Lett,* 349**,** 275-80.

TOFARIS, G. K., PATTERSON, P. H., JESSEN, K. R. & MIRSKY, R. 2002. Denervated Schwann cells attract macrophages by secretion of leukemia inhibitory factor (LIF) and monocyte chemoattractant protein-1 in a process regulated by interleukin-6 and LIF. *J Neurosci,* 22**,** 6696-703.

TSUKADA, M. & OHSUMI, Y. 1993. Isolation and characterization of

autophagy-defective mutants of Saccharomyces cerevisiae. *FEBS Lett,* 333**,** 169-74.

VALLABHAPURAPU, S. & KARIN, M. 2009. Regulation and function of NF-kappaB transcription factors in the immune system. *Annu Rev Immunol,* 27**,** 693-733.

VAN ANTWERP, D. J., MARTIN, S. J., KAFRI, T., GREEN, D. R. & VERMA, I. M. 1996. Suppression of TNF-alpha-induced apoptosis by NF-kappaB. *Science,* 274**,** 787-9.

VANLANGENAKKER, N., VANDEN BERGHE, T., BOGAERT, P., LAUKENS, B., ZOBEL, K., DESHAYES, K., VUCIC, D., FULDA, S., VANDENABEELE, P. & BERTRAND, M. J. M. 2010. cIAP1 and TAK1 protect cells from TNF-induced necrosis by preventing RIP1/RIP3-dependent reactive oxygen species production. *Cell Death Differ,* 18**,** 656.

VARFOLOMEEV, E. & VUCIC, D. 2016. Intracellular regulation of TNF activity in health and disease. *Cytokine*.

VARGAS, M. E. & BARRES, B. A. 2007. Why is Wallerian degeneration in the CNS so slow? *Annu Rev Neurosci,* 30**,** 153-79.

VOGELSTEIN, B., PAPADOPOULOS, N., VELCULESCU, V. E., ZHOU, S., DIAZ, L. A., JR. & KINZLER, K. W. 2013. Cancer genome landscapes. *Science,* 339**,** 1546-58.

WALCZAK, H. 2011. TNF and ubiquitin at the crossroads of gene activation, cell death, inflammation, and cancer. *Immunol Rev,* 244**,** 9-28.

WANG, C. Y., MAYO, M. W., KORNELUK, R. G., GOEDDEL, D. V. & BALDWIN, A. S., JR. 1998. NF-kappaB antiapoptosis: induction of TRAF1 and TRAF2 and c-IAP1 and c-IAP2 to suppress caspase-8 activation. *Science,* 281**,** 1680-3.

WANG, L., DU, F. & WANG, X. 2008. TNF-alpha induces two distinct caspase-8 activation pathways. *Cell,* 133**,** 693-703.

WANG, Q., LIU, Y. & ZHOU, J. 2015. Neuroinflammation in Parkinson's disease and its potential as therapeutic target. *Transl Neurodegener,* 4**,** 19.

WANG, X. & LIN, Y. 2008. Tumor necrosis factor and cancer, buddies or foes? *Acta Pharmacol Sin,* 29**,** 1275-88.

WELLMANN, H., KALTSCHMIDT, B. & KALTSCHMIDT, C. 2001. Retrograde transport of transcription factor NF-kappa B in living neurons. *J Biol Chem,* 276**,** 11821-9.

WENIGER, M. A., GESK, S., EHRLICH, S., MARTIN-SUBERO, J. I., DYER, M. J., SIEBERT, R., MOLLER, P. & BARTH, T. F. 2007. Gains of REL in primary mediastinal B-cell lymphoma coincide with nuclear accumulation of REL protein. *Genes Chromosomes Cancer,* 46**,** 406-15.

WESTERMARK, B., PONTEN, J. & HUGOSSON, R. 1973. Determinants for

the establishment of permanent tissue culture lines from human gliomas. *Acta Pathol Microbiol Scand A,* 81**,** 791-805.

WHITE, E. & DIPAOLA, R. S. 2009. The double-edged sword of autophagy modulation in cancer. *Clin Cancer Res,* 15**,** 5308-16.

WIDERA, D., KLENKE, C., NAIR, D., HEIDBREDER, M., MALKUSCH, S., SIBARITA, J. B., CHOQUET, D., KALTSCHMIDT, B., HEILEMANN, M. & KALTSCHMIDT, C. 2016. Single-particle tracking uncovers dynamics of glutamate-induced retrograde transport of NF-kappaB p65 in living neurons. *Neurophotonics,* 3**,** 041804.

WIDERA, D., MIKENBERG, I., ELVERS, M., KALTSCHMIDT, C. & KALTSCHMIDT, B. 2006. Tumor necrosis factor alpha triggers proliferation of adult neural stem cells via IKK/NF-kappaB signaling. *BMC Neurosci,* 7**,** 64.

WURSTLE, S., SCHNEIDER, F., RINGEL, F., GEMPT, J., LAMMER, F., DELBRIDGE, C., WU, W. & SCHLEGEL, J. 2017. Temozolomide induces autophagy in primary and established glioblastoma cells in an EGFR independent manner. *Oncol Lett,* 14**,** 322-328.

XIA, Y., SHEN, S. & VERMA, I. M. 2014. NF-kappaB, an active player in human cancers. *Cancer Immunol Res,* 2**,** 823-30.

XIA, Y., YEDDULA, N., LEBLANC, M., KE, E., ZHANG, Y., OLDFIELD, E., SHAW, R. J. & VERMA, I. M. 2012. Reduced cell proliferation by IKK2 depletion in a mouse lung-cancer model. *Nat Cell Biol,* 14**,** 257-65.

YAN, Z., ZHAO, N., WANG, Z., LI, B., BAO, C., SHI, J., HAN, W. & ZHANG, Y. 2006. A mutated human tumor necrosis factor-alpha improves the therapeutic index in vitro and in vivo. *Cytotherapy,* 8**,** 415-23.

YDENS, E., LORNET, G., SMITS, V., GOETHALS, S., TIMMERMAN, V. & JANSSENS, S. 2013. The neuroinflammatory role of Schwann cells in disease. *Neurobiol Dis,* 55**,** 95-103.

YOSHIDA, A., SHIMIZU, A., ASANO, H., KADONOSONO, T., KONDOH, S. K., GERETTI, E., MAMMOTO, A., KLAGSBRUN, M. & SEO, M. K. 2015. VEGF-A/NRP1 stimulates GIPC1 and Syx complex formation to promote RhoA activation and proliferation in skin cancer cells. *Biol Open,* 4**,** 1063-76.

YUE, Z., JIN, S., YANG, C., LEVINE, A. J. & HEINTZ, N. 2003. Beclin 1, an autophagy gene essential for early embryonic development, is a haploinsufficient tumor suppressor. *Proc Natl Acad Sci U S A,* 100**,** 15077-82.

ZARE-SHAHABADI, A., MASLIAH, E., JOHNSON, G. V. & REZAEI, N. 2015. Autophagy in Alzheimer's disease. *Rev Neurosci,* 26**,** 385-95.

ZHANG, J., CLARK, K., LAWRENCE, T., PEGGIE, M. W. & COHEN, P. 2014a. An unexpected twist to the activation of IKKbeta: TAK1 primes IKKbeta for activation by autophosphorylation. *Biochem J,* 461**,** 531-7.

ZHANG, X., CHEN, S., SONG, L., TANG, Y., SHEN, Y., JIA, L. & LE, W.

2014b. MTOR-independent, autophagic enhancer trehalose prolongs motor neuron survival and ameliorates the autophagic flux defect in a mouse model of amyotrophic lateral sclerosis. *Autophagy,* 10**,** 588-602.

8. Acknowledgments

I received great help and support during the time of my PhD thesis, for which I would like to express my gratitude.

In particular, I wish to thank my supervisor Prof. Dr. Barbara Kaltschmidt for help and guidance throughout my time but also for critical remarks. Additionally, I want to thank Prof. Dr. Christian Kaltschmidt for his interesting project ideas, in which I was allowed to participate and for numerous critical discussions.

I am very grateful to Dr. Peter Heimann for great help within the "Plekhg5-project". Without his knowledge and skills, many experiments would not have been possible.

I would like to thank all current and former members of the Department of Cell Biology for support and the nice working atmosphere. In particular, I would like to mention Angela Kralemann-Köhler for her outstanding technical assistance and Dr. Johannes Greiner.

Special thanks I would like to dedicate to Dr. Patrick Lüningschrör for numerous interesting and constructive phone conferences and his great input within the "Plekhg5-project".

I thank all the co-authors of the papers published and the manuscripts that hopefully will be published soon for their great contributions.

Furthermore, I would like to thank my family for steady support. They always showed interest in what I was doing, even when I was not able to explain it to them properly.

Marie, I cannot describe how much your support and love means to me. We managed the long distance during our PhD time and I am sure we will manage the rest of our lives together.

9. Declaration

I hereby declare that I am the sole author of the dissertation

"**Analysis of the NF-κB signal transduction pathway in neurological disorders and cancer**"

and did not use any material or sources other than the ones I have named. Passages that use wording (or words of that effect), tables or pictures of other sources have always been duly acknowledged with a reference to the original material.

This dissertation or similar versions have not been previously submitted for a degree.

Bielefeld, 20.12.2017   _____

10. Curriculum vitae

Personal information

Date of birth:	October 6th, 1987
Place of birth:	Lemgo, Germany
Nationality:	German
Current address:	Wellensiek 89, 33619 Bielefeld
Email:	carsten.slotta@uni-bielefeld.de

Education

11/2013 – present	Ph.D. studies, University of Bielefeld, Department of Cell Biology
10/2011 – 10/2013	Master of Science in Molecular Cell Biology, University of Bielefeld *final mark: 1.0*
10/2008 – 09/2011	Bachelor of Science in Cell Biology, University of Osnabrueck *final mark: 1.7*
09/2007 – 05/2008	Civilian service at Stiftung Eben-Ezer, 32657 Lemgo
08/1998 – 06/2007	Secondary school "Weser-Gymnasium Vlotho", 32602 Vlotho School certificate: Abitur (A-Level), *final mark: 2.4*

Professional experience

11/2013 – present	Research assistant (Ph.D. student), University of Bielefeld, Department of Cell Biology

Teaching experience

Organization of and demonstrating in practical courses

Supervision and marking of academic theses:

Nina Pfisterer, "Detailed analysis of TNFα-mediated Cell Death in IKKα/β-deficient Cells", Bachelor thesis (B.Sc.), SS2017, University of Bielefeld

Fabian Essfeld, "Quantitative analyses of IκBα involved in NF-κB Dynamics", Bachelor thesis (B.Sc.), SS2017, University of Bielefeld

Angelika Kitke, "CRISPR/Cas9-mediated knockout of PLEKHG5 in human glioma cells", Bachelor thesis (B.Sc.), SS2017, University of Bielefeld

Jonathan Storm, "CRISPR/Cas9-mediated knockout of IKBKA and IKBKB in HEK293 FT-cells results in TNFα-induced cell death", Bachelor thesis (B.Sc.), SS2017, University of Bielefeld

Ann-Christin Groh, "PLEKHG5 signaling pathway – Investigations via embryonic stem cell differentiation and Yeast-two-Hybrid system", WS2014/15, University of Bielefeld

Publications

Slotta C, Friedrich KE, Kitke A, Greiner JFW, Kaltschmidt C & Kaltschmidt B. Impaired clearance of autolysosomes in *PLEKHG5*-deficient human glioma cells. *In preparation*

Slotta C, Lüningschrör P, Weikert UM, Briese M, Appenzeller S, Heimann P, Sendtner M, Kaltschmidt C & Kaltschmidt B. Plekhg5 mediates myelin breakdown by regulating the immune response in peripheral nerves. *In submission*

Slotta C, Storm J, Kleinwächter S, Pfisterer N, Pieper M, Ruiz-Perera L, Henkel E, Greiner JFW, Kaltschmidt B & Kaltschmidt C. CRISPR/Cas9-mediated deficiency of human *IKBK1*/*IKBK2* leads to TNFα-induced programmed cell death in an NF-κB-independent manner. *Under review*

Lüningschrör P, Binotti B, Dombert B, Heimann P, Perez-Lara A, **Slotta C**, Thau-Habermann N, Rüdt von Collenberg C, Karl F, Damme M, *et al*. Plekhg5-regulated autophagy of synaptic vesicles reveals a pathogenic mechanism in motoneuron disease. Nat.Commun. 2017 Oct 30;8(1):678

Slotta C, Schlüter T, Ruiz-Perera L, Kadhim H, Tertel T, Henkel E, Hübner W, Greiner JFW, Huser T, Kaltschmidt B & Kaltschmidt C. CRISPR/Cas9-mediated knockout of *c-REL* in HeLa cells results in profound defects of the cell cycle. PLoS ONE 12(8): e0182373

Slotta C, Müller J, Tran L, Hauser S, Widera D, Kaltschmidt B & Kaltschmidt C. (2014) An Investigation of the Specificity of Research Antibodies against NF-kappaB-subunit p65. *J Histochem Cytochem,* 62**,** 157-61.

Nguyen TD, Widera D, Greiner J, Müller J, Martin I, **Slotta C**, Hauser S, Kaltschmidt C & Kaltschmidt B. (2013) Prolonged cultivation of hippocampal neural precursor cells shifts their differentiation potential and selects for aneuploid cells. *Biol Chem,* 394, 1623-36.

Patents

DUAL INHIBITION OF IKK1 AND IKK2 FOR THE TREATMENT OF PROLIFERATIVE DISEASES. App. No EP17184522.5, *pending*

Scientific exchange

Invited talks

2017	"Impaired Schwann cell autophagy in a late onset motoneuron disease" 12th Goettingen Meeting of the German Neuroscience Society March 22-25, 2017, Goettingen, Germany
2016	"Loss of Schwann cell autophagy might contribute to a late onset motoneuron disease in Plekhg5 deficient mice" 8th Westerberger Herbsttagung September 22-24, 2016, Osnabrueck, Germany

Posters

2017	"Impaired Schwann cell autophagy contributes to a late onset motoneuron disease in Plekhg5 deficient mice" **C. Slotta**, P. Heimann, P. Lüningschrör, B. Kaltschmidt, C. Kaltschmidt 4th Symposium on Current Topics in Myelin Research March 2-4, 2017, Kassel, Germany
2016	"Loss of Schwann cell autophagy might contribute to a late onset motoneuron disease in Plekhg5 deficient mice"

65

C. Slotta, P. Heimann, P. Lüningschrör, B. Kaltschmidt, C. Kaltschmidt
8th Westerberger Herbsttagung
September 22-24, 2016, Osnabrueck, Germany

"Genome editing of NF-kappaB family member c-Rel using mCRISPR/Cas9n for future applications in the nervous system"
T. Schlüter, A. Kralemann-Köhler, **C. Slotta**, B. Kaltschmidt, C. Kaltschmidt
8th Westerberger Herbsttagung
September 22-24, 2016, Osnabrueck, Germany

2015

"Plekhg5 regulates Neuregulin-1 mediated Axon-Schwann Cell Interaction for Long-Term Motoneuron Maintenance"
C. Slotta, P. Lüningschrör, M. Sendtner, B. Kaltschmidt, C. Kaltschmidt
NeuroVisionen 11
November 13-14, Muenster, Germany

11. Publications

Plekhg5-regulated autophagy of synaptic vesicles reveals a pathogenic mechanism in motoneuron disease

Patrick Lüningschrör[1,2], Beyenech Binotti[3], Benjamin Dombert[1], Peter Heimann[2], Angel Perez-Lara [3], Carsten Slotta[2], Nadine Thau-Habermann[4], Cora R. von Collenberg[1], Franziska Karl[5], Markus Damme[6], Arie Horowitz [7], Isabelle Maystadt[8], Annette Füchtbauer[9], Ernst-Martin Füchtbauer[9], Sibylle Jablonka[1], Robert Blum[1], Nurcan Üçeyler[5], Susanne Petri[4,10], Barbara Kaltschmidt[2,11], Reinhard Jahn[3], Christian Kaltschmidt[2] & Michael Sendtner [1]

Autophagy-mediated degradation of synaptic components maintains synaptic homeostasis but also constitutes a mechanism of neurodegeneration. It is unclear how autophagy of synaptic vesicles and components of presynaptic active zones is regulated. Here, we show that Pleckstrin homology containing family member 5 (Plekhg5) modulates autophagy of synaptic vesicles in axon terminals of motoneurons via its function as a guanine exchange factor for Rab26, a small GTPase that specifically directs synaptic vesicles to preautophagosomal structures. *Plekhg5* gene inactivation in mice results in a late-onset motoneuron disease, characterized by degeneration of axon terminals. Plekhg5-depleted cultured motoneurons show defective axon growth and impaired autophagy of synaptic vesicles, which can be rescued by constitutively active Rab26. These findings define a mechanism for regulating autophagy in neurons that specifically targets synaptic vesicles. Disruption of this mechanism may contribute to the pathophysiology of several forms of motoneuron disease.

[1] Institute of Clinical Neurobiology, University Hospital Würzburg, 97078 Würzburg, Germany. [2] Department of Cell Biology, University of Bielefeld, 33501 Bielefeld, Germany. [3] Department of Neurobiology, Max Planck Institute for Biophysical Chemistry, 37077 Göttingen, Germany. [4] Department of Neurology, Hannover Medical School, 30625 Hannover, Germany. [5] Department of Neurology, University Hospital Würzburg, 97078 Würzburg, Germany. [6] Institut für Biochemie, Christian-Albrechts-Universität zu Kiel, 24098 Kiel, Germany. [7] Cardeza Vascular Biology Center, Departments of Medicine and Cancer Biology, Sidney Kimmel Medical College, Thomas Jefferson University, Philadelphia, PA 19107, USA. [8] Centre de Génétique Humaine, Institut de Pathologie et de Génétique, 6041 Gosselies, Belgium. [9] Department of Molecular Biology and Genetics, Aarhus University, 8000 Aarhus C, Denmark. [10] Integrated Research and Treatment Center Transplantation (IFB-Tx) Hannover, Hannover Medical School 30625 Hannover, Germany. [11] Molecular Neurobiology, University of Bielefeld, 33615 Bielefeld, Germany. Beyenech Binotti, Benjamin Dombert, Peter Heimann, Christian Kaltschmidt and Michael Sendtner contributed equally to this work. Correspondence and requests for materials should be addressed to C.K. (email: c.kaltschmidt@uni-bielefeld.de) or to M.S. (email: Sendtner_M@ukw.de)

In neurons, autophagosome biogenesis predominantly takes places in axon terminals. Newly synthesized autophagosomes mature during retrograde transport to the soma and fuse with lysosomes[1, 2]. Autophagy-mediated degradation of synaptic components is involved in neuronal network remodeling, presynaptic neurotransmission and synaptic pruning at polyinnervated neuromuscular junctions during development, but could also represent a mechanism of neurodegeneration[3–6].

Selective elimination of axon terminals marks disease onset in familial amyotrophic lateral sclerosis (ALS) and loss of synaptic vesicles precedes axon degeneration in SOD1 G93A mice[7], indicating that autophagy temporally regulates degradation of synaptic vesicles in axon terminals. Neuron-specific disruption of autophagy by depletion of Atg5 or Atg7 results in progressive deficits of motor function and neurodegeneration[8, 9]. Modulation of the autophagy pathway modifies disease onset and progression in SOD1 G93A mice, which further points to the contribution of autophagy to the pathology of motoneuron disease[10, 11]. However, the molecular mechanisms that differentially regulate autophagy of synaptic vesicles and components of presynaptic active zones are not known.

Here, we show that Plekhg5 (also known as Syx, Tech or GEF720)[12–14] regulates autophagy of synaptic vesicles in motoneurons via its function as a guanine exchange factor (GEF) for Rab26, a small GTPase selectively delivering synaptic vesicles into preautophagosomes[15]. Plekhg5 is a pleckstrin homology domain containing member of the GEF family. It is predominantly expressed in the nervous system[12, 14]. While several studies provided evidence for a function of Plekhg5 in endothelial cell migration and angiogenesis in zebrafish and mice[13, 16], its function in the nervous system remained elusive. Mutations in the PLEKHG5 gene have been associated with different forms of motoneuron diseases such as distal spinal muscular atrophy type IV (DSMA-IV)[17], intermediate Charcot-Marie-Tooth disease (CMT)[18, 19] and ALS[20]. The PLEKHG5-mutations identified so far in CMT disease patients produce premature stop codons and are predicted to result in a functional null allele[18, 19]. In contrast, mutations described to be causative for a recessive lower motoneuron disease with childhood onset lead to an exchange of one amino acid within the pleckstrin homology domain[17, 20].

To analyze the function of Plekhg5 in the nervous system and its involvement in motoneuron disease, we generated Plekhg5-deficient mice using a gene-trap approach[21]. Plekhg5-deficient mice develop a late-onset motoneuron disease, characterized by degeneration of motoneuron axon terminals. Plekhg5-depleted cultured motoneurons show defective autophagy resulting in accumulation of synaptic vesicles at axon terminals and impaired axon growth. Furthermore, Plekhg5-deficient cells show a reduced activity of Rab26. In a cell-free system Plekhg5 is able to promote GTP exchange of Rab26. Finally, constitutively active Rab26 rescues autophagy and axon growth deficits of cultured motoneurons. Our data indicate that the function of Plekhg5 as a GEF for Rab26 is essential for axonal integrity, and that defective autophagy of synaptic vesicles is a pathogenic mechanism in this specific form of motoneuron disease.

Results

Plekhg5 deficiency causes a late-onset motoneuron disease.
To analyze the cellular function of Plekhg5, we generated Plekhg5-deficient mice using an embryonic stem-cell line harboring a gene-trap cassette within the Plekhg5 allele (Fig. 1), (Supplementary Fig. 1)[21]. Plekhg5-deficient mice developed normally without obvious disease phenotype up to adulthood. However, within 24 months after birth 33 out of 100 homozygous mice died, in contrast to 10 out of 100 heterozygous and 5 out of

100 wild-type animals (Fig. 1a). Affected mice developed hind-limb paralysis at 15 months (Fig. 1b). A reduction in body weight became apparent in 18–24 months old Plekhg5-deficient mice (Fig. 1c). To assess the impact of Plekhg5 deficiency on motor performance in more detail, grip strength (Fig. 1e, f) and rotarod performance (Fig. 1g) were analyzed in animals of different ages. These data indicate that the disease starts late at about 12 months of age and progresses from hindlimbs (Fig. 1f) to forelimbs (Fig. 1e). Correlating with reduced grip strength, we observed a loss of motoneurons starting at 12 months as shown by quantification of Nissl-stained lumbar spinal cord sections (Fig. 1d, h). This decrease was more prominent in 24-month-old animals (Fig. 1d).

We complemented the phenotypic characterization of the motor system with nerve conduction and electromyography studies of the gastrocnemius and plantaris muscles (Fig. 1j–l, o). In both muscles we observed a significantly delayed motor latency time (Fig. 1i). The measurements in the gastrocnemius muscles also showed a marked reduction of motor unit potential (MUP) amplitudes following sciatic nerve-stimulation (Fig. 1j). Our analyses revealed elevated single motor unit potentials (SMUP) (Fig. 1k) and a decrease in motor unit number estimation (MUNE) (Fig. 1l) in the gastrocnemius muscle, suggestive of sprouting of surviving motoneurons to re-innervate muscle fibers that have been denervated upon motoneuron loss. This finding is also supported by the observed fiber grouping as shown by succinate dehydrogenase (SDH) staining (Fig. 1m). These data are similar to the observed sprouting phenotype reported in SOD G93A mice[22]. As previously described for Plekhg5 mutant mice[19], we also detected a modest decrease in nerve conduction velocities (NCVs) (Fig. 1o).

Next, we investigated β-GEO reporter-activity of the gene-trap cassette in mutant mice. In contrast to spinal cord, β-galactosidase activity was not detected in skeletal muscle (Fig. 1n). Therefore, loss of Plekhg5 apparently does not affect the skeletal muscle directly, but rather indirectly via denervation and motoneuron loss.

We also assessed the impact of Plekhg5 deficiency on sensory and cognitive function. Sensory function was analyzed using the von Frey and Hargreaves tests (Fig. 1p, q). Whereas Plekhg5-deficient mice did not show major changes in mechanical withdrawal thresholds as compared to wild-type littermates (Fig. 1p), they displayed hypersensitivity to heat (Fig. 1p), indicating that sensory perception is not reduced in these mice.

To address whether Plekhg5 deficiency impairs cognitive function, we performed behavioral tests in 12–14-month-old mice (Supplementary Fig. 2), before motor disease symptoms occur. Plekhg5-deficient mice performed similarly in the open field test (Supplementary Fig. 2a, b) indicating that anxiety-related behavior is not altered. They also did not display differences in object recognition (Supplementary Fig. 2c, d) and fear conditioning (Supplementary Fig. 2e, f) suggestive for unaffected learning and memory.

Plekhg5 modulates synaptic vesicle turnover in motoneurons.
Next, we studied neuromuscular junctions (NMJs) within the gastrocnemius muscle to analyze whether the degenerative process in Plekhg5^{−/−} mice involves terminal axons (Fig. 2a, c; Supplementary Fig. 3). Wild-type animals exhibited regular pretzel-like NMJs at an age of 12 months, as indicated by bungarotoxin (BTX) staining for labeling of postsynaptic acetylcholine-receptors and synaptophysin immunoreactivity for the corresponding presynaptic compartment (Fig. 2a; Supplementary Fig. 3). In contrast, the presynaptic nerve
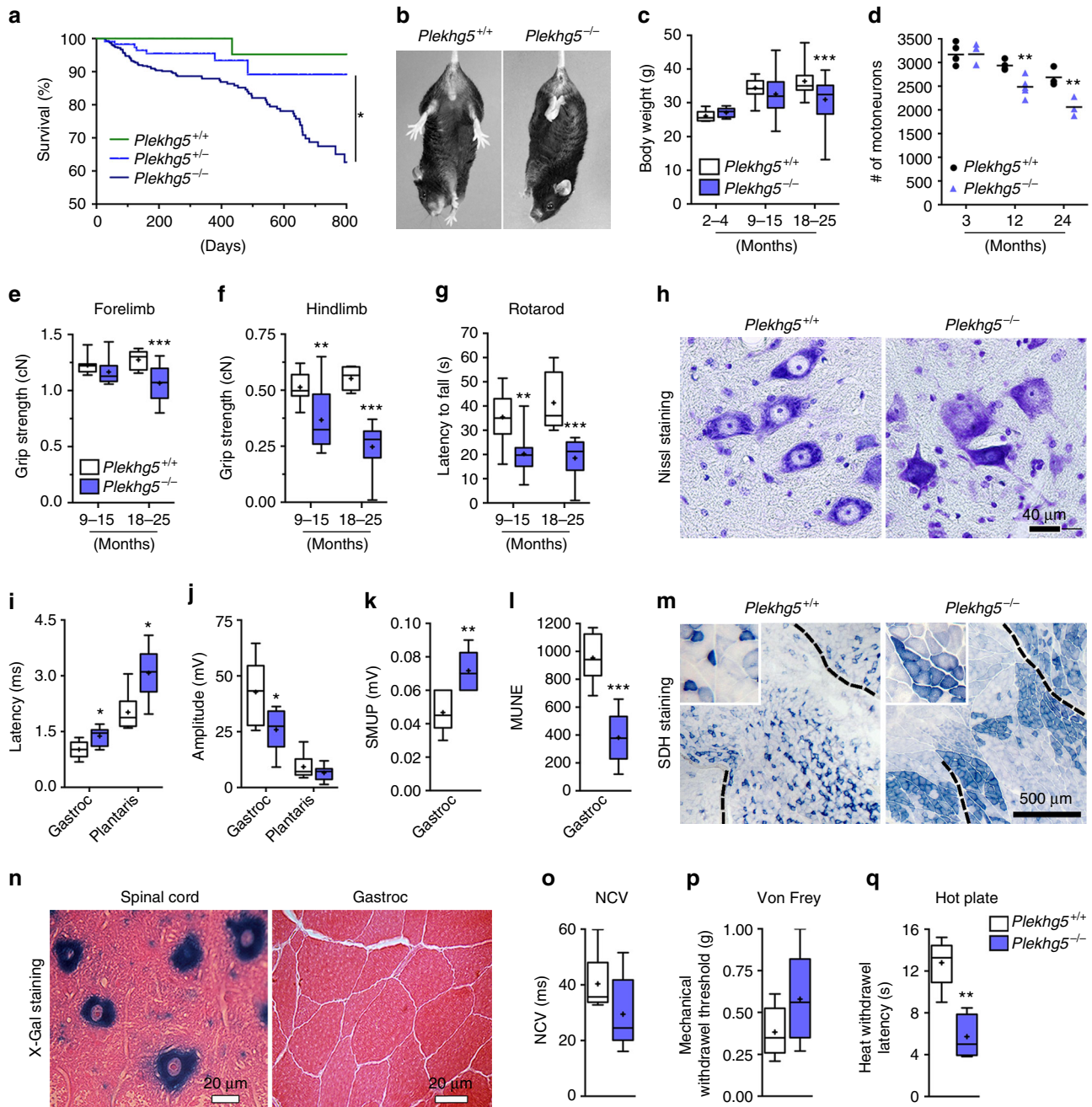
Fig. 1 Plekhg5-deficient mice develop a motoneuron disease with late onset. **a** Survival analysis of *Plekhg5* mutant mice. (Mean survival after 24 months: *Plekhg5*$^{+/+}$: 95%, *n* = 48; *Plekhg5*$^{+/−}$: 89%, *n* = 112; *Plekhg5*$^{−/−}$: 68%, *n* = 351; *p* = 0.0068; log-rank test) **b** Hind-limb clasping defects in 15-month-old Plekhg5-deficient mice. **c** Body weight measurements of Plekhg5-deficient and control mice of different ages (2−4 months, *Plekhg5*$^{+/+}$: *n* = 12, *Plekhg5*$^{−/−}$: *n* = 9; 9−15 months, *Plekhg5*$^{+/+}$: *n* = 19, *Plekhg5*$^{−/−}$: *n* = 42; 18−25 months, *Plekhg5*$^{+/+}$: *n* = 18, *Plekhg5*$^{−/−}$: *n* = 36; two-way ANOVA; Bonferroni post-test). **d** Number of motoneurons was counted in lumbar spinal cord sections (3 months, *n* = 5; 12 months, *n* = 5; 24 months, *n* = 3; unpaired *t*-test; two-tailed). **e**, **f** Grip strength measurements of fore- **e** and hindlimbs **f**. **g** Rotarod performance (9−15 months, *Plekhg5*$^{+/+}$: *n* = 9, *Plekhg5*$^{−/−}$: *n* = 10; 18 −24 months, *Plekhg5*$^{+/+}$: *n* = 11, *Plekhg5*$^{−/−}$: *n* = 8; two-way ANOVA; Bonferroni post-test). **h** Nissl-stained motoneurons in spinal sections from *Plekhg5*$^{+/+}$ and *Plekhg5*$^{−/−}$ mice. *Scale bar*: 40 μm. **i−l** Electrophysiological recordings of gastrocnemius and plantaris muscles (*Plekhg5*$^{+/+}$: *n* = 6, *Plekhg5*$^{−/−}$: *n* = 6; unpaired *t*-test; two-tailed). Latency **i** and amplitude **j** of muscle depolarization upon stimulation of the sciatic nerve. **k**, **l** Single motor unit potential (SMUP) **k** and motor unit number estimation (MUNE) **l** of the gastrocnemius muscle. **m** Succinate dehydrogenase (SDH) staining of the gastrocnemius muscle. *Scale bar*: 500 μm. **n** X-Gal staining of cross-sectioned spinal cord and gastrocnemius muscle. *Scale bar*: 20 μm. **o** Sciatic nerve conduction velocities (*Plekhg5*$^{+/+}$: *n* = 6, *Plekhg5*$^{−/−}$: *n* = 6; unpaired *t*-test; two-tailed) **p**, **q** Box- and whisker-plots show mechanical withdrawal thresholds **p** and heat withdrawal latencies (s) **q** of naive male *Plekhg5*$^{−/−}$ and control littermates. Mechanical withdrawal thresholds did not differ between genotypes **p**. *Plekhg5*$^{−/−}$ mice showed heat hypersensitivity as compared to control littermates (*Plekhg5*$^{+/+}$: *n* = 5, *Plekhg5*$^{−/−}$: *n* = 5; Mann−Whitney *U*-test)
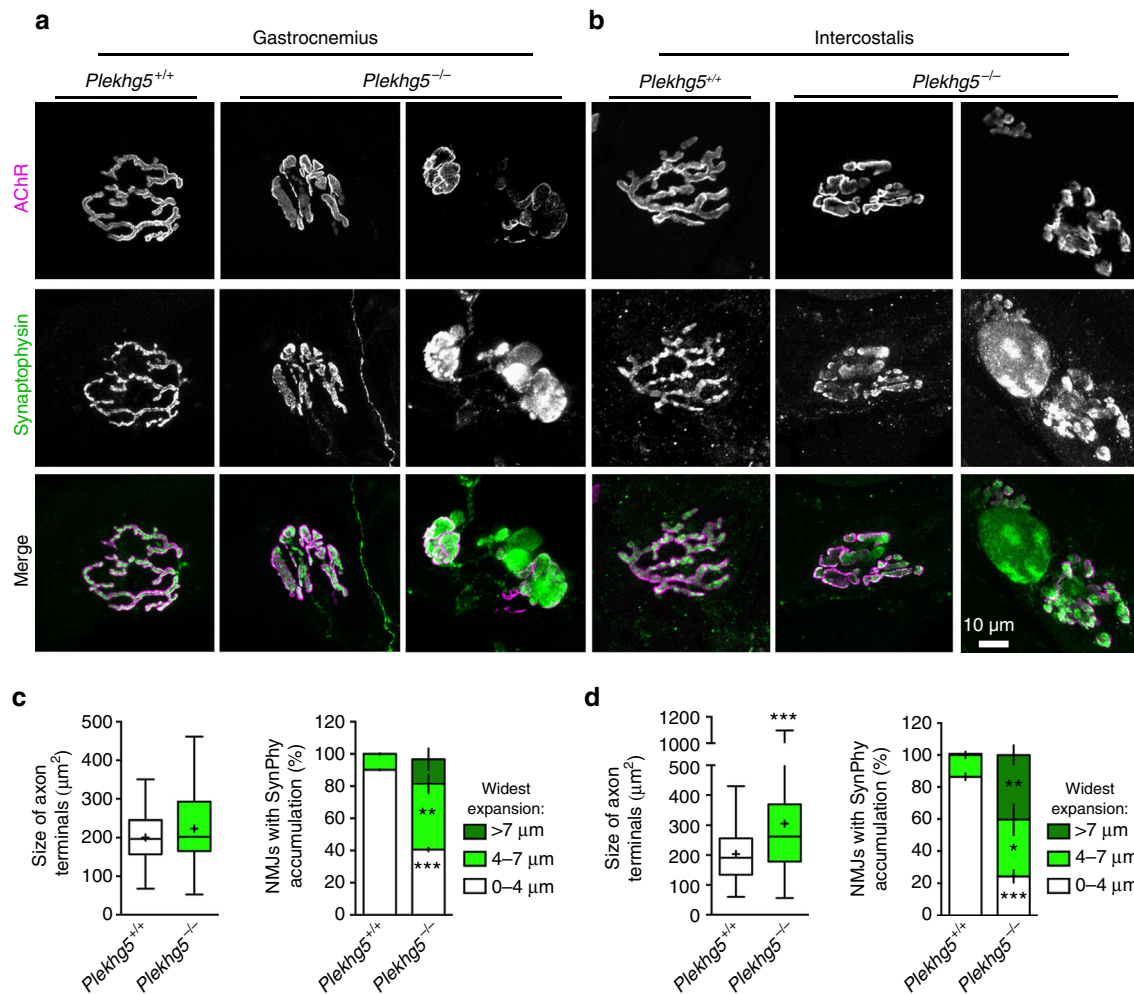
Fig. 2 Degradation of neuromuscular junctions in Plekhg5-deficient mice. **a**, **b** NMJs within the gastrocnemius **a** and intercostal **b** muscles stained for BTX and synaptophysin. *Scale bar*: 10 μm. **c**, **d** Quantification of presynaptic area by evaluation of synaptophysin staining and measurement of the widest expansion of presynaptic sites (three animals per genotype with at least 15 NMJs analyzed per animal; mean ± SEM; two-way ANOVA; Bonferroni post-test)

terminals of $Plekhg5^{-/-}$ mice appeared swollen with accumulations of synaptophysin (Fig. 2a, c; Supplementary Fig. 3) and neurofilament-H (NF-H) (Supplementary Fig. 3).

Respiratory failure due to progressive impairment of the neuromuscular system has been reported as a main cause of death in ALS and the major trigger for premature death in SOD1 G93A mice[23]. We therefore investigated whether NMJs within intercostal muscles of Plekhg5-deficient mice also show signs of degeneration. We observed a phenotype similar as in the gastrocnemius muscle with deformed and swollen axon terminals (Fig. 2b, d), indicating that muscles necessary for respiration become denervated which could make a major contribution to premature death.

At the ultrastructural level, axon terminals of Plekhg5-deficient mice were filled with membrane fragments and cytoplasmic inclusions (Fig. 3a–e), similar as those observed in patients with ALS[24, 25]. Strikingly, synaptic vesicles in $Plekhg5^{-/-}$ motoneuron terminals were frequently enlarged, in contrast to synaptic vesicles in wild-type mice, which appeared smaller and of a more uniform size (Fig. 3f–h). Furthermore, the organization of actin filaments in axon terminals appeared altered, with more actin fibers in close neighborhood of synaptic vesicles in active zones (Fig. 3f, g). In line with these findings we detected elevated protein levels of several synaptic vesicle markers in sciatic nerve

lysates of $Plekhg5^{-/-}$ mice (Fig. 3i, j). The ultrastructural examination of NMJs also revealed axonal swellings in distal axons (Fig. 4a). Axons showed a highly disorganized cytoskeleton (Fig. 4b, c). Axonal swellings were also frequently detectable in spinal cord and sciatic nerve cross-sections (Fig. 4d–j). In contrast, we detected no axonal swelling in wild-type animals (Fig. 4j). Taken together, these data indicate that Plekhg5 deficiency results in degradation of axon terminals, but also affects axonal integrity in proximal parts of axons.

Next, we studied the impact of Plekhg5 deficiency on synapse-morphology in the central nervous system and stained brain sections for synaptophysin and Tuj1 (Supplementary Fig. 4). The overall morphology and layering of the hippocampus, cerebellum and cortex appeared normal (Supplementary Fig. 4). In contrast to the abnormally swollen appearance of motoneuron terminals with synaptophysin-accumulations, synapses within the brain appeared unaffected in Plekhg5-deficient mice (Supplementary Fig. 4). These observations are in line with our data on normal cognitive function in Plekhg5-deficient mice.

Plekhg5 regulates autophagy in motoneurons. Under physiological conditions damaged organelles are removed from axon terminals by autophagy[1, 2, 6]. To assess whether
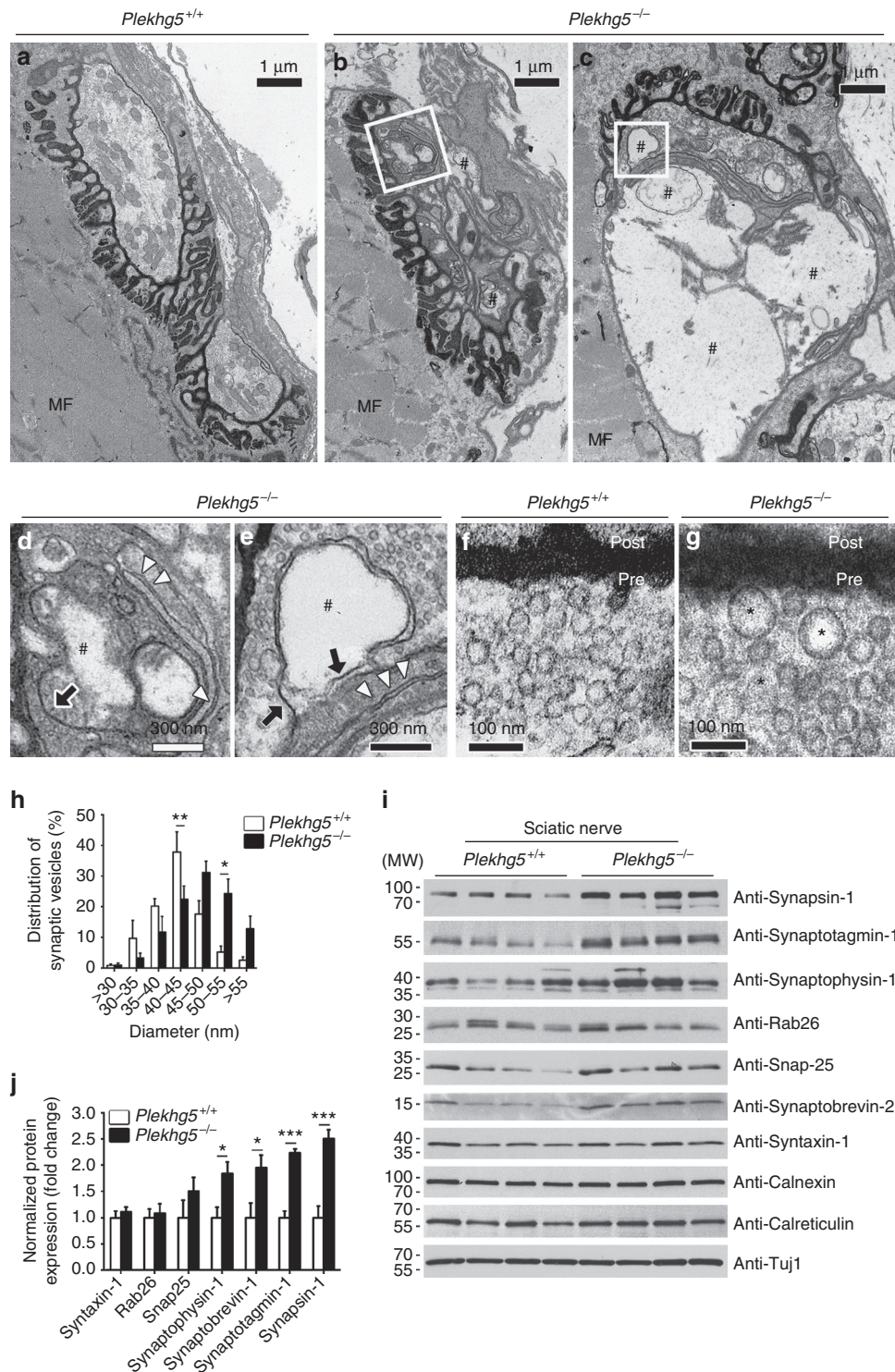
Fig. 3 Structural alterations and accumulation of synaptic vesicle proteins in Plekhg5-deficient mice. **a–c** Neuromuscular junction of *Plekhg5*^{+/+} **a** and *Plekhg5*^{−/−} **b**, **c** mice. # labels empty inclusions. *MF* myofibers. *Scale bar*: 1 μm. **d** Membrane fragments in nerve terminals of Plekhg5-deficient mice. *Scale bar*: 300 nm. **e** Double membrane fragment forming an inclusion. Arrow points to single membrane. Arrowheads point to double membrane structures. # labels inclusions. *Scale bar*: 300 nm. **f**, **g** Synaptic vesicles in Plekhg5-deficient mice **g** appear frequently enlarged, in contrast to synaptic vesicles in wild-type mice **f**, which appear smaller and more uniform in size. Asterisks label enlarged synaptic vesicles. *Scale bar*: 100 nm. **h** Quantification of synaptic vesicle diameter. (Synaptic vesicles of five NMJs were analyzed per genotype. Mean ± SEM; two-way ANOVA; Bonferroni post-test). **i** Expression of several synaptic vesicle markers in sciatic nerve lysates of four mice per genotype. **j** Quantification of western blot analysis. Mean ± SEM; two-way ANOVA; Bonferroni post-test). Images have been cropped for presentation. Full size images are presented in Supplementary Fig. 7
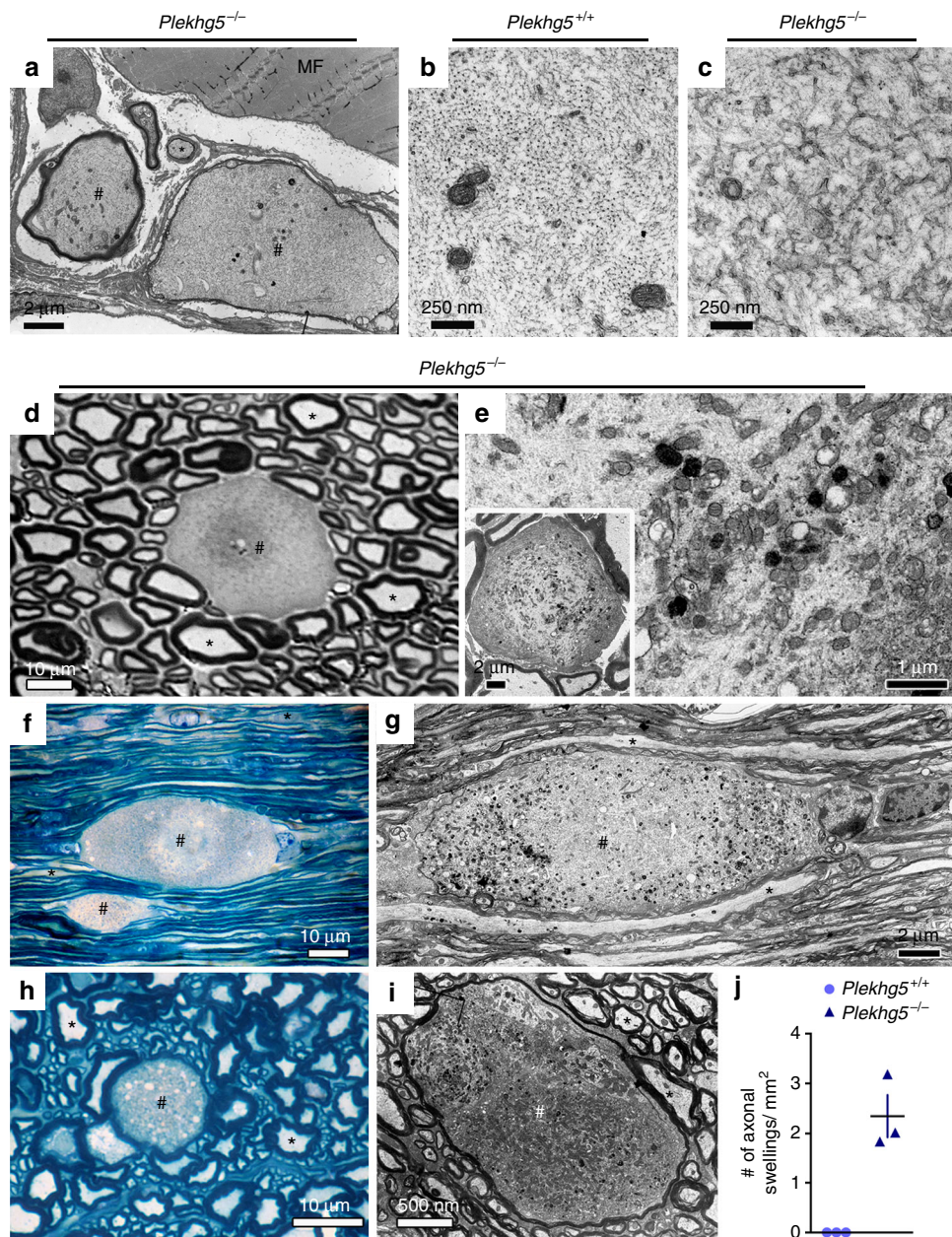
Fig. 4 Loss of Plekhg5 impairs axonal integrity. **a** Swellings in distal motor axons. MF, muscle fiber. *Scale bar*: 2 μm. **b**, **c** High magnification micrographs of axons from wild-type **b** and Plekhg5-deficient **c** mice with altered cytoskeleton organization in *Plekhg5$^{-/-}$* mice. *Scale bar*: 250 nm. **d** Semi-thin cross-section of sciatic nerve from Plekhg5-deficient mice showing an axonal swelling. *Scale bar*: 10 μm. **e** High magnification micrograph of an axonal swelling from sciatic nerve. *Scale bar*: 1 μm. *Inset, Scale bar*: 2 μm. **f–i** Longitudinal- **f**, **g** and cross- **h**, **i** sections of lumbar spinal cord showing axonal swellings within the white matter of *Plekhg5$^{-/-}$* mice. **f**, **h** *Scale bar*: 10 μm. **g**, **i** Fine structure of axonal swellings in spinal cord white matter of Plekhg5-deficient mice. # labels axon swellings; asterisks label axons with unaltered morphology. **g** *Scale bar*: 2 μm. **h** *Scale bar*: 10 μm. **i** *Scale bar*: 500 nm. **j** Quantification of axonal swellings in spinal cord semi-thin cross-sections. Three animals per genotype were analyzed. Each *data point* represents the mean of 10 sections from individual animals with a distance of 100 μm between each section

dysregulated autophagy causes the accumulation of synaptic vesicles at nerve terminals we examined the autophagic flux in Plekhg5-deficient motoneurons (Fig. 5). Since autophagosomes rapidly fuse with lysosomes, changes in the biogenesis of autophagosomes are hardly detectable under basal conditions[26, 27]. Therefore, cultured motoneurons were transduced with lentiviruses expressing GFP-RFP-LC3 and treated with bafilomycin A1 after 7 days in culture (Fig. 5a–c). Bafilomycin A1 blocks the fusion of autophagosomes and lysosomes resulting in an enrichment of LC3-II positive autophagosomes. Since fusion of autophagosomes and lysosomes quenches the fluorescence of

GFP, RFP positive structures selectively mark autolysosomes, whereas autophagosomes appear positive for both RFP and GFP[27]. Under basal conditions we detected no difference in the number of autophagosomes and autolysosomes in the soma of wild-type and *Plekhg5$^{-/-}$* cells. However, upon treatment with bafilomycin A1 Plekhg5-deficient cells displayed a significantly reduced number of autophagosomes in comparison to wild-type motoneuron somata (Fig. 5a, b). In axons of *Plekhg5$^{-/-}$* motoneurons, a reduced number of autophagosomes was detected in both untreated cells and bafilomycin A1 treated cells (Fig. 5a, c). In agreement with previous reports we only identified very few

autolysosomes in axons of cultured motoneurons, confirming that full maturation of autophagosomes to lysosomes mostly occurs within or close to the soma[1, 26]. The number of autolysosomes was not altered indicating that acidification of autolysosomes, as a late step of maturation, was unaffected (Fig. 5a–c). To examine whether Plekhg5 deficiency causes impaired axonal transport of autophagosomes, motoneurons were transduced with RFP-GFP-LC3, and the movement of GFP-LC3^{+} structures was analyzed (Fig. 5d–f). $Plekhg5^{-/-}$ motoneurons showed a reduced number of autophagosomes

moving retrogradely towards the soma (Fig. 5f), whereas the relative number of retrogradely moving autophagosomes appeared unaltered (Fig. 5e; Supplementary Movie 1, 2). Reduced protein levels of endogenous LC3-II were also biochemically detected in Plekhg5-deficient neurosphere-derived neurons upon treatment with bafilomycin A1 by western blotting (Fig. 5g, h). This reduction of LC3-II levels was also apparent in spinal cord extracts of 24-month-old mice (Fig. 5i, j). Taken together, these data emphasize that the biogenesis of autophagosomes is impaired in Plekhg5-deficient motoneurons
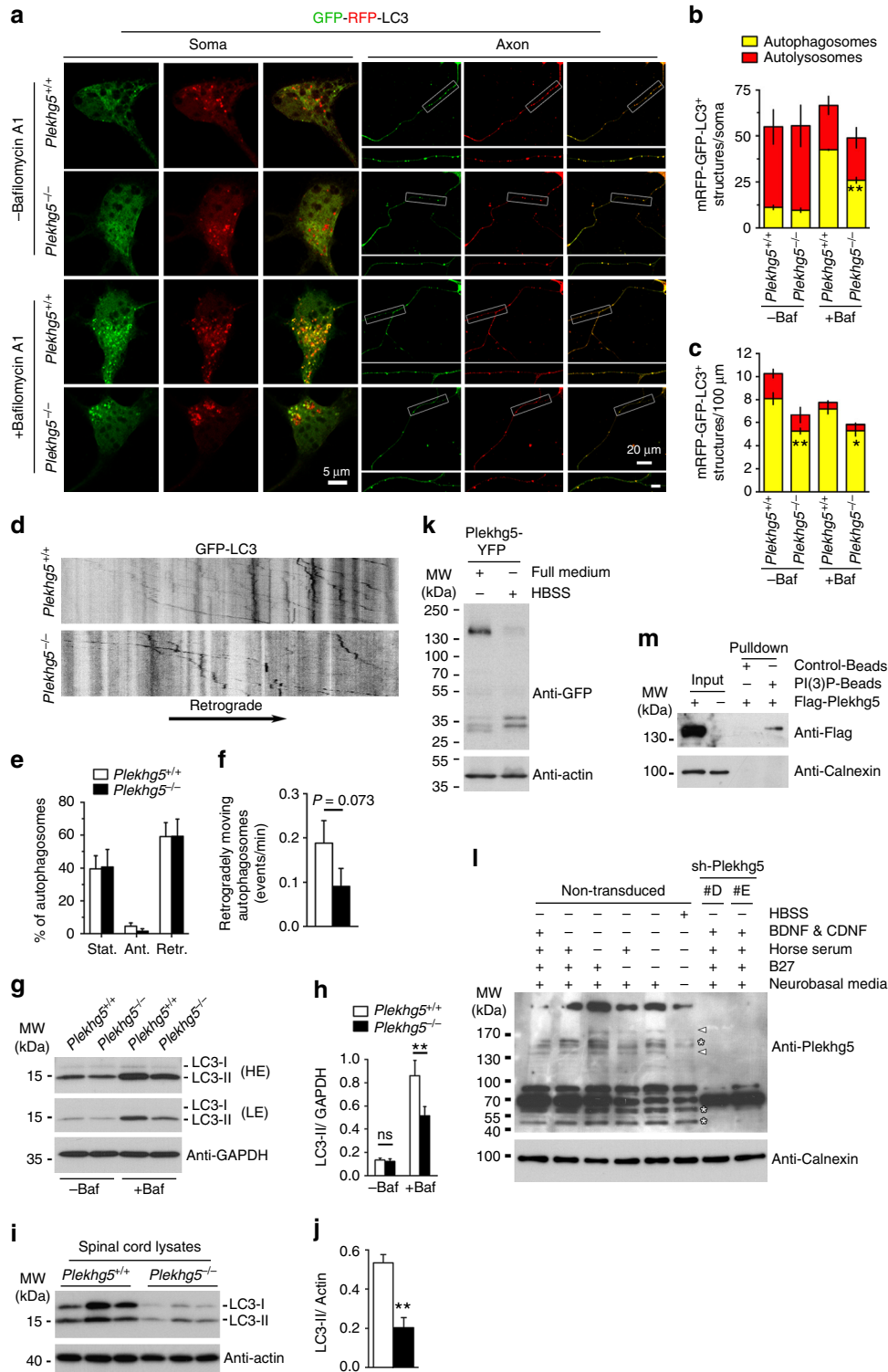
resulting in a reduced number of retrogradely transported autophagosomes. The remaining autophagosomes are transported normally.

An essential process for autophagosome formation is the production of phosphatidylinositol 3-phosphate (PI(3)P) by phosphatidylinositol-3-kinase class III at preautophagosomal membranes[28]. Pleckstrin homology (PH) domains form a conserved family that mediates protein association to inositol lipids like PI(3)P. We analyzed whether Plekhg5 binds to PI(3)P using extracts from mouse motoneuron-like hybrid cells (NSC34) expressing Flag-tagged Plekhg5. We could precipitate Plekhg5 with PI(3)P-coated beads but not with control beads (Fig. 5m) suggesting that Plekhg5 is able to associate with PI(3)P at preautophagosomal membranes[28]. For monitoring the fate of Plekhg5 upon induction of autophagy, Plekhg5-YFP transfected NSC34 cells were starved for 4 h in HBSS and the expression of Plekhg5-YFP was analyzed by western blot (Fig. 5k). In contrast to a marked reduction of full-length Plekhg5-YFP, the signal for smaller protease-resistant YFP-positive fragments increased (Fig. 5k). Nutrient deprivation differently affects cell lines and primary neurons. Therefore, we also performed this experiment with cultured motoneurons by replacing enriched motoneuron-media with different media each deprived of specific nutrient components (Fig. 5l). As observed in NSC34 cells, nutrient deprivation resulted in degradation of Plekhg5. In contrast to overexpressed Flag-Plekhg5, endogenous Plekhg5 appeared as multiple bands that were differently affected by nutrient deprivation (Fig. 5l). The identity of the bands that were detected by western blot analysis was controlled by sh-RNA-mediated knockdown of Plekhg5 (Fig. 5l; Supplementary Fig. 5a, b). In summary, these experiments suggest that Plekhg5 is able to bind PI(3)P, placing Plekhg5 to the inner autophagosomal membrane. This idea is further supported by the degradation of Plekhg5 upon autophagy induction. Fusion of autophagosomes with lysosomes results in digestion of proteins in the lumen of the autophagosome including proteins localized to the inner autophagosomal membrane[29].

Next, we determined whether impaired autophagy affects survival and/or morphology of Plekhg5-depleted motoneurons in vitro. Plekhg5-depleted motoneurons grew shorter axons, whereas cell survival and dendritic complexity was not affected (Fig. 6a, b; Supplementary Fig. 5). In order to find out how altered autophagy leads to axonal growth defects, we characterized the morphology of axon terminals in Plekhg5−/− motoneurons. Growth cones of cultured Plekhg5−/− motoneurons appeared atrophic with a significantly smaller size and with dysmorphic densely packed accumulation and clustering of synaptophysin-positive synaptic vesicles leading to a reduced number of F-actin filaments (Fig. 6c, d). We next looked at the expression pattern

of Rab26 in axons of cultured motoneurons. Rab26 is a small GTPase enriched on synaptic vesicles designated for delivery to preautophagosomal structures[15]. In its GTP-bound form Rab26 is an effector of Atg16L leading to recruitment of the autophagy machinery to synaptic vesicles. In Plekhg5-deficient cells Rab26-positive structures accumulate in regions directly at active zones, in contrast to wild-type motoneurons where these structures are found in more proximal areas of axonal growth cones (Fig. 6c, d).

To examine these morphological alterations in more depth, we performed SIM microscopy (Fig. 6e). These high-resolution images confirmed the data obtained by confocal microscopy providing additional evidence that the number of Rab26-positive vesicles increased, and the actin cytoskeleton disorganized (Fig. 6e). These findings support the in vivo structural analyses demonstrating marked alterations in cytoskeletal structures (Fig. 4b, c), which might cause the defect in axon growth.

Plekhg5 functions as a GEF for Rab26. Activation of GTPases requires dissociation of protein-bound GDP, an intrinsically slow process that is accelerated by specific GEFs[30]. To explore whether Plekhg5 regulates the activity of Rab26, neurosphere-derived cortical neurons were transduced with EGFP-Rab26 and labeled with ^{32}P for 4 h. Subsequently, EGFP-Rab26 was immunoprecipitated and GTP- or GDP-bound Rab26 was separated by thin layer chromatography (TLC) (Fig. 7a), revealing a significantly reduced GTP/GDP ratio (Fig. 7b). Next, we asked whether Plekhg5 is able to directly act as a GEF for Rab26 in a cell-free system (Fig. 7c–h). Using homogenously purified recombinant proteins we analyzed the ability of Plekhg5 to catalyze GDP dissociation of Rab26 and observed a marked acceleration of GTP exchange in the presence of the DH-PH (Dbl-homologous-Pleckstrin homology) tandem domain of Plekhg5 for Rab26 (Fig. 7g, h), but not for Rab5, Rab27b, or Rab33b (Fig. 7d–f). These data demonstrate that Plekhg5 acts as a GEF for Rab26.

We then followed this line of experiments and tested wild-type and a constitutively active form of Rab26, Rab26Q123L (Rab26-QL), in cultured motoneurons (Fig. 8). As previously described, wild-type EGFP-Rab26 accumulated in vesicles within axons[15]. In Plekhg5-deficien motoneurons, the size of these vesicles was significantly reduced (Fig. 8a, c), and the number of EGFP-Rab26 vesicles was also modestly reduced (Fig. 8a, d). With constitutive active EGFP-Rab26, the number and size of these vesicles normalized and no differences between wild-type and Plekhg5-deficient cells were detectable (Fig. 8a, c, d). In correlation with these findings, EGFP-Rab26-QL also fully restored axon growth

---

Fig. 5 Plekhg5 regulates biogenesis of autophagosomes. **a** Motoneurons of Plekhg5+/+ and Plekhg5−/− mice were transduced with mRFP-GFP-LC3-expressing lentiviruses and cultured for seven days. At day seven cells were treated with Bafilomycin A1 for four hours or left untreated and the number of autophagosomes (mRFP+-GFP+-LC3) and autolysosomes (mRFP+-GFP−-LC3) was determined in the soma **b** and axon **c** (three independent experiments with 15 cells analyzed in each experiment; mean ± SEM; two-way ANOVA; Bonferroni post-test). Soma, scale bar: 5 μm. Axon, scale bar: 20 μm. Axon (blow up), scale bar: 5 μm. **d** Representative kymographs of autophagosome motility. Cultured motoneurons were transduced with mRFP-GFP-LC3 and the movement of GFP positive punctae in axons was monitored for 20 min. **e** Proportion of retrogradely, anterogradely or stationary/bidirectionally moving autophagosomes (mean ± SEM; n = 10 cells; two-way ANOVA; Bonferroni post-test). **f** Number of retrogradely moving autophagosomes per minute (mean ± SEM; n = 10 cells; Student's t-test; one-tailed). **g** Western blot analysis of LC3 expression in neurosphere-derived cortical neurons from control and Plekhg5-deficient mice. Cells were treated with 400 nM Bafilomycin A1 for 4 h or left untreated. LE low exposure, HE high exposure. **h** Quantification of LC3 western blots. (Mean ± SEM; n = 3; mean ± SEM; one-way ANOVA). **i** Expression of LC3 in spinal cord lysates of three mice per genotype. **j** Quantification of LC3 Western blots from spinal cord extracts. (mean ± SEM; n = 4; mean ± SEM; Student's t-test; two-tailed). **k** NSC34 cells were transfected with Plekhg5-YFP. Seventy-two hours after transfection, cells were starved for 4 h in HBSS or left untreated. The expression of Plekhg5-YFP was analyzed by western blot. **l** Motoneurons were cultured for seven days in motoneuron-media. At day seven cells were cultured for 4 h with different media each deprived of specific components. Subsequently, motoneurons were lysed and the expression of endogenous Plekhg5 was analyzed by western blot. Asterisks label bands that do not change upon nutrient deprivation. Arrowheads point to bands that change upon nutrient deprivation. **m** NSC34 cells were transfected with Flag-Plekhg5. Seventy-two hours after transfection, cells were lysed and Flag-Plekhg5 was pulled-down with PI(3)P-coated beads. Western blot images have been cropped for presentation. Full size images are presented in Supplementary Fig. 7
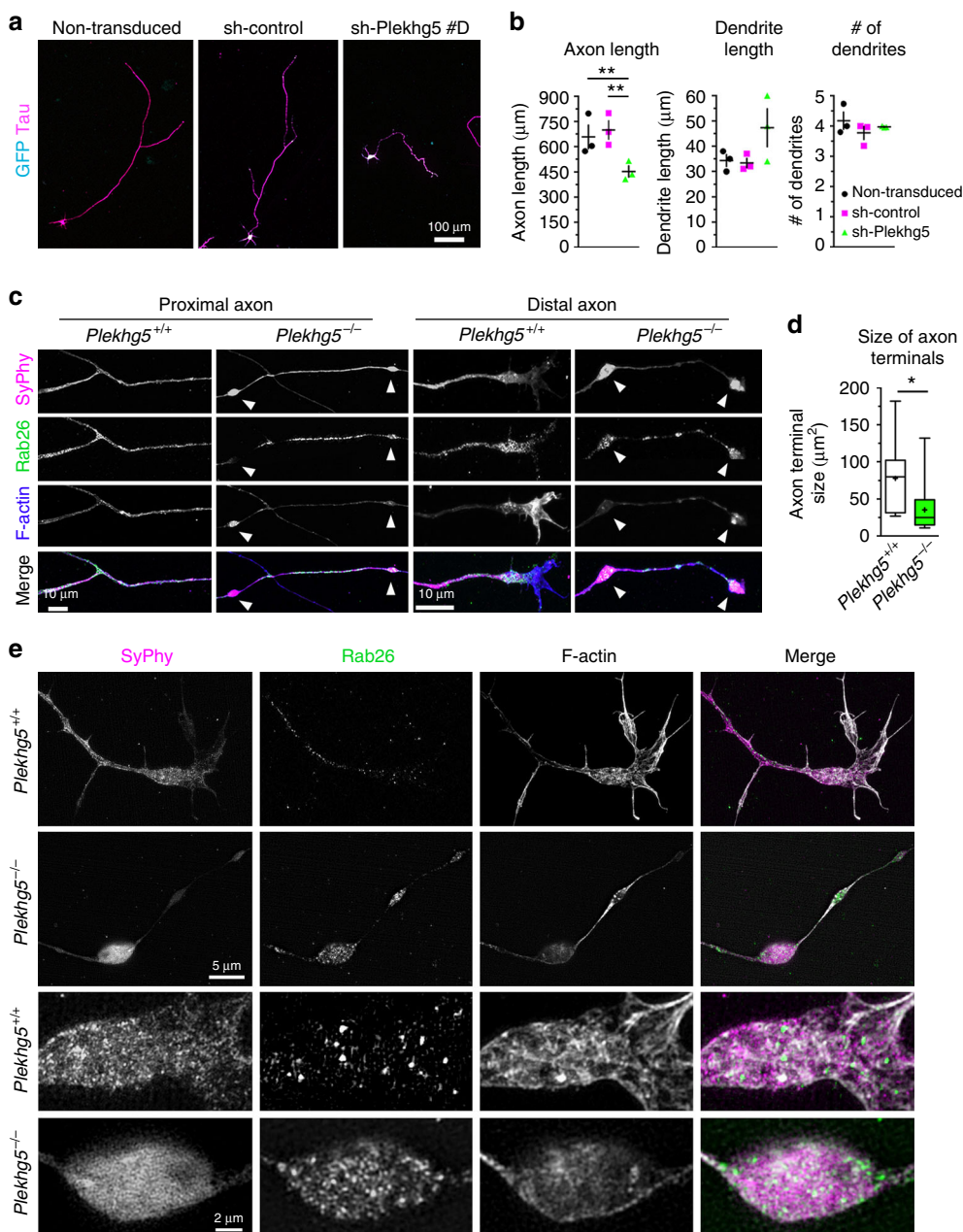
Fig. 6 Depletion of Plekhg5 results in axon growth defects and degeneration of axon terminals in vitro. **a** Motoneurons were transduced with sh-control or sh-Plekhg5 #D lentiviruses or left untreated. *Scale bar*: 100 μm. **b** Seven days after sh-RNA transduction, knockdown of Plekhg5 reduced axon length, whereas dendrite length and number of dendrites were not affected. Each data point represents the mean of one individual experiment with at least 20 cells analyzed. One-way ANOVA, Bonferroni post-test. **c–e** Motoneurons were cultured for seven days and stained for synaptophysin, Rab26 and F-actin and imaged by confocal **c** and SIM microscopy **e**. **c** *Scale bar*: 10 μm. **d** Quantification of axon terminal size ($n = 15$ cells; unpaired t-test; two-tailed). **e** Motoneurons were cultured for 7 days and stained for synaptophysin, Rab26 and F-actin and imaged by SIM microscopy. Axons of Plekhg5$^{-/-}$ motoneurons display synaptophysin positive swellings. *Scale bar*: 10 μm. *Scale bar* (*blow up*): 2 μm

defects of Plekhg5-deficient motoneurons (Fig. 8b, e). In contrast, EGFP-Rab26-QL only moderately enhanced axon growth in wild-type cells (Fig. 8b, e).

In order to study the effects of constitutive Rab26 on axonal autophagy, we constructed lentiviral vectors that simultaneously express RFP-GFP-LC3 and Flag-Rab26-WT or Flag-Rab26-QL (Fig. 8f, g), respectively. We then quantified the number of RFP-GFP-LC3 positive structures in proximal axons and found that the number of autophagosomes was reduced in Plekhg5-deficient motoneurons (Fig. 8h, i). This reduction did not occur in Plekhg5$^{-/-}$ motoneurons expressing constitutive active Rab-QL (Fig. 8h, i). In agreement with the data shown in

Fig. 5a–c, the number of autolysosomes remained unaltered. These data confirm the conclusion that Plekhg5 acts as a GEF for Rab26 and contributes to autophagosome biogenesis.

Plekhg5 modifies ER-stress in SOD1 G93A motoneurons. Protein misfolding and endoplasmatic reticulum (ER) stress is a common disease mechanism in different models of motoneuron disease[31–36]. Deficiency of global autophagy in neurons results in an impairment of proteostasis characterized by accumulation of polyubiquitinated proteins in inclusion bodies[8, 9]. Plekhg5-deficient mice did not show any accumulation of
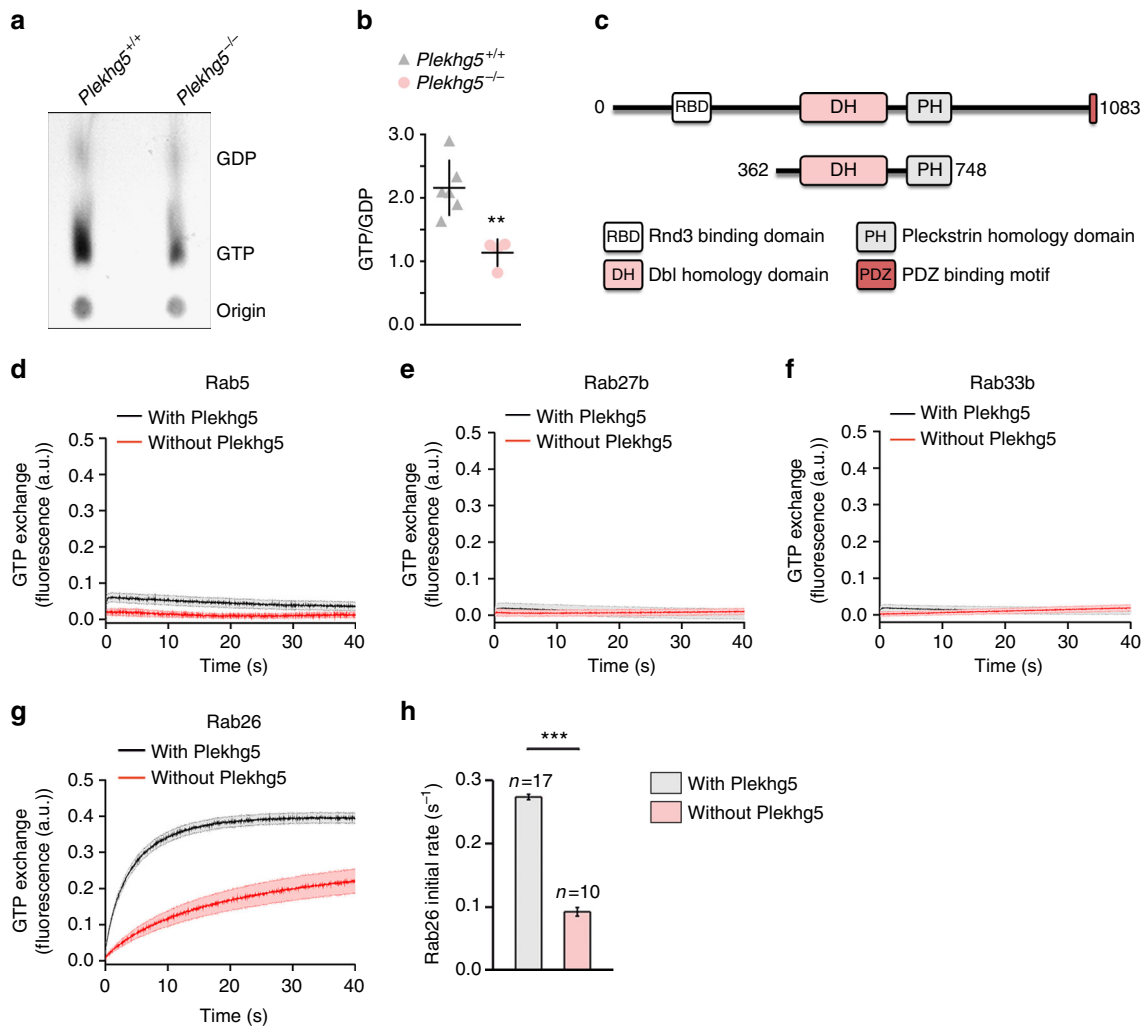
Fig. 7 Plekhg5 functions as a GEF for Rab26. **a** Neurosphere-derived cortical neurons were transduced with EGFP-Rab26 and labeled with P^{32} for 4 h. EGFP-Rab26 was immunoprecipitated and GTP- or GDP-bound Rab26 was separated by TLC. **b** Densitometric quantification of GTP/GDP ratios (each *data point* represents one independent experiment. Mean ± SEM; unpaired *t*-test; two-tailed). **c–h** Exchange activity of Plekhg5 on different GTPases. **c** Scheme of the DH-PH tandem domain, which was purified and used for the biochemical assays. Exchange activity of Plekhg5 on Rab5 **d**, Rab27b **e**, Rab33b **f**, and Rab26 **g** was measured by monitoring the fluorescent increase of Mant-GppNHp upon binding to Rab proteins. **g** The initial GTP exchange rate of Rab26 was evaluated using the first 10 s of each time course. (Mean ± SEM; Student's *t*-test; two-tailed)

polyubiquitinated proteins at axon terminals or in motoneuron cell bodies as shown by immunohistochemical staining (Supplementary Fig. 6a, b). In addition, we were not able to detect any differences in the levels of polyubiquitinated proteins by western blotting (Supplementary Fig. 6c). In contrast, the levels of Chop and IRE1α were markedly elevated in *Plekhg5*$^{-/-}$ spinal cord extracts (Fig. 9c, d). Thus, the unfolded protein response (UPR) seems to be activated in Plekhg5-deficient mice. We also tested the expression levels of heat shock protein family members HSP70 and HSP90 and the ER chaperone Calreticulin by western blot analyses and found significantly decreased expression of all three chaperones (Fig. 9a, b). Together, these data suggest that Plekhg5 deficiency results in ER-stress without affecting the turnover of polyubiquitinated proteins.

In order to investigate the relevance of impaired synaptic vesicle autophagy for motoneuron vulnerability in a well-characterized model of ALS we depleted Plekhg5 in SOD1 G93A motoneurons in vitro (Fig. 9e–g). We analyzed the effect of Plekhg5 knockdown with two independent sh-RNA lentiviral constructs on embryonic SOD1 G93A motoneurons and investigated ER-stress as a pathogenic mechanism. ER-stress

precedes disease onset in SOD1 transgenic mice[37] and modulation of the UPR has been shown to modulate disease onset and progression in SOD1 transgenic mice[38, 39]. PERK phosphorylation, BIP expression and Chop activation were enhanced in a supra-additive manner in SOD G93A motoneurons with additional Plekhg5 depletion (Fig. 9e, f). Upon knockdown of Plekhg5, SOD1 G93A motoneurons also showed a decrease in survival (Fig. 9g). Interestingly, this effect was observed in embryonic motoneurons representing a developmental stage long before disease becomes apparent in vivo. We did not observe any significant changes in the levels of endogenous and transgenic SOD1 when Plekhg5 is depleted (Fig. 9e, f). Therefore, Plekhg5 is not involved in the degradation of the mutant SOD1 protein. These data indicate that both disease mechanisms have additive effects, cumulating in an elevated load of ER-stress.

Discussion

In summary, our data show that Plekhg5 functions as a GEF for Rab26, and thus regulates autophagy of synaptic vesicles in axon terminal of motoneurons. Disruption of this process leads
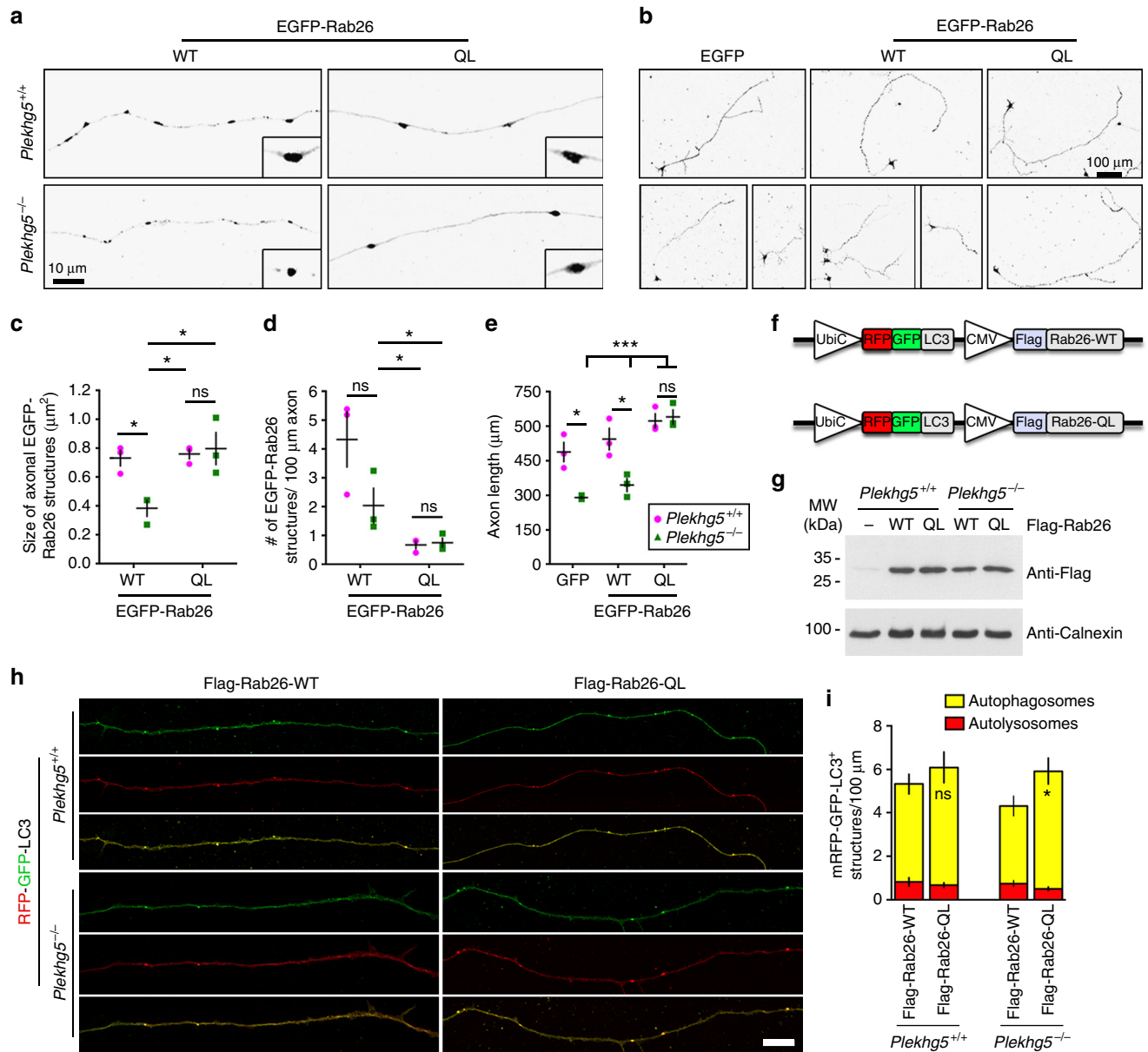
Fig. 8 Expression of constitutively active Rab26 rescues axonal growth and autophagy defects in Plekhg5-deficient cells. **a** Representative images of GFP-Rab26-WT or GFP-Rab26-QL positive structures in axons of control cells and Plekhg5-deficient cells. *Scale bar*: 10 μm. **b** Morphology of GFP, GFP-Rab26-WT or GFP-Rab26-QL expressing motoneurons cultured for 7 days. *Scale bar*: 100 μm. **c, d** Size and number of axonal EGFP-Rab26 structures. **e** Axon length of GFP, GFP-Rab26-WT, or GFP-Rab26-QL expressing motoneurons isolated from *Plekhg5*^{+/+} and *Plekhg5*^{−/−} mice (each *data point* represents one individual experiment with 15 cells analyzed in each experiment; mean ± SEM; two-way ANOVA). **f** Scheme of lentiviral vectors for simultaneous expression of RFP-GFP-LC3 and Flag-Rab26-WT or Flag-Rab26-QL, respectively. **g** Western blot analysis of Flag-Rab26-WT and Flag-Rab26-QL expression. Images have been cropped for presentation. Full size images are presented in Supplementary Fig. 7. **h** Motoneurons of *Plekhg5*^{+/+} and *Plekhg5*^{−/−} mice expressing mRFP-GFP-LC3 and Flag-Rab26-WT or Flag-Rab26-QL were cultured for 7 days and the number of mRFP-GFP-LC3 positive structures was analyzed. *Scale bar*: 10 μm. **i** Number of autophagosomes and autolysosomes upon expression of Flag-Rab26-WT and Flag-Rab26-QL (three independent experiments with 10 cells analyzed in each experiment; mean ± SEM; two-way ANOVA; Bonferroni post-test)

to enlarged synaptic vesicles and accumulation of synaptic proteins resulting in dysfunction of neuromuscular junctions and motoneuron disease.

Our data suggest that Plekhg5 associates with PIP(3) on preautophagosomal membranes and regulates the activity of Rab26 by exchanging GDP to GTP. The observation that Plekhg5 does not regulate Rab5, Rab27b, or Rab33b activity suggests relative specificity, but does not exclude the possibility that Plekhg5 could also regulate the activity of other small GTPases. However, the observation that constitutively active Rab26 rescues

the phenotype in Plekhg5-deficient motoneurons suggests that the GEF activity for Rab26 is central for altered autophagy of synaptic vesicles in motoneurons. In its GTP-bound form Rab26 recruits Atg16l to synaptic vesicles for initiating the delivery of synaptic vesicles to autophagosomes. Two previously identified interaction partners of Plekhg5, Synectin[13], and the 14-3-3γ-protein[40], are involved in autophagy regulation[41, 42]. Both proteins have been described to interact with PI(3)P-kinase, resulting in the inhibition of autophagy biogenesis. The 14-3-3γ-protein acts as a scaffold that inhibits the activity of PI(3)P-kinase. In the

same manner, the 14-3-3γ-protein inhibits the GEF activity of Plekhg5. Furthermore, protein kinase D mediated phosphorylation of Ser92 at the N-terminus of Plekhg5 prevents the interaction between these proteins[40]. It is tempting to speculate

that phosphorylation of Plekhg5 is the upstream signal to release 14-3-3γ protein from the complex with Plekhg5 and probably also from PI(3)P-kinase. This might result in initiation of autophagy and activation of Rab26.
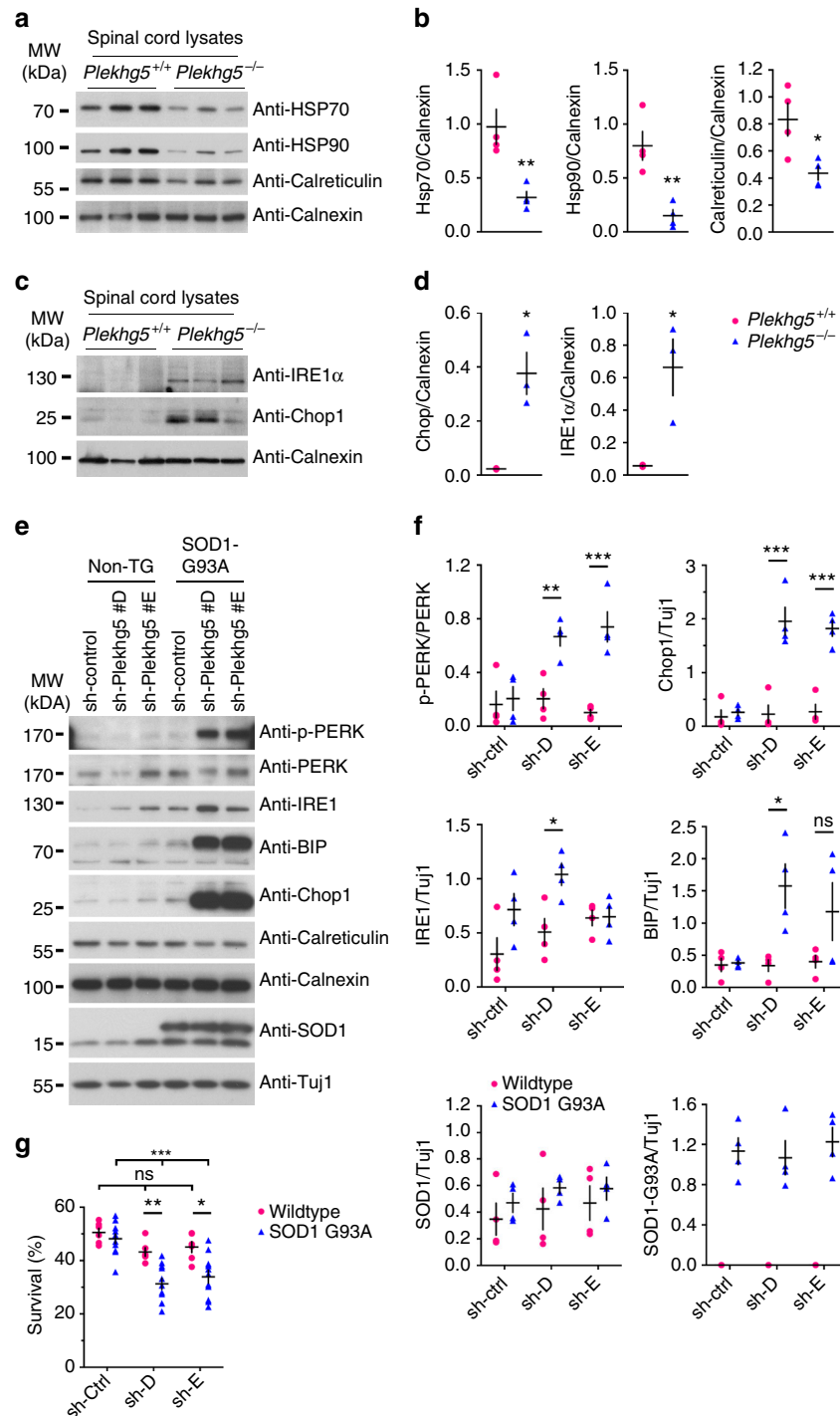

Fig. 9 Plekhg5 depletion in SOD1 G93A motoneurons results in elevated ER-stress. **a** Expression of HSP70, HSP90, Calreticulin, and Calnexin in spinal cord lysates from three animals per genotype. **b** Quantification of western blot shown in **a** (each *data point* represents expression levels of one animal; unpaired *t*-test; two-tailed). **c** Expression of IRE1α and Chop1 in spinal cord lysates from three animals per genotype. **d** Quantification of western blot shown in **c** (each *data point* represents expression levels of one animal; unpaired *t*-test; two-tailed). **e** SOD1 G93A and non-transgenic motoneurons were depleted of Plekhg5 and several ER-stress markers were examined after 7 days in culture. **f** Quantification of western blots shown in **e** (each *data point* represents one individual experiment; mean ± SEM; unpaired *t*-test; two-tailed). **g** Survival of SOD1 G93A motoneurons decreased upon knockdown of Plekhg5 using two independent sh-RNA constructs (each *data point* represents the % of motoneuron-survival from one individual embryo. At least 50 motoneurons were evaluated from one embryo; mean ± SEM; two-way ANOVA; Bonferroni post-test). Images have been cropped for presentation. Full size images are presented in Supplementary Fig. 7

Deficiency of global autophagy in neurons results in an impairment of proteostasis characterized by accumulation of polyubiquitinated proteins in inclusion bodies[8, 9]. Our data suggest that Plekhg5 deficiency does not impair global protein homeostasis indicating that the defect in $Plekhg5^{-/-}$ mice is restricted to synaptic vesicles and does not involve misfolding or aggregation of cytosolic proteins. Thus, $Plekhg5^{-/-}$ mice represent a model of motoneuron disease without poly-ubiquitinated protein inclusion in which defective autophagy of synaptic vesicles stands in the center of the pathophysiology. Such cases of motoneuron disease without polyubiquitinated inclusions have been described[43] and they seem to correlate with forms of motoneuron disease with prolonged survival, or with unusual familial cases of progressive muscular atrophy[43].

NMJs might be particularly vulnerable to defects in synaptic vesicle turnover due to their large presynaptic size and large number of synaptic vesicles compared to other synapses[44]. This idea is supported by the lack of behavioral deficits in Plekhg5-deficient mice and by the relatively preserved morphology of synapses in hippocampus, cerebral cortex and cerebellum.

Azzedine et al.[19] had previously characterized Plekhg5-deficient mice until 12 months of age, and had not detected motoneuron loss at this stage. In our model, symptoms of motoneuron disease did not start before 12 months (Fig. 1c, e–g). Furthermore, motoneuron loss was not detectable before 12 months of age, and it progresseed until 24 months (Fig. 1d). Therefore, it is possible that motoneuron loss would have become apparent in the model described by Azzedine et al.[19] in mice older than 12 months. Furthermore, different strategies for generation of the null-allele could contribute to the severity of disease. The model described by Azzedine et al.[19] had been generated by insertion of loxP sites flanking exon 9–13. Excision of this target region results in a truncated protein lacking the RhoGEF domain but still containing the PH domain. In our model, the protein lacks both domains.

Our findings add to previous reports that neuron-specific disruption of autophagy by depletion of $Atg5$ or $Atg7$ results in progressive degeneration of motoneurons[8, 9] and that missense mutations in the autophagy receptors p62/SQSTM1 and opti-neurin are causative for ALS[45, 46]. Both proteins are substrates of Traf family member-associated NF-kappa-B activator (TANK)-binding kinase 1 (TBK1). Upon phosphorylation, p62/SQSTM1 and optineurin are recruited to mitochondria during PTEN-induced putative kinase protein 1 (PINK1)/Parkin-mediated mitophagy[47], a mechanism implicated in the pathogenesis of Parkinson's disease[48]. Previous reports on $TBK1$ mutations in ALS[49, 50] and the recently identified interaction of the putative Rab GTPase GEF chromosome 9 open reading frame 72 (C9ORF72) with WD repeat-containing protein 41 (WDR41) and Smith-Magenis syndrome chromosomal region candidate gene 8 protein (SMCR8)[51] support the idea that impaired autophagy could make major contributions to the pathophysiology of motoneuron disease. Our study provides a first mechanism to explain how autophagy of synaptic vesicles is regulated in axon terminals of motoneurons and adds further weight to the hypothesis that dysregulated autophagy constitutes a major pathogenic mechanism in motoneuron disease.

Methods

Statistics. Whiskers in box–whisker plots show minima and maxima. Boxes extend from the first to the third quartiles with cross lines at the median. Means are depicted by plus signs. In dot plots, dots represent individual experiments with cross lines at the mean ± SEM. When comparing two groups, statistics were performed using two-tailed Student's t-tests for unpaired samples assuming unequal variance. When comparing multiple groups, one-way ANOVA or two-way ANOVA (grouped analysis) was performed. P values below 0.05 were considered significant (*$P < 0.05$; **$P < 0.01$; ***$P < 0.001$). For multiple comparisons of individual groups, the Bonferroni post-test was performed. No statistical tests were used to predetermine sample sizes, but our sample sizes are similar to those generally employed in the field. Normal distribution of data was assumed, but not formally tested. All statistical analyses were performed using GraphPad Prism 6.00.

Generation of transgenic mice. To generate Plekhg5-deficient mice, embryonic stem cells (ESCs) with a disruption of one $Plekhg5$ allele from gene-trap clone E277F07 (cell line: E14TG2a.4 (ES cells 129P2 (formerly 129/Ola))) were injected into blastocysts of B6D2F2 (C58bl6/DBA2) mice[52] and transferred into pseudo-pregnant NMRI-foster mothers. Correct insertion site of the gene-trap cassette was verified by sequencing. Offspring were genotyped by PCR using the following primers: a 5′primer located in the intron upstream of the GT-Cassette (5′ TAAAAGCTGGCAGCCTGAAT 3′), a 3′ primer located in the GT-Cassette (5′ GCTAGCACAACCCCTCACTC 3′), and a 3′primer located in the intron downstream of the GT-Cassette (5′ ACCCCAAGGTCTGTCCTCTT 3′).

Mice were backcrossed for at least four generations onto C57Bl/6 background. Genders within genotypes were grouped, as differences between them were not statistically significant. The age of mice used for individual experiments is indicated accordingly throughout the results section.

This study was approved by the local veterinary authority (Veterinaeramt der Stadt Wuerzburg) and Committee on the Ethics of Animal Experiments, i.e., Regierung von Unterfranken, Wuerzburg (License number 55.2-2531.01-8/14).

RNA extraction and RT-PCR. Dissected tissues were frozen in liquid nitrogen and RNA was extracted using standard phenol–chloroform extraction. 1 µg of total RNA was treated with DNase I (Fermentas) and reverse transcribed with First Strand cDNA Synthesis Kit (Fermentas). cDNA was diluted 1:5 and 1 µl was subsequently used as template for RT-PCR reactions.

The following primers were used to validate gene-trap cassette functionality. According to www.ensemble.org, the murine Plekhg5 locus is can generate four different protein-coding transcripts. Specific 5′ primers were used for each transcript: Isoform 001 and 004: 5′ GAGCTACCCTCCCCAGACTC 3′ (ENSMUSE00000523883), Isoform 003: 5′ CTGCAGAGGAGAAGGGACTG 3′ (ENSMUSE00000594961), Isoform 002: 5′ GGTACCTAGAGGCCCGAAAC 3′ (ENSMUSE00000667027). A common 3′ primer was used for the wild-type-allele: 5′ GGTGCTGTGGAACTTGCTATC 3′ (ENSMUSE00000594961). The following 3′ primer was used to detect expression of the gene-trap-allele: 5′ GGCCTCTTCGCTATTACGC 3′.

Using 3′ primers specific for exons 6 and exon 9, we confirmed that insertion of the GT-cassette did not disturb the normal splicing pattern by altering the order of 5′exons or elimination of 5′ exons. The following 3′ primer specific to exon 6 (ENSMUSE00000594959) was used: 5′ GGCTGGCACAATTTCTGTTT 3′. The following 3′ primer specific to exon 9 (ENSMUSE00000594955) was used: 5′ GCAGAGAACAGCTGGAAGGT 3′.

Grip strength measurements. Force measurements were performed on a thin metal mesh connected to a force meter detecting forces within a range of 0–200 cN. Mice were suspended and allowed to hold on the grid, and, after they had grasped the grid using both paws, a force was applied to pull the mice from the grid. The force required to detach the mice from the grid was recorded, and the mean value from five attempts was taken as one data point and considered as the grip strength.

Nissl staining and quantification of spinal motoneurons. Mice were deeply anaesthetized and trans-cardially perfused with 4% PFA. 12.5 µm paraffin serial sections of the spinal cord were produced for Nissl staining, as described previously[53]. Cresyl violet intensively stains acidic structures within cells, and renders the nucleolus and the rough endoplasmic reticulum visible. Only motoneurons with a clearly distinguishable nucleolus, that had Nissl-stained rough endoplasmic reticulum-like structure in the cell body were counted in every tenth section of the lumbar spinal cord (L1–L8). Raw counts were corrected for double counting of split nucleoli as described[53].

Succinate dehydrogenase enzyme activity. Succinate dehydrogenase (SDH) stain was used to distinguish between oxidative and glycolytic fibers on 10 µm thick cryosections of tibialis anterior leg muscles. SDH staining was performed on fresh, untreated 10 µm cryosections that were incubated for 5 min in the dark at room temperature in standard SDH-substrate solution (0.2 M Na-succinat, 10 mM KCN, 10 mM nitro-blue tetrazolium, 2 mM phenazin methosulfate in phosphate buffer at pH 7.2). Reaction was stopped with 3,7% buffered formaldehyde. Stained sections were photographed under identical conditions.

Immunohistochemical staining of neuromuscular junctions. Staining of NMJs was carried out as previously described[54]. Briefly, mice were deeply anaesthetized and trans-cardially perfused with 4% paraformaldehyde (PFA). Subsequently, the muscles were dissected and post-fixed in 4% PFA for at least 2 hours. The tissue was washed in PBS-T (0.1% Tween-20) for 20 min at room temperature (RT) and incubated with ω-Bungarotoxin-Alexa-488 (Invitrogen) for 25 min at RT. The tissue was then incubated overnight at 4 °C with a blocking solution (2% BSA, 0.1%

Tween-20 and 10% donkey serum), followed by incubation with the primary antibodies for 3 days at 4 °C. After washing with PBS at pH 7.4 (PAA Laboratories) thrice for 15 min, the appropriate secondary antibodies were applied for 1 h at RT. The tissue was washed again as above, and embedded in Aqua Polymount (Polysciences). The following primary antibodies were used: anti-NF-H (1:5000; Millipore, AB5539), anti-Synaptophysin-1 (1:500; Synaptic Systems, 101 004). Alexa-647 and Alexa-546-conjugated secondary antibodies were from Jackson Immuno-Research Laboratories.

Immunofluorescence staining of free-floating sections. Mice were deeply anaesthetized and trans-cardially perfused with 4% PFA. After removal of the spinal cord, spinal cord was post-fixed in 4% PFA overnight and subsequently incubated in 30% sucrose at 4 °C overnight. Thirty-five micrometers of thick free-floating sections were cut on a Leica 9000 s sliding microtome as described previously[62] and collected in 0.1 M phosphate buffer (PB) pH 7.4. After incubation of the sections for 1 h with 4% normal goat or donkey serum and 0.3% Triton X-100 for blocking of nonspecific binding at room temperature, sections were incubated overnight at 4 °C with primary antibodies in blocking solution. After three times 10 min washing in 0.25% Triton X-100 in PB at room temperature, sections were incubated in with fluorescently labeled secondary antibodies, washed again and finally mounted with Mowiol/DABCO. The following primary antibodies were used: anti-NeuN (1:1000; Millipore, MAB377, clone A60), ChAT (1:1000; Millipore, MAB144P), anti-Ubiquitin (1:500; DAKO, Z0458), anti-Synaptophysin-1 (1:500; Synaptic Systems, 101 004). Alexa-647-, Alexa-488-, and Alexa-546-conjugated secondary antibodies were from Jackson Immuno-Research Laboratories. For visualization of F-actin Alexa Flour 532 conjugated Phalloidin (Invitrogen) was used.

Electron microscopy. Mice were anesthetized and trans-cardially perfused according to local institutional guidelines in 3 steps, slightly modified according to Forssmann et al.[55] with 3% paraformaldehyde, 3% glutaraldehyde, 0.5% picric acid in 0.1 M sodium phosphate buffer, pH 7.2 for 10 min. Dissected organs were fixed in the same solution for additional 1–2 h at 4 °C, post-fixed in buffered 2% osmium tetroxide (2.5 h, 4 °C), and embedded in Araldite.

To analyze the ultrastructure of NMJs, animals were trans-cardially perfused under deep anesthesia for 40 s with heparin/procaine followed by 2% formaldehyde and 4% glutaraldehyde in 0.1 M cacodylate buffer with 2 mM $MgCl_2$ and 3 mM $CaCl_2$ for 10 min. Dissected organs were further fixed for 2–4 h at 4 °C and post-fixed with 2% OsO_4 and 0.15% potassium hexacyanoferrate(III) to enhance visibility of the extracellular matrix.

For identification of target regions by optical microscopy, 1.5 µm-thick sections were stained with Richardson's blue (1% w/v methylene blue, 1% w/v Azur II) for 3 min at 80 °C. 60–80 nm sections (stained for 40 min in uranyl acetate and 8 min in lead citrate) were used for electron microscopy (Zeiss EM 109).

Primary motoneuron culture. Murine embryonic spinal motoneurons were isolated and cultured as described[56]. Briefly, after dissection of the ventrolateral part of E12.5 embryos, spinal cord tissues were incubated for 15 min in 0.05% trypsin in Hank's balanced salt solution. Cells were triturated and incubated in Neurobasal medium (Invitrogen), supplemented with 1× Glutamax (Invitrogen) on Nunclon plates (Nunc) pre-coated with antibodies against the p75 NGF receptor (MLR2, kind gift of Robert Rush, Flinders University, Adelaide, Australia) for 45 min. Plates were washed with Neurobasal medium, and the remaining motoneurons were recovered from the plate with depolarization solution (0.8% NaCl, 35 mM KCl and 2 mM $CaCl_2$) and collected in full medium (2% horse serum, 1× B27 in Neurobasal medium with 1× Glutamax). After counting, cell number was adjusted to 1000 in 100 µl, and 1000 cells were plated on four-well dishes (Greiner, Cellstar) pre-coated with poly-ornithine/laminin (Invitrogen). Cells were cultured in the presence of the neurotrophic factor BDNF. For survival assays, motoneurons were counted 4 h after plating to find the total number of plated cells. Cells were counted again after 5 and after 7 days in vitro (DIV).

For lentiviral transduction, motoneurons were incubated with viral particles for 10 min at RT directly before plating.

Culture of neurospheres. The forebrain was dissected from 11.5 to 12.5-day-old mouse embryos and transferred to 100 µl HBSS. After treatment with trypsin (Gibco; 0.05%, 15 min), cell suspensions were generated by trituration. Trypsin was inactivated with egg yolk sack trypsin inhibitor (Sigma; 0.05%), and cells were plated on 75 ml flasks (Greiner) in 5 ml Neurobasal medium (Invitrogen) containing Glutamax (1:100), B27 supplement (Invitrogen), basic fibroblast growth factor (bFGF), and epidermal growth factor (EGF) (Peprotech), each at a final concentration of 10 ng/ml. Cells were passaged at least once before being used in the first experiment. For differentiation, neurospheres were dissociated using 0.05% trypsin and plated on Poly-L-ornithine-coated dishes at a density of 20,000 cells per cm^2. One day after plating, cells were transferred to an EGF and bFGF-depleted medium, and cultured for the indicated time intervals.

Immunocytochemistry. For immunocytochemistry, cells grown on glass coverslips were fixed with buffered PFA for 20 min at RT, washed three times with PBS for 15 min, and blocked for 30 min with blocking buffer containing 10% donkey serum

and 0.3% Triton X-100 in TBST (TBS-Tween). After three washes with TBST for 5 min at room temperature, cells were incubated with primary antibodies overnight at 4 °C, followed by three washes in TBST at RT for 15 min, and then incubated with the appropriate fluorophore-conjugated secondary antibodies for 1 h. Subsequently, cells were washes three times with TBST for 15 min. The coverslips were mounted on glass slides with Aqua Polymount. Cells were imaged using an Olympus Fluoview 1000i confocal microscope. The following primary antibodies were used: anti-phospho-Tau (Ser199/202) (1:500; Sigma-Aldrich, T6819), anti-Rab26 (1:500; Synaptic Systems, 269 011, clone 163E12), anti-Synaptophysin-1 (1:500; Synaptic Systems, 101 004). Alexa-647-, Alexa-488- and Alexa-546-conjugated secondary antibodies were purchased from Jackson Immuno-Research Laboratories. For visualization of F-actin Alexa Flour 532 conjugated Phalloidin (Invitrogen) was used.

Plasmid construction. FUW-RFP-GFP-LC3 was generated by digestion of the FUWG plasmid by Xba and EcoRI, and the resulting 10 kB fragment was purified by gel extraction. pmRFP-GFP-rLC3[57] was digested by NheI and EcoRI, and the resulting insert was purified by gel extraction and cloned into the FUW backbone by ligation. The XbaI site was destroyed during cloning.

For generation of FUW-EGFP-Rab26-WT and FUW-EGFP-Rab26-QL[15], pEGFP-Rab26-WT, and pEGFP-Rab26-WT were digested by BamHI and NheI and the resulting fragments purified by gel extraction. Subsequently, both inserts were ligated into the BamHI and XbaI sites of FUWG.

For generation of FUW-mRFP-GFP-LC3-CMV-Flag-Rab26, pCMV-Tag2a-Flag-Rab26 was digested by SalI and the resulting CMV-Flag-Rab26 fragment was purified, blunted and phosphorylated. FUW-RFP-GFP-LC3 was digested by EcoRI and blunted. Subsequently, both fragments were ligated.

To generate Plekhg5 knockdown constructs, different short hairpin (sh)-sequences were synthesized as sense and antisense oligos, and cloned into the BamHI and EcoRI restriction sites of pSIH-H1-eGFP. The following sequences were validated for their ability to knockdown Plekhg5: sh-A: 5′ TCAAGTCGGTGCTAAGGAA 3′; sh-B: 5′ ATAGCAAGATGGACGTGTA 3′; sh-C: 5′ GGACACTATTTACAACGCA 3′; sh-D: 5′ GGACGAATCTT CTCTCAGT 3′; sh-E: 5′ CGCAAGAACATGTCTGAAT 3′. Sh-D was used in the experiments, if not indicated otherwise.

The DH-PH domain of Pleghg5 was generated by amplifying the coding DNA from cDNA of human Plekhg5 (BC042606) as a template using following primers (uppercase letters indicate gene-specific nucleotides): 5′ atctggttccgcgtggatccGATGGGCATGAGAAGCTG 3′, 5′ tcacgatgcggccgctcgagTCACTGTGCACGCAGCTG 3′. The PCR product was cloned into the pGEX-4T vector using the Gibson assembly kit (New England Biolabs) according to the manufacturer's protocol.

GST-hRab26WT and GST-mRab5WT were cloned into pGEX-2T as described.

Lentivirus production. Lentivirus was produced by co-transfecting HEK 293T cells with the indicated expression and packaging plasmids using Lipofectamine 2000 (Invitrogen). The medium was replaced 24 h after transfection and collected 24 h later. Subsequently, the virus was concentrated by ultracentrifugation.

Western blotting. Equal amounts of protein were separated by SDS-PAGE, and transferred to PVDF or nitrocellulose membranes (Pall). Membranes were blocked in TBST with 5% milk powder for 1 h at RT, probed with primary antibodies overnight at 4 °C, and incubated with horseradish peroxidase-conjugated secondary antibodies for 1 h at RT. The following primary antibodies were used: anti-LC3 (1:2000; Novus Biologicals, NB100-2220), anti-Calreticulin (1:8000; Thermo Scientific, PA1-902A), anti-Calnexin (1:8000; Enzo, ADI-SPA-860), anti-HSP90 (1:4000; Enzo, ADI-SPA-830-D, clone AC88), anti-HSP70 (1:2000; Cell Signaling, 4872 T), anti-BiP (1:2000; Cell Signaling, 3177P, clone C50B12), anti-CHOP (1:1000; Cell Signaling, 2895, clone L63F7), anti-PERK (1:1000; Sigma-Aldrich, P0074), anti-phospho-Perk (Thr980) (1:1000; Cell Signaling, 3179, clone 16F8), anti-Tuj1 (1:4000; Neuromics, MO15013), anti-Flag (1:10,000, Sigma-Aldrich, F7425), anti-Actin (1:8000; Millipore, MAB1501R), anti-Gapdh (1:8000; Calbiochem, CB1001, clone 6C5), anti-IRE1α (1:1000; Cell Signaling, 3294), anti-Ubiquitin (1:1000, Enzo, BML-PW0930, clone P4D1), anti-Rab26 (1:1000; Cell Signaling 269 011, clone 163E12), anti-Synaptophysin-1 (1:1000; Synaptic Systems, 101 004), anti-Synapsin-1 (1:4000; Synaptic Systems, 106 103), anti-Syntaxin 1A (1:1000; Synaptic Systems, 110 111, clone 78.3), anti-Synaptotagmin-1 (1:1000; Synaptic Systems, 105 011,clone 41.1), anti-Synaptobrevin-2 (1:1000; Synaptic Systems, 104 211, clone 69.1), anti-Snap 25 (1:1000, Synaptic Systems, 111 011, clone 71.1) Appropriate peroxidase-conjugated secondary antibodies were from Jackson Immuno-Research Laboratories.

Culture and transfection of NSC34 cells. NSC34 cells were cultured in Dulbecco's modified Eagle's medium (DMEM, Gibco) containing 10% FCS, 1× Glutamax and 1× Penicillin/Streptomycin and transfected with Turbofect (Life Technologies). For pull-down experiments, 1 day prior to transfection 2×10^6 cells were plated on 6 cm dishes and transfected using 8 µg plasmid and 24 µl Turbofect. For starvation experiments 1×10^6 cells were plated on six-well plates one day before transfection. The next day, cells were transfected using

4 µg plasmid and 12 µl Turbofect. Transfections were carried out according to the manufactures instructions. All subsequent assays were performed 72 h after transfection.

Lipid beads pull-down assay. Lipid beads pull-down assays were performed as described[58], with minor modifications. NSC34 cells transiently expressing Plekhg5-Flag were suspended in lipid-binding buffer (20 mM Tris-HCl, 150 mM NaCl, and 1 mM EDTA, pH 7.5). The cells were extruded 10 times through a G25 syringe needle and sonicated on ice. After removal of insoluble debris by high-speed centrifugation at 13,000×g for 1 h at 4 °C, a 50 µl slurry of PI(3)P-conjugated or unconjugated beads (Echelon Bioscience) was added to the tube and rotated for 2 h at 4 °C. After washing the rotating beads five times for 20 min at 4 °C with lipid-wash buffer (10 mM HEPES, pH 7.4, 150 mM NaCl, 0.25% NP-40), bound proteins were eluted by boiling in 2× Laemmli buffer.

Metabolic labeling, IP and thin layer chromatography. 10^6 cells from dissociated neurospheres were plated on PORN-coated 10 cm dishes. A day after plating, the growth medium was replaced by bFGF and EGF-depleted medium. Three days after plating, cells were transduced with FUW-Rab26-WT and cultured for additional 96 h. Thirty minutes before ^{32}P labeling, cells were switched to phosphate-free medium. Subsequently, cells were labeled for 4 h in phosphate-free medium containing 1 mCi^{32}Pi in a volume of 6 ml phosphate-free medium. After labeling, cells were washed once with 5 ml ice-cold PBS and placed in 500 µl lysis buffer (50 mM Tris-Cl, pH 7.5, 150 mM NaCl, 5 mM MgCl$_2$, 1% Triton X-100, 0.5% CHAPS supplemented with protease inhibitors). Plates were kept on ice for 10 min, and then centrifuged for 3 min at maximum speed. A lysate aliquot was retained for Western blotting to test loading similarity of the samples.

Supernatants were transferred to microfuge tubes containing 30 µl GFP antibody conjugated to agarose (clone RQ2, MBL) and incubated for 2 h at 4 °C while mixing. Beads were then washed five times in ice-cold lysis buffer and nucleotides bound to the GTPase were eluted in 20 µl elution buffer (2 mM EDTA, 1 mM GTP, 0.2% SDS, 5 mM DTT) at 65 °C for 5 min. Ten microlitre eluate was spotted on 20 × 20 cm polyethylenimine (PEI) cellulose plates (Macherey-Nagel) and separated in a chromatography chamber saturated with 0.75 M KH$_2$PO$_4$ (pH 3.4). Chromatography chambers were prepared one day in advance by filling the bottom with 50 ml potassium phosphate solution. GDP and GTP were separated by placing the dry TLC sheet upright in a sealed chamber until the solvent has ascended to 70% of its length. After drying, TLC plates were exposed to an X-ray film for 3–5 days.

Protein expression and purification. The GST-tagged DH-PH domain (amino acids 362–748) of human Plekhg5 protein, GST-tagged human Rab26-WT and GST-tagged mouse Rab5-WT were expressed in BL21 (DE3) E. Coli. One litre of Terrific Broth supplemented with salt and 100 mg/ml of ampicillin was inoculated with 200 ml of an overnight (o.n.) culture for 3 h at 37 °C to an OD of 0.8. Subsequently, expression was induced by adding 0.2 mM IPTG and bacteria were incubated o.n. at 22 °C. Bacteria were pelleted at 4000 r.p.m. for 15 min. Pellets were washed in 1× PBS, centrifuged again as above, and resuspended in Plekhg5 (20 mM HEPES pH 7.4, 500 mM NaCl, 1 mM DTT, 5 mM EDTA and 10% glycerol), or Rab26/Rab5 (20 mM Tris pH 7.4, 500 mM NaCl, 5 mM MgCl$_2$, 100 µM GDP and 5 mM DTT) protein buffer. Cell suspensions were lysed with lysozym (Roth), supplemented with inhibitor cocktail (Roche), 1 mg/l DNase (Applichem), and 1% Triton X-100. Lysates were sonicated (Branson Sonifier 450) four times for 30 s. In between, lysates were and kept on ice for 30 s. Lysates were pre-cleared by centrifugation at 13,000 r.p.m. for 45 min. Supernatants were filtered through a 0.45 µm (Whatman) filter, and rotated with glutathione conjugated to sepharose (Amersham Bioscience) for 2 h at 4 °C. After collecting the flow-through, the bound fraction was washed with 1 l of protein buffer supplemented with 1 mM ATP and 0.1% Triton X-100 for the DH-PH domain of PleghG5, 1% Triton X-100 for Rab26, or no additive for Rab5. Subsequently, Rab5 and Rab26 samples were digested in protein buffer supplemented with 150 mM NaCl and 5 mg/ml thrombin o.n. at 4 °C. The Rab5 sample was loaded on a Superdex 75 16/60 column (GE healthcare). The GST-DH/PH domain was eluted by 30 mM free and reduced glutathione. The beads were incubated four times with 10 ml of elution buffer for 10 min. Fraction were examined by SDS-PAGE. The protein-containing fractions were combined and dialyzed in protein buffer containing 150 mM NaCl and 0,1% Triton X-100 o.n. Purified proteins were snap frozen and stored at −80 °C.

For Rab27B and Rab33B the beads were washed with 500 ml wash buffer containing 20 mM HEPES pH 7.4, 500 mM NaCl, 5 mM MgCl$_2$ and 50 mM HEPES pH 7.5, 200 mM NaCl, 5 mM MgCl$_2$, respectively.

The proteins were eluted in their respective wash buffer supplemented with 400 mM imidazole 4–5 times with 7 ml buffer each elution fraction. Then the proteins were dialyzed with wash buffer containing reduced salt concentration of 150 mM NaCl. Rab33B was dialyzed in wash buffer containing 30 mM HEPES. All the purified proteins were snap frozen and stored at −80 °C for downstream experiments such as GEF assay.

Measurement of rapid kinetics. Nucleotide binding to Rab GTPases was analyzed by stopped flow instrument (SX-20 MV, Applied Photophysics) using Mant-GppNHp (Jena Bioscience GmbH). An aliquot of 100 nM Mant-GppNHp, either in the presence or absence of 10 µm Plekhg5, was rapidly mixed with 1 µm Rab GTPase in 10 mM MgCl$_2$, 20 mM HEPES, pH 7.4, 150 mM NaCl, 1 mM DTT and 5% glycerol. Mant-GppNHp was excited at 366 nm and fluorescence emission was monitored using a passing cut-off filter (KV395, Schott).

Electrophysiological analyses. For the electrophysiological tests six wild-type (3 female, 3 male) and six knockout (2 female, 4 male) animals were used. Electrophysiological experiments were carried out in accordance with the internationally accepted principles in the care and use of experimental animals, approved by the local Institutional Animal Care and Research Advisory Committee and permitted by the local government (Lower Saxony, Germany; AZ 13/1070). Mice were housed under controlled conditions in the Central Animal Facility of Hannover Medical School for nearly one week before measurements. Animals were anaesthetized by isoflurane (1.5–2% with pure oxygen (1 l/min); Baxter AG, Unterschleißheim, Germany). Prior to the electrophysiological measurements Carprofen (0.01 ml/100 g; 5 mg/kg; Rimadyl, Pfizer GmbH, Karlsruhe, Germany) was given subcutaneously for analgesia, and dexpanthenol eye ointment (Bepanthen Augen-und Nasensalbe, Bayer Vital GmbH, Leverkusen, Germany) was applied to the eyes to prevent corneal dehydration. During measurements, body temperature of the animals, monitored and recorded rectally, was maintained between 33 and 37 °C by using a thermostat heating plate (direct current). Portable EMG equipment (Natus Keypoint Focus, Natus Europe GmbH, Planegg, Germany) along with the Keypoint.net (version 2.32) computer program was used. For nerve conduction studies, the sciatic nerve of ~ 24-month-old animals was stimulated percutaneously by single pulses of 0.1 ms and 1 Hz delivered through a pair of needle electrodes (Spes Medica disposable monopolar needle electrode, 13 mm × 33 G, GVB geliMED KG, Bad Segeberg, Germany) placed proximally at the sciatic notch and distally at the popliteal fossa. The distance between both stimulation electrodes was measured. Reference electrodes were inserted subcutaneously a few millimeters apart from the stimulation electrodes. The maximal compound muscle action potential (CMAP) was recorded using needle electrodes (same as for stimulation) at the gastrocnemius, anterior tibial or plantaris muscles. The reference electrode for all three muscles was placed in the fourth toe. The ground electrode was inserted subcutaneously rostral to the stimulation electrodes. Amplitude (baseline-peak, mean proximal/ distal) and latency (time from stimulus to the onset of first negative deflection, mean proximal/ distal) were measured. Nerve conduction velocity (NCV) was calculated via the latency differences of the proximal and distal stimulation and the stimulation distance (mean NCV per muscle gastrocnemius/ tibialis). Motor unit number estimation (MUNE) was performed subsequently to the nerve conduction study, based on the description in Arnold et al.[59]. At least ten single motor unit potentials (SMUPs; baseline-peak amplitude) were obtained by incremental stimulation technique (1 Hz, 0.1 ms, 0.02 mA increase). Only increases over 25 µV in the amplitude were recorded trying to minimize the influence of alternation. The incremental values of the SMUPs were averaged in order to determine the size of the mean SMUP. In the end, the estimated number of motor units within the tibialis and gastrocnemius muscle was calculated by dividing the respective mean SMUP into the maximum CMAP amplitude.

Mechanical sensitivity. To determine mechanical paw withdrawal thresholds, we used the von Frey test based on the up-and-down-method of Chaplan et al.[60]. Experimental mice were placed on a wire mesh in individual acrylic-glas cages and the plantar surface of the hind paws was alternately touched with a calibrated von Frey filament applying mild pressure leading to a slight bending of the filament; the experiment was started at 0.69 g. Upon hind paw withdrawal the next thinner von Frey filament was used. If the hind paw was not withdrawn, the next thicker von Frey filament was used. Each hind paw was assessed three consecutive times and the 50% withdrawal threshold (i.e. force of the von Frey hair to which an animal reacts in 50% of the administrations) was calculated.

Heat sensitivity. To determine paw withdrawal latencies upon heat stimulation we applied a standard algometer (Ugo Basile, Gemonio, Italy) based on the method of Hargreaves et al.[61]. Experimental mice were placed on a glass surface in individual plexiglas cages and a radiant heat source (25 IR) was placed under one hind paw each. Time until paw withdrawal was recorded automatically. Heat application was limited to 16 s to avoid tissue damage. Each hind paw was tested three times consecutively.

Behavior. Plekhg5-deficient ($n = 10$) and control mice ($n = 11$), at age of 12–14 months with no symptoms of motoneuron disease were used for behavioral analysis. Genders within genotypes were grouped, as differences between them were not statistically significant. Mice were housed individually under a 12 h light/dark cycle (6:00 a.m.–6:00 p.m.) with *ad libitum* access to food and water. The cages (Tecniplast, 1264 C Eurostandard Typ II, 267 × 207 × 140 mm) were kept in a Scantainer (Scanbur Ltd. Denmark) assuring stable conditions through a constant airflow and maintaining a temperature of about 21 °C and air humidity of about

55%. Experimental procedures took place during the light phase of the cycle between 8:00 a.m. and 5:00 p.m. Mice were transported in their home cage to a separate room and allowed to calm down for half an hour. Then mice were taken individually in their home cages to the experimental room for experiments. The experimenter was unaware of the genotype to keep experiments unbiased.

For the Open Field test, mice were placed in the middle of an open field arena (48 × 48 cm, height 50 cm, evenly illuminated to ~40 lux) and filmed for 10 min with a webcam-based system (Logitech). Movements of the mice were tracked with VideoMot2 (TSE, Germany) and the following parameters were analyzed: time spent in center, number of entries into center. The area was cleaned thoroughly with water after each trial.

The Object Recognition experiments took place in the open field arena. For the object recognition task two kinds of objects were used: a cell culture flask and a tower of about the same size built of differently colored Lego bricks. The objects were placed in diagonally opposing corners of the arena with 12 cm distance to from both sides of the wall. On day 1 half of the animals were presented with two cell culture flasks, the other half with two Lego towers. Mice were placed in the middle of the arena and allowed to explore the arena and the objects for 10 min. On day 2 one of the objects was replaced by a novel object (either cell culture flask or Lego tower) at either position 1 or 2 in a pseudo-randomized manner to avoid position bias. Each mouse was therefore confronted with a familiar and a novel object and was allowed to explore freely for 10 min. Mice were automatically tracked (see above). We scored exploratory behavior toward objects manually whenever the mouse sniffed the object or touched the object while looking at it. After each trial, the arena and the objects were cleaned with water.

Fear conditioning was performed in a fear conditioning apparatus (mouse multi-conditioning system, 256060 series, TSE, Germany). Fear conditioning took place in context A, which consisted of a square arena with two blackened sides placed on a metal grid. Context B, a round arena, which was placed on a black plastic ground, served as new context. To support context discrimination, mild olfactory cues were introduced into the arenas by wiping them with tissue paper moistened with 70% ethanol for context A and 1% acetic acid for context B. The conditioning consisted of two phases. On day 1 (fear acquisition), mice were exposed to context A for 180 s before a tone (CS, 80 dB, 5000 Hz) was presented for 10 s and co-terminated with an electric foot shock of 0.7 mA for 1 s (US). The CS and the US were presented three times with an inter-stimulus-interval (ISI) of 20 s. After the last presentation, mice stayed in context A for 150 s before being returned to the home cage. On day 2, mice were placed in context B to test for context discrimination. For fear retrieval, after 60 s of free exploration the CS was presented without the US for 12 times with an ISI of 20 s. After another 60 s mice were returned to their home cage. Mice were video tracked and movement was recorded by a light beam system. Freezing behavior, defined as immobility except for respiration movements, was analyzed with a software-assisted system (TSE MCS FCS) and a freezing threshold of 2 s. After each trial, the context was cleaned with 70% ethanol or 1% acetic acid, respectively.

To account for statistical differences between genotypes and conditions depending on the experiment, two-way ANOVAs with post hoc Sidak's multiple comparison test or unpaired t-tests were performed. Analyses were performed with GraphPad Prism 6 and are represented as ± SEM. Results were considered statistically significant at $P < 0.05$.

Data availability. The authors declare that all data supporting the findings of this study are available within the article and its Supplementary Information files or from the corresponding author on reasonable request.

References

1. Maday, S., Wallace, K. E. & Holzbaur, E. L. Autophagosomes initiate distally and mature during transport toward the cell soma in primary neurons. *J. Cell Biol.* **196**, 407–417 (2012).
2. Maday, S. & Holzbaur, E. L. Autophagosome biogenesis in primary neurons follows an ordered and spatially regulated pathway. *Dev. Cell* **30**, 71–85 (2014).
3. Shen, D. N., Zhang, L. H., Wei, E. Q. & Yang, Y. Autophagy in synaptic development, function, and pathology. *Neurosci. Bull.* **31**, 416–426 (2015).
4. Shen, W. & Ganetzky, B. Nibbling away at synaptic development. *Autophagy* **6**, 168–169 (2010).
5. Hernandez, D. et al. Regulation of presynaptic neurotransmission by macroautophagy. *Neuron* **74**, 277–284 (2012).
6. Menzies, F. M., Fleming, A. & Rubinsztein, D. C. Compromised autophagy and neurodegenerative diseases. *Nat. Rev. Neurosci.* **16**, 345–357 (2015).
7. Pun, S., Santos, A. F., Saxena, S., Xu, L. & Caroni, P. Selective vulnerability and pruning of phasic motoneuron axons in motoneuron disease alleviated by CNTF. *Nat. Neurosci.* **9**, 408–419 (2006).
8. Hara, T. et al. Suppression of basal autophagy in neural cells causes neurodegenerative disease in mice. *Nature* **441**, 885–889 (2006).
9. Komatsu, M. et al. Loss of autophagy in the central nervous system causes neurodegeneration in mice. *Nature* **441**, 880–884 (2006).
10. Nassif, M. et al. Pathogenic role of BECN1/Beclin 1 in the development of amyotrophic lateral sclerosis. *Autophagy* **10**, 1256–1271 (2014).
11. Castillo, K. et al. Trehalose delays the progression of amyotrophic lateral sclerosis by enhancing autophagy in motoneurons. *Autophagy* **9**, 1308–1320 (2013).
12. Marx, R., Henderson, J., Wang, J. & Baraban, J. M. Tech: a RhoA GEF selectively expressed in hippocampal and cortical neurons. *J. Neurochem.* **92**, 850–858 (2005).
13. Liu, M. & Horowitz, A. A PDZ-binding motif as a critical determinant of Rho guanine exchange factor function and cell phenotype. *Mol. Biol. Cell* **17**, 1880–1887 (2006).
14. De Toledo, M., Coulon, V., Schmidt, S., Fort, P. & Blangy, A. The gene for a new brain specific RhoA exchange factor maps to the highly unstable chromosomal region 1p36.2-1p36.3. *Oncogene* **20**, 7307–7317 (2001).
15. Binotti, B. et al. The GTPase Rab26 links synaptic vesicles to the autophagy pathway. *Elife* **4**, e05597 (2015).
16. Garnaas, M. K. et al. Syx, a RhoA guanine exchange factor, is essential for angiogenesis in vivo. *Circ. Res.* **103**, 710–716 (2008).
17. Maystadt, I. et al. The nuclear factor kappaB-activator gene PLEKHG5 is mutated in a form of autosomal recessive lower motor neuron disease with childhood onset. *Am. J. Hum. Genet.* **81**, 67–76 (2007).
18. Kim, H. J. et al. Mutations in the PLEKHG5 gene is relevant with autosomal recessive intermediate Charcot-Marie-Tooth disease. *Orphanet. J. Rare Dis.* **8**, 104 (2013).
19. Azzedine, H. et al. PLEKHG5 deficiency leads to an intermediate form of autosomal-recessive Charcot-Marie-Tooth disease. *Hum. Mol. Genet.* **22**, 4224–4232 (2013).
20. Ozoguz, A. et al. The distinct genetic pattern of ALS in Turkey and novel mutations. *Neurobiol. Aging* **36**, e1769-1718 (2015).
21. Schnutgen, F. et al. Genomewide production of multipurpose alleles for the functional analysis of the mouse genome. *Proc. Natl Acad. Sci. USA* **102**, 7221–7226 (2005).
22. Gurney, M. E. et al. Motor neuron degeneration in mice that express a human Cu,Zn superoxide dismutase mutation. *Science* **264**, 1772–1775 (1994).
23. Tankersley, C. G., Haenggeli, C. & Rothstein, J. D. Respiratory impairment in a mouse model of amyotrophic lateral sclerosis. *J. Appl. Physiol.* **102**, 926–932 (2007).
24. Chou, S. M. (1992) in *Handbook of Amyotrophic Lateral Sclerosis* (ed. R. A. Smith) CRC Press, USA.
25. Bruneteau, G. et al. Endplate denervation correlates with Nogo-A muscle expression in amyotrophic lateral sclerosis patients. *Ann. Clin. Transl. Neurol.* **2**, 362–372 (2015).
26. Maday, S. & Holzbaur, E. L. Compartment-Specific Regulation of Autophagy in Primary Neurons. *J. Neurosci.* **36**, 5933–5945 (2016).
27. Mizushima, N., Yoshimori, T. & Levine, B. Methods in mammalian autophagy research. *Cell* **140**, 313–326 (2010).
28. Carlsson, S. R. & Simonsen, A. Membrane dynamics in autophagosome biogenesis. *J. Cell Sci.* **128**, 193–205 (2015).
29. Shibutani, S. T. & Yoshimori, T. A current perspective of autophagosome biogenesis. *Cell Res.* **24**, 58–68 (2014).
30. Vetter, I. R. & Wittinghofer, A. The guanine nucleotide-binding switch in three dimensions. *Science* **294**, 1299–1304 (2001).
31. Hetz, C. & Mollereau, B. Disturbance of endoplasmic reticulum proteostasis in neurodegenerative diseases. *Nat. Rev. Neurosci.* **15**, 233–249 (2014).
32. Matus, S., Valenzuela, V., Medinas, D. B. & Hetz, C. ER Dysfunction and Protein Folding Stress in ALS. *Int. J. Cell Biol.* **2013**, 674751 (2013).
33. Ng, S. Y. et al. Genome-wide RNA-Seq of human motor neurons implicates selective ER stress activation in spinal muscular atrophy. *Cell Stem Cell* **17**, 569–584 (2015).
34. Carra, S. et al. Alteration of protein folding and degradation in motor neuron diseases: Implications and protective functions of small heat shock proteins. *Prog. Neurobiol.* **97**, 83–100 (2012).
35. Luo, W., Sun, W., Taldone, T., Rodina, A. & Chiosis, G. Heat shock protein 90 in neurodegenerative diseases. *Mol. Neurodegener.* **5**, 24 (2010).
36. Marcu, M. G. et al. Heat shock protein 90 modulates the unfolded protein response by stabilizing IRE1alpha. *Mol. Cell Biol.* **22**, 8506–8513 (2002).
37. Saxena, S., Cabuy, E. & Caroni, P. A role for motoneuron subtype-selective ER stress in disease manifestations of FALS mice. *Nat. Neurosci.* **12**, 627–636 (2009).
38. Wang, L., Popko, B. & Roos, R. P. An enhanced integrated stress response ameliorates mutant SOD1-induced ALS. *Hum. Mol. Genet.* **23**, 2629–2638 (2014).
39. Wang, L., Popko, B. & Roos, R. P. The unfolded protein response in familial amyotrophic lateral sclerosis. *Hum. Mol. Genet.* **20**, 1008–1015 (2011).

40. Ngok, S. P., Geyer, R., Kourtidis, A., Storz, P. & Anastasiadis, P. Z. Phosphorylation-mediated 14-3-3 protein binding regulates the function of the rho-specific guanine nucleotide exchange factor (RhoGEF) Syx. *J. Biol. Chem.* **288**, 6640–6650 (2013).

41. Bhattacharya, S. et al. GAIP interacting protein C-terminus regulates autophagy and exosome biogenesis of pancreatic cancer through metabolic pathways. *PLoS ONE* **9**, e114409 (2014).

42. Pozuelo-Rubio, M. 14-3-3zeta binds class III phosphatidylinositol-3-kinase and inhibits autophagy. *Autophagy* **7**, 240–242 (2011).

43. Ince, P. G. in *Amyotrophic Lateral Sclerosis*. 1st edn (eds E. R. H. M. Brown Jr, V. & Swash, M.) (Dunitz, Martin, 2000).

44. Rizzoli, S. O. & Betz, W. J. Synaptic vesicle pools. *Nat. Rev. Neurosci.* **6**, 57–69 (2005).

45. Maruyama, H. et al. Mutations of optineurin in amyotrophic lateral sclerosis. *Nature* **465**, 223–226 (2010).

46. Fecto, F. et al. SQSTM1 mutations in familial and sporadic amyotrophic lateral sclerosis. *Arch. Neurol.* **68**, 1440–1446 (2011).

47. Herhaus, L. & Dikic, I. Expanding the ubiquitin code through post-translational modification. *EMBO Rep.* **16**, 1071–1083 (2015).

48. Pickrell, A. M. & Youle, R. J. The roles of PINK1, parkin, and mitochondrial fidelity in Parkinson's disease. *Neuron* **85**, 257–273 (2015).

49. Cirulli, E. T. et al. Exome sequencing in amyotrophic lateral sclerosis identifies risk genes and pathways. *Science* **347**, 1436–1441 (2015).

50. Freischmidt, A. et al. Haploinsufficiency of TBK1 causes familial ALS and fronto-temporal dementia. *Nat. Neurosci.* **18**, 631–636 (2015).

51. Sellier, C. et al. Loss of C9ORF72 impairs autophagy and synergizes with polyQ Ataxin-2 to induce motor neuron dysfunction and cell death. *EMBO J.* **35**, 1276–1297 (2016).

52. Wertz, K. & Füchtbauer, E. M. B6D2F1 - An improved mouse hybrid strain for the production of ES cell germ line chimeras. *Transgene* **1**, 277–280 (1994).

53. Masu, Y. et al. Disruption of the CNTF gene results in motor neuron degeneration. *Nature* **365**, 27–32 (1993).

54. Dombert, B., Sivadasan, R., Simon, C. M., Jablonka, S. & Sendtner, M. Presynaptic localization of Smn and hnRNP R in axon terminals of embryonic and postnatal mouse motoneurons. *PLoS ONE* **9**, e110846 (2014).

55. Forssmann, W. G. et al. An improved perfusion fixation method for the testis. *Anat. Rec.* **188**, 307–314 (1977).

56. Wiese, S. et al. Isolation and enrichment of embryonic mouse motoneurons from the lumbar spinal cord of individual mouse embryos. *Nat. Protoc.* **5**, 31–38 (2010).

57. Kimura, S., Noda, T. & Yoshimori, T. Dissection of the autophagosome maturation process by a novel reporter protein, tandem fluorescent-tagged LC3. *Autophagy* **3**, 452–460 (2007).

58. Vicinanza, M. et al. PI(5)P regulates autophagosome biogenesis. *Mol. Cell* **57**, 219–234 (2015).

59. Arnold, W. D. et al. Electrophysiological motor unit number estimation (MUNE) measuring compound muscle action potential (CMAP) in mouse hindlimb muscles. *J. Vis. Exp.* (2015).

60. Chaplan, S. R., Bach, F. W., Pogrel, J. W., Chung, J. M. & Yaksh, T. L. Quantitative assessment of tactile allodynia in the rat paw. *J. Neurosci. Methods* **53**, 55–63 (1994).

61. Hargreaves, K., Dubner, R., Brown, F., Flores, C. & Joris, J. A new and sensitive method for measuring thermal nociception in cutaneous hyperalgesia. *Pain* **32**, 77–88 (1988).

62. Damme. M. et al Impaired lysosomal trimming of N-linked oligosaccharides leads to hyperglycosylation of native lysosomal proteins in mice with α-mannosidosis. *Mol. Cell. Biol.* **30**, 273–283 (2009).

Acknowledgements

Author contributions

Additional information

Supplementary Figure 1

Generation of Plekhg5 deficient mice. (**a**) Scheme of the mutant *Plekhg5* locus. The gene trap cassette (GT-cassette) consisted of a splice acceptor, a *β-geo* gene and a poly-adenylation signal. Correct insertion of the GT-cassette within the *Plekhg5* locus was verified by sequencing. According to ensemble.org, the murine *Plekhg5* locus is able to generate four different protein-coding transcripts (isoforms 001-004) with three distinct N-termini. Isoform

001 and 004 only differ in their PDZ-binding motif, comprising three amino acids at the C-terminus. The GT-cassette is inserted within the fourth intron of the *Plekhg5* gene and affects transcription of all predicted splice variants. Frt/F3 flippase recognition target; loxP/lox511 Cre recognition sites; SA, splice acceptor; pA, bovine growth hormone polyadenylation sequence; β-GEO, β-galactosidase/neomycin phosphotransferase fusion gene. (**b - d**) Splice events at the wildtype (**b, c**) and gene-trap (**d, e**) locus, characterized by RT-PCR. To investigate which isoforms are expressed within the spinal cord, RT-PCRs were carried out with specific 5′ primers for each splice variant. For the wildtype-allele one common 3′ primer was used, located in the next downstream exon (ENSMUSE00000594961) of the GT-cassette (**b**). For detection of the GT-cassette a specific 3′ primer was applied (**d**). In wildtype-animals, *Plekhg5* is dominantly expressed within the spinal cord as isoform 003 (E2-E5) (**c**). We hardly detected any *Plekhg5* transcripts in homozygous mutant animals (**c**). Conversely, expression of the GT-cassette was only detectable in mutant animals (**e**). Thus, the gene-trap locus predominantly generates a truncated protein consisting of 28 amino acids (Exon 2 and 3 of isoform-003) fused to β-GEO. The 28 amino acids of the original protein contain neither the RhoGEF nor PH-domain. (**f, g**) Using 5′ primers specific for exon 6 and exon 9 (**f, g**) we confirmed that insertion of the GT-cassette did not disturb the normal splicing pattern by altering the order of 5′ exons or elimination of 5′ exons (**f, g**). These data demonstrate functionality of the GT-cassette and confirm the absence of wildtype-transcripts within the spinal cord of mutant mice. (**h**) Using an antibody directed against the C-terminus of Plekhg5, we detected a vesicular staining within the cytosol. As indicated by co-staining against NeuN and choline acetyltransferase (ChAT), expression of Plekhg5 was identified in NeuN^{+} neurons including ChAT[+] motoneurons. In *Plekhg5*^{-/-} mice, Plekhg5 staining was completely abolished, providing further evidence for functionality of the GT-cassette.

Supplementary Figure 2
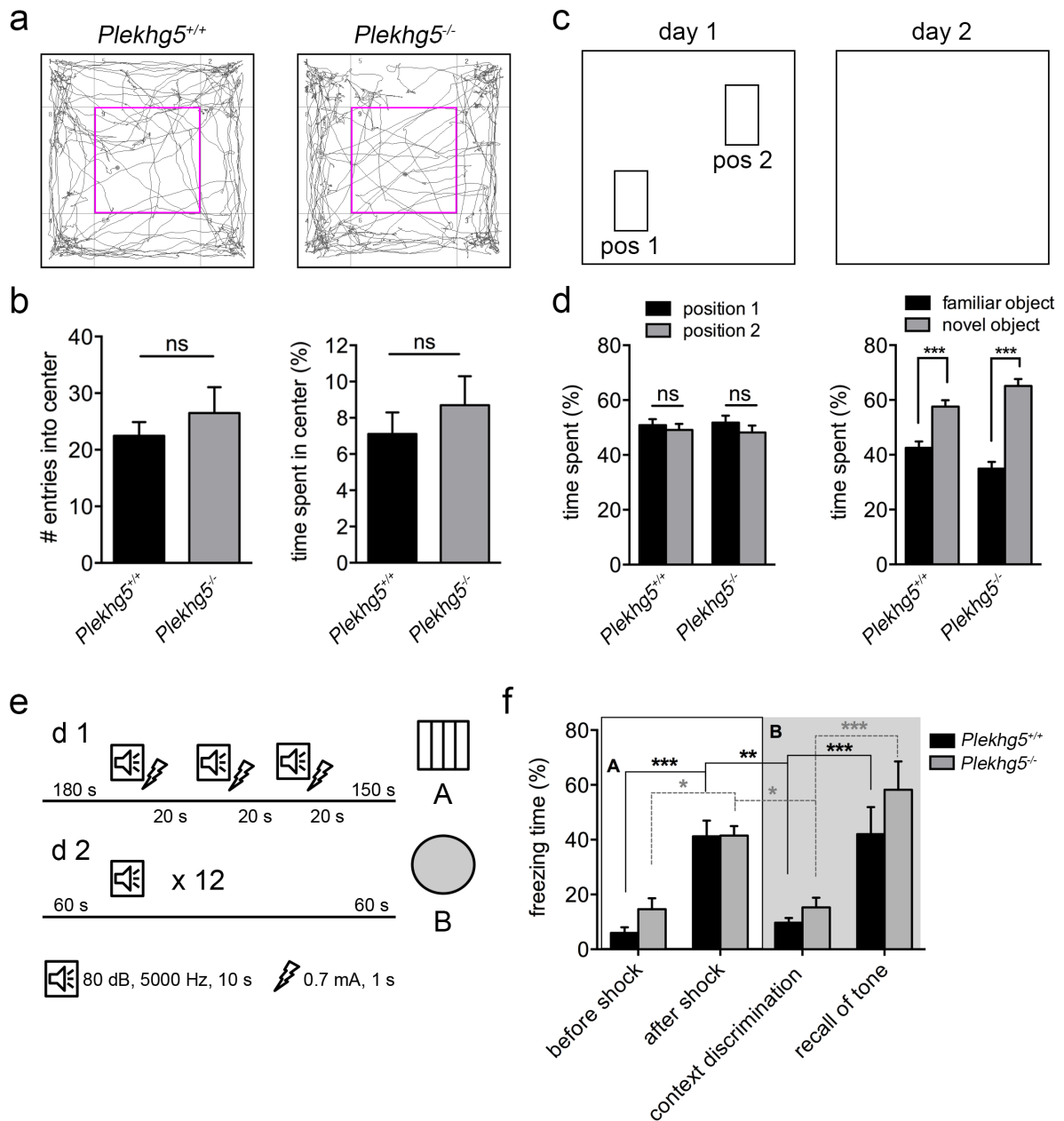
Plekhg5 deficiency does not impair cognitive function. (**a**, **b**) Control- and Plekhg5 deficient mice were placed in the center of the open field arena and their movement was monitored for 10 minutes. (**a**) Representative trajectories of control- and Plekhg5 deficient mice show the behavior of both groups in the open field test. (**b**) Plekhg5 deficient mice spent the same amount of time in the center as compared to control animals. Both groups also showed the same number of entries into the center. (**c**, **d**) To assess the memory skills of Plekhg5 deficient mice the object recognition test was performed. (**c**) The first day two identical objects were presented and placed in two diagonally opposing corners of the box. Mice were

placed in the middle of the box and monitored and tracked for 10 minutes. The next day one of the objects was replaced with a novel object. Whether the novel object is presented at position 1 or 2 was randomized to avoid position bias. Again, mice were placed in the middle of the box and monitored and tracked for 10 minutes. (**d**) At day 1, control- and Plekhg5 deficient mice spent half of the time at both objects. The second day both groups spent significantly more time at the novel object suggesting that both groups are able to recall the familiar object and recognize the new object. (**e**, **f**) We investigated fear acquisition and context discrimination of Plekhg5 deficient mice in a paradigm of fear conditioning. (**e**) At day 1, mice were trained to associate a tone with a foot shock in context A. After a 180 s habituation phase, mice received a 10 s tone of which the last second is accompanied by an electric foot shock delivered via the metal grid in the cage. The stimuli are presented 3 times with an inter stimulus interval (ISI) of 20 s. At day 2, mice have to recall the acquisition in context B. After a 60 s habituation phase, mice receive a 10s tone that is not accompanied by an electric foot shock. The sound is presented 12 times with an ISI of 20s. (**f**) Quantification of freezing time. During acquisition (context A) both groups show a significant increase in freezing time after receiving an electric foot shock. At day 2 both, control and Plekhg5 deficient mice are able to recall the acquisition in context B. Both groups show a significantly increase in freezing time after receiving the tone without electric foot shock.

Supplementary Figure 3
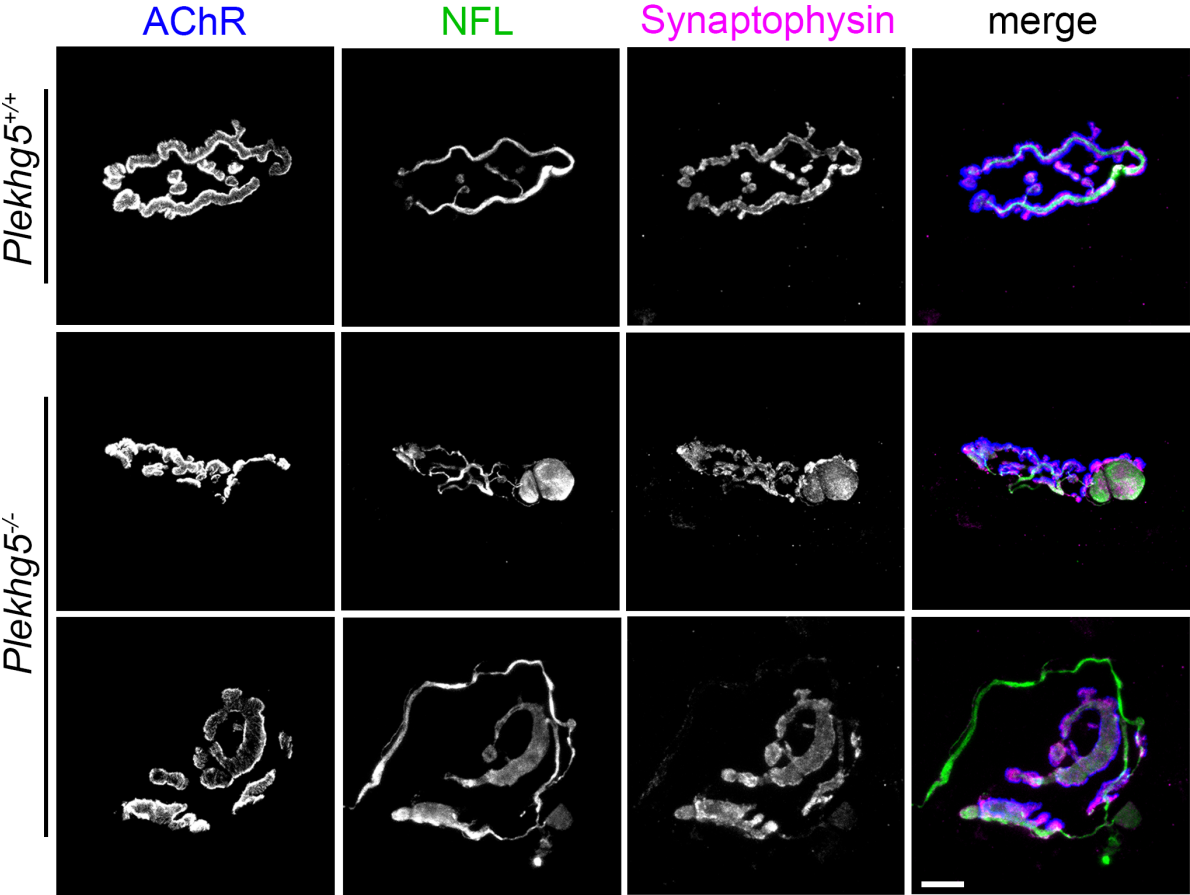
Degradation of neuromuscular junctions in Plekhg5 deficient mice. Representative images of neuromuscular junctions within the gastrocnemius muscle of adult mice stained for acetylcholine receptors (BTX labeling), NFM and synaptophysin. Scale bar: 10 μm.

Supplementary Figure 4
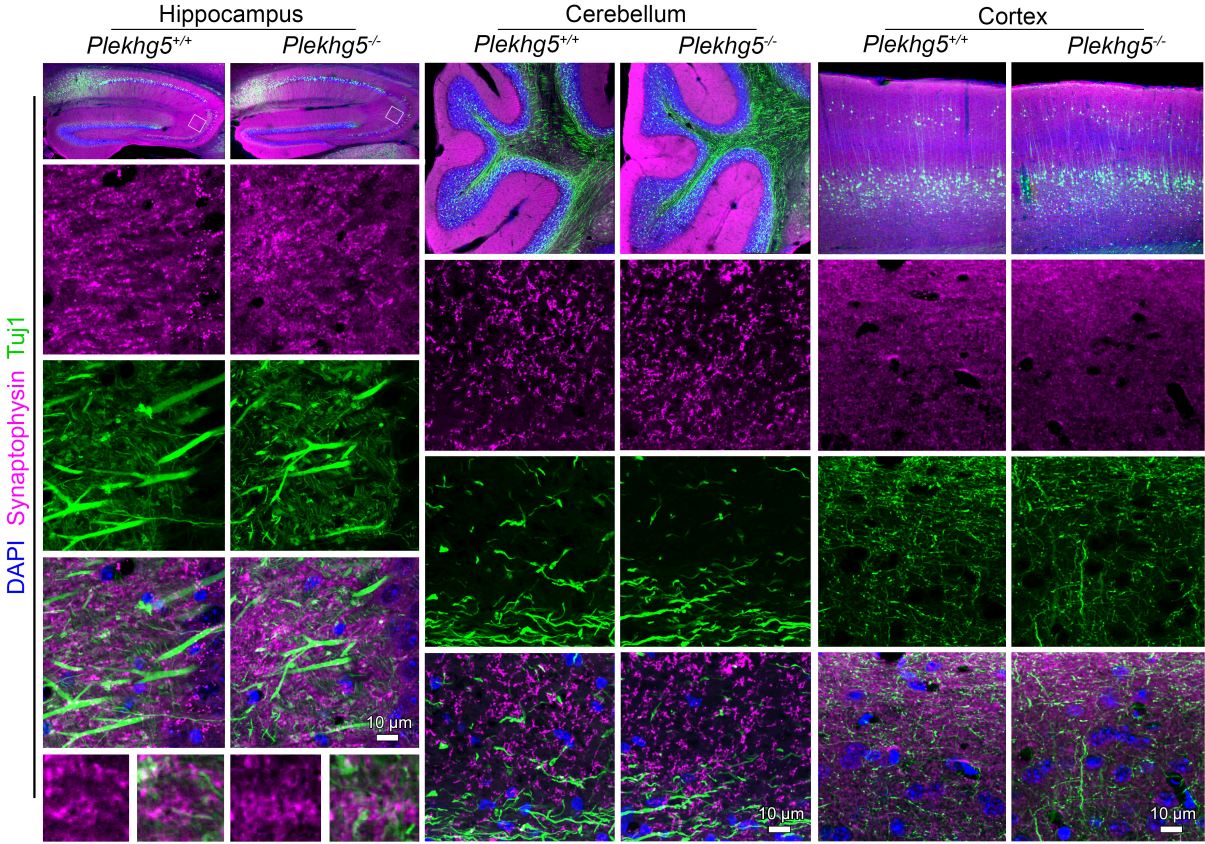
Histological analysis of major brain areas. Brain sections of control and Plekhg5 deficient mice were stained for synaptophysin, Tuj1 and DAPI. The morphology and layering of major brain areas as well as the synapse morphology appeared normal in Plekhg5 deficient mice as compared to controls animals.

Supplementary Figure 5
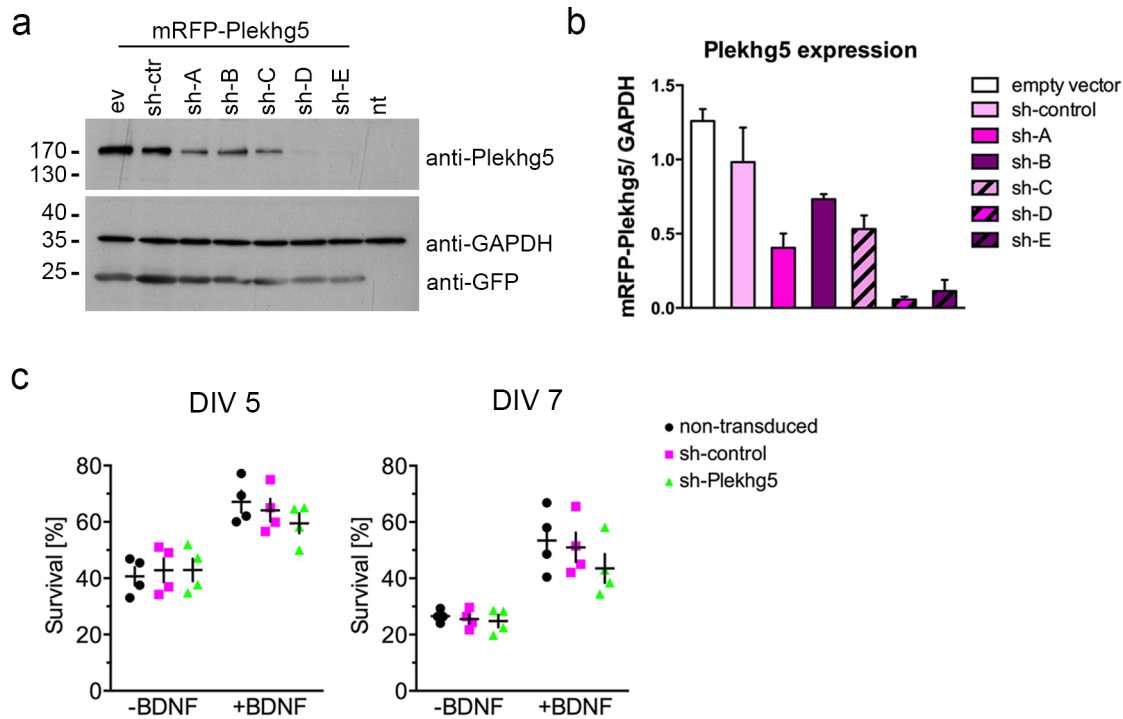
Depletion of Plekhg5 does not impair survival of cultured motoneurons. (a, b) Different sh-RNA constructs were validated for their ability to knockdown Plekhg5. Co-transfection of HEK293T cells with mRFP-Plekhg5 and different sh-RNAs targeting Plekhg5. After 48h, cells were lysed and submitted to SDS-PAGE and Western blotting. Images have been cropped for presentation. Full size images are presented in Supplementary Fig. 7. **(c)** After five and seven days, knockdown of Plekhg5 with construct # D did not significantly affect motoneuron survival when cultured with or without BDNF (each data point represents one individual experiment; Mean ± SEM; Two-way ANOVA; Bonferroni post-test).

Supplementary Figure 6
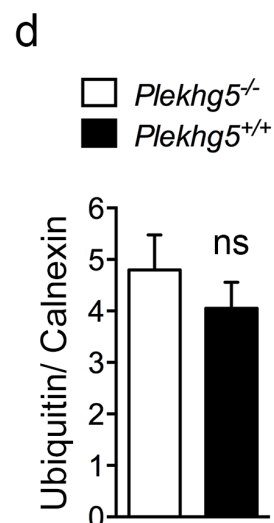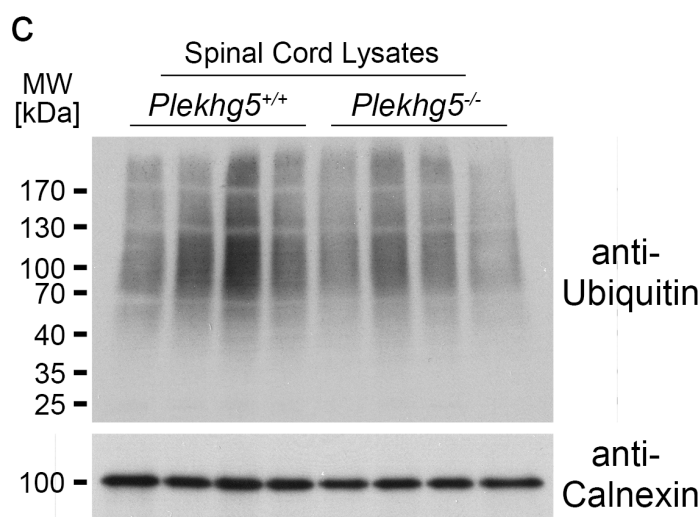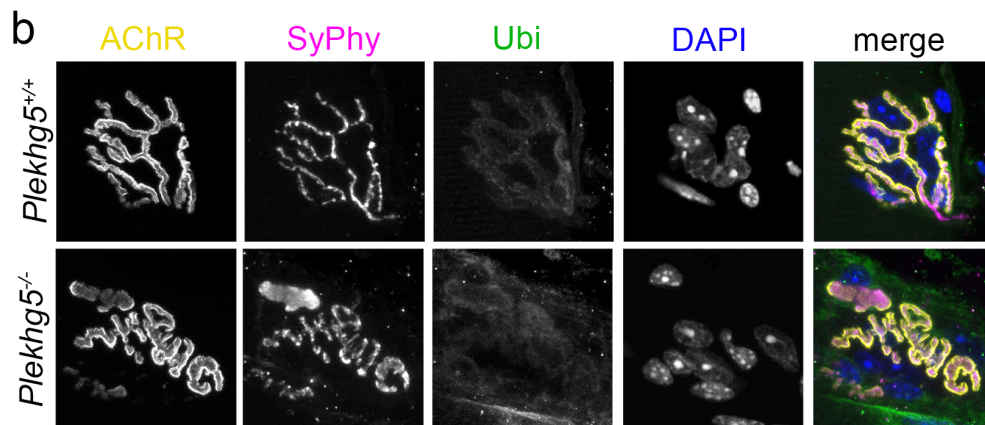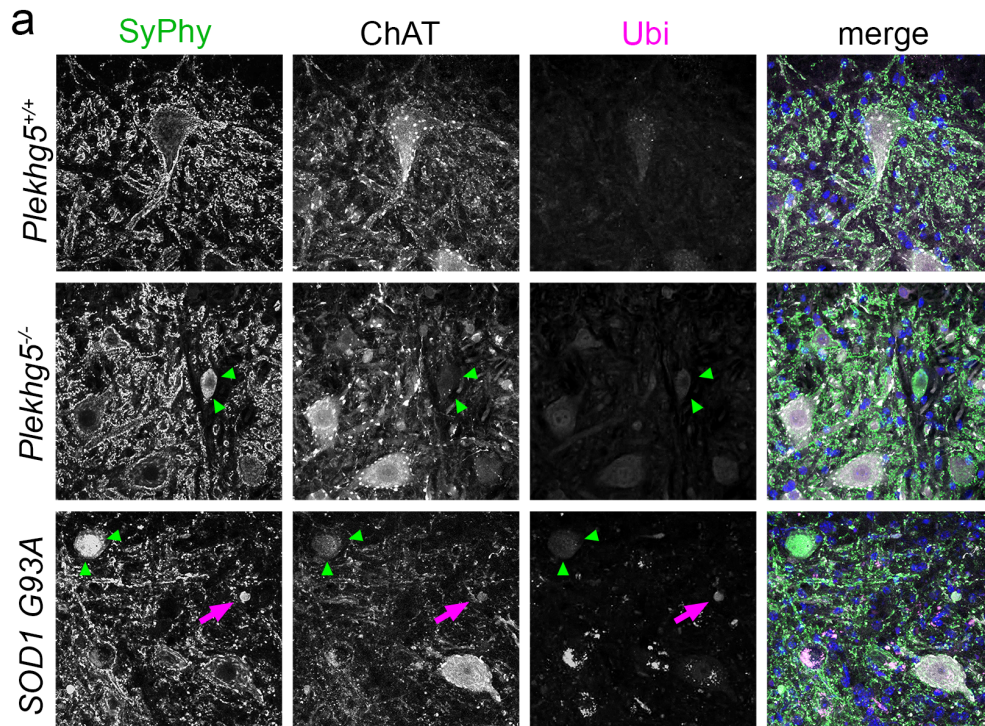
Global protein homeostasis is not impaired by Plekhg5 deficiency. (**a**) Ubiquitin staining of spinal cord cross-sections from control-, Plekhg5 deficient- and SOD1 G93A mice. Plekhg5 deficient mice showed no enrichment for polyubiquitinated protein inclusions, in contrast to SOD1 G93A mice. Arrowheads point to Synaptophysin accumulations. Arrows point to accumulations positive for Synaptophysin and Ubiquitin. (**b**) Ubiquitin staining of NMJs. Ubiquitinated protein inclusions were not detectable at NMJs of Plekhg5 deficient mice. (**c**) Western bot analysis of spinal cord extracts probed for Ubiquitin. Plekhg5 deficient mice did not reveal any enrichment for polyubiquitinated proteins. (**d**) Western blot quantification. (Four animals per genotype were analyzed; Mean ± SEM; unpaired t-test; two-tailed)

Supplementary Figure 7

Figure 3 i

Figure 5 i & 9 a

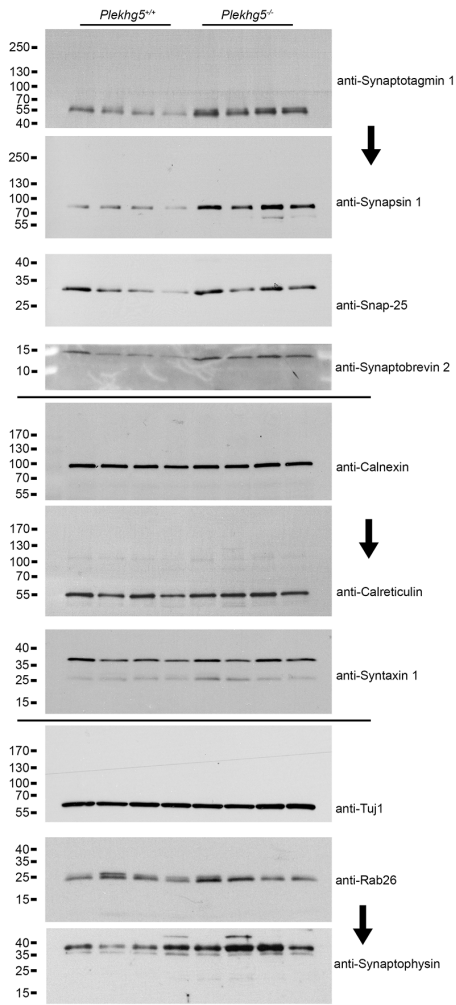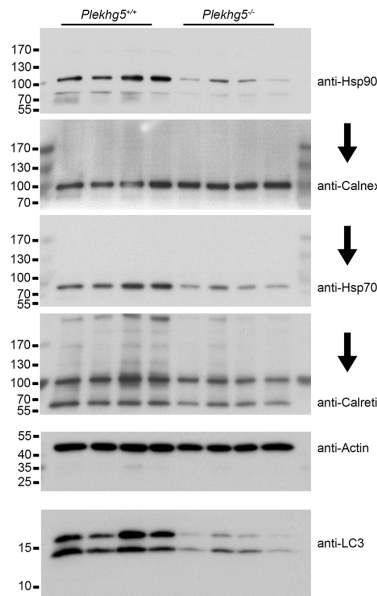

Figure 5 g
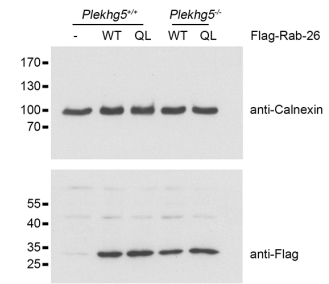
Figure 8 g

Figure 9 c
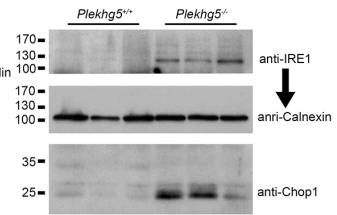
Figure 9 e
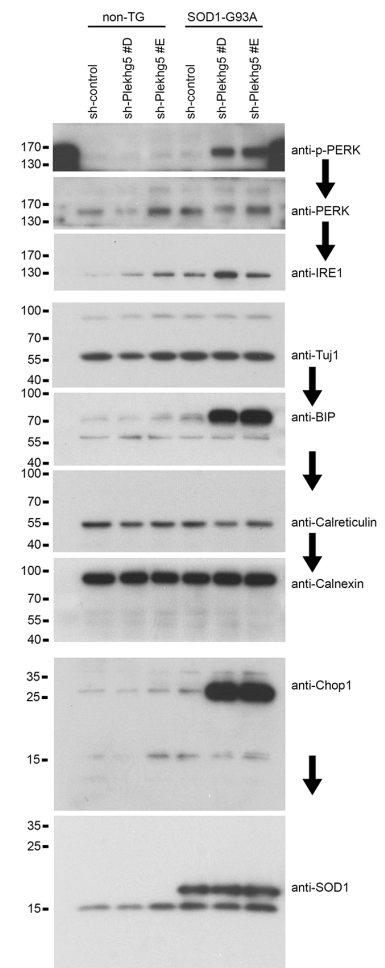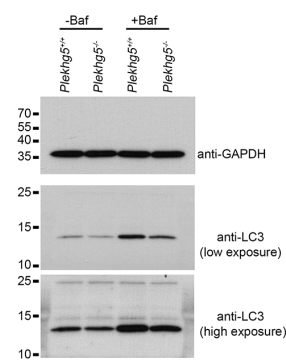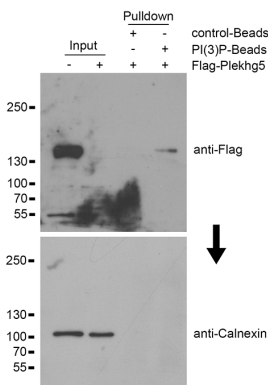
Supplementary Figure 5 a

Figure 5 m
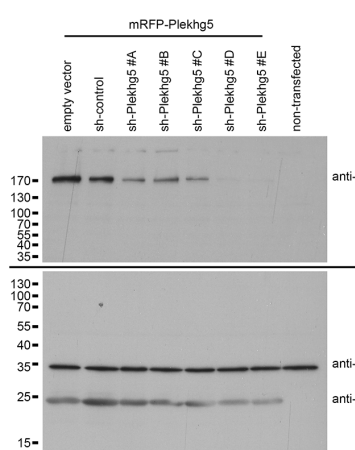
Full size images of Western blots. Arrows indicate reprobing of Western blots. Lines separate individual Western blots.

Plekhg5 mediates myelin breakdown by regulating the immune response in peripheral nerves

Carsten Slotta[1,2+], Patrick Lüningschrör[3+], Ulrich M. Weikert[1], Michael Briese[3], Silke Appenzeller[4,5], Peter Heimann[1], Michael Sendtner[3], Christian Kaltschmidt[1+], Barbara Kaltschmidt[1,2+*]

[1] Department of Cell Biology, University of Bielefeld, Universitaetsstr. 25, 33501 Bielefeld, Germany

[2] Molecular Neurobiology, University of Bielefeld, Universitaetsstr. 25, 33501 Bielefeld, Germany

[3] Institute of Clinical Neurobiology, University Hospital Wuerzburg, 97078 Wuerzburg, Germany

[4] Core Unit Systems Medicine, University of Wuerzburg, 97080 Wuerzburg, Germany

[5] Comprehensive Cancer Center Mainfranken, University Hospital Wuerzburg, 97080 Wuerzburg, Germany

+ These authors contributed equally to this work

* Corresponding Author:

Barbara Kaltschmidt, Molecular Neurobiology, Department of Cell Biology, University of Bielefeld, Universitaetsstr. 25, 33501 Bielefeld, Germany,

Tel.: + 49 521 106 5624; Fax: + 49 521 106 5654; E-Mail: c.kaltschmidt@uni-bielefeld.de

Abstract

Inflammation and an active immune response are hallmarks of several neurodegenerative diseases. An activated immune response is considered as the cause for myelin breakdown in demyelinating disorders. In the peripheral nervous system, myelin can be degraded in an autophagy-dependent manner directly by Schwann cells or by recruitment of immune cells. Here, we show that the NF-κB activator Pleckstrin homology containing family member 5 (Plekhg5) regulates both, Schwann cell autophagy and recruitment of T-lymphocytes in peripheral nerves during motoneuron disease. *Plekhg5*-deficient mice show myelin infoldings and hypermyelination in peripheral nerves during motoneuron disease. Even at late stages *Plekhg5*-deficient mice do not show any signs for demyelination and inflammation. Using RNAseq we unraveled a transcriptional signature for an impaired immune response in sciatic nerves, which manifested in a reduced number of CD4$^+$ and CD8$^+$ T-cells. These findings identify Plekhg5 as a promising target to impede myelin breakdown in demyelinating PNS disorders.

Introduction

The myelin sheath is an essential cellular component for axonal integrity and function. While oligodendrocytes generate myelin in the central nervous system (CNS), in the peripheral nervous system (PNS) it is formed by Schwann cells (Nave & Werner, 2014). Nerve conduction velocity is highly dependent on an intact myelin sheath. However, in pathological situations, e.g. upon infections or in the context of neurodegenerative diseases, such as hereditary motor and sensory neuropathies (HSMN), myelin breakdown (demyelination) can occur leading to impairments in axonal integrity and function but also to axonal loss. At the same time several demyelinating neuropathies are associated with excessive myelin production that appears histologically as myelin outfoldings or focal thickening of the myelin sheath ('tomacula') (Chung et al, 2011; Fabrizi et al, 2000; Quattrone et al, 1996). Excessive myelin production in these disorders precedes demyelination and axon loss (Adlkofer et al, 1995).

Abnormalities of the myelin architecture, especially in the context of neurodegenerative diseases, are often linked to inflammation and an immune response. By impairing the immune response, myelin maintenance was improved in mouse models for a demyelinating CNS disorder (Ip et al, 2006) and for Charcot Marie Tooth (CMT) disease (Schmid et al, 2000). While myelin breakdown in the CNS is mediated predominantly by macrophages (Brosius Lutz & Barres, 2014), within the PNS an additional mechanism for initial myelin degradation has been described. After acute injury Schwann cells degrade their own myelin sheath via a specific form of autophagy (myelinophagy) in response to axonal stress (Gomez-Sanchez et al, 2015).

A key regulator of inflammation and immune response is the transcription factor NF-κB (Kaltschmidt & Kaltschmidt, 2009; Tak & Firestein, 2001). Besides its involvement in acute injury such as viral infections of the CNS, NF-κB is also tightly linked to neurodegenerative diseases such as Alzheimer's, Parkinson's disease or the demyelinating disease multiple sclerosis (MS) (reviewed in (Mattson & Meffert, 2006)). Increased amount of nuclear NF-κB has been found within oligodendrocytes and microglia next to lesion sites of MS patients (Bonetti et al, 1999). Consequently, substances such as fingolimod that directly or indirectly modulate NF-κB activity are already being used in MS therapy (Sanford, 2014).

The guanine exchange factor (GEF) Plekhg5 (also known as Syx or Tech) is a known activator of NF-κB (Matsuda et al, 2003; Maystadt et al, 2007), which is highly expressed within the nervous system (De Toledo et al, 2001; Marx et al, 2005). Mutations within the human *PLEKHG5* gene are associated with different motoneuron diseases such as an intermediate form of CMT, distal spinal muscular atrophy type (DSMA) IV and amyotrophic lateral sclerosis (ALS) (Azzedine et al, 2013; Kim et al, 2013; Maystadt et al, 2007; Ozoguz et al, 2015). Mice lacking Plekhg5 developed a late-onset motoneuron disease caused by an impaired autophagy-mediated clearance of synaptic vesicles at the neuromuscular junctions (Luningschror et al, 2017).

Within the nervous system, expression of Plekhg5 is not limited to neuronal cells. Especially in Schwann cells a high expression of Plekhg5 was demonstrated (Azzedine et al, 2013). In line with moderately decreased nerve conduction velocities (NCVs) observed in *Plekhg5*-deficient mice (Azzedine et al, 2013; Luningschror et al, 2017), a direct or indirect role of Plekhg5 in myelin maintenance can be hypothesized. In contrast, based on RNA-sequencing data, expression in myelinating oligodendrocytes – the CNS counterpart – appears to be very low suggesting this potential function of Plekhg5 to be PNS-specific (Zhang et al, 2014).

In this study, we analyzed the role of Plekhg5 in Schwann cells and its role in myelination. We detected myelin abnormalities, mostly characterized by infoldings of the myelin sheath and by a modest hypermyelination. Strikingly, using RNA-sequencing we found prominent downregulation of genes in the context of immune response. In line with that, we observed a reduced number of T-lymphocytes within the sciatic nerve indicating an impaired immune response despite axonal pathology. A significant subset of the downregulated genes were validated target genes of the transcription factor NF-κB. We hypothesize a reduced NF-kB activation due to *Plekhg5*-deficiency to be the cause of impaired immune response within peripheral nerves. Targeting Plekhg5 and/or NF-κB in Schwann cells therefore appears to be promising regarding therapeutic approaches in demyelinating PNS disorders.

Results/discussion

Plekhg5-deficiency results in profound alterations of the myelin sheath in peripheral nerves

To investigate a putative role of Plekhg5 in Schwann cells, we histologically analyzed the sciatic nerve of *Plekhg5*-deficient mice. Most prominently, we observed profound alterations of the myelin sheath in the sciatic (Fig. 1) and the phrenic nerve (Fig. S1). Particularly infoldings of the myelin sheath could be detected (Fig. 1A, F-I). The number of fibers with an altered myelination progressed with age and significantly differed in comparison to control mice at 12 months and older (Fig. 1B). Additionally, we detected a significantly reduced axonal diameter in *Plekhg5*-deficient animals (Fig. 1C) and a hypermyelination in 24 months old animals as indicated by g-ratio analysis (Fig. 1D, E). Notably, fibers with myelin alterations were excluded in this analysis. Focal in- and outfoldings of the myelin sheath have been described to precede demyelination in several demyelinating neuropathies (Chung et al, 2011; Fabrizi et al, 2000; Quattrone et al, 1996). Moreover, myelin alterations have been described in different mouse models for demyelinating PNS disorders (Cai et al, 2006; Lee et al, 2013; Robinson et al, 2008). However, we detected no signs of demyelination, even in 24 months old mice, suggesting an impaired myelin breakdown in *Plekhg5*-deficient mice.

Next, we wondered whether Schwann cell dysfunction caused the myelin alterations and the lack of subsequent myelin degradation. Using qPCR we analyzed the expression of several Schwann cell markers within the sciatic nerve (Fig. 1J). With significantly altered expression of several markers for both, mature and immature Schwann cells we hypothesized a Schwann cell dysfunction in *Plekhg5*-deficient mice. In line with this, we observed an increase in the number of Schwann cells within the sciatic nerve of *Plekhg5*-deficient mice compared to control mice. Notably, this increase was already significant in 3 months old animals (Fig. 1K) and persisted in older animals (Fig. S2).

Impaired formation of autophagosomes in *Plekhg5*-deficient Schwann cells

Since we did not detect any signs for demyelination within peripheral nerves, we aimed to promote demyelination by an *ex vivo* approach investigating general impairments in myelin breakdown. As previously described, we cultivated segments of the sciatic nerve from *Plekhg5*-deficient mice to simulate sciatic nerve injury

5

resulting in demyelination of the axons predominantly by Schwann cells due to the absence of invading macrophages (Fernandez-Valle et al, 1995). After 5 days in culture, we counted the remaining intact myelin sheaths and observed a significantly increased number in segments derived from mutant mice compared to wildtype (Fig. 2A, B). Recently, Schwann cell-specific autophagy (myelinophagy) was described for initial myelin breakdown following injury (Gomez-Sanchez et al, 2015). In teased fiber preparations of cultivated nerve segments, we detected fragments positive for the myelin protein zero (P0) in control mice but not in mutant mice (Fig. 2C).

We recently described Plekhg5 to be involved in regulating the autophagy-mediated clearance of synaptic vesicles in motoneurons (Luningschror et al, 2017). To analyze, whether *Plekhg5*-deficiency additionally results in autophagy impairments within Schwann cells, we cultivated primary Schwann cells of mutant mice transduced with a lentiviral GFP-RFP-LC3 reporter. Using this reporter, autophagosomes and autolysosomes can be distinguished based on their fluorescent signals, as the GFP signal is rapidly lost after fusion of autophagosomes and lysosomes due to the pH drop. Structures positive for RFP alone are therefore classified as autolysosomes, whereas structures positive for both, GFP and RFP, are considered as autophagosomes. Under basal conditions, a modestly reduced number of autophagosomes was observed in *Plekhg5*-deficient Schwann cells although not reaching statistical significance (Fig. 2D, E). Upon treatment with Bafilomycin A1, which blocks the fusion of autophagosomes and lysosomes, the increase in the number of autophagosomes in Plekhg5-depleted cells was significantly lowered compared to wildtype cells indicating an impaired autophagosome biogenesis. This observation is comparable to previous results in cultured motoneurons of *Plekhg5*-deficient mice (Luningschror et al, 2017).

Reduced recruitment of T-lymphocytes within the sciatic nerve

Schwann cell autophagy-mediated myelin degradation was described as the initial response to injury (Gomez-Sanchez et al, 2015). However, after this initial phase, myelin is being degraded via phagocytosis mediated by macrophages (Brosius Lutz & Barres, 2014). Furthermore, in mouse models for demyelinating PNS disorders, increased levels of both T-lymphocytes and macrophages have been found contributing to myelin breakdown (Ip et al, 2006; Wang Ip et al, 2006). We therefore

wondered whether a defective immune response also contributes to the impaired myelin breakdown.

For an unbiased approach, we performed RNAseq with RNA derived from the sciatic nerve of 12 months old animals. Strikingly, a high number of the 95 significantly (q<0.05) downregulated genes (Fig. 3A) were associated with the gene ontology (GO) term "immune response" (Fig. 3B). A significant subset of the downregulated genes in *Plekhg5*-deficient mice represented validated target genes of the transcription factor NF-κB (Fig. 3C). Among these, the chemokines Ccl22, Ccl5 and Cxcl9 are known mediators of T-cell recruitment and activation (Charo & Ransohoff, 2006; Gobert et al, 2009; Miyagishi et al, 1997). Furthermore, we detected a reduced expression of the chemokine receptor Ccr7, which is expressed in T-cells and binds the chemokines Ccl21 and Ccl19. Ccr7 regulates T-cell migration and recruitment from peripheral tissues (Noor & Wilson, 2012). A reduced expression of Cx3cl1, which is also a potent chemoattractant of T-cells (Imai et al, 1997), further points to an impaired T-cell infiltration into the sciatic nerve of *Plekhg5*-deficient mice. Schwann cells reportedly have the capability to act as facultative antigen presenting cells, expressing MHC complex II molecules (Bergsteinsdottir et al, 1992; Meyer zu Horste et al, 2010). In addition, several myelin proteins were described as autoantigens in neuropathologies (Braun et al, 1982; de Rosbo & Ben-Nun, 1998; Kaushansky et al, 2010). Antigens presented by Schwann cells are recognized by T-lymphocytes to initiate macrophage-mediated clearance. To confirm a reduced number of T-lymphocytes in sciatic nerves of *Plekhg5*-deficient mice, we performed immunostainings of sciatic nerve cross-sections for CD4 and CD8 and detected reduced numbers of both, CD4- and CD8-positive T-lymphocytes in sciatic nerves of *Plekhg5*-deficient mice (Fig. 3E, F).

In addition to the macrophage-secreted chemokines Ccl22 and Cxcl9, the RNAseq data also revealed a reduced expression of Siglec-1, a macrophage-restricted adhesion molecule. Depletion of Siglec-1 in P0-mutant mice results in an attenuated demyelination and a reduced number of CD8^{+} T-lymphocytes (Kobsar et al, 2006). To address whether the reduced expression of Ccl22, Cxcl9 and Siglec-1 was caused by a reduced number of macrophages we stained sciatic nerve cross-section for F4-80 and CD68. Notably, we detected no elevated levels of F4-80- positive macrophages (Fig. 3G) or CD68-positive activated macrophages (Fig. 3H) indicating that the impaired expression of the aforementioned genes is rather caused by

macrophage dysfunction. Recently, expression of Plekhg5 in macrophages was reported (Iwatake et al, 2017). Moreover, elevated activation of NF-κB in microglial cells – the resident CNS macrophages – was reported to be causative for motoneuron death within the spinal cord in amyotrophic lateral sclerosis (ALS) (Frakes et al, 2014). While NF-κB in macrophages within peripheral nerves was not evaluated, high numbers of macrophages are reportedly being observed in the sciatic nerve of SOD1 G93A mice, a model for ALS (Chiu et al, 2009). It is therefore tempting to speculate, that *Plekhg5*-deficiency additionally leads to macrophages dysfunction within the sciatic nerve and thereby results in an impaired immune response during motoneuron disease.

Taken together our data suggest that *Plekhg5*-deficiency results in defective Schwann cell autophagy and in an impaired recruitment of T-lymphocytes to Schwann cells leading to myelin infoldings and hypermyelination. Recent reports on *TBK1* mutations in ALS (Freischmidt et al, 2015) and the identification of a putative role for *C9ORF72* in immune response regulation (Burberry et al, 2016) further support the idea that the immune system makes major contributions to the pathophysiology of motoneuron disease. Furthermore, OPTN has recently been described to suppress receptor-interacting kinase 1 (RIPK1) signaling for maintenance of axonal integrity. Notably, loss of OPTN from oligodendrocytes and myeloid cells, but not from astrocytes or motoneurons resulted in RIPK1-mediated axon degeneration by promoting inflammation and necroptosis (Ito et al, 2016). Our data add further weight to the notion that the interaction between the immune system and the nervous system needs to be tightly regulated and that a dysregulation of this interplay contributes to the axon pathology in demyelinating PNS disorders and motoneuron disease. We therefore hypothesize that targeting Plekhg5 and/or NF-κB in Schwann cells represents a potential therapeutic approach in demyelinating PNS disorders and motoneuron disease.

Materials and methods

Statistical analysis

Statistical evaluation was done using GraphPad Prism 5 (GraphPad Software, La Jolla, USA). Data is presented as the mean ± SEM if not stated otherwise. The statistical test used for each experiment is listed within the respective figure legend.

Animals

Plekhg5-deficient mice were described previously (Luningschror et al, 2017). Animals were kept under specific pathogen free conditions as defined by the Federation European Laboratory Animal Science Association (FELASA) in the central animal facility of the University of Bielefeld.

Light and electron microscopy

Mice were anaesthetized and transcardially perfused according to local institutional guide lines in 3 steps essentially as described by Forssmann and colleagues (Forssmann et al, 1977) with 3 % paraformaldehyde, 3 % glutaraldehyde, 0.5 % picric acid in 0.1 M sodium phosphate buffer, pH 7.4 for 10 minutes. After dissection, organs were fixed in the same solution for additional 2 hours at 4°C followed by 2 h postfixation in buffered 2% osmium tetroxide at 4°C. Afterwards they were embedded in Araldite. For light microscopy, semi-thin sections were stained with Richardson's blue (1% w/v methylene blue, 1% w/v Azur II) for 3 min, 80°C. For electron microscopy using Zeiss EM 109, ultra-thin (60-80 nm) sections (stained for 40 min in uranyl acetate and 7 min in lead citrate) were prepared.

Determination of g-ratio and counting of Schwann cell nuclei

Semi-thin sections stained with Richardson's blue as stated above were used for analyzing the g-ratio of myelinated axons within the sciatic nerve. High Resolution images were taken and afterwards stitched together with Photoshop CS software (Adobe Systems) resulting in a high resolution image of the whole sciatic nerve cross-section. Using the g-ratio plugin for ImageJ software (Goebbels et al, 2012), 100 randomly chosen axons per cross-section were measured. Fibers with myelin abnormalities were excluded. In addition, nuclei within these images were counted, distinguishing between Schwann cell and other nuclei according to Patzig et al.. A

nucleus in direct contact to an axon was considered to be a Schwann cell nucleus (Patzig et al, 2016).

RNA extraction and qPCR

For extraction of total RNA TRIReagent (Sigmal-Aldrich) was used according to the manufacturer's protocol. 500 ng of RNA were used for cDNA synthesis. cDNA was diluted 1:50 and 2 µL/reaction were used. qPCR was carried out with SYBR Green Master Mix (Thermo Fisher Scientic). The following primers were used: Ppia (fwd 5'-GTCTCCTTCGAGCTGTTTGC-3', rev 5'-GTCTCCTTCGAGCTGTTTGC-3'), EeF2 (fwd 5'-GGAACATGTCAGTCATCGCC-3'; rev 5'-GGAACATGTCAGTCATCGCC-3'), RPLP0 (fwd 5'-TGGGCAAGAACACCATGATG-3'; rev 5' AGTTTCTCCAGAGCTGGGTTGT-3'), Plp1 (fwd 5'-CTCCAAAAACTACCAGGACTATGAG-3'; rev 5'-AGGGCCCCATAAAGGAAGA-3'), Mag (fwd 5'-TGATAAGTATGAGTCCAGAGAGGTC-3'; rev 5'-TGATAAGTATGAGTCCAGAGAGGTC-3'), Sox10 (fwd 5'-TGATAAGTATGAGTCCAGAGAGGTC-3'; rev 5'-TTCGTTCAGCAACCTCCAGA-3'), Egr2 (fwd 5'-GCCAAGGCCGTAGACAAAAT-3'; rev 5'-AATGTTGATCATGCCATCTCCC-3'), Pmp-22 (fwd 5'-AATGTTGATCATGCCATCTCCC-3'; rev 5'-CGGTGCCTGTTTCAGTTCAA-3') P0 (fwd 5'-TTCTTTGGTGCTCTCTCCAGC-3'; rev 5'-TTCTTTGGTGCTCTCTCCAGC-3'), c-Jun (fwd 5'-CCTTCTACGACGATGCCCTC-3'; rev 5'-CCTTCTACGACGATGCCCTC-3'), p75 (fwd 5'-GGGCACATACTCAGATGAAGC-3'; rev 5'-CGTAGACCTTGTGATCCATCG-3').

RNAseq

Total RNA was isolated from sciatic nerves using TRIReagent (Sigmal-Aldrich) according to the manufacturer's guidelines and cDNA library generation was performed using the SENSE mRNA-Seq Library Prep Kit V2 (Lexogen, Vienna, Austria) according to the manufacturer's protocol. Libraries were pooled and sequenced on the Illumina NextSeq 500 with the High Output Kit v2 (75 cycles). Adapters and low quality reads were trimmed with TrimGalore, v0.4.0 (http://www.bioinformatics.babraham.ac.uk/projects/trim_galore/) powered by Cutadapt, v1.8 (https://cutadapt.readthedocs.io/en/stable) (Martin, 2011). Additionally, the first nine nucleotides were removed as described in the Lexogen

user manual. Reads were then mapped using STAR v2.5.0a (https://github.com/alexdobin/STAR) and differentially expressed transcripts were determined using the Cufflinks package v2.2.1 (http://cufflinks.cbcb.umd.edu/) as described before (Briese et al, 2016). Venn diagrams were generated using BioVenn (Hulsen et al, 2008). For gene ontology (GO) analysis we used the Database for Annotation, Visualization and Integrated Discovery (DAVID, http://david.abcc.ncifcrf.gov/home.jsp) (Huang da et al, 2009). As background dataset for the GO term analysis we used all expressed genes which we defined as those transcripts with an average FPKM≥0.1 in either the *Plekhg5*-deficient or wildtype sciatic nerve datasets. NF-κB targets were extracted from https://www.bu.edu/nf-kb/gene-resources/target-genes/. The sequencing files have been deposited in NCBI's Gene Expression Omnibus (Edgar et al, 2002) and are accessible through GEO Series accession number GSEXXX.

Immunohistochemical stainings

Mice were sacrificed by cervical dislocation, the sciatic nerve was dissected, embedded in Tissue-Tec O.C.T. compound (Sakura Finetek) and frozen in 2-methylbutane at -30°C. 10 µm thick sections were cut using CM1900 microtome (Leica Microsystems). Frozen sections were shortly thawed and depending on primary antibody, they were fixed using -20° C cold acetone for 10 minutes, with 4% paraformaldehyde for 10 min or left unfixed. Following repetitive washing using phosphate buffered saline (PBS), sections were incubated in PBS containing 5% BSA to block non-specific bindings. Primary antibodies were applied for overnight at 4° C, followed by washing in PBS and application of secondary fluorochrome-conjugated antibodies. For nuclear counterstaining DAPI (1 µg/ml; AppliChem) was used. After washing, sections were finally cover slipped with Mowiol/DABCO.

For stainings of cultivated nerve segments, segments were fixed in 4 % PFA for 1h, followed by repetitive washing. Teased fiber preparations were done using fine forceps. Fibers were placed on collagen-coated coverslips and after permeabilization using 0.3 % Triton X-100, staining was performed as stated above.

Primary antibodies used according to the manufacturer's protocol were: CD4 (YTS191.1), CD8 (YTS169.4) F4-80 (Cl:A3-1), CD68 (FA-11) (all from Serotec), MPZ/P0 (ab39375; Abcam)

Primary Schwann cell culture

Murine neonatal Schwann cells were cultured essentially as described (Honkanen et al, 2007). Neonatal animals were sacrificed by decapitation at postnatal day five and six. The sciatic nerves were dissected and maintained in ice-cold PBS until all nerves were prepared. Remaining connective tissue was removed and the nerves were transferred to a new dish containing fresh ice-cold PBS, where they were shredded with forceps. Following enzymatic digestion using trypsin (final concentration 0.125%) and collagenase A (final concentration 0.05%) for 30 min at 37°C, nerve fragments were centrifuged for 5 min at 190 x g. After three washing steps with 7 mL DMEM containing 10% horse serum and centrifugation for 5 min at 190 x g, the pellet was resuspended in basic growth medium (DMEM containing 10% horse serum, 4 mM L-Glutamine, 100 u/mL Penicillin/Streptomycin, 2ng/mL human heregulin-β1 and 0.5 μM forskolin), plated on a poly-D-lysine coated 60 mm tissue culture dish and incubated at 37° C and 5% CO2. After two days in culture, basic growth medium was replaced and the cells were allowed to grow for two additional days. To get rid of upcoming fibroblasts, complement-mediated cytolysis was done at day four in culture. Medium was removed and the cells were rinsed with HBSS in 20 mM HEPES, followed by rinsing with HMEM (DMEM containing 10% horse serum, 4 mM L-glutamine, 100 u/mL penicillin/streptomycin and 20 mM HEPES). Anti-mouse CD90 antibody was diluted in HMEM to a final concentration of 4 μg/mL and added to the cells. After 15 min at 37°C complement sera was added and incubation continued for additional two hours. Cells were rinsed twice with HBSS containing 20 mM HEPES and finally Schwann cell growth medium (basic growth medium containing 10 ng/mL FGF-2 and 20 μg/mL bovine pituitary extract) was added. Medium was changed every two days and cells were subcultured when reaching 80% confluency. All cells were passaged at least once before being used for experiments.

Cultivation of sciatic nerve segments

Sciatic nerve segments were cultivated as described (Gomez-Sanchez et al, 2015). Briefly, adult mice were sacrificed by cervical dislocation and the sciatic nerves were prepared and placed on ice in HBSS. Connective tissue was removed and the desheathed nerves were cut into 5 mm long segments. Segments were transferred to culture medium (DMEM containing 5 % FCS) and cultivated for 5 days at 37° C and 5% CO_2.

Lentivirus production

For lentivirus production, HEK 293FT cells were transfected with the plasmids indicated and packaging plasmids VSV-G and delta8.91 using standard calcium phosphate precipitation. 8 hours after transfection, medium was exchanged and 48 to 72 h after transfection supernatants were collected and concentrated by ultracentrifugation. For transduction, lentiviral particles were diluted in the respective growth medium and polybrene was added to a final concentration of 8 µg/mL.

Acknowledgement

Author contributions

CS and PL designed and performed experiments, analyzed data and wrote the manuscript. UW performed experiments PH designed and performed experiments. MB and SA analyzed data. MS provided resources. BK designed experiments. CK designed experiments, provided resources and supervised the study.

References

Adlkofer K, Martini R, Aguzzi A, Zielasek J, Toyka KV, Suter U (1995) Hypermyelination and demyelinating peripheral neuropathy in Pmp22-deficient mice. Nature genetics 11**:** 274-280

Azzedine H, Zavadakova P, Plante-Bordeneuve V, Vaz Pato M, Pinto N, Bartesaghi L, Zenker J, Poirot O, Bernard-Marissal N, Arnaud Gouttenoire E et al (2013) PLEKHG5 deficiency leads to an intermediate form of autosomal-recessive Charcot-Marie-Tooth disease. Human molecular genetics 22**:** 4224-4232

Bergsteinsdottir K, Kingston A, Jessen KR (1992) Rat Schwann cells can be induced to express major histocompatibility complex class II molecules in vivo. Journal of neurocytology 21**:** 382-390

Bonetti B, Stegagno C, Cannella B, Rizzuto N, Moretto G, Raine CS (1999) Activation of NF-kappaB and c-jun transcription factors in multiple sclerosis lesions. Implications for oligodendrocyte pathology. The American journal of pathology 155**:** 1433-1438

Braun PE, Frail DE, Latov N (1982) Myelin-associated glycoprotein is the antigen for a monoclonal IgM in polyneuropathy. Journal of neurochemistry 39**:** 1261-1265

Briese M, Saal L, Appenzeller S, Moradi M, Baluapuri A, Sendtner M (2016) Whole transcriptome profiling reveals the RNA content of motor axons. Nucleic acids research 44**:** e33

Brosius Lutz A, Barres BA (2014) Contrasting the glial response to axon injury in the central and peripheral nervous systems. Developmental cell 28**:** 7-17

Burberry A, Suzuki N, Wang JY, Moccia R, Mordes DA, Stewart MH, Suzuki-Uematsu S, Ghosh S, Singh A, Merkle FT et al (2016) Loss-of-function mutations in the C9ORF72 mouse ortholog cause fatal autoimmune disease. Science translational medicine 8**:** 347ra393

Cai Z, Finnie JW, Blumbergs PC, Manavis J, Ghabriel MN, Thompson PD (2006) Early paranodal myelin swellings (tomacula) in an avian riboflavin deficiency model of demyelinating neuropathy. Experimental neurology 198**:** 65-71

Charo IF, Ransohoff RM (2006) The many roles of chemokines and chemokine receptors in inflammation. The New England journal of medicine 354**:** 610-621

Chiu IM, Phatnani H, Kuligowski M, Tapia JC, Carrasco MA, Zhang M, Maniatis T, Carroll MC (2009) Activation of innate and humoral immunity in the peripheral nervous system of ALS transgenic mice. Proceedings of the National Academy of Sciences of the United States of America 106**:** 20960-20965

Chung KW, Hyun YS, Lee HJ, Jung HK, Koo H, Yoo JH, Kim SB, Park CI, Kim HN, Choi BO (2011) Two recessive intermediate Charcot-Marie-Tooth patients with GDAP1 mutations. Journal of the peripheral nervous system : JPNS 16**:** 143-146

de Rosbo NK, Ben-Nun A (1998) T-cell responses to myelin antigens in multiple sclerosis; relevance of the predominant autoimmune reactivity to myelin oligodendrocyte glycoprotein. Journal of autoimmunity 11**:** 287-299

De Toledo M, Coulon V, Schmidt S, Fort P, Blangy A (2001) The gene for a new brain specific RhoA exchange factor maps to the highly unstable chromosomal region 1p36.2-1p36.3. Oncogene 20**:** 7307-7317

Edgar R, Domrachev M, Lash AE (2002) Gene Expression Omnibus: NCBI gene expression and hybridization array data repository. Nucleic acids research 30**:** 207-210

Fabrizi GM, Taioli F, Cavallaro T, Rigatelli F, Simonati A, Mariani G, Perrone P, Rizzuto N (2000) Focally folded myelin in Charcot-Marie-Tooth neuropathy type 1B with Ser49Leu in the myelin protein zero. Acta neuropathologica 100**:** 299-304

Fernandez-Valle C, Bunge RP, Bunge MB (1995) Schwann cells degrade myelin and proliferate in the absence of macrophages: evidence from in vitro studies of Wallerian degeneration. Journal of neurocytology 24**:** 667-679

Forssmann WG, Ito S, Weihe E, Aoki A, Dym M, Fawcett DW (1977) An improved perfusion fixation method for the testis. The Anatomical record 188**:** 307-314

Frakes AE, Ferraiuolo L, Haidet-Phillips AM, Schmelzer L, Braun L, Miranda CJ, Ladner KJ, Bevan AK, Foust KD, Godbout JP et al (2014) Microglia induce motor neuron death via the classical NF-kappaB pathway in amyotrophic lateral sclerosis. Neuron 81**:** 1009-1023

Freischmidt A, Wieland T, Richter B, Ruf W, Schaeffer V, Muller K, Marroquin N, Nordin F, Hubers A, Weydt P et al (2015) Haploinsufficiency of TBK1 causes familial ALS and fronto-temporal dementia. Nature neuroscience 18**:** 631-636

Gobert M, Treilleux I, Bendriss-Vermare N, Bachelot T, Goddard-Leon S, Arfi V, Biota C, Doffin AC, Durand I, Olive D et al (2009) Regulatory T cells recruited through CCL22/CCR4 are selectively activated in lymphoid infiltrates surrounding primary breast tumors and lead to an adverse clinical outcome. Cancer research 69**:** 2000-2009

Goebbels S, Oltrogge JH, Wolfer S, Wieser GL, Nientiedt T, Pieper A, Ruhwedel T, Groszer M, Sereda MW, Nave KA (2012) Genetic disruption of Pten in a novel mouse model of tomaculous neuropathy. EMBO molecular medicine 4**:** 486-499

Gomez-Sanchez JA, Carty L, Iruarrizaga-Lejarreta M, Palomo-Irigoyen M, Varela-Rey M, Griffith M, Hantke J, Macias-Camara N, Azkargorta M, Aurrekoetxea I et al (2015) Schwann cell autophagy, myelinophagy, initiates myelin clearance from injured nerves. The Journal of cell biology 210**:** 153-168

Honkanen H, Lahti O, Nissinen M, Myllyla RM, Kangas S, Paivalainen S, Alanne MH, Peltonen S, Peltonen J, Heape AM (2007) Isolation, purification and expansion of myelination-competent, neonatal mouse Schwann cells. The European journal of neuroscience 26**:** 953-964

Huang da W, Sherman BT, Lempicki RA (2009) Systematic and integrative analysis of large gene lists using DAVID bioinformatics resources. Nature protocols 4**:** 44-57

Hulsen T, de Vlieg J, Alkema W (2008) BioVenn - a web application for the comparison and visualization of biological lists using area-proportional Venn diagrams. BMC genomics 9**:** 488

Imai T, Hieshima K, Haskell C, Baba M, Nagira M, Nishimura M, Kakizaki M, Takagi S, Nomiyama H, Schall TJ et al (1997) Identification and molecular characterization of fractalkine receptor CX3CR1, which mediates both leukocyte migration and adhesion. Cell 91**:** 521-530

Ip CW, Kroner A, Bendszus M, Leder C, Kobsar I, Fischer S, Wiendl H, Nave KA, Martini R (2006) Immune cells contribute to myelin degeneration and axonopathic changes in mice overexpressing proteolipid protein in oligodendrocytes. The Journal of neuroscience : the official journal of the Society for Neuroscience 26**:** 8206-8216

Ito Y, Ofengeim D, Najafov A, Das S, Saberi S, Li Y, Hitomi J, Zhu H, Chen H, Mayo L et al (2016) RIPK1 mediates axonal degeneration by promoting inflammation and necroptosis in ALS. Science 353**:** 603-608

Iwatake M, Nishishita K, Okamoto K, Tsukuba T (2017) The Rho-specific guanine nucleotide exchange factor Plekhg5 modulates cell polarity, adhesion, migration, and podosome organization in macrophages and osteoclasts. Experimental cell research 359**:** 415-430

Kaltschmidt B, Kaltschmidt C (2009) NF-kappaB in the nervous system. Cold Spring Harbor perspectives in biology 1**:** a001271

Kaushansky N, Eisenstein M, Zilkha-Falb R, Ben-Nun A (2010) The myelin-associated oligodendrocytic basic protein (MOBP) as a relevant primary target autoantigen in multiple sclerosis. Autoimmunity reviews 9**:** 233-236

Kim HJ, Hong YB, Park JM, Choi YR, Kim YJ, Yoon BR, Koo H, Yoo JH, Kim SB, Park M et al (2013) Mutations in the PLEKHG5 gene is relevant with autosomal recessive intermediate Charcot-Marie-Tooth disease. Orphanet journal of rare diseases 8**:** 104

Kobsar I, Oetke C, Kroner A, Wessig C, Crocker P, Martini R (2006) Attenuated demyelination in the absence of the macrophage-restricted adhesion molecule sialoadhesin (Siglec-1) in mice heterozygously deficient in P0. Molecular and cellular neurosciences 31**:** 685-691

Lee SM, Sha D, Mohammed AA, Asress S, Glass JD, Chin LS, Li L (2013) Motor and sensory neuropathy due to myelin infolding and paranodal damage in a transgenic mouse model of Charcot-Marie-Tooth disease type 1C. Human molecular genetics 22**:** 1755-1770

Luningschror P, Binotti B, Dombert B, Heimann P, Perez-Lara A, Slotta C, Thau-Habermann N, C RvC, Karl F, Damme M et al (2017) Plekhg5-regulated autophagy

of synaptic vesicles reveals a pathogenic mechanism in motoneuron disease. Nature communications 8**:** 678

Martin M (2011) Cutadapt removes adapter sequences from high-throughput sequencing reads. 2011 17

Marx R, Henderson J, Wang J, Baraban JM (2005) Tech: a RhoA GEF selectively expressed in hippocampal and cortical neurons. Journal of neurochemistry 92**:** 850-858

Matsuda A, Suzuki Y, Honda G, Muramatsu S, Matsuzaki O, Nagano Y, Doi T, Shimotohno K, Harada T, Nishida E et al (2003) Large-scale identification and characterization of human genes that activate NF-kappaB and MAPK signaling pathways. Oncogene 22**:** 3307-3318

Mattson MP, Meffert MK (2006) Roles for NF-kappaB in nerve cell survival, plasticity, and disease. Cell death and differentiation 13**:** 852-860

Maystadt I, Rezsohazy R, Barkats M, Duque S, Vannuffel P, Remacle S, Lambert B, Najimi M, Sokal E, Munnich A et al (2007) The nuclear factor kappaB-activator gene PLEKHG5 is mutated in a form of autosomal recessive lower motor neuron disease with childhood onset. American journal of human genetics 81**:** 67-76

Meyer zu Horste G, Heidenreich H, Mausberg AK, Lehmann HC, ten Asbroek AL, Saavedra JT, Baas F, Hartung HP, Wiendl H, Kieseier BC (2010) Mouse Schwann cells activate MHC class I and II restricted T-cell responses, but require external peptide processing for MHC class II presentation. Neurobiology of disease 37**:** 483-490

Miyagishi R, Kikuchi S, Takayama C, Inoue Y, Tashiro K (1997) Identification of cell types producing RANTES, MIP-1 alpha and MIP-1 beta in rat experimental autoimmune encephalomyelitis by in situ hybridization. Journal of neuroimmunology 77**:** 17-26

Nave KA, Werner HB (2014) Myelination of the nervous system: mechanisms and functions. Annual review of cell and developmental biology 30**:** 503-533

Noor S, Wilson EH (2012) Role of C-C chemokine receptor type 7 and its ligands during neuroinflammation. Journal of neuroinflammation 9**:** 77

Ozoguz A, Uyan O, Birdal G, Iskender C, Kartal E, Lahut S, Omur O, Agim ZS, Eken AG, Sen NE et al (2015) The distinct genetic pattern of ALS in Turkey and novel mutations. Neurobiology of aging 36**:** 1764 e1769-1764 e1718

Patzig J, Kusch K, Fledrich R, Eichel MA, Luders KA, Mobius W, Sereda MW, Nave KA, Martini R, Werner HB (2016) Proteolipid protein modulates preservation of peripheral axons and premature death when myelin protein zero is lacking. Glia 64**:** 155-174

Quattrone A, Gambardella A, Bono F, Aguglia U, Bolino A, Bruni AC, Montesi MP, Oliveri RL, Sabatelli M, Tamburrini O et al (1996) Autosomal recessive hereditary

motor and sensory neuropathy with focally folded myelin sheaths: clinical, electrophysiologic, and genetic aspects of a large family. Neurology 46**:** 1318-1324

Robinson FL, Niesman IR, Beiswenger KK, Dixon JE (2008) Loss of the inactive myotubularin-related phosphatase Mtmr13 leads to a Charcot-Marie-Tooth 4B2-like peripheral neuropathy in mice. Proceedings of the National Academy of Sciences of the United States of America 105**:** 4916-4921

Sanford M (2014) Fingolimod: a review of its use in relapsing-remitting multiple sclerosis. Drugs 74**:** 1411-1433

Schmid CD, Stienekemeier M, Oehen S, Bootz F, Zielasek J, Gold R, Toyka KV, Schachner M, Martini R (2000) Immune deficiency in mouse models for inherited peripheral neuropathies leads to improved myelin maintenance. The Journal of neuroscience : the official journal of the Society for Neuroscience 20**:** 729-735

Tak PP, Firestein GS (2001) NF-kappaB: a key role in inflammatory diseases. The Journal of clinical investigation 107**:** 7-11

Wang Ip C, Kroner A, Fischer S, Berghoff M, Kobsar I, Maurer M, Martini R (2006) Role of immune cells in animal models for inherited peripheral neuropathies. Neuromolecular medicine 8**:** 175-190

Zhang Y, Chen K, Sloan SA, Bennett ML, Scholze AR, O'Keeffe S, Phatnani HP, Guarnieri P, Caneda C, Ruderisch N et al (2014) An RNA-sequencing transcriptome and splicing database of glia, neurons, and vascular cells of the cerebral cortex. The Journal of neuroscience : the official journal of the Society for Neuroscience 34**:** 11929-11947
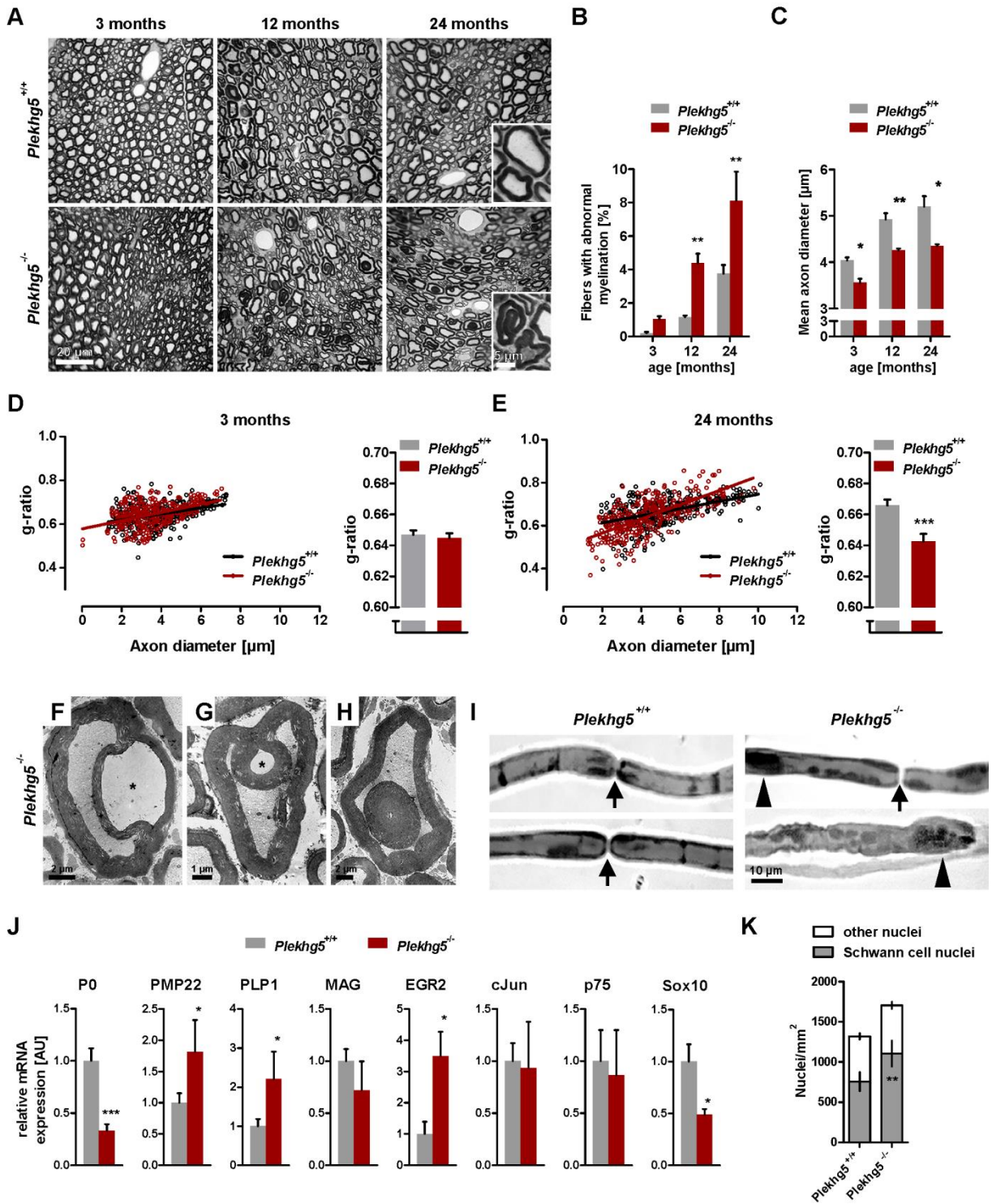
Figures

Figure 1

Figure 1 – Histopathological analysis of the sciatic nerve

A   Semi-thin sections of the sciatic nerve of wildtype (*Plekhg5*$^{+/+}$) and mutant mice (*Plekhg5*$^{-/-}$) at different ages. Scale bars: 20 µm and 5 µm (blow-up).

B   Relative amount of axons with myelin alterations. Five animals per genotype and age (n=5, unpaired, two-tailed t-test).

C   Mean axonal diameter of wildtype and mutant mice at different ages. Three animals per genotype and age (n=3, unpaired, two-tailed t-test)

D, **E**   G-ratio analysis of 3 (D) and 24 (E) months old mice. Three animals per age and genotype, 100 axons per animal were analyzed.

F, **G**, **H**   Electromicrographs of *Plekhg5*-deficient mice depicting myelin infoldings at different stages. Scale bars: 2 µm (F, H) and 1 µm (G)

I   Teased fiber preparations of wildtype and mutant mice. Arrows point to nodes of Ranvier, arrowheads to myelin accumulations. Scale bar: 10 µm

J   qPCR analysis of several Schwann cell markers within the sciatic nerve of wildtype and mutant mice (n = 5/6 (wildtype/mutant), unpaired, two-tailed t-test).

K   Number of nuclei within the sciatic nerve of 3 months old mice distinguishing between Schwann cell nuclei and others. Three animals per genotype (n=3, two-way ANOVA with Bonferroni posttest).
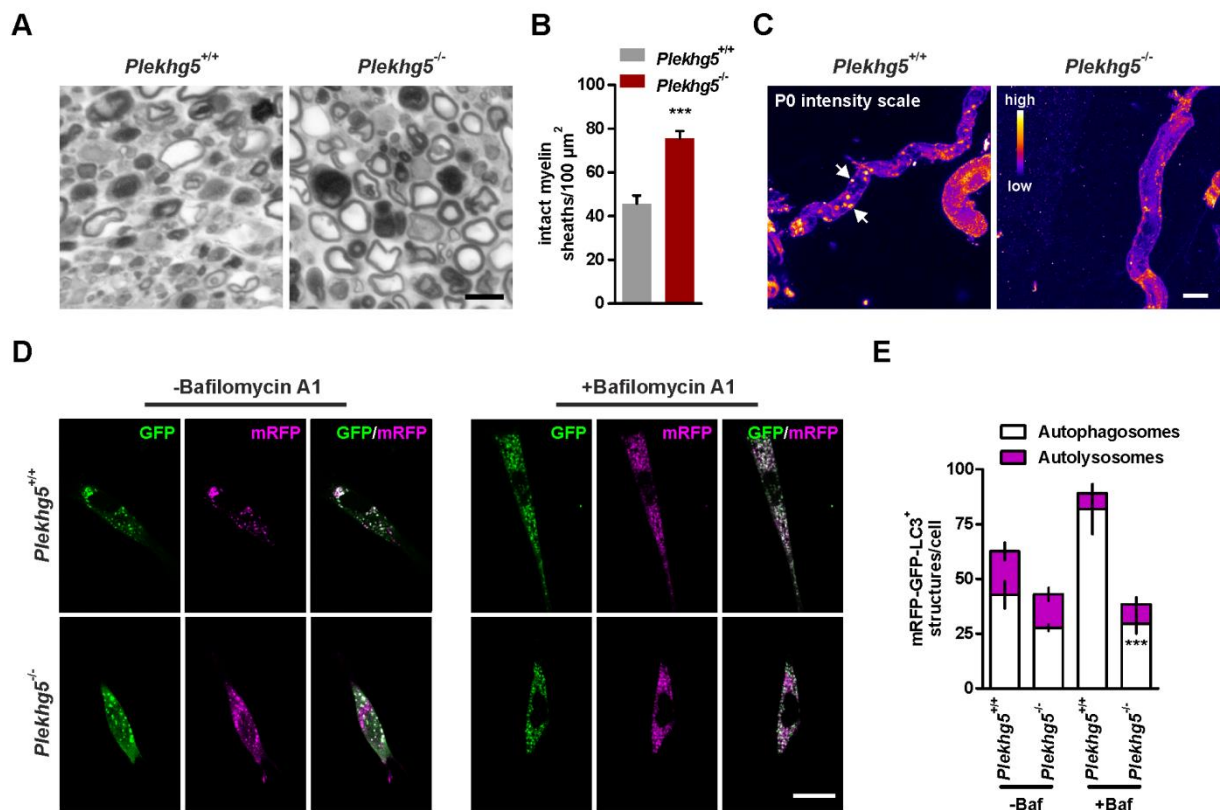
Figure 2

Figure 2 – Impairments in Schwann cell autophagy upon *Plekhg5*-deficiency

A Representative images of semi-thin sections of sciatic nerve fragments from wildtype and mutant mice cultivated for 5 days.

B Amount of intact myelin sheaths, normalized to the area of the section analyzed. At least 5 sections per animal were analyzed; 3 animals per genotype (n=3, unpaired, two-tailed t-test).

C Immunohistochemical stainings of teased fiber preparations derived from cultivated sciatic nerve fragments against the myelin protein zero (P0). Arrows point to degraded myelin. Scale bar: 10 μm

D Immunofluorescent analysis of primary Schwann cells transduced with mRFP-GFP-LC3 reporter. Prior to fixation, cells were treated with 400 nM Bafilomycin A1 for 4 hours or left untreated.

E Quantitative analysis of fluorescent structures within transduced Schwann cells. GFP$^+$-RFP$^+$-structures were defined as autophagosomes, GFP$^-$-RFP$^+$-structures as autolysosomes. At least 5 cells per experiment were analyzed; 3 independent experiments (n = 3, two-way ANOVA with Bonferroni posttest).

Figure 3
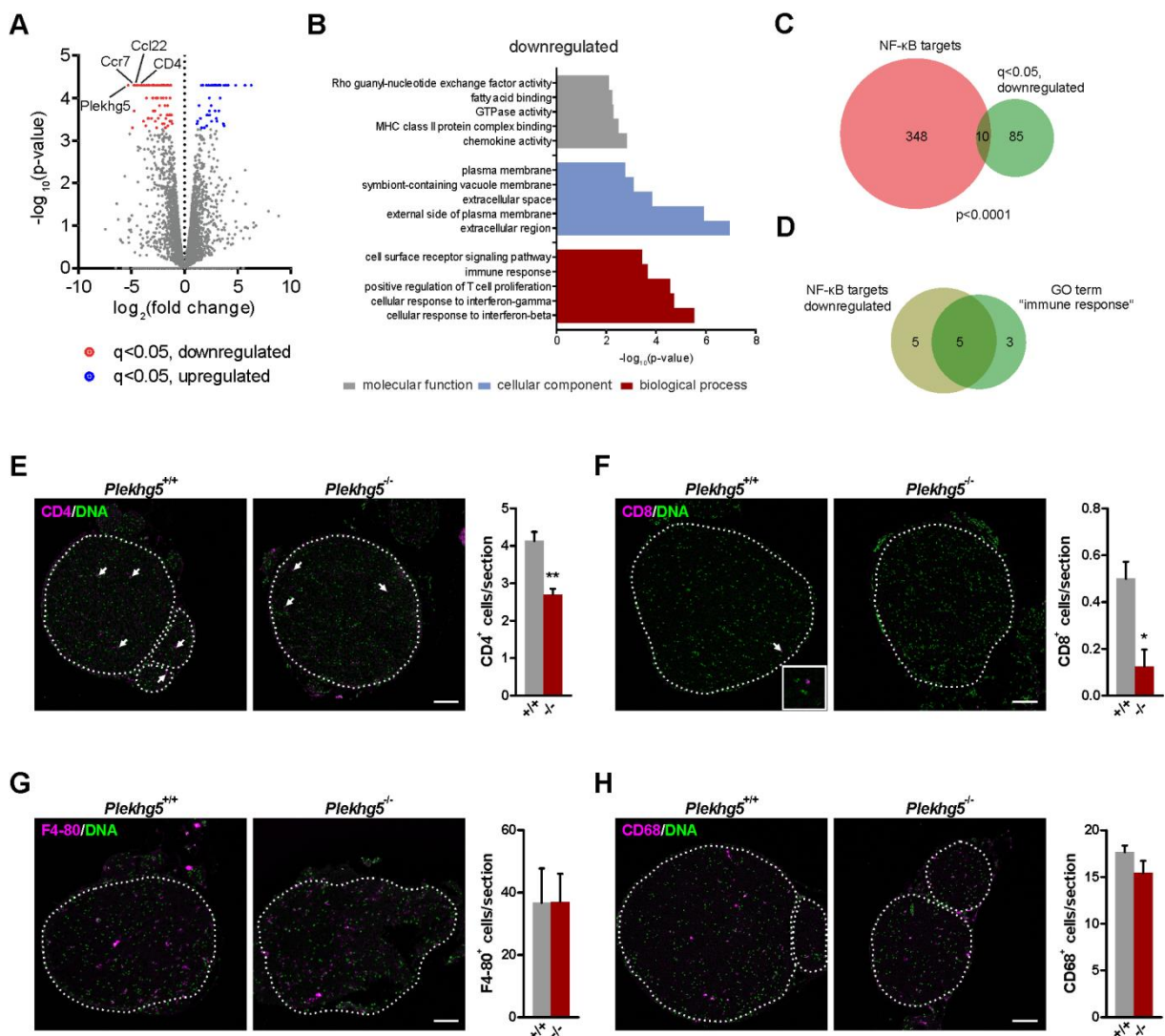
Figure 3 – Lack of Plekhg5 results in a reduced immune response within the sciatic nerve

A Volcano plot showing the significance of transcript change [$-\log_{10}$(p-value)] vs. the magnitude of change [$\log_2$(fold change)]. Downregulated transcripts with $q<0.05$ are marked in red, upregulated transcripts with $q<0.05$ are marked in blue. Data points for transcripts with log2FC<-10 or >10 (all of which were not significantly altered) were omitted for visualization purposes.

B Gene-ontology (GO) term analysis of significantly downregulated genes

C,D Venn diagrams depicting the number of NF-κB targets within (C) all downregulated genes and (D) within the GO term "immune response".

E-H Immunohistochemical stainings of sciatic nerve sections against the T-lymphocyte markers CD4 (C) and CD8 (D) and the macrophage markers F4-80 (E)

and CD-68 (H). For each marker at least 8 sections per animal were analyzed. Three animals per genotype (n=3, unpaired, two-tailed t-test). Scale bars: 100 µm

Supplementary figures

Figure S1
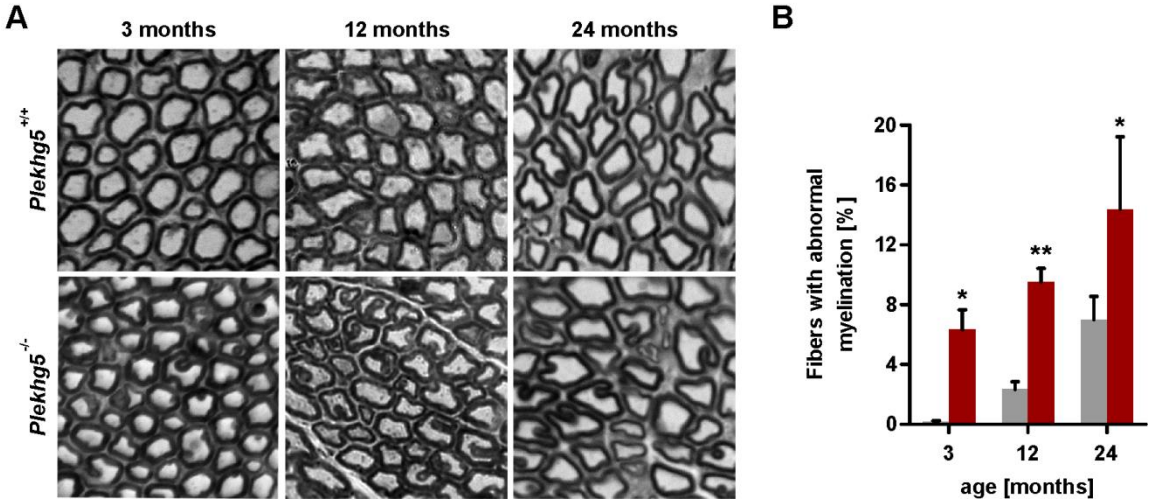
Figure S1 – Histopathological analysis of the phrenic nerve

A   Semi-thin sections of the phrenic nerve of wildtype and mutant mice at different ages.

B   Relative amount of axons with myelin alterations. Five animals per genotype and age (n=5, unpaired, two-tailed t-test).

Figure S2

A

B
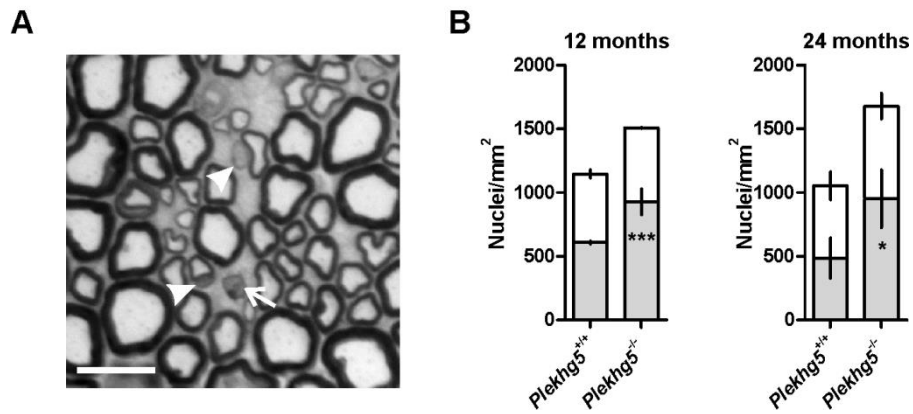
Figure S2 – Elevated numbers of Schwann cells in *Plekhg5*-deficient mice

A   Semi-thin section of a sciatic nerve. Arrowheads point to Schwann cell nuclei, arrows to other nuclei. Scale bar: 10 µm

B   Number of nuclei within the sciatic nerve of 12 and 24 months old mice distinguishing between Schwann cell nuclei and others. Three animals per genotype and age (n=3, two-way ANOVA with Bonferroni posttest).

Figure S3

A

B
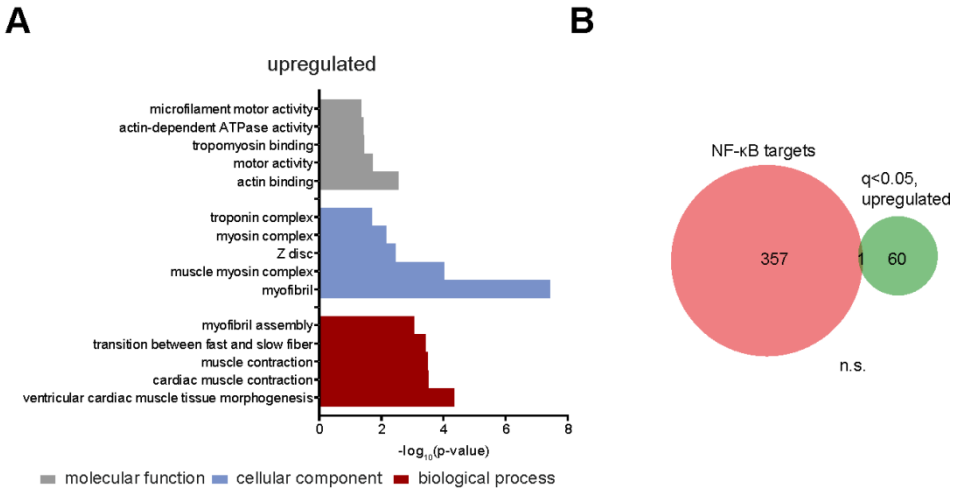
Figure S3 – Upregulated genes within the sciatic nerve of *Plekhg5*^{-/-} mice

A   Gene-ontology (GO) term analysis of significantly upregulated genes.

B   Venn diagram showing the number of NF-κB target genes among the upregulated genes.

Impaired clearance of autolysosomes in *PLEKHG5*-deficient human glioma cells

Carsten Slotta[1,2], Kaya E. Friedrich[1,2], Angelika Kitke[1], Johannes F.W. Greiner[1], Christian Kaltschmidt[1+], Barbara Kaltschmidt[1,2+*]

[1] Department of Cell Biology, University of Bielefeld, Universitaetsstr. 25, 33501 Bielefeld, Germany

[2] Molecular Neurobiology, University of Bielefeld, Universitaetsstr. 25, 33501 Bielefeld, Germany

[+] These authors contributed equally to this work

* Corresponding Author:

Barbara Kaltschmidt, Molecular Neurobiology, Department of Cell Biology, University of Bielefeld, Universitaetsstr. 25, 33501 Bielefeld, Germany,

Tel.: + 49 521 106 5624; Fax: + 49 521 106 5654; E-Mail: barbara.kaltschmidt@uni-bielefeld.de

Abstract

The autophagy-mediated degradation of cellular components recently is the focus of cancer research. Cancer cells rely on autophagy for survival. Moreover, elevated autophagy is associated with increased resistance of tumor cells during therapy.

Here, we applied CRISPR/Cas9-mediated genome editing to perform a knockout of *PLEKHG5* in U251-MG cells as a model for glioblastoma multiforme. Homozygous deletions within the *PLEKHG5* gene resulted in the lack of Plekhg5 protein, validated using genomic PCR and immunocytochemistry. Profound changes of cellular morphology and significantly impaired proliferation was observed after depletion of Plekhg5. Changes in the procession of autophagy within *PLEKHG5*-deficient cells, as demonstrated by highly elevated levels of autolysosomes indicating an impaired clearance. Targeting autophagy remains a promising approach within anticancer therapy, in particular for chemo-resistant tumors such as glioblastoma. Thus, the findings presented in this study have direct clinical implications and point towards new therapy options for glioblastoma.

Introduction

Autophagy is a cellular process, in which damaged or non-used biomolecules such as lipids, proteins or even organelles are being degraded and recycled (reviewed in (Boya et al, 2013)). It serves both as an alternative energy source for the cell during metabolic stress and in preventing the accumulation of e.g. aggregated proteins. In the context of disease, particularly in cancer, opposing effects of autophagy have been reported. While the contribution of autophagy on tumor formation remains a matter of scientific debate (Thorburn, 2014), inhibition of autophagic processes might generally be beneficial within anticancer therapy (Amaravadi et al, 2007; Levy et al, 2017). Presumably due to a higher metabolic rate, tumor cells rely on autophagy as an important recycling mechanism for cell survival (Rabinowitz & White, 2010). Importantly, elevated autophagy was described as essential for cell survival in hypoxic tumor regions (Degenhardt et al, 2006).

Malignant glioblastomas (GBM) are the most common and lethal primary brain tumors (Stupp et al, 2009). Although immuno- and chemotherapies are one therapy option, surgical resection remains the most applied treatment for glioblastoma. However, even with maximum treatment, survival time is no longer than 14 months (Koshy et al, 2012). Major obstacles preventing successful therapy are the heterogeneity of the tumor cells (hence the name "multiforme") and the variety of underling causative mutationsm. Moreover, Glioblastoma cells are particularly resistant against chemotherapeutics, which in turn leads to tumor recurrence and decreased survival. Upregulation of autophagy upon chemotherapeutic treatment increases glioblastoma cell survival, suggestively contributing to therapy resistance and recurrence (Knizhnik et al, 2013; Wurstle et al, 2017). The cell line U251-MG derived from a grade III-IV malignant glioma and was isolated in 1973 (Ponten & Macintyre, 1968; Westermark et al, 1973). Since then U251-MG cells were used extensively as a model to study cellular mechanisms of glioblastoma cells.

The Pleckstrin homology containing family member 5 (Plekhg5) is a guanine exchange factor (GEF). Plekhg5 is highly expressed in endothelial cells, within the nervous system as well as in cancer cells (Dachsel et al, 2013; Liu & Horowitz, 2006; Marx et al, 2005). In skin cancer cells, Plekhg5 was reported to function in VEGF-induced proliferation (Yoshida et al, 2015). In U251-MG cells, it was demonstrated to regulate polarity-orientated cell migration (Dachsel et al, 2013). Recently, a novel role of Plekhg5 in the regulation of autophagy-mediated clearance of synaptic vesicles

was described (Luningschror et al, 2017). We hypothesized Plekhg5-mediated regulation of autophagy not to be restricted to motoneurons and aimed to analyze its putative function within cancer cells.

In this study, we generated a CRISPR/Cas9-mediated knockout of the *PLEKHG5* gene in U251-MG cells. Clonally grown Plekhg5-depleted cells showed significantly reduced proliferation and profound loss of cellular polarity. Moreover, lack of Plekhg5 resulted in a significantly increased number of autolysosomes. As the formation of autophagosomes was not altered, an impaired termination of autophagy was suggested. Targeting autophagy is a promising approach to sensitize tumor cells to chemotherapeutic agents. Importantly, autophagy is particularly relevant for the survival and recurrence of glioblastoma. Thus, the observations made in this study have direct implications for the development of new treatment strategies.

Results

Successful generation of *PLEKHG5*-deficient cells using CRISPR/Cas9

To target autophagy-mediated recycling processes in glioblastoma cells, we first generated U251-MG cells deficient for *PLEKHG5* by applying CRISPR/Cas9. In first instance, a genomic deletion spanning the boundary of intron 2 and exon 3 to efficiently knockout the gene was designed (Fig. 1A). The genomic deletion in clonally grown cells was detected using genomic PCR with primers flanking the desired deletion (Fig. 1B). Using immunocytochemistry, a clear reduction in the intensity of the fluorescent signal was detected in mutant cells when compared to wildtype cells (Fig. 1C). Thus, we confirmed that the genomic deletion resulted in a lack of PLEKHG5 protein in U251-MG.
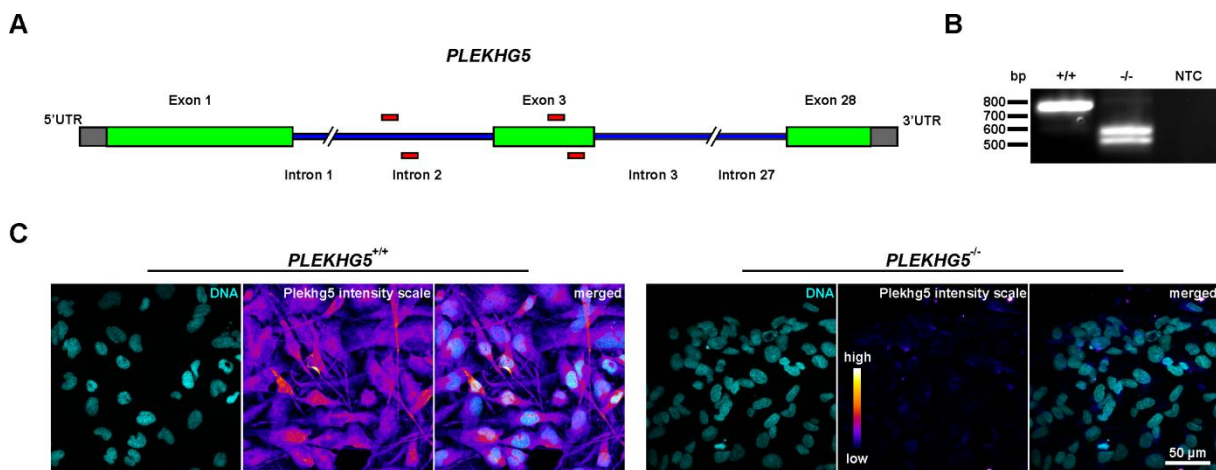
Figure 1. Generation of CRISPR/Cas9-mediated *PLEKHG5* knockout in U251-MG cells. (A) Target design for the genomic deletion. sgRNAs used are depicted in red**. (B)** Clonally grown cells display the desired genomic deletion as shown by genomic PCR using primers flanking the deletion**. (C)** Immunocytochemistry revealed a nearly complete loss of Plekhg5 protein in mutant cells compared to wildtype cells.

Knockout of *PLEKHG5* results in a loss of cellular polarity and a markedly reduced proliferation

We wanted to further analyze potential effects of *PLEKHG5*-deficiency on cellular polarity and proliferation. Cells lacking Plekhg5 displayed prominent morphological changes (Fig. 2A, B). In general, cell polarization was markedly reduced, as was observed by light microscopy (Fig. 2A). Phalloidin staining clearly revealed an altered organization of the actin cytoskeleton (Fig. 2B). In contrast to a mostly bipolar structure of wildtype cells, mutant cells rather appeared apolar. As a consequence of

the loss of polarity, a markedly reduced migratory behavior was observed. In contrast to wildtype cells, which usually grow homogenously distributed, mutant cells grew in local spots without spreading out. However, despite their clonal origin, mutant cells rapidly adapted a heterogenic phenotype. This was particularly apparent in terms of cell polarity ranging from complete apolar (Fig. 2B) to multipolar cells (Fig. S1). Of note, migratory behavior of the mutant cells did not change over time.

Mutant cells additionally displayed reduced proliferation. The population doubling time of 29.3 ± 2.1 hours was significantly elevated compared to 22.9 ± 0.9 hours observed in wildtype cells to (Fig. 2C). In line with this, using Orangu™ Cell Proliferation Assay Kit dehydrogenase activity measured in *PLEKHG5*-deficient cells was significantly reduced (Fig. 2D).
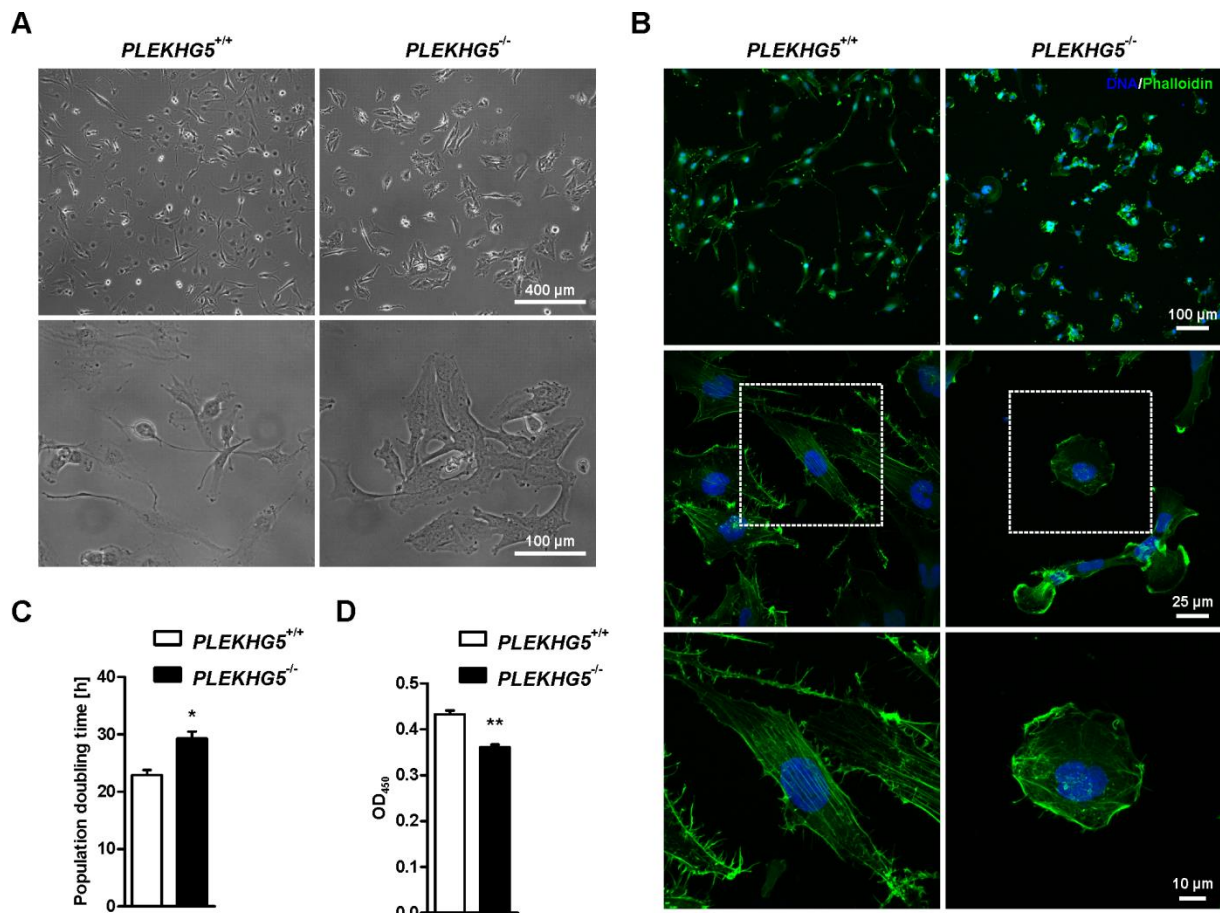
Figure 2. *PLEKHG5*-deficiency in U251-MG resulted in adaptation of an apolar phenotype and decreased proliferation. (A) Lightmicroscopic images of wildtype and mutant cells display differences in cellular morphology. **(B)** Immunofluorescent stainings of f-actin using phalloidin reveals de-organization of the actin cytoskeleton in *PLEKHG5*-deficient cells. **(C)** Significantly reduced population doubling tome of *PLEKHG5*-deficient cells (n=3; unpaired, two-tailed t-test). **(D)** Reduced absorbance due to reduced dehydrogenase activity was shown in knockout-cells compared to wildtype cells (n=6; unpaired, two-tailed t-test).

PLEKHG5^{-/-} cells display an impaired clearance of autolysosomes

Previously, we demonstrated direct involvement of Plekhg5 in the formation of autophagosomes within motoneurons (Luningschror et al, 2017). We therefore wanted to test potential effects on the autophagic process within the newly generated mutant cells. We biochemically assessed the levels of LC3-II as a marker for autophagosomes. Mutant and wildtype cells were treated for 4 h with 200 nM Bafilomycin A1 to block fusion of autophagosomes and autolysosomes, resulting in an enrichment of LC3-II-positive autophagosomes. No differences in the LC3-II levels were detectable in mutant cells under basal conditions as well as upon treatment with Bafilomycin A1, as compared to wildype cells (Fig. 3A).
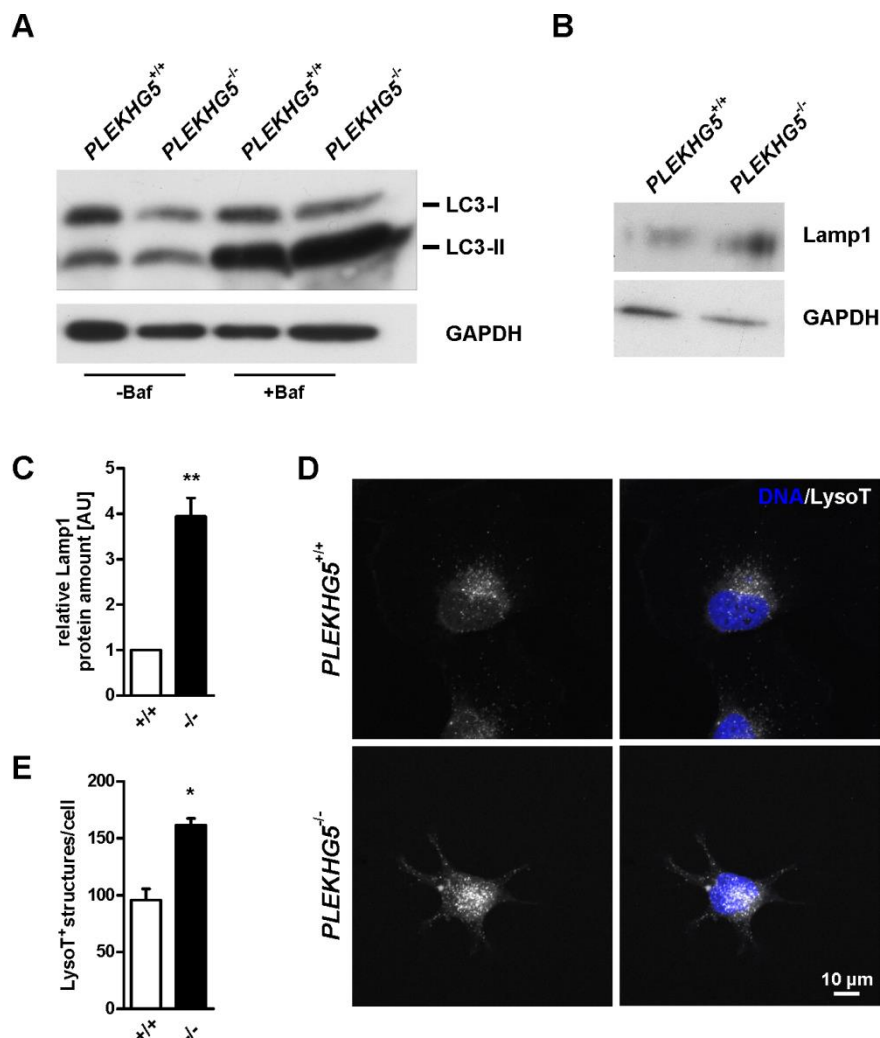
Figure 3 Lack of Plekhg5 leads to accumulation of acidic organelles. (A) Formation of autophagosomes assessed by LC3-II levels is not altered under basal conditions and upon treatment with Bafilomycin A1 (Baf) in *PLEKHG5*-deficient cells **(B, C)** Western blot analysis reveals a significantly elevated Lamp1 protein amount in mutant cells (n=4, paired, two-tailed t-test). **(D, E)** Staining of acidic organelles using Lysotracker Deep Red revealed increased numbers of acidic organelles in *PLEKHG5*-deficient cells (five cells per experiment and genotype were analyzed, n=3, unpaired, two-tailed t-test).

7

However, we observed a significantly increased number of acidic organelles in *PLEKHG5*-deficient cells after applying LysoTracker Deep Red (Fig. 3D, E). In line with that, significantly elevated protein levels of the lysosomal marker Lamp1 were detected using Western blot (Fig 3B, C).

Next we addressed, whether the acidic and Lamp1-positive structures marked autolysosomes. Thus, a RFP-GFP-LC3 reporter was stably introduced into wildtype and mutant cells. Fusion of autophagosomes and lysosome quenches the GFP fluorescence due to the pH drop (Mizushima et al, 2010). Therefore, structures positive for both RFP and GFP mark autophagosomes, whereas structures positive only for RFP mark autolysosomes. In line with the endogenous levels of LC3-II (Fig. 3A), no differences in the number of autophagosomes were detected (Fig. 4A, B). However, the number of autolysosomes was highly significantly increased in mutant cells (Fig. 4A, B). Upon treatment with Bafilomycin A1, the number of autolysosomes decreased back to wildtype levels. This indicates an impaired clearance of autolysosomes and by this a delayed termination of autophagy.
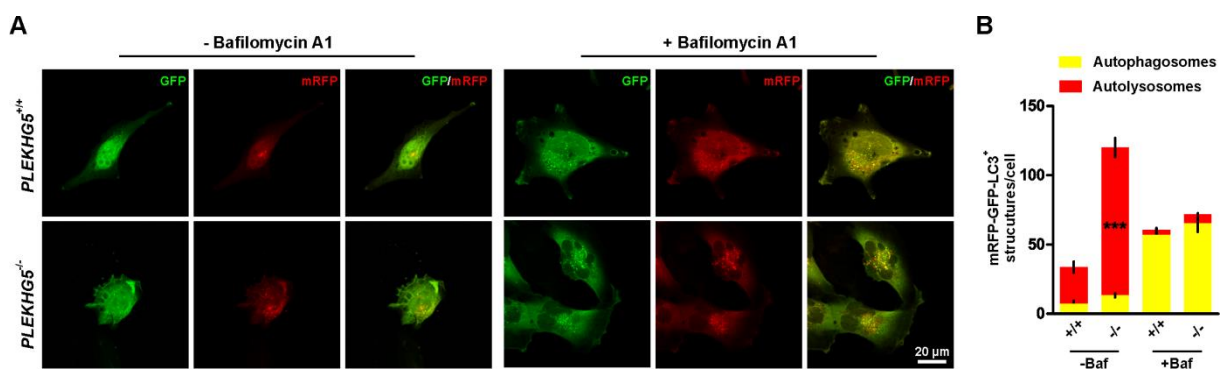
Figure 4 Clearance of autolysosomes is impaired in *PLEKHG5*-deficient cells. (A) Wildtype and mutant cells were transduced with lentiviral GFP-RFP-LC3 reporter. Cells were treated with 400 nM Bafilomycin A1 for 4 hours or left untreated. **(B)** The number of autophagosomes (GFP$^+$-RFP$^+$-LC3) and autolysosomes (GFP$^-$-RFP$^+$-LC3) was determined (five cells per experiment and genotype, n=3, two-way ANOVA with Bonferroni post-test).

Discussion

The present study showed the successful CRISPR/Cas9-mediated knockout of the GEF Plekhg5 in U251-MG cells, a broadly applied model for glioblastoma. *PLEKHG5*-deficiency in U251 cells resulted in profound changes in the cellular morphology, as well as in significantly reduced proliferation. Moreover, an increased number of autolysosomes were detected in *PLEKHG5*$^{-/-}$ cells. Thus, it was suggested that Plekhg5 has a particular function in the termination of autophagy in glioblastoma cells.

The role of Plekhg5 was particularly investigated in cells of the nervous system and in endothelial cells (Liu & Horowitz, 2006; Luningschror et al, 2017; Marx et al, 2005). However, several reports described Plekhg5 to be expressed in a variety of cancer cells. To understand the involvement of Plekhg5 in glioblastoma, we first developed a PLEKHG5-specific knockout cell line using CRISPR/Cas9 genome editing. We were able to confirm a successful knockout on both mRNA and protein level (Fig 1). In order to understand the cellular mechanisms Plekhg5 is involved in, particularly in cancer cells, we further characterized the cell line generated. Plekhg5 was originally described to be a GEF specific for RhoA. Here, it was reported that Plekhg5 has a specific function on the actin cytoskeleton, which is known to be regulated by RhoA (Sit & Manser, 2011). In U251-MG cells, Plekhg5 influenced the migratory behavior of these cells by activating RhoA and its downstream kinase Dia1 (Dachsel et al, 2013). Recently, similar results were obtained in macrophages and osteoclasts demonstrating impairments in polarity and migration upon shRNA-mediated knockdown of Plekhg5 (Iwatake et al, 2017). In line with this, we demonstrated profound changes in the arrangement of the actin cytoskeleton upon knockout of *PLEKHG5,* which also resulted in a reduced migratory behavior.

In the human skin cancer cell line DJM-1, activation of the VEGF-A receptor neuropilin (NRP1) was demonstrated to lead to the recruitment of Plekhg5 to the receptor and subsequent activation of RhoA (Yoshida et al, 2015). Active RhoA was reported to induce the degradation of the cyclin-dependent kinase (CDK) inhibitor p27. This degradation initiates the transition of the G1 phase to the S-phase of the cell cycle (Hu et al, 1999; Mammoto et al, 2004). The reduced proliferation of *PLEKHG5*-deficient U251-MG cells presented here is presumably caused by reduced RhoA activation and improper degradation of p27.

The role of autophagy in tumor formation remains a matter of scientific debate (for an overview see (Thorburn, 2014)). However, reports describe beneficial effects of targeting autophagy in cancer therapy (reviewed in (Levy et al, 2017)). Particularly, this appears to be a promising approach for glioblastoma. Glioblastoma cells are very resistant to conventional anticancer therapy. Partly, this is caused by an upregulation of autophagy during therapy (Paglin et al, 2001; Sui et al, 2013). Treatment with temozolomide (TMZ), a chemotherapeutic agent regularly used for GBM (Messaoudi et al, 2015; Stupp et al, 2005; Wait et al, 2015), results in profoundly elevated levels of autophagy and thereby increases cell survival (Knizhnik et al, 2013; Wurstle et al, 2017).

We recently described that Plekhg5regulates autophagy-mediated clearance of synaptic vesicles in motoneurons (Luningschror et al, 2017). In contrast to previous studies which focused on RhoA, Plekhg5 was reported to directly act as a GEF on Rab26. Importantly, Rab26 was previously reported to mediate degradation of synaptic vesicles via autophagy (Binotti et al, 2015). Notably, in motoneurons derived from *Plekhg5*-deficient mice, an impaired formation of autophagosomes was demonstrated (Luningschror et al, 2017). In contrast, an impaired clearance of autolysosomes upon *PLEKHG5* knockout in human glioma cells was reported in the present study. Plekhg5 was shown to associate to phosphatidylinositol 3-phosphate (PI(3)P) (Luningschror et al, 2017), which is an essential component of the autophagosome membrane (Carlsson & Simonsen, 2015). This indicates that Plekhg5 resides within the membranes of autophagosomes, however it remains unclear, how this influences the degradation of the formed autolysosomes after fusion with the lysosome. In 2015, impaired clearance of autolysosomes was reported in HeLa cells upon shRNA-mediated knockdown of Rab24 (Yla-Anttila et al, 2015). However, Rab24 was described as an unusual Rab protein occurring in a predominantly GTP-bound state due to a low intrinsic GTPase activity (Erdman et al, 2000). Its function therefore might not rely on a GEF. We analyzed the colocalization of Rab24 to LC3-positive structures in wildtype and *Plekhg5*-deficient cells and observed no differences (data not shown). Therefore, an involvement of Rab24 in the observed phenotypewas excluded. In comparison to the initiation and maturation of the autophagic process, termination of autophagy is poorly understood. Potentially, different termination mechanisms exist, depending on the initial stimulus for autophagy induction. Nutrient-depletion

10

results in the induction of autophagy via initial inhibition of the mammalian target of rapamycin complex 1 (mTORC1). Notably, mTORC1 later resides in the lysosomal membrane and is reactivated, when nutrients are replenished (Efeyan et al, 2013; Yu et al, 2010). Moreover, mTORC1 is also involved in the extrusion of proto-lysosomal tubules from autolysosomes, which subsequently matured into lysosomes (Yu et al, 2010). In general, evidence was provided leading to the suggestion that preventing autophagy termination increases the sensitivity to cell death stimuli (Antonioli et al, 2014; Liu et al, 2016).

In summary, our findings demonstrate the involvement of Plekhg5 in multiple cellular processes, which are directly linked to cancer progression and recurrence. As such, Plekhg5 appears to be a promising target with regard to anticancer therapy.

Materials and methods

Statistics

Statistical tests used in this study were performed using GraphPad Prism 5 (GraphPad Software, La Jolla, USA). The specific test used is displayed within the respective figure legend. ns, not significant, $*p<0.05$, $**p<0.01$, $***p<0.001$.

Target design and cloning

Design of single guide RNAs (sgRNAs) was done using the online prediction tool from the University of Heidelberg (Stemmer et al, 2015). We took advantage of the Cas9n (D10A) nickase mutant (Ran et al, 2013a) to minimize putative off-side effects and chose nicking pairs accordingly. To effectively generate a gene knockout, two nicking pairs were chosen to create a genomic deletion spanning an intron-exon boundary. Each sgRNA was cloned into pSpCas9n(BB)-2A-Puro (PX462) V2.0 (Addgene plasmid #62987) as already described (Ran et al, 2013b). Oligos used for sgRNA design were: oligo 1 (fwd 5'-CACCgACAGCACCATGCATTATGA-3'; rev 5'-AAACTCATAATGCATGGTGCTGTC-3'), oligo 2 (fwd 5'-CACCgGCTGTCACAGGCCTCGCAG-3'; rev 5'-AAACCTGCGAGGCCTGTGACAGCC-3'), oligo 3 (fwd 5'-CACCgGGGAGAGGGGGGACTGCTG-3'; rev 5'-AAACCAGCAGTCCCCCCTCTCCCC-3'), oligo 4 (fwd 5'-CACCgCATCAAGTTTCCCCTCTGC-3'; rev 5'-AAACGCAGAGGGGAAACTTGATGC-3').

Cell culture and transfection

U251-MG and HEK293 FT cells were cultivated in in Dulbecco's Modified Eagle's Medium (DMEM) (Sigma Aldrich, Taufkirchen, Germany) supplemented with 10% (v/v) heat-inactivated fetal calf serum (FCS) (VWR, Darmstadt, Germany), 2 mM L-glutamine (Sigma Aldrich) and 100 U/ml Penicillin/Streptomycin (P/S) (Sigma Aldrich) at 37°C and 5% CO_2 at saturated humidity.

U251-MG cells were transfected using TurboFect transfection reagent (Thermo Fisher Scientific) according to the manufacturer's guidelines.

Genomic PCR

For DNA isolation, cells were lysed in cell lysis buffer (0.1 µg/mL Gelatine, 50 mM KCl, 1.5 mM MgCl2, 0.45% NP40, 10 mM TRIS pH 8.3, 0.45 % TWEEN 20, 200 µg/mL proteinase K) for 1 h at 55°C followed by 5 min at 95°C. Lysate was directly used as template for genomic PCR. Primers used for genomic PCR were: Plekhg5 (fwd 5'-TTGTCCTTATGACGCCCTAGC-3'; rev 5'-CACTGCACTCCCTGTCTCAAAGAA-3').

Western bloting

Cells were lysed in RIPA buffer (1 mM EGTA, 150 mM NaCl, 1 mM Na_2EDTA, 1 mM Na_3VO_4, 1% (w/v) NP-40, 1 µg/mL leupeptin, 1 % (w/v) sodium deoxycholate, 2.5 mM sodium pyrophosphate, 20 mM Tris-HCl (pH 7,5), 1 mM β-glycerophosphate). Equal amounts of protein were separated by SDS-PAGE and transferred to a PVDF membrane using a semi-dry blotter. Non-specific binding was blocked with PBS containing 0.05% Tween 20 and 5% milk powder for 1 h at 37°C, followed by probing with primary antibodies LC3B (#2775; Cell Signaling) and Lamp1 (deposited to the DSHB by August, J.T. / Hildreth, J.E.K. (DSHB Hybridoma Product H4A3) overnight at 4°C. Horseradish peroxidase-conjugated secondary antibodies were applied for 1h at room temperature and blots were developed using enhanced chemiluminescence. As loading control, protein amounts of GAPDH (#32233; Santa-Cruz Biotechnology) were detemined.

Immunocytochemistry

For immunocytochemical stainings, cells were cultivated on tissue-culture treated coverslips. Cells were fixed for 10 min at RT using 4 % paraformaldehyde (PFA). Prior to applying primary antibodies (1 h at RT), non-specific binding was blocked with PBS containing 5 % goat serum for 30 min. Secondary fluorochrome-conjugated antibodies were added for 1 h at RT under exclusion of light. DAPI (1 µg/mL) was used for nuclear counterstaining and samples were mounted using Mowiol/DABCO. Imaging was accomplished by confocal laser scanning microscopy (LSM 780, Carl Zeiss, Oberkochen, Germany) and image processing with Fiji (Schindelin et al, 2012) and Corel Draw X5 (Corel Corporation, Ottawa, Canada).

Proliferation assay

For conventional proliferation assay, 5 x 10^4 cells were seeded in 6-well multiwell plates and cultivated for 2 days. Cells were counted again and population-doubling-time was calculated.

The Orangu™ Cell Proliferation Assay Kit (Cell Guidance Systems) was used according to the manufacturer's protocol. Briefly, 2000 cells were seeded and cultivated for 2 days before applying Orangu™ solution. After 2 hours, the absorbance at 450 nm was measured.

Lentivirus production

For the production of lentiviral particles, HEK293 FT cells were transfected with FUW-RFP-GFP-LC3 (Luningschror et al, 2017) and the packaging plasmids VSV-G and Δ8.91 using standard calcium phosphate precipitation. 72 h after transfection, the supernatant was collected and subsequently concentrated by ultracentrifugation.

Author contributions

CS designed the study, designed and performed experiments, analyzed data and wrote the manuscript. KEF and JFWG performed experiments and analyzed data. AK performed experiments. BK and CK provided resources and supervised the study.

References

Amaravadi RK, Yu D, Lum JJ, Bui T, Christophorou MA, Evan GI, Thomas-Tikhonenko A, Thompson CB (2007) Autophagy inhibition enhances therapy-induced apoptosis in a Myc-induced model of lymphoma. The Journal of clinical investigation 117**:** 326-336

Antonioli M, Albiero F, Nazio F, Vescovo T, Perdomo AB, Corazzari M, Marsella C, Piselli P, Gretzmeier C, Dengjel J et al (2014) AMBRA1 interplay with cullin E3 ubiquitin ligases regulates autophagy dynamics. Developmental cell 31**:** 734-746

Binotti B, Pavlos NJ, Riedel D, Wenzel D, Vorbruggen G, Schalk AM, Kuhnel K, Boyken J, Erck C, Martens H et al (2015) The GTPase Rab26 links synaptic vesicles to the autophagy pathway. eLife 4**:** e05597

Boya P, Reggiori F, Codogno P (2013) Emerging regulation and functions of autophagy. Nature cell biology 15**:** 713-720

Carlsson SR, Simonsen A (2015) Membrane dynamics in autophagosome biogenesis. Journal of cell science 128**:** 193-205

Dachsel JC, Ngok SP, Lewis-Tuffin LJ, Kourtidis A, Geyer R, Johnston L, Feathers R, Anastasiadis PZ (2013) The Rho guanine nucleotide exchange factor Syx regulates the balance of dia and ROCK activities to promote polarized-cancer-cell migration. Molecular and cellular biology 33**:** 4909-4918

Degenhardt K, Mathew R, Beaudoin B, Bray K, Anderson D, Chen G, Mukherjee C, Shi Y, Gelinas C, Fan Y et al (2006) Autophagy promotes tumor cell survival and restricts necrosis, inflammation, and tumorigenesis. Cancer cell 10**:** 51-64

Efeyan A, Zoncu R, Chang S, Gumper I, Snitkin H, Wolfson RL, Kirak O, Sabatini DD, Sabatini DM (2013) Regulation of mTORC1 by the Rag GTPases is necessary for neonatal autophagy and survival. Nature 493**:** 679-683

Erdman RA, Shellenberger KE, Overmeyer JH, Maltese WA (2000) Rab24 is an atypical member of the Rab GTPase family. Deficient GTPase activity, GDP dissociation inhibitor interaction, and prenylation of Rab24 expressed in cultured cells. The Journal of biological chemistry 275**:** 3848-3856

Hu W, Bellone CJ, Baldassare JJ (1999) RhoA stimulates p27(Kip) degradation through its regulation of cyclin E/CDK2 activity. The Journal of biological chemistry 274**:** 3396-3401

Iwatake M, Nishishita K, Okamoto K, Tsukuba T (2017) The Rho-specific guanine nucleotide exchange factor Plekhg5 modulates cell polarity, adhesion, migration, and podosome organization in macrophages and osteoclasts. Experimental cell research 359**:** 415-430

Knizhnik AV, Roos WP, Nikolova T, Quiros S, Tomaszowski KH, Christmann M, Kaina B (2013) Survival and death strategies in glioma cells: autophagy, senescence

and apoptosis triggered by a single type of temozolomide-induced DNA damage. PloS one 8**:** e55665

Koshy M, Villano JL, Dolecek TA, Howard A, Mahmood U, Chmura SJ, Weichselbaum RR, McCarthy BJ (2012) Improved survival time trends for glioblastoma using the SEER 17 population-based registries. Journal of neuro-oncology 107**:** 207-212

Levy JMM, Towers CG, Thorburn A (2017) Targeting autophagy in cancer. Nature reviews Cancer 17**:** 528-542

Liu CC, Lin YC, Chen YH, Chen CM, Pang LY, Chen HA, Wu PR, Lin MY, Jiang ST, Tsai TF et al (2016) Cul3-KLHL20 Ubiquitin Ligase Governs the Turnover of ULK1 and VPS34 Complexes to Control Autophagy Termination. Molecular cell 61**:** 84-97

Liu M, Horowitz A (2006) A PDZ-binding motif as a critical determinant of Rho guanine exchange factor function and cell phenotype. Molecular biology of the cell 17**:** 1880-1887

Luningschror P, Binotti B, Dombert B, Heimann P, Perez-Lara A, Slotta C, Thau-Habermann N, C RvC, Karl F, Damme M et al (2017) Plekhg5-regulated autophagy of synaptic vesicles reveals a pathogenic mechanism in motoneuron disease. Nature communications 8**:** 678

Mammoto A, Huang S, Moore K, Oh P, Ingber DE (2004) Role of RhoA, mDia, and ROCK in cell shape-dependent control of the Skp2-p27kip1 pathway and the G1/S transition. The Journal of biological chemistry 279**:** 26323-26330

Marx R, Henderson J, Wang J, Baraban JM (2005) Tech: a RhoA GEF selectively expressed in hippocampal and cortical neurons. Journal of neurochemistry 92**:** 850-858

Messaoudi K, Clavreul A, Lagarce F (2015) Toward an effective strategy in glioblastoma treatment. Part I: resistance mechanisms and strategies to overcome resistance of glioblastoma to temozolomide. Drug discovery today 20**:** 899-905

Mizushima N, Yoshimori T, Levine B (2010) Methods in mammalian autophagy research. Cell 140**:** 313-326

Paglin S, Hollister T, Delohery T, Hackett N, McMahill M, Sphicas E, Domingo D, Yahalom J (2001) A novel response of cancer cells to radiation involves autophagy and formation of acidic vesicles. Cancer research 61**:** 439-444

Ponten J, Macintyre EH (1968) Long term culture of normal and neoplastic human glia. Acta pathologica et microbiologica Scandinavica 74**:** 465-486

Rabinowitz JD, White E (2010) Autophagy and metabolism. Science 330**:** 1344-1348

Ran FA, Hsu PD, Lin CY, Gootenberg JS, Konermann S, Trevino AE, Scott DA, Inoue A, Matoba S, Zhang Y et al (2013a) Double nicking by RNA-guided CRISPR Cas9 for enhanced genome editing specificity. Cell 154**:** 1380-1389

Ran FA, Hsu PD, Wright J, Agarwala V, Scott DA, Zhang F (2013b) Genome engineering using the CRISPR-Cas9 system. Nature protocols 8**:** 2281-2308

Schindelin J, Arganda-Carreras I, Frise E, Kaynig V, Longair M, Pietzsch T, Preibisch S, Rueden C, Saalfeld S, Schmid B et al (2012) Fiji: an open-source platform for biological-image analysis. Nature methods 9**:** 676-682

Sit ST, Manser E (2011) Rho GTPases and their role in organizing the actin cytoskeleton. Journal of cell science 124**:** 679-683

Stemmer M, Thumberger T, Del Sol Keyer M, Wittbrodt J, Mateo JL (2015) CCTop: An Intuitive, Flexible and Reliable CRISPR/Cas9 Target Prediction Tool. PloS one 10**:** e0124633

Stupp R, Hegi ME, Mason WP, van den Bent MJ, Taphoorn MJ, Janzer RC, Ludwin SK, Allgeier A, Fisher B, Belanger K et al (2009) Effects of radiotherapy with concomitant and adjuvant temozolomide versus radiotherapy alone on survival in glioblastoma in a randomised phase III study: 5-year analysis of the EORTC-NCIC trial. The Lancet Oncology 10**:** 459-466

Stupp R, Mason WP, van den Bent MJ, Weller M, Fisher B, Taphoorn MJ, Belanger K, Brandes AA, Marosi C, Bogdahn U et al (2005) Radiotherapy plus concomitant and adjuvant temozolomide for glioblastoma. The New England journal of medicine 352**:** 987-996

Sui X, Chen R, Wang Z, Huang Z, Kong N, Zhang M, Han W, Lou F, Yang J, Zhang Q et al (2013) Autophagy and chemotherapy resistance: a promising therapeutic target for cancer treatment. Cell death & disease 4**:** e838

Thorburn A (2014) Autophagy and its effects: making sense of double-edged swords. PLoS biology 12**:** e1001967

Wait SD, Prabhu RS, Burri SH, Atkins TG, Asher AL (2015) Polymeric drug delivery for the treatment of glioblastoma. Neuro-oncology 17 Suppl 2**:** ii9-ii23

Westermark B, Ponten J, Hugosson R (1973) Determinants for the establishment of permanent tissue culture lines from human gliomas. Acta pathologica et microbiologica Scandinavica Section A, Pathology 81**:** 791-805

Wurstle S, Schneider F, Ringel F, Gempt J, Lammer F, Delbridge C, Wu W, Schlegel J (2017) Temozolomide induces autophagy in primary and established glioblastoma cells in an EGFR independent manner. Oncology letters 14**:** 322-328

Yla-Anttila P, Mikkonen E, Happonen KE, Holland P, Ueno T, Simonsen A, Eskelinen EL (2015) RAB24 facilitates clearance of autophagic compartments during basal conditions. Autophagy 11**:** 1833-1848

Yoshida A, Shimizu A, Asano H, Kadonosono T, Kondoh SK, Geretti E, Mammoto A, Klagsbrun M, Seo MK (2015) VEGF-A/NRP1 stimulates GIPC1 and Syx complex

formation to promote RhoA activation and proliferation in skin cancer cells. Biology open 4**:** 1063-1076

Yu L, McPhee CK, Zheng L, Mardones GA, Rong Y, Peng J, Mi N, Zhao Y, Liu Z, Wan F et al (2010) Termination of autophagy and reformation of lysosomes regulated by mTOR. Nature 465**:** 942-946
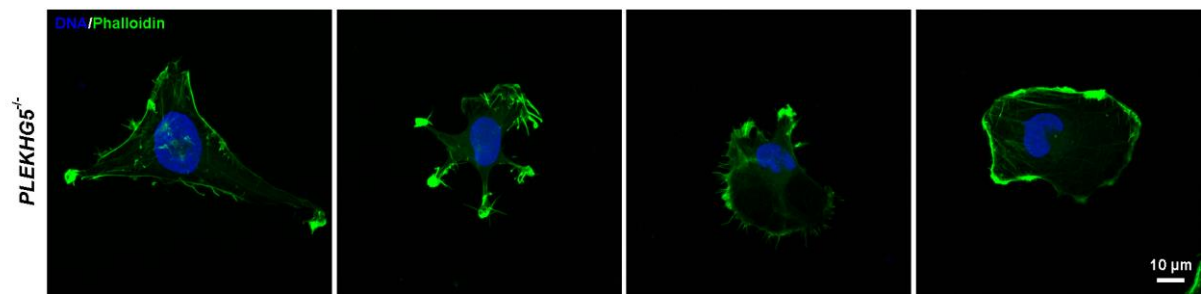
Figure S1

Figure S1. Heterogeneity of clonally grown *PLEKHG5*-deficient cells. Despite of their clonal origin, mutant cells rapidly developed a heterogenic organization of the actin cytoskeleton, assessed by phalloidin staining.

CRISPR/Cas9-mediated knockout of *c-REL* in HeLa cells results in profound defects of the cell cycle

Carsten Slotta[1]◉, Thomas Schlüter[1]◉, Lucia M. Ruiz-Perera[2], Hussamadin M. Kadhim[1], Tobias Tertel[1], Elena Henkel[1], Wolfgang Hübner[3], Johannes F. W. Greiner[1], Thomas Huser[3], Barbara Kaltschmidt[1,2], Christian Kaltschmidt[1] *

1 Department of Cell Biology, University of Bielefeld, Bielefeld, Germany, **2** AG Molecular Neurobiology, University of Bielefeld, Bielefeld, Germany, **3** Biomolecular Photonics, University of Bielefeld, Bielefeld, Germany

◉ These authors contributed equally to this work.

* c.kaltschmidt@uni-bielefeld.de

Abstract

Cervical cancer is the fourth common cancer in women resulting worldwide in 266,000 deaths per year. Belonging to the carcinomas, new insights into cervical cancer biology may also have great implications for finding new treatment strategies for other kinds of epithelial cancers. Although the transcription factor NF-κB is known as a key player in tumor formation, the relevance of its particular subunits is still underestimated. Here, we applied CRISPR/Cas9n-mediated genome editing to successfully knockout the NF-κB subunit *c-REL* in HeLa Kyoto cells as a model system for cervical cancers. We successfully generated a homozygous deletion in the *c-REL* gene, which we validated using sequencing, qPCR, immunocytochemistry, western blot analysis, EMSA and analysis of off-target effects. On the functional level, we observed the deletion of *c-REL* to result in a significantly decreased cell proliferation in comparison to wildtype (wt) without affecting apoptosis. The impaired proliferative behavior of *c-REL*$^{-/-}$ cells was accompanied by a strongly decreased amount of the H2B protein as well as a significant delay in the prometaphase of mitosis compared to *c-REL*$^{+/+}$ HeLa Kyoto cells. *c-REL*$^{-/-}$ cells further showed significantly decreased expression levels of *c-REL* target genes in comparison to wt. In accordance to our proliferation data, we observed the *c-REL* knockout to result in a significantly increased resistance against the chemotherapeutic agents 5-Fluoro-2'-deoxyuridine (5-FUDR) and cisplatin. In summary, our findings emphasize the importance of c-REL signaling in a cellular model of cervical cancer with direct clinical implications for the development of new treatment strategies.

Introduction

Cervical cancer is an epithelial cancer, also called carcinoma, and the fourth common cancer in women worldwide with an estimated 5-year survival rate of 70% following diagnosis [1, 2]. Based on the degenerated cell type in the uterus, cervical cancer can be classified into

squamous cell cancer and adenocarcinoma [1]. The most common reason for cervical cancer is an infection by the human papilloma virus (HPV), namely by HPV 16 and HPV 18 causing malignant transformations or carcinogenesis in 85% of the diagnosed cases [3, 4]. Treatment strategies of cervical cancer highly depend on the stage of progression and range from radio-therapy and surgery [5] to chemotherapy with cisplatin or 5-fluorouracil (5-FU) [6, 7].

Discovered in 1986 [8, 9], the transcription factor nuclear factor kappa-light-chain-enhancer of activated B-cells (NF-κB) has been shown to play a key role in various cellular processes as cell growth, differentiation, apoptosis, inflammation, learning and memory as well as immunity [10, 11]. Given the importance of NF-κB in these processes, deregulation of its signaling is directly associated to the formation of tumors and cancer progression [12–14], particularly regarding breast cancer [15] and cervical carcinomas [1]. In 2003, Nair and coworkers showed a constitutive activation of the NF-κB subunit p65 during human cervical cancer progression. Here, NF-κB p65 was demonstrated to be particularly activated in high-grade squamous intraepithelial lesions and squamous cell carcinomas of the human uterine cervix [16]. Next to NF-κB p65, the subunit c-REL was shown to possess a key role in tumor formation. Initial studies demonstrated severe B-cell lymphomas in chickens infected with avian reticuloendotheliosis comprising V-REL [17]. Expression of wildtype human *c-REL* in primary chicken spleen cell cultures was likewise shown to result in malignant transformation events [18], although respective mutations increasing the oncogenicity of the c-REL protein in the avian system were not observable in human cancers (reviewed in [19]). However, amplification of *c-REL* was observed in a broad range of human B-cell lymphomas [20, 21]. In terms of human cervical cancer, Shehata and coworkers demonstrated a 6-fold slowed cell growth in cultivated cervical cancer cells by expression of the *c-REL* homolog Xrel3 from *Xenopus laevi* [22]. Accordingly, downregulation of *c-REL* by small interfering RNA was shown to result in reduced proliferation of human keratinocytes [23], directly correlating *c-REL* signaling to impaired cell cycle progression in a non-cancerous environment. Expression of the *c-REL* homolog Xrel3 in human cervical cancer cells was further shown to lead to anti- or pro-apoptotic effects during cisplatin-treatment in a concentration-dependent manner. These findings emphasize the importance of *c-REL*-signaling in resistance of cervical carcinoma to chemotherapeutic agents [24].

The present study further extends these promising findings by showing a profound overexpression of *c-REL* in cancers located in human ovary, cervix and endometrium using database mining. To investigate the role of *c-REL* in human cervical cancers in more detail, we applied CRISPR/Cas9n-mediated genome editing in a multiplex way to delete *c-REL* in HeLa Kyoto cells. Initially discovered as a part of adaptive immune system of bacteria and archaea [25], the clustered regularly interspaced short palindromic repeats (CRISPR) system has been developed to a state-of-the-art technique for editing the human genome [26, 27]. Applications of the CRISPR/Cas9-system particularly include cancer modeling [28] or knockout studies using human cancer cell lines [27, 29]. In the present study, we applied a Cas9 nickase mutant (Cas9n) inducing single-strand breaks to minimize the possibility of off-target cleavage in turn increasing the specificity of genome editing [30].

Using the CRISPR/Cas9n approach, we successfully deleted the *c-REL* gene on chromosomes 2 of HeLa Kyoto cells (*c-REL$^{-/-}$*). In comparison to wildtype, *c-REL$^{-/-}$* HeLa Kyoto cells showed a significantly decreased proliferation accompanied by strongly reduced amounts of histone H2B, a delay in the prometaphase of mitosis and decreased expression levels of *c-REL* target genes. We further observed a significantly increased resistance against the chemotherapeutic agents 5-Fluoro-2'-deoxyuridine (5-FUDR) and cisplatin in HeLa Kyoto cells with *c-REL* deletion compared to wildtype (wt). Our findings emphasize the importance of *c-REL*

Materials and methods

Target design and cloning

The design of the sgRNAs was done using the CRISPR/Cas9n Target Online Predictor from University of Heidelberg (crispr.cos.uni-heidelberg.de). The gene sequence was taken from Ensembl Genome Browser (ensembl.org). Two nicking pairs were designed resulting in two double strand breaks creating a deletion. Nicking pairs were chosen according to the criteria described by Ran and coworkers [30]. All oligos designed were cloned into one vector essentially as described [31].

Cell culture and transfection

HeLa Kyoto cells [32] were cultured in Dulbecco's Modified Eagle's Medium (DMEM) (Sigma Aldrich, Taufkirchen, Germany) containing high glucose (25 mM), and sodium pyruvate (1 mM). This medium was supplemented with 10% (v/v) heat-inactivated fetal calf serum (FCS) (VWR, Darmstadt, Germany), 2 mM L-glutamine (Sigma Aldrich), 100 U/ml Penicillin/Streptomycin (P/S) (Sigma Aldrich), and 0.5 mg/ml geneticin (G418) (Sigma Aldrich). Cells were cultivated at 37°C with 5% CO_2 at saturated humidity.

Transfection of HeLa Kyoto cells (3×10^5 cells / transfection) was performed by electroporation using Amaxa Cell Line Nucleofector Kit R (Lonza, Basel, Schweiz) according to the manufacturer's protocol. 48 hours after transfection knockout generation was checked by genomic PCR and cells were used for limiting dilution to obtain clonal *c-REL* knockout cells.

Genomic PCR and Native PAGE

For cell lysis, cells were harvested at 300 g for 5 min and resuspended in cell lysis buffer (0.1 μg/mL gelatine, 50 mM KCl, 1.5 mM $MgCl_2$, 0.45% NP40, 10 mM TRIS pH 8.3, 0.45% TWEEN 20). Proteinase K (20 mg/ml, Serva Electrophoresis, Heidelberg, Germany) was added followed by incubation of the cell lysate for at least 1 h at 55°C and 5 min at 95°C. 2 μL were used for PCR (*c-REL* primers: Fw `5´-TGCATTTTCATTTTCAGTGAATGGT-3´`, Rev `5´-ACCTGTGGAGATGACTGTGAAG-3´`). Resulting bands on agarose gels were extracted using NucleoSpin Gel and PCR Clean up Kit (Macherey Nagel) according to manufacturer's guidelines and subsequently analyzed by sequencing.

For Native PAGE, DNA of the PCR product was denaturized and re-annealed (5 min at 95°C, -2°C/s from 95°C to 85°C and 0.1°C/s from 85°C to 25°C). PCR product was separated on a 10% native Polyacrylamide-gel for 2 h at 150 V. Gene Ruler DNA Ladder Mix (Thermo Fisher Scientific, Waltham, MA, USA) served as marker, gel was immersed in 0.05% ethidium bromide (Carl Roth GmbH, Karlsruhe, Germany) for 5 min prior to visualization.

Quantitative real-time PCR

RNA isolation was done with NucleoSpin®RNA Kit (Macherey-Nagel) according to manufacturer's guidelines. 500 ng RNA were used for cDNA synthesis. Quantitative real-time PCR (qPCR) was performed using SYBR Green Master Mix (Thermo Fisher Scientific). cDNA was diluted 1:50 and 2 μL/reaction were used as template. Primer sequences were `5´-CTCCTGACTGACTGACTGCG-3´` (Fw *c-REL* target deletion), `5´-TACGGGTTATACGCACCGGA-3´` (Rev *c-REL* target deletion), `5´-CCTGGAGCAGGCTATCAGTC-3´` (Fw *RELA*), `5´-CACTGTCACCTGGAAGCAGA-3´` (Rev *RELA*), `5´-ACATCAAGGAGAACGGCTTCG-3´`

(Fw *RELB*), 5´-GACACTAGTCGGCCCAGG-3´ (Rev *RELB*), 5´-GCACCCTGACCTTGCCTA TT-3´ (Fw *NFKB1*), 5´-GCTCTTTTTCCCGATCTCCCA-3´ (Rev NFKB1), 5´-CAACCCAG GTCTGGATGGTA-3´ (Fw *NFKB2*), 5´-CTGCTTAGGCTGTTCCACGA-3´ (Rev NFKB2), 5´-TGACAGTGAGCCCTGAAAGC-3´ (Fw *IKBKE*), 5´-CCGGATTTCCCACACTCTGA-3´ (Rev *IKBKE*), 5´-CGGAGACCCGGCTGGTATAA-3´ (Fw *TBK1*), 5´-ATCCACTGGACGAAG GAAGC-3´ (Rev *TBK1*), 5´-CTGAAAACGAACGGTGACGG-3´ (Fw *A20*), 5´-TCCAGTTG CCAGCGGAATTT-3´ (Rev *A20*), 5´-CAGGATAACGGAGGCTGGGATG-3´ (Fw *BCL2*), 5´-TTCACTTGTGGCCCAGATAGG-3´ (Rev *BCL2*), 5´-GCTTGGATGGCCACTTACCT-3´ (Fw *BCL-XL*), 5´-ACAAAAGTATCCCAGCCGCC-3´ (Rev *BCL-XL*), 5´-GCAAGTGGACATCAA CGGGT-3´ (Fw *TGFB1*), 5´-TCCGTGGAGCTGAAGCAATA-3´ (Rev *TGFB1*), 5´-GTAGT GGAAAACCAGCAGCC-3´ (Fw *MYC*), 5´-AGAAATACGGCTGCACCGAG-3´ (Rev *MYC*), 5´-ATGGCAACGACTCCTTCTCG-3´ (Fw *ICAM-1*), 5´-GCCGGAAAGCTGTAGATGGT-3´ (Rev *ICAM-1*). Ct values were normalized to reference genes *GAPDH* (Fw 5´-CATGAGAAG TATGACAACAGCCT-3´, Rev 5´-AGTCCTTCCACGATACCAAAGT-3´), *RPLP0* (Fw 5´-TGGGCAAGAACACCATGATG-3´, Rev 5´-AGTTTCTCCAGAGCTGGGTTGT-3´) and *eEF2* (Fw 5´-AGGTCGGTTCTACGCCTTTG-3´, 5´-TTCCCACAAGGCACATCCTC-3´).

Western blotting

For analysis of RELA and A20, *c-REL*⁻/⁻ and *c-REL*⁺/⁺ cells were treated with human recombinant TNFα (10ng/ml, Calbiochem, Merck, Darmstadt, Germany) for 24h prior to protein isolation. Protein extracts were made using cell lysis buffer (0.01 M TRIS, 3 mM EDTA, 1% SDS) and equal amounts of protein were separated by SDS-PAGE and transferred to a PVDF membrane. Membranes were blocked using PBS containing 0.05% Tween 20 and 5% milk powder and probed with primary antibodies (rabbit anti-c-REL (#4727), Cell Signaling Technology, Danvers, MA, USA); rabbit anti-p65 (#8242), Cell Signaling; mouse anti-A20 (sc-166692), Santa Cruz Biotechnology, Heidelberg, Germany) overnight at 4°C. Horseradish peroxidase-conjugated secondary antibodies were applied for 1h at room temperature and blots were subsequently developed using enhanced chemiluminescence.

Electrophoretic mobility shift assay

Electrophoretic Mobility Shift Assay was performed using DIG Gel Shift Kit, 2nd generation (Deutschland Holding GmbH, Grenzach-Wyhlen, Germany) according to manufacturer's guidelines. For *c-REL* probe sequence (5´-TCGAGGGCTCGGGCTTTCCATCTCTCGA-3´), *c-REL* binding site CGGGCTTTCC was assessed using the JASPAR Tool (jaspar.genereg.net). Protein isolation procedure and unspecific competitor sequence were applied as described by Tokunaga and coworkers [33]. PAGE was performed as described above.

Immunocytochemistry and fluorescence imaging of H2B-mcherry

For immunostaining and imaging of H2B-mCherry cells were seeded and cultivated on coverslips. Fixation was done by adding 4% paraformaldehyde (PFA) for 10 min. After repetitive washing using phosphate-buffered saline (PBS), cells were either directly mounted with Mowiol/DABCO or carried over to immunostaining. For immunocytochemistry, cells were blocked and permeabilized using 0.02% PBST (PBS with Triton X-100) containing 5% goat serum for 30 min at RT. Primary antibody (rabbit anti-c-REL (#4727), Cell Signaling; mouse anti-CD54/ICAM MAB1379, Chemicon, Merck) was applied for 1 h at RT. After washing, cells were incubated with secondary antibody (goat anti-rabbit Alexa Fluor 647, Thermo Fisher Scientific) for 1 h at RT under exclusion of light. Finally, coverslips were mounted with Mowiol/DABCO. Imaging was done by confocal laser scanning microscopy (LSM 780, Carl Zeiss,

Oberkochen, Germany) and image processing was done using Fiji) and Adobe Photoshop CS6 (Adobe Systems, San José, USA) or Corel Draw (Corel Corporation, Ottawa, Canada).

Proliferation & survival assay

Proliferation was analyzed with Orangu Cell Proliferation Assay Kit (Cell Guidance Systems, Cambridge, UK) used following the manufacturer's protocol. Cells were counted with Cellometer Auto T4 Cell Viability Counter (Nexcelom, Lawrence, USA). For a calibrating curve 1000, 2500, 5000, 7500, 10000 and 15000 wildtype cells were seeded and incubated for 24 h at 37˚C. For correct cell number determination after one day, one well of each condition was recounted.

For survival assay 5000 cells in 100 µl were seeded one day before treatment. Cells were incubated with chemotherapeutic agents cisplatin (CDDP) (P4394, Sigma Aldrich) and 5-Fluoro-2´-deoxyuridine (5-FUDR) (Sigma Aldrich) for 21 h and subsequently Orangu Cell Proliferation Assay Kit was applied.

Flow cytometric analysis of the cell cycle, apoptosis and histone H2B-mCherry

DNA content measurement for analyzing cell cycle parameters was performed according to Kaltschmidt and colleagues [34] by harvesting 1×10^6 cells at 300 g for 5 min followed by fixation with 70% (v/v) ethanol. After centrifugation at 300 x g for 10 minutes, staining solution (PBS containing 1 mg/ml glucose (Carl Roth GmbH), 4´,6-diamidino-2-phenylindole (DAPI; 0.5 mg/ml; Sigma-Aldrich), and 100 Kunitz units RNaseA (Thermo Fisher Scientific) was applied for 60 min under exclusion of light.

For apoptosis measurement, 1×10^6 cells were labeled with Annexin V-PE (Miltenyi Biotec, Bergisch Gladbach, Germany) according to the manufacturer's instructions. For analysis of H2B-mCherry, 1×10^6 c-REL$^{+/+}$ and c-REL$^{-/-}$ cells were harvested and directly applied for flow cytometric analysis without additional staining procedures.

DAPI or Annexin V-PE-labeled cells as well as unstained cells (H2B-mCherry) were analyzed using a Gallios™ 10/3 flow cytometer (Beckman Coulter, Brea, CA, USA). Data analysis was performed using FlowJo Software (TreeStar, Olten, Switzerland), doublet discrimination for cell cycle analysis was assured by appropriate gating strategies.

Live cell imaging

We imaged H2B-mCherry alpha-tubulin-eGFP expressing HeLa Kyoto c-REL+/+ and c-REL -/- cells in growth conditions at 37 degrees for more than 20 hours with a DeltaVision Elite imaging system (GE Healthcare). At 20x magnification (Olympus UPlanSApo 20x 0.75), we recorded on a CoolSNAP HQ2 (Photometrics, USA) CCD camera 15 different lateral positions with 3 axial position with 1µm spacing for each c-REL+/+ and c-REL-/- cells respectively every 10 minutes for each fluorescent emission channels (LED excitation source 461-489nm, 553-597nm and emission filtered at 501-549nm, 603-647nm respectively). A DIC image was recorded for reference at each timepoint. The fluorescent images were deconvolved with the appropriate OTF in SoftWoRx (version 6.1.3, GE Healthcare), analysed with Fiji and figures were prepared with Omero.

Promoter analysis

Sequence of promoter regions (1500 bp downstream and 100 bp upstream to respective ATG, 5000 bp downstream for c-Myc promoter) of interest were taken from Eukaryotic Promoter

Database (epd.vital-ti.ch) for *Homo sapiens*. Binding sites for gene of interest in chosen promoter sequence were looked up using JASPAR Tool (jaspar.genereg.net). A relative score threshold of 85% was used. *RELA* and *c-REL* binding sites were compared in promoter regions of selected target genes.

Statistics

All statistical tests were performed with PrismGraph Pad 5 (GraphPad Software, La Jolla, USA). Statistical significance of qPCR results and fluorescence intensity quantification was analyzed using unpaired t-test. Welch correction was performed, if variances were significantly different. Data of proliferation and survival assays were shown to be not normally distributed (Shapiro-Wilk test) and analyzed using Kruskal-Wallis test with Dunn post-hoc test.

Results

c-REL is overexpressed in human cervical cancers

To assess the clinical implications of a *c-REL* knockout, we assessed levels of *c-REL* overexpression in human cancers by database mining using COSMIC [35]. We found *c-REL* to be profoundly overexpressed in human cancers, particularly within those located in human ovary, cervix and endometrium in comparison to oesophagus (Fig 1A, cancer.sanger.ac.uk; 02-14-2017 16:00; 02-21-2017 15:10). Due to their human cervix origin, we decided to apply HeLa Kyoto cells for the CRISPR/Cas9n-mediated *c-REL* knockout.

Successful knockout of *c-REL* in HeLa Kyoto cells using CRISPR/Cas9n

To generate a *c-REL* knockout in HeLa Kyoto cells, we designed a target deletion around 450 bp between intron 1 and exon 2 of chromosome 2 using the CRISPR/Cas9 Target Online Predictor tool (Fig 1B, [36], crispr.cos.uni-heidelberg.de). All designed oligonucleotides were cloned into an all-in-one vector according to Golden Gate Assembly method (mCRISPR, [31]) allowing easier generation of knockouts. Genomic PCR depicted a profound deletion of the
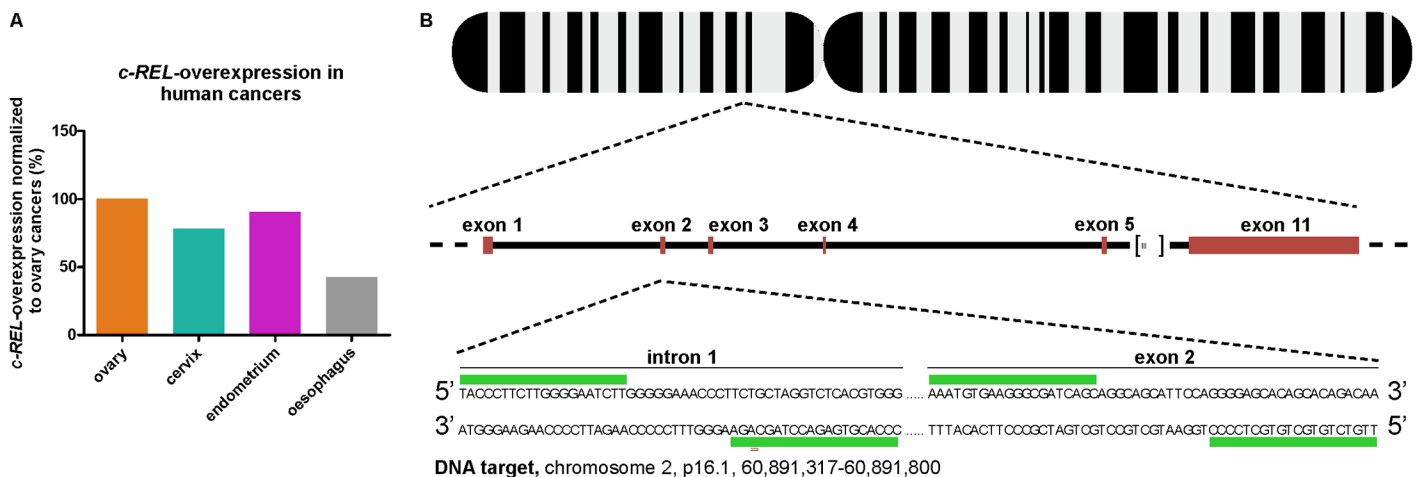
Fig 1. Assessment of *c-REL* overexpression in human cancers and target design of CRISPR/Cas9n-mediated *c-REL* knockout. A: Database mining revealed more profound overexpression of *c-REL* in cancers from human ovary, cervix and endometrium compared to oesophagus ([35], sancer. sanger.ac.uk; 02-14-2017 16:00; 02-21-2017 15:10). **B**: Target design showing the proposed *c-REL* knockout with an expected deletion around 450 bp targeting the intron 1-exon 2-boundary of the *c-REL* gene. The design was done with the CRISPR/Cas9n Target Online Predictor from the University of Heidelberg [36], crispr.cos.uni-heidelberg.de) and the gene sequence was taken from Ensembl Genome Browser (ensembl.org).

Fig 2. Successful validation of the *c-REL* knockout in HeLa Kyoto cells on DNA, mRNA and protein level. A: Genomic PCR depicting a profound deletion of the *c-REL* gene in the *c-REL* knockout clone (band at 300 bp) compared to the wt clone (band at 700 bp). **B:** Sequencing analysis confirmed the knockout in exon 2 of *c-REL*. **C:** qPCR with specific primers in targeted deletion of exon 2 showed no expression of *c-REL* on mRNA level in the *c-REL* knockout clone in comparison to wt. **D:** Western blot analysis validated 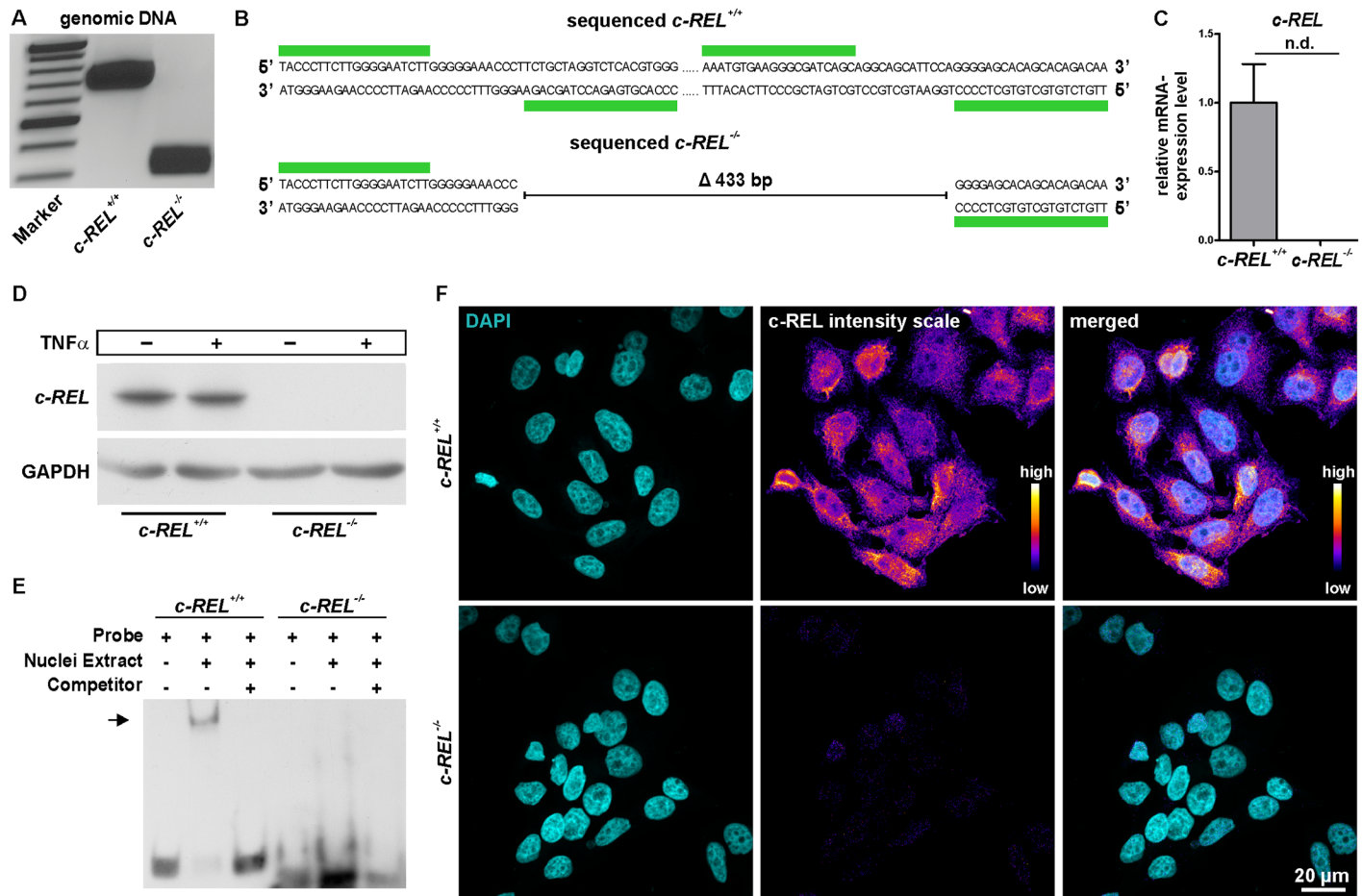the knockout of *c-REL* on protein level. **E:** Electrophoretic mobility shift assays (EMSA) showed DNA-binding of c-REL in HeLa Kyoto wt cells (arrow), which was not observable in the *c-REL* KO clone. **F:** Immunocytochemistry depicted a nearly complete loss of c-REL-protein in *c-REL* knockout clone compared to HeLa Kyoto wt cells.

c-REL gene in clonally grown HeLa Kyoto cells after transfection with the constructed CRISPR/Cas9 vector in comparison to untransfected HeLa Kyoto wt cells (Fig 2A). Sequencing analysis confirmed the knockout of around 433 bp in exon 2 of *c-REL* within the transfected HeLa Kyoto clone.

CRISPR/Cas9n-mediated *c-REL* knockout can be validated on mRNA and protein level

After initial analysis of the *c-REL* knockout on DNA level, we assessed the expression level of *c-REL* in the HeLa Kyoto knockout clone by qPCR with primers in the targeted deletion. In contrast to HeLa Kyoto wt cells showing a robust expression of *c-REL* on mRNA level, no expression was detectable in the *c-REL* knockout clone (Fig 2C). Notably, we analysed the top three predicted exonic off-targets and detected no significant signs of off-target effects in the *c-REL* kockout clone (S1 Fig).

In contrast to HeLa Kyoto wt cells, no c-REL protein was detectable in knockout cells by western blot analysis even after TNFα-dependent stimulation, confirming the knockout of *c-REL* on protein level (Fig 2D). Assessing a potential loss in functionality of the c-REL protein, we investigated DNA binding activity of c-REL using electrophoretic mobility shift assay (EMSA). *c-REL*$^{-/-}$ cells showed no DNA-binding activity of c-REL (Fig 2E), whereas a clear shift was observable using HeLa Kyoto wt cells (Fig 2E, arrow). Immunocytochemistry further validated the *c-REL* knockout in the transfected HeLa Kyoto clone by showing a nearly complete loss of c-REL protein in comparison to HeLa Kyoto wt cells (Fig 2F).

CRISPR/Cas9n-mediated deletion of *c-REL* results in a decreased proliferation of HeLa Kyoto cells without affecting apoptosis

We next analyzed potential effects of the *c-REL* knockout on proliferation and apoptosis of HeLa Kyoto cells. Using Orangu Cell Proliferation Assay Kit (Cell Guidance Systems), proliferation of *c-REL* knockout and wt cells was assessed after 2 days. HeLa Kyoto *c-REL*$^{-/-}$ cells showed a strongly increased population doubling time of 26.54 h compared to wt HeLa Kyoto cells displaying a population doubling time of 15.68 h (Fig 3A). This robustly decreased proliferative behavior of *c-REL* knockout cells was accompanied by a 0.81 fold decrease in the amount of mitotic cells compared to wildtype, as shown by cell cycle analysis using flow cytometric DNA content measurements (Fig 3B). However, we observed only slightly increased levels of Annexin V-positive apoptotic cells in *c-REL*$^{-/-}$ cells compared to wt cells (Fig 3C), indicating the effect of the *c-REL* knockout on proliferation of HeLa Kyoto cells to be apoptosis-independent.

c-REL$^{-/-}$ HeLa Kyoto cells reveal strongly reduced levels of histone H2B accompanied by a significantly delayed prometaphase or complete arrest of the cell cycle

Assessing the reduced proliferative behavior of *c-REL*$^{-/-}$ HeLa Kyoto cells in more detail, we analyzed the protein level of histone H2B, which is fused to mCherry in HeLa Kyoto cells [32]. Flow cytometric analysis of H2B-mCherry showed a strongly decreased amount of the H2B protein in 41.48% of *c-REL*$^{-/-}$ HeLa Kyoto cells. On the contrary, we observed a reduced H2B protein level in only 8.67% of HeLa Kyoto wt cells (Fig 3D). Taking advantage of the H2B-mCherry and alpha-tubulin-EGFP fusion in HeLa Kyoto cells, we further visualized the different stages of mitosis in fixed cell samples and living cells. Fluorescence imaging of fixed cells revealed a significantly increased amount of *c-REL*$^{-/-}$ HeLa Kyoto cells within the prometaphase compared to wt cells (Fig 4E). We investigated this effect of the *c-REL* deletion in more detail by live cell imaging. Here, *c-REL*$^{-/-}$ cells showed a length of the prometaphase of 39.50 ± 9.96 min, which was significantly delayed in comparison to wt cells revealing a duration of the prometaphase of 18.42 ± 1.58 min (Fig 4A–4C, S1 Movie). In addition, we observed only 5.4% of wt cells but 25.7% of *c-REL*$^{-/-}$ cells (n = 40) to arrest during mitosis without entry of the G2 phase of the cell cycle (Fig 4D, S2 Fig).

c-REL knockout leads to significantly decreased expression levels of NF-κB family members and cell cycle-associated *c-REL* target genes

Analyzing effects of the *c-REL* knockout in HeLa Kyoto cells on other NF-κB family members, we assessed respective gene expression levels by qPCR. *c-REL* knockout cells revealed significantly decreased mRNA levels of *RELA*, *NFKB1 (p50)*, *NFKB2 (p52)*, IκB-Kinase ε (*IKBKE*)
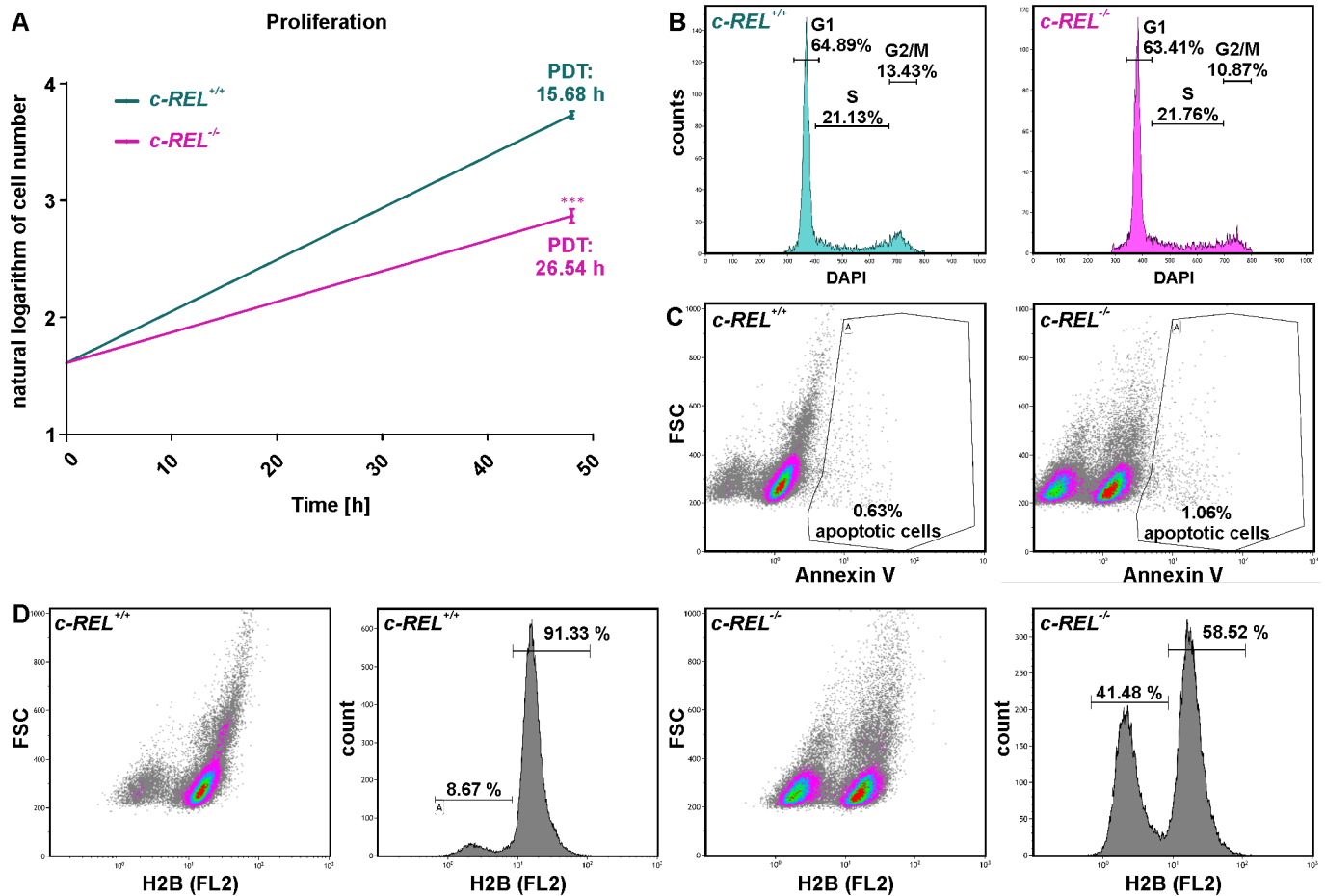
Fig 3. CRISPR/Cas9-mediated deletion of *c-REL* results in a decreased proliferation of HeLa Kyoto cell accompanied by strongly reduced amounts of histone H2B. A: Cell number assessed by Orangu Cell Proliferation Assay Kit (Cell Guidance Systems) set against cultivation time showed a strongly increased population doubling time of *c-REL* knockout cells compared to wt HeLa Kyoto cells. PDT: Population doubling time. **B:** Flow cytometric DNA content measurements of DAPI-stained *c-REL* knockout cells showed a decrease in the amount of mitotic cells in *c-REL* knockout cells compared to wildtype. **C:** Flow cytometric analysis of Annexin V-stained *c-REL*⁻/⁻ and wt HeLa Kyoto cells revealed only slightly increased amounts of apoptotic cells upon *c*-REL deletion in comparison to wt. **D:** Flow cytometric analysis of histone H2B-mCherry showed a strongly decreased amount of the H2B protein in 41.48% of *c-REL*⁻/⁻ HeLa Kyoto cells, which was observable in only 8.67% of HeLa Kyoto wt cells.

and TANK-binding kinase 1 (*TBK1*) compared to wildtype cells (Fig 5A). On the contrary, expression levels of *RELB* were not significantly affected in the *c-REL* knockout clone (Fig 5A).

In accordance to the observed decrease in proliferation and in *c-REL* knockout cells, we further observed significantly decreased mRNA levels in cell cycle-related *c-REL* target genes. In particular, expression levels of A20 (*TNFAIP3*), B-cell lymphoma 2 (*BCL2*), B-cell lymphoma-extra large (*BCLXL*, *BCL2L1*) and transforming growth factor beta 1 (*TGFB1*) were found to be significantly decreased in comparison to HeLa Kyoto wildtype cells (Fig 5B). In addition, expression levels of the *c-REL* target genes *MYC* and Intercellular Adhesion Molecule 1 (*ICAM-1*) were likewise significantly decreased compared to wildtype HeLa Kyoto cells (Fig 5C).

Promoter analysis was further performed using the JASPAR Tool (jaspar.genereg.net) to validate the analyzed genes to be direct *c-REL* target genes. Binding sites for *c-REL* and *RELA* were analyzed in each promoter region and their presence confirmed *IKBKE*, *TBK1*, *A20*, *BCL2*, *BCL-XL*, *TGFB1*, *MYC* and *ICAM-1* to be direct *c-REL* target genes (S3 Fig).
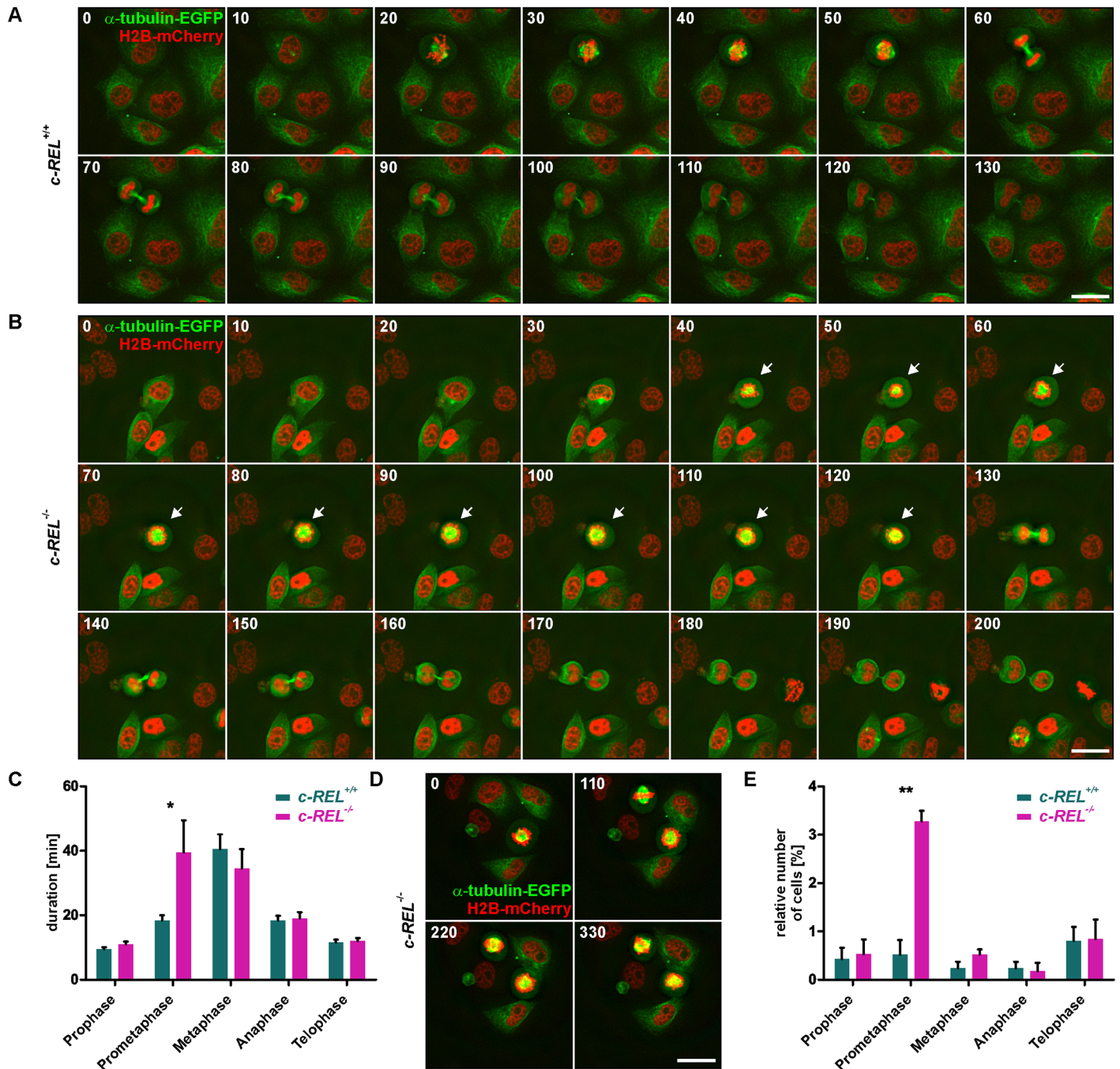
Fig 4. Knockout of *c-REL* leads to a significantly delayed prometaphase or even complete arrest of the cell cycle. A-B: Live cell imaging of *c-REL*^-/- and *c-REL*^+/+ cells showed delayed duration of the prometaphase in *c-REL*^-/- (arrows) in comparison to wildtype. Mitosis was visualized by H2B-mCherry and alpha-tubulin-EGFP. **C:** Quantification of life cell imaging validated the significant delay of *c-REL*^-/- *in* length of the prometaphase (39.50 ± 9.96 min) in comparison to wt (18.42 ± 1.58 min) (n = 20). **D:** Exemplary images of *c-REL*^-/- cells arresting during mitosis without entry of the G2 phase of the cell cycle. **E:** Fluorescence imaging of H2B-mCherry in fixed cells displayed a significantly increased amount of *c-REL*^-/- HeLa Kyoto cells within the prometaphase compared to wt cells. (>1000 cells quantified per genotype, n = 3). Scale bar: 25 µm.
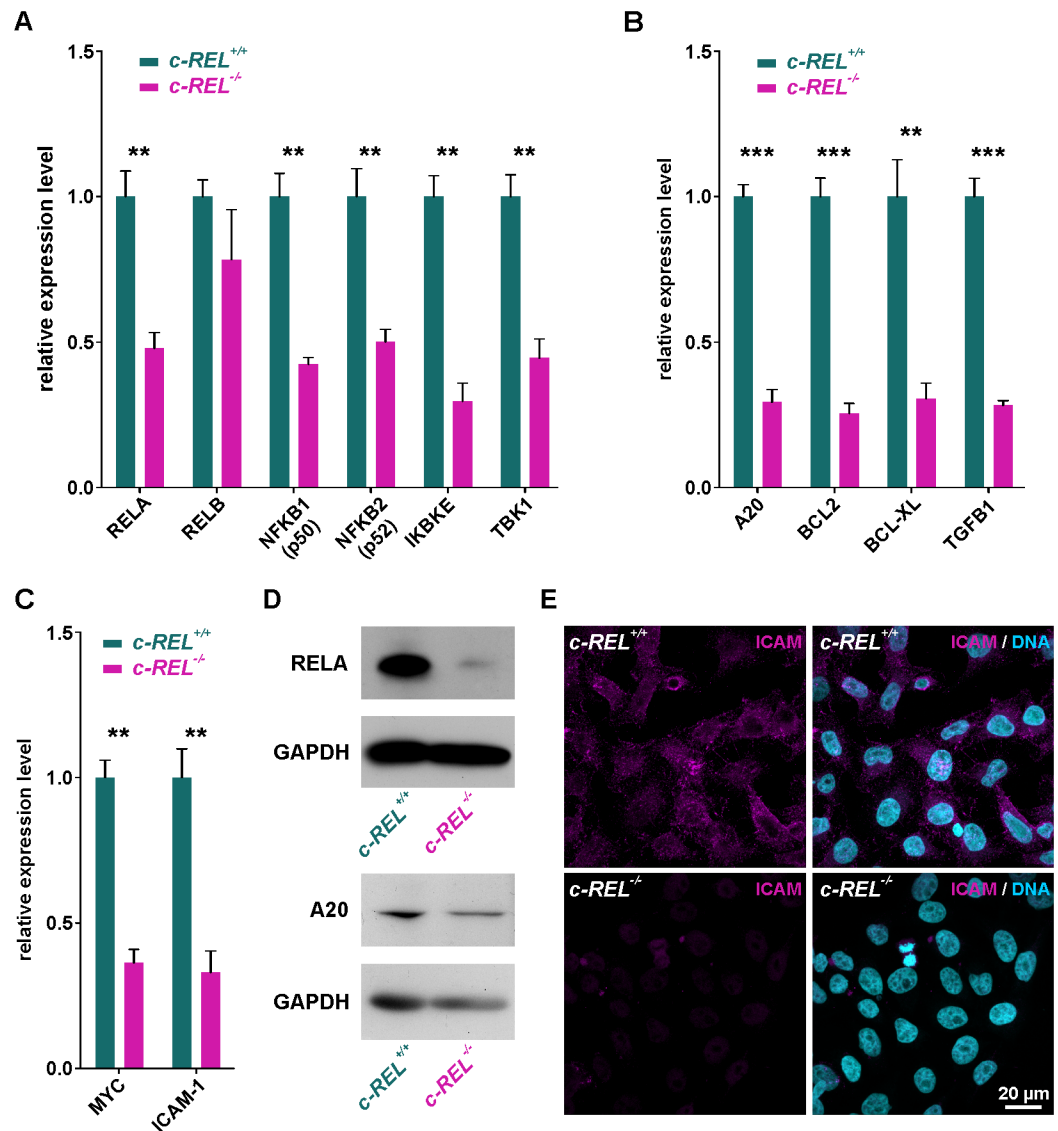
Fig 5. *c-REL* **knockout leads to significantly decreased expression levels of NF-κB family member and cell cycle-associated genes. A:** qPCR analysis showing significantly decreased mRNA levels of NF-κB family members *RELA*, *NFKB1 (p50)*, *NFKB2* (*p52*), *IKBKE* and *TBK1* in *c-REL* knockout cells compared to wildtype cells. **B-C:** Expression levels of cell cycle-related *c-REL* target genes *A20*, *BCL2*, *BCL-XL* and *TGFB1* and *c-REL* target genes *MYC* and *ICAM-1* were significantly decreased in *c-REL* knockout cells in comparison to HeLa Kyoto wildtype cells. **D:** Western blot analysis validated the reduced expression levels of RELA and A20 in *c-REL*⁻/⁻ cells in comparison to wt on protein level. WB were performed after TNFα-dependent stimulation of *c-REL*⁻/⁻ and *c-REL*⁺/⁺ cells. **E:** Immunocytochemistry revealed a strongly decreased protein amount of ICAM in *c-REL*⁻/⁻ cells in comparison to wt.

https://doi.org/10.1371/journal.pone.0182373.g005

To validate the decreased expression levels of *c-REL* target genes in *c-REL*⁻/⁻ HeLa Kyoto cells on protein level, we performed western blot analysis and immunocytochemistry. Western blot analysis revealed reduced amounts of RELA and A20 protein in *c-REL*⁻/⁻ cells in comparison to wt (Fig 5D). We further observed a nearly complete loss of ICAM protein in *c-REL*⁻/⁻ cells by immunocytochemistry, while HeLa Kyoto wt cells showed an unchanged amount of ICAM protein (Fig 5E).

Fig 6. Significantly increased resistance against chemotherapeutic agents in HeLa Kyoto cells with *c-REL* deletion. A: Although both HeLa Kyoto wildtype and *c-REL* knockout cells showed cell death after treatment with 5-Fluoro-2'-deoxyuridine, the *c-REL* knockout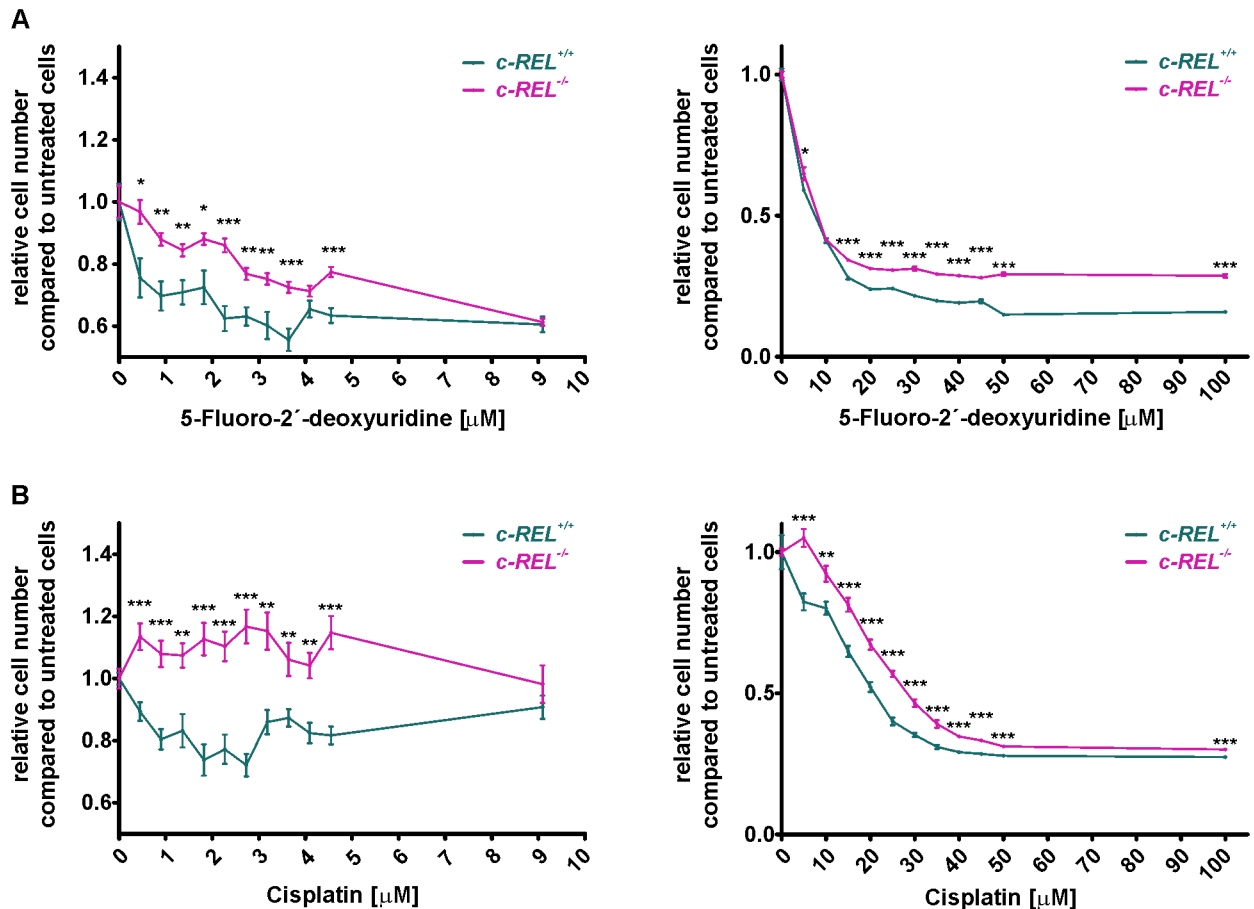 clone showed significantly elevated cell numbers in comparison to wildtype cells. Cells were exposed to chemotherapeutic agents for 21 h, cell numbers were assessed using Orangu Cell Proliferation Assay Kit (Cell Guidance Systems) after 2 h of incubation. Cell number of untreated cells were set to 1 and used for comparison. **B:** Although cisplatin-treatment of 1–4 μM led to cell death of wildtype cells, survival of the *c-REL* knockout clone was significantly increased even in comparison to untreated control. Increasing concentrations of cisplatin (10–100 μM) affected survival of *c-REL* knockout cells, but cell numbers were still significantly elevated compared to wildtype. Cells were exposed to chemotherapeutic agents for 21 h, cell numbers were assessed using Orangu Cell Proliferation Assay Kit (Cell Guidance Systems) after 2 h of incubation. Cell number of untreated cells were set to 1 and used for comparison (n = 8).

HeLa Kyoto cells with *c-REL* deletion show a significantly increased resistance against chemotherapeutic agents

With regards to the assessed overexpression of *c-REL* in human cancers ([Fig 1A](#)), potential clinical implications of the *c-REL* knockout were assessed by determining cell survival upon exposure to the chemotherapeutic agents 5-Fluoro-2'-deoxyuridine (5-FUDR) and cisplatin. Here, treatment with increasing concentration of 0.45–100 μM 5-FUDR for 21 h led to cell death of both *c-REL*$^{-/-}$ and wildtype cells ([Fig 6A](#)).

However, 5-FUDR-treated *c-REL* knockout clone showed significantly increased cell numbers in comparison to wildtype cells, indicating a profoundly increased resistance against 5-FUDR ([Fig 6A](#)). We likewise observed this effect after treatment of HeLa Kyoto wildtype and knockout cells with cisplatin. While cisplatin-treatment of 0.45–4.5 μM led to cell death of wildtype cells, assessed cell numbers of the *c-REL* knockout clone were significantly increased

even in comparison to untreated control ([Fig 6B]). Although exposure to increasing concentrations of cisplatin (10–100 µM) also resulted in cell death of *c-REL* knockout cells, cell number were still found to be significantly increased compared to wildtype, validating a robust resistance against cisplatin ([Fig 6B]).

Discussion

The present study shows a successful CRISPR/Cas9n-mediated knockout of the NF-κB subunit *c-REL* in HeLa Kyoto cells. HeLa cells are one of the most frequently used model systems for epithelial and in particular cervical cancers [37–39]. Here, we observed a significantly decreased proliferation of *c-REL*$^{-/-}$ cells accompanied by a significant decline in expression levels of NF-κB target genes in comparison to wt cells. HeLa Kyoto cells with *c-REL* deletion further revealed a significantly increased resistance against the chemotherapeutic agents 5-Fluoro-2'-deoxyuridine (5-FUDR) and cisplatin. These are commonly used as the trademarked chemotherapeutics Platinol® and FUDR® in the clinic.

With NF-κB being involved in many cellular processes [10, 11], a broad range of genes were described to be direct targets of NF-κB, including cytokines, chemokines, cell adhesion molecules, cell surface receptors, regulators of apoptosis and growth factors [40]. Interestingly, particular subunits of NF-κB were only rarely directly linked to specific target genes. In the present study, *c-REL*$^{-/-}$ HeLa Kyoto cells showed significantly decreased expression levels of NF-κB family members *RELA*, *NFKB1*, *NFKB2* as well as *IKBKE* and *TBK1*. We also observed several *c-REL* binding sites in the promoter region of the *TBK1* and *IKBKE* gene, suggesting *TBK1* and *IKBKE* as direct *c-REL* target genes. In addition to their role in phosphorylating NF-κB p65 [41], TBK1 and IKBKE were in turn described to directly phosphorylate the C-terminal domain of the c-REL protein resulting in its nuclear accumulation [42]. Extending these promising findings, we suggest a positive feedback loop by *c-REL*-mediated expression of *TBK1* and IKBKE in turn leading to a pronounced activation of *c-REL*. Being also closely linked to the pathogenesis of breast cancer by promoting activation of NF-κB [43], targeting *IKBKE* may be an interesting future perspective for developing new treatment strategies against cervical cancer. Next to *TBK1* and *IKBKE*, *c-REL* knockout was observed to be sufficient to downregulate the expression of *MYC* in growing HeLa cells by more than 50% with the relative *MYC* expression being highly elevated in comparison to other target genes. Accordingly, Grumont and coworkers showed an impaired expression of *MYC* in stage III thymocytes with a *RELA/c-REL* double knockout [44]. We also demonstrated the presence of three *c-REL* binding sites in the downstream region of the *MYC* promoter, further validating *MYC* as a direct target gene of *c-REL*.

In comparison to wildtype, *c-REL*$^{-/-}$ HeLa Kyoto cells further revealed a significantly decreased expression of *BCL-2*, *BCL-XL* and *A20*, which are commonly known as anti-apoptotic genes [45, 46]. In accordance to our promoter analysis depicting *c-REL*-binding sites, *BCL-XL* and *BCL2* were described to be direct *c-REL* target genes [47, 48]. Expression of *TGFB1*, already known as direct target of *c-REL* [49] and a common inducer of cell proliferation [50], was also significantly reduced in *c-REL*$^{-/-}$ HeLa Kyoto cells. On functional level, we observed the *c-REL* knockout to result in a significantly reduced proliferation, which we suggest to be at least in part mediated by the depicted decline in pro-proliferative target gene expression. In consistence with these findings, knockdown of the *c-REL* target gene *IKBKE* in HeLa cells was also shown to result in a suppression of proliferation [51]. In human keratinocytes, small interfering RNA-mediated knockdown of c-REL was reported to directly affect cell cycle progression by cell cycle delay of the G2/M phase [23]. The present study further extended these findings by showing the CRISPR-Cas9n-mediated knockout of *c-REL* to result in a robustly delayed prometaphase of mitosis accompanied by strongly reduced levels of

Table 1. Overexpression of *REL* in human cancers.

tissue type	% of *REL* overexpression	no. tested
Ovary	7.52	266
Lung	7.26	1019
Urinary tract	7.11	408
Endometrium	6.81	602
Pancreas	6.7	179
Haematopoietic and lymphoid	6.33	221
Soft tissue	6.08	263
Cervix	5.86	307
Upper aerodigestive tract	5.75	522
Kidney	5.5	600
Thyroid	5.46	513
Large intestine	4.92	610
Stomach	4.91	285
Liver	4.83	373
CNS	4.73	697
Prostate	4.62	498
Breast	3.71	1104
Skin	3.59	473
Oesophagus	3.2	125
Adrenal gland	2.53	79

https://doi.org/10.1371/journal.pone.0182373.t001

histone H2B protein. In addition, we observed a novel linkage between the decreased amount of histone H2B protein and the prolonged prometaphase in *c-REL*^{-/-} cells. In mice, silencing of c-Rel by siRNA was shown to lead to a reduction of mitosis in a B cell tumor cell line [52]. Grumont and coworkers likewise demonstrated a cell cycle arrest in B-cells of *c-Rel*^{-/-} mice [53]. Our present findings for the first time transfer these promising data to the human cancerous systems and provide deeper insights into the biology of cervical cancers in relation to *c-REL*-signaling. In this regard, we were also able to observe significantly reduced expression levels of *ICAM1* in *c-REL*^{-/-} HeLa Kyoto cells. Downregulation of this adhesion molecule was described to result in a suppression of human breast cancer cell invasion with the level of expression being directly correlated to their metastatic potential [54]. Accordingly, inhibition of MYC protein family members have been shown to induce regression of lung cancer in mice [55], suggesting the downregulation of *MYC* observed here likewise to be linked to the reduced proliferation of *c-REL*^{-/-} cells.

The NF-κB subunit *c-REL* is also directly linked to cancer development and progression. In 1999, Krappmann and colleagues described a constitutive NF-κB-activity with NF-κB-complexes containing RELA and c-REL in malignant cells derived from Hodgkin's disease [56]. Whereas *c-REL* was currently discussed as being mutated in hematopoietic and lymphoid tumors [57], a high throughput database analysis performed in the present study including 3397 hematopoietic and lymphoid tumors detected mutations in only a few samples [35, 58]. In 2004, Futreal and coworkers described a 'census' of human cancers indicating mutations in >1% of genes of the human genome to contribute to cancer, although genes showing solely altered expression levels were not included in this initial 'census' [59]. Here, we applied database mining using the COSMIC database [35] and observed profound overexpression of *c-REL* in various human tumors (Table 1), which is in accordance to the observed amplification of *c-REL* in human B-cell lymphomas [20, 21]. Likewise in line with previous studies, *c-REL* can be

considered as one of the most oncogenic members of the NF-κB family, in fowl reticuloendotheliosis virus also contains mutated oncogenic *v-Rel* [18, 19, 52, 60].

In the present study, knockout of *c-REL* in a cellular model of cervical carcinoma resulted in a significantly increased resistance against the chemotherapeutic agents 5-FUDR and cisplatin. Due to direct interaction of cisplatin and 5-fluorouracil with the DNA, highly proliferating cells are exposed to DNA damage resulting in cell-cycle arrest and cell death [61, 62]. Thus, we suggest the reduced proliferation of HeLa *c-REL*−/− cells to account for the observed increase in resistance against cisplatin and 5-FUDR. Although activation of NF-κB was also described to lead to a decreased sensitivity of cancer cells against chemotherapeutic treatment [63, 64], our present findings propose a subunit specificity of NF-κB in terms of chemoresistance. While a knockout of *c-REL* promoted survival of HeLa cells to chemotherapy, expression of the *c-REL* homolog *Xenopus* Xrel3 in cervical cancer cells treated with 5 μM cisplatin was shown to result in increased apoptosis [24].

In summary, our findings emphasize the importance of *c-REL*-signaling in a cellular model of cervical cancer particularly in terms of proliferation and resistance to chemotherapeutic agents. Considering the proposed NF-κB-subunit specificity of chemoresistance, we provide deeper insights into cervical cancer biology with direct clinical implications for the development of new treatment strategies.

Supporting information

S1 Fig. PAGE-analysis of top three predicted exonic off-targets revealed no signs of off-target effects in the *c-REL* knockout clone.
(TIF)

S2 Fig. Live cell imaging showing *c-REL*−/− cells, which arrested during mitosis without entry of the G2 phase of the cell cycle. Scale bar: 25 μm.
(TIF)

S3 Fig. Promoter analysis using the JASPAR Tool (jaspar.genereg.net) validated *IKBKE*, *TBK1*, *A20*, *BCL2*, *BCL-XL*, *TGFB1*, *MYC* and *ICAM*-1 to be direct *c-REL* target genes. *c-REL* binding site is shown in magenta, *RELA* binding site is depicted in cyan and common binding sites are shown in purple.
(TIF)

S1 Movie. Live cell imaging of *c-REL*−/− and *c-REL*+/+ cells showed delayed duration of the prometaphase in *c-REL*−/− in comparison to wildtype. Mitosis was visualized by H2B-mCherry and alpha-tubulin-EGFP.
(MP4)

Acknowledgments

Author Contributions

Conceptualization: Barbara Kaltschmidt, Christian Kaltschmidt.

Data curation: Barbara Kaltschmidt, Christian Kaltschmidt.

Formal analysis: Carsten Slotta, Thomas Schlüter, Johannes F. W. Greiner.

Funding acquisition: Barbara Kaltschmidt, Christian Kaltschmidt.

Investigation: Carsten Slotta, Thomas Schlüter, Lucia M. Ruiz-Perera, Hussamadin M. Kadhim, Tobias Tertel, Elena Henkel, Wolfgang Hübner.

Methodology: Carsten Slotta, Thomas Schlüter, Barbara Kaltschmidt, Christian Kaltschmidt.

Project administration: Barbara Kaltschmidt, Christian Kaltschmidt.

Resources: Thomas Huser, Barbara Kaltschmidt, Christian Kaltschmidt.

Supervision: Barbara Kaltschmidt, Christian Kaltschmidt.

Validation: Carsten Slotta, Johannes F. W. Greiner, Barbara Kaltschmidt, Christian Kaltschmidt.

Visualization: Carsten Slotta, Thomas Schlüter, Johannes F. W. Greiner.

Writing – original draft: Carsten Slotta, Thomas Schlüter, Johannes F. W. Greiner.

Writing – review & editing: Carsten Slotta, Lucia M. Ruiz-Perera, Hussamadin M. Kadhim, Tobias Tertel, Elena Henkel, Wolfgang Hübner, Johannes F. W. Greiner, Thomas Huser, Barbara Kaltschmidt, Christian Kaltschmidt.

References

1. Shehata MF. Rel/Nuclear factor-kappa B apoptosis pathways in human cervical cancer cells. Cancer cell international. 2005; 5(1):10. Epub 2005/04/29. https://doi.org/10.1186/1475-2867-5-10 PMID: 15857509

2. Stewart BW, Wild CP, (Editors). World Cancer Report 2014. World Health Organization; 2014.

3. Schiffman M, Castle PE, Jeronimo J, Rodriguez AC, Wacholder S. Human papillomavirus and cervical cancer. Lancet. 2007; 370(9590):890–907. Epub 2007/09/11. https://doi.org/10.1016/S0140-6736(07)61416-0 PMID: 17826171

4. Garland SM. Human papillomavirus update with a particular focus on cervical disease. Pathology. 2002; 34(3):213–24. Epub 2002/07/12. PMID: 12109780

5. Kang YJ, O'Connell DL, Tan J, Lew JB, Demers A, Lotocki R, et al. Optimal uptake rates for initial treatments for cervical cancer in concordance with guidelines in Australia and Canada: Results from two large cancer facilities. Cancer epidemiology. 2015; 39(4):600–11. Epub 2015/05/26. https://doi.org/10.1016/j.canep.2015.04.009 PMID: 26004990

6. Lorusso D, Petrelli F, Coinu A, Raspagliesi F, Barni S. A systematic review comparing cisplatin and carboplatin plus paclitaxel-based chemotherapy for recurrent or metastatic cervical cancer. Gynecologic oncology. 2014; 133(1):117–23. Epub 2014/02/04. https://doi.org/10.1016/j.ygyno.2014.01.042 PMID: 24486604

7. Nishiyama M, Yamamoto W, Park JS, Okamoto R, Hanaoka H, Takano H, et al. Low-dose cisplatin and 5-fluorouracil in combination can repress increased gene expression of cellular resistance determinants to themselves. Clinical cancer research: an official journal of the American Association for Cancer Research. 1999; 5(9):2620–8. Epub 1999/09/28.

8. Sen R, Baltimore D. Inducibility of kappa immunoglobulin enhancer-binding protein Nf-kappa B by a posttranslational mechanism. Cell. 1986; 47(6):921–8. Epub 1986/12/26. PMID: 3096580

9. Sen R, Baltimore D. Multiple nuclear factors interact with the immunoglobulin enhancer sequences. Cell. 1986; 46(5):705–16. Epub 1986/08/29. PMID: 3091258

10. Kaltschmidt B, Kaltschmidt C. NF-kappaB in the nervous system. Cold Spring Harbor perspectives in biology. 2009; 1(3):a001271. Epub 2010/01/13. https://doi.org/10.1101/cshperspect.a001271 PMID: 20066105

11. Perkins ND. Integrating cell-signalling pathways with NF-kappaB and IKK function. Nature reviews Molecular cell biology. 2007; 8(1):49–62. Epub 2006/12/22. https://doi.org/10.1038/nrm2083 PMID: 17183360

12. Xia Y, Shen S, Verma IM. NF-kappaB, an active player in human cancers. Cancer immunology research. 2014; 2(9):823–30. Epub 2014/09/05. https://doi.org/10.1158/2326-6066.CIR-14-0112 PMID: 25187272

13. Li Q, Withoff S, Verma IM. Inflammation-associated cancer: NF-kappaB is the lynchpin. Trends in immunology. 2005; 26(6):318–25. Epub 2005/06/01. https://doi.org/10.1016/j.it.2005.04.003 PMID: 15922948

14. Ben-Neriah Y, Karin M. Inflammation meets cancer, with NF-kappaB as the matchmaker. Nature immunology. 2011; 12(8):715–23. Epub 2011/07/21. https://doi.org/10.1038/ni.2060 PMID: 21772280

15. Sovak MA, Bellas RE, Kim DW, Zanieski GJ, Rogers AE, Traish AM, et al. Aberrant nuclear factor-kappaB/Rel expression and the pathogenesis of breast cancer. The Journal of clinical investigation. 1997; 100(12):2952–60. Epub 1998/01/31. https://doi.org/10.1172/JCI119848 PMID: 9399940

16. Nair A, Venkatraman M, Maliekal TT, Nair B, Karunagaran D. NF-kappaB is constitutively activated in high-grade squamous intraepithelial lesions and squamous cell carcinomas of the human uterine cervix. Oncogene. 2003; 22(1):50–8. Epub 2003/01/16. https://doi.org/10.1038/sj.onc.1206043 PMID: 12527907

17. Gilmore TD. Multiple mutations contribute to the oncogenicity of the retroviral oncoprotein v-Rel. Oncogene. 1999; 18(49):6925–37. Epub 1999/12/22. https://doi.org/10.1038/sj.onc.1203222 PMID: 10602467

18. Gilmore TD, Cormier C, Jean-Jacques J, Gapuzan ME. Malignant transformation of primary chicken spleen cells by human transcription factor c-Rel. Oncogene. 2001; 20(48):7098–103. Epub 2001/11/13. https://doi.org/10.1038/sj.onc.1204898 PMID: 11704834

19. Gilmore TD, Kalaitzidis D, Liang MC, Starczynowski DT. The c-Rel transcription factor and B-cell proliferation: a deal with the devil. Oncogene. 2004; 23(13):2275–86. Epub 2004/02/03. https://doi.org/10.1038/sj.onc.1207410 PMID: 14755244

20. Rosenwald A, Wright G, Chan WC, Connors JM, Campo E, Fisher RI, et al. The use of molecular profiling to predict survival after chemotherapy for diffuse large-B-cell lymphoma. The New England journal of medicine. 2002; 346(25):1937–47. Epub 2002/06/21. https://doi.org/10.1056/NEJMoa012914 PMID: 12075054

21. Houldsworth J, Olshen AB, Cattoretti G, Donnelly GB, Teruya-Feldstein J, Qin J, et al. Relationship between REL amplification, REL function, and clinical and biologic features in diffuse large B-cell lymphomas. Blood. 2004; 103(5):1862–8. Epub 2003/11/15. https://doi.org/10.1182/blood-2003-04-1359 PMID: 14615382

22. Shehata M, Shehata F, Pater A. Apoptosis effects of Xrel3 c-Rel/Nuclear Factor-kappa B homolog in human cervical cancer cells. Cell biology international. 2005; 29(6):429–40. Epub 2005/08/02. https://doi.org/10.1016/j.cellbi.2004.12.014 PMID: 16054560

23. Lorenz VN, Schon MP, Seitz CS. c-Rel downregulation affects cell cycle progression of human keratinocytes. The Journal of investigative dermatology. 2014; 134(2):415–22. Epub 2013/07/31. https://doi.org/10.1038/jid.2013.315 PMID: 23892589

24. Shehata M, Shehata F, Pater A. Dual apoptotic effect of Xrel3 c-Rel/NF-kappaB homolog in human cervical cancer cells. Cell biology international. 2004; 28(12):895–904. Epub 2004/11/30. https://doi.org/10.1016/j.cellbi.2004.09.002 PMID: 15566959

25. Horvath P, Barrangou R. CRISPR/Cas, the immune system of bacteria and archaea. Science. 2010; 327(5962):167–70. Epub 2010/01/09. https://doi.org/10.1126/science.1179555 PMID: 20056882

26. Cong L, Ran FA, Cox D, Lin S, Barretto R, Habib N, et al. Multiplex genome engineering using CRISPR/Cas systems. Science. 2013; 339(6121):819–23. Epub 2013/01/05. https://doi.org/10.1126/science.1231143 PMID: 23287718

27. Mali P, Yang L, Esvelt KM, Aach J, Guell M, DiCarlo JE, et al. RNA-guided human genome engineering via Cas9. Science. 2013; 339(6121):823–6. Epub 2013/01/05. https://doi.org/10.1126/science.1232033 PMID: 23287722

28. Matano M, Date S, Shimokawa M, Takano A, Fujii M, Ohta Y, et al. Modeling colorectal cancer using CRISPR-Cas9-mediated engineering of human intestinal organoids. Nature medicine. 2015; 21 (3):256–62. Epub 2015/02/24. https://doi.org/10.1038/nm.3802 PMID: 25706875

29. Jinek M, East A, Cheng A, Lin S, Ma E, Doudna J. RNA-programmed genome editing in human cells. eLife. 2013; 2:e00471. Epub 2013/02/07. https://doi.org/10.7554/eLife.00471 PMID: 23386978

30. Ran FA, Hsu PD, Lin CY, Gootenberg JS, Konermann S, Trevino AE, et al. Double nicking by RNA-guided CRISPR Cas9 for enhanced genome editing specificity. Cell. 2013; 154(6):1380–9. Epub 2013/09/03. https://doi.org/10.1016/j.cell.2013.08.021 PMID: 23992846

31. Sakuma T, Nishikawa A, Kume S, Chayama K, Yamamoto T. Multiplex genome engineering in human cells using all-in-one CRISPR/Cas9 vector system. Scientific reports. 2014; 4:5400. Epub 2014/06/24. https://doi.org/10.1038/srep05400 PMID: 24954249

32. Neumann B, Walter T, Heriche JK, Bulkescher J, Erfle H, Conrad C, et al. Phenotypic profiling of the human genome by time-lapse microscopy reveals cell division genes. Nature. 2010; 464(7289):721–7. Epub 2010/04/03. https://doi.org/10.1038/nature08869 PMID: 20360735

33. Tokunaga S, Stegeman JJ. Elimination of nonspecific bands in non-radioactive electrophoretic mobility shift assays using the digoxigenin system. Analytical biochemistry. 2014; 465:70–2. Epub 2014/07/09. https://doi.org/10.1016/j.ab.2014.06.020 PMID: 25004462

34. Kaltschmidt B, Kaltschmidt C, Hehner SP, Droge W, Schmitz ML. Repression of NF-kappaB impairs HeLa cell proliferation by functional interference with cell cycle checkpoint regulators. Oncogene. 1999; 18(21):3213–25. Epub 1999/06/08. https://doi.org/10.1038/sj.onc.1202657 PMID: 10359527

35. Forbes SA, Beare D, Gunasekaran P, Leung K, Bindal N, Boutselakis H, et al. COSMIC: exploring the world's knowledge of somatic mutations in human cancer. Nucleic acids research. 2015; 43(Database issue):D805–11. Epub 2014/10/31. https://doi.org/10.1093/nar/gku1075 PMID: 25355519

36. Stemmer M, Thumberger T, Del Sol Keyer M, Wittbrodt J, Mateo JL. CCTop: An Intuitive, Flexible and Reliable CRISPR/Cas9 Target Prediction Tool. PloS one. 2015; 10(4):e0124633. Epub 2015/04/25. https://doi.org/10.1371/journal.pone.0124633 PMID: 25909470

37. Zhao Y, Yao R, Ouyang L, Ding H, Zhang T, Zhang K, et al. Three-dimensional printing of Hela cells for cervical tumor model in vitro. Biofabrication. 2014; 6(3):035001. Epub 2014/04/12. https://doi.org/10.1088/1758-5082/6/3/035001 PMID: 24722236

38. Vidya Priyadarsini R, Senthil Murugan R, Maitreyi S, Ramalingam K, Karunagaran D, Nagini S. The flavonoid quercetin induces cell cycle arrest and mitochondria-mediated apoptosis in human cervical cancer (HeLa) cells through p53 induction and NF-kappaB inhibition. European journal of pharmacology. 2010; 649(1–3):84–91. Epub 2010/09/23. https://doi.org/10.1016/j.ejphar.2010.09.020 PMID: 20858478

39. Hamada K, Alemany R, Zhang WW, Hittelman WN, Lotan R, Roth JA, et al. Adenovirus-mediated transfer of a wild-type p53 gene and induction of apoptosis in cervical cancer. Cancer research. 1996; 56 (13):3047–54. Epub 1996/07/01. PMID: 8674061

40. Gilmore TD. NF-kB Target Genes. https://www.bu.edu/nf-kb/gene-resources/target-genes/: Boston University Biology; [cited 2017 13.02.].

41. Buss H, Dorrie A, Schmitz ML, Hoffmann E, Resch K, Kracht M. Constitutive and interleukin-1-inducible phosphorylation of p65 NF-{kappa}B at serine 536 is mediated by multiple protein kinases including I {kappa}B kinase (IKK)-{alpha}, IKK{beta}, IKK{epsilon}, TRAF family member-associated (TANK)-binding kinase 1 (TBK1), and an unknown kinase and couples p65 to TATA-binding protein-associated factor Il31-mediated interleukin-8 transcription. The Journal of biological chemistry. 2004; 279(53):55633–43. Epub 2004/10/19. https://doi.org/10.1074/jbc.M409825200 PMID: 15489227

42. Harris J, Oliere S, Sharma S, Sun Q, Lin R, Hiscott J, et al. Nuclear accumulation of cRel following C-terminal phosphorylation by TBK1/IKK epsilon. J Immunol. 2006; 177(4):2527–35. Epub 2006/08/05. PMID: 16888014

43. Eddy SF, Guo S, Demicco EG, Romieu-Mourez R, Landesman-Bollag E, Seldin DC, et al. Inducible IkappaB kinase/IkappaB kinase epsilon expression is induced by CK2 and promotes aberrant nuclear factor-kappaB activation in breast cancer cells. Cancer research. 2005; 65(24):11375–83. Epub 2005/12/17. https://doi.org/10.1158/0008-5472.CAN-05-1602 PMID: 16357145

44. Grumont R, Lock P, Mollinari M, Shannon FM, Moore A, Gerondakis S. The mitogen-induced increase in T cell size involves PKC and NFAT activation of Rel/NF-kappaB-dependent c-myc expression. Immunity. 2004; 21(1):19–30. Epub 2004/09/04. https://doi.org/10.1016/j.immuni.2004.06.004 PMID: 15345217

45. Grey ST, Arvelo MB, Hasenkamp W, Bach FH, Ferran C. A20 inhibits cytokine-induced apoptosis and nuclear factor kappaB-dependent gene activation in islets. The Journal of experimental medicine. 1999; 190(8):1135–46. Epub 1999/10/19. PMID: 10523611

46. Boise LH, Gonzalez-Garcia M, Postema CE, Ding L, Lindsten T, Turka LA, et al. bcl-x, a bcl-2-related gene that functions as a dominant regulator of apoptotic cell death. Cell. 1993; 74(4):597–608. Epub 1993/08/27. PMID: 8358789

47. Grossmann M, O'Reilly LA, Gugasyan R, Strasser A, Adams JM, Gerondakis S. The anti-apoptotic activities of Rel and RelA required during B-cell maturation involve the regulation of Bcl-2 expression. The EMBO journal. 2000; 19(23):6351–60. Epub 2000/12/02. https://doi.org/10.1093/emboj/19.23.6351 PMID: 11101508

48. Chen C, Edelstein LC, Gelinas C. The Rel/NF-kappaB family directly activates expression of the apoptosis inhibitor Bcl-x(L). Molecular and cellular biology. 2000; 20(8):2687–95. Epub 2000/03/25. PMID: 10733571

49. De Siervi A, De Luca P, Moiola C, Gueron G, Tongbai R, Chandramouli GV, et al. Identification of new Rel/NFkappaB regulatory networks by focused genome location analysis. Cell Cycle. 2009; 8 (13):2093–100. Epub 2009/06/09. https://doi.org/10.4161/cc.8.13.8926 PMID: 19502793

50. Strutz F, Zeisberg M, Renziehausen A, Raschke B, Becker V, van Kooten C, et al. TGF-beta 1 induces proliferation in human renal fibroblasts via induction of basic fibroblast growth factor (FGF-2). Kidney international. 2001; 59(2):579–92. Epub 2001/02/13. https://doi.org/10.1046/j.1523-1755.2001. 059002579.x PMID: 11168939

51. Adli M, Baldwin AS. IKK-i/IKKepsilon controls constitutive, cancer cell-associated NF-kappaB activity via regulation of Ser-536 p65/RelA phosphorylation. The Journal of biological chemistry. 2006; 281 (37):26976–84. Epub 2006/07/15. https://doi.org/10.1074/jbc.M603133200 PMID: 16840782

52. Tian W, Liou HC. RNAi-mediated c-Rel silencing leads to apoptosis of B cell tumor cells and suppresses antigenic immune response in vivo. PloS one. 2009; 4(4):e5028. Epub 2009/04/07. https://doi.org/10. 1371/journal.pone.0005028 PMID: 19347041

53. Grumont RJ, Rourke IJ, O'Reilly LA, Strasser A, Miyake K, Sha W, et al. B lymphocytes differentially use the Rel and nuclear factor kappaB1 (NF-kappaB1) transcription factors to regulate cell cycle progression and apoptosis in quiescent and mitogen-activated cells. The Journal of experimental medicine. 1998; 187(5):663–74. Epub 1998/03/28. PMID: 9480976

54. Rosette C, Roth RB, Oeth P, Braun A, Kammerer S, Ekblom J, et al. Role of ICAM1 in invasion of human breast cancer cells. Carcinogenesis. 2005; 26(5):943–50. Epub 2005/03/19. https://doi.org/10. 1093/carcin/bgi070 PMID: 15774488

55. Soucek L, Whitfield JR, Sodir NM, Masso-Valles D, Serrano E, Karnezis AN, et al. Inhibition of Myc family proteins eradicates KRas-driven lung cancer in mice. Genes & development. 2013; 27(5):504–13. Epub 2013/03/12.

56. Krappmann D, Emmerich F, Kordes U, Scharschmidt E, Dorken B, Scheidereit C. Molecular mechanisms of constitutive NF-kappaB/Rel activation in Hodgkin/Reed-Sternberg cells. Oncogene. 1999; 18 (4):943–53. Epub 1999/02/19. https://doi.org/10.1038/sj.onc.1202351 PMID: 10023670

57. Perkins ND, Gilmore TD. Good cop, bad cop: the different faces of NF-kappaB. Cell death and differentiation. 2006; 13(5):759–72. Epub 2006/01/18. https://doi.org/10.1038/sj.cdd.4401838 PMID: 16410803

58. Forbes SA. cancer.sanger.ac.uk [cited 2017 14.02].

59. Futreal PA, Coin L, Marshall M, Down T, Hubbard T, Wooster R, et al. A census of human cancer genes. Nature reviews Cancer. 2004; 4(3):177–83. Epub 2004/03/03. https://doi.org/10.1038/nrc1299 PMID: 14993899

60. Wilhelmsen KC, Eggleton K, Temin HM. Nucleic acid sequences of the oncogene v-rel in reticuloendotheliosis virus strain T and its cellular homolog, the proto-oncogene c-rel. Journal of virology. 1984; 52(1):172–82. Epub 1984/10/01. PMID: 6090694

61. Wang D, Lippard SJ. Cellular processing of platinum anticancer drugs. Nature reviews Drug discovery. 2005; 4(4):307–20. Epub 2005/03/25. https://doi.org/10.1038/nrd1691 PMID: 15789122

62. Peters GJ, Backus HH, Freemantle S, van Triest B, Codacci-Pisanelli G, van der Wilt CL, et al. Induction of thymidylate synthase as a 5-fluorouracil resistance mechanism. Biochimica et biophysica acta. 2002; 1587(2–3):194–205. Epub 2002/06/27. PMID: 12084461

63. Wang CY, Cusack JC Jr., Liu R, Baldwin AS Jr.. Control of inducible chemoresistance: enhanced antitumor therapy through increased apoptosis by inhibition of NF-kappaB. Nature medicine. 1999; 5 (4):412–7. Epub 1999/04/15. https://doi.org/10.1038/7410 PMID: 10202930

64. Yang L, Zhou Y, Li Y, Zhou J, Wu Y, Cui Y, et al. Mutations of p53 and KRAS activate NF-kappaB to promote chemoresistance and tumorigenesis via dysregulation of cell cycle and suppression of apoptosis in lung cancer cells. Cancer letters. 2015; 357(2):520–6. Epub 2014/12/17. https://doi.org/10.1016/j. canlet.2014.12.003 PMID: 25499080
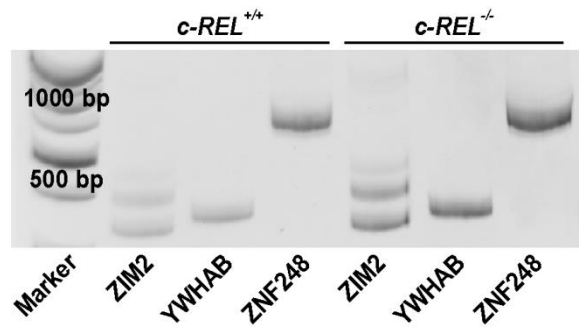
Supplementary Data

Figure S1

Figure S2
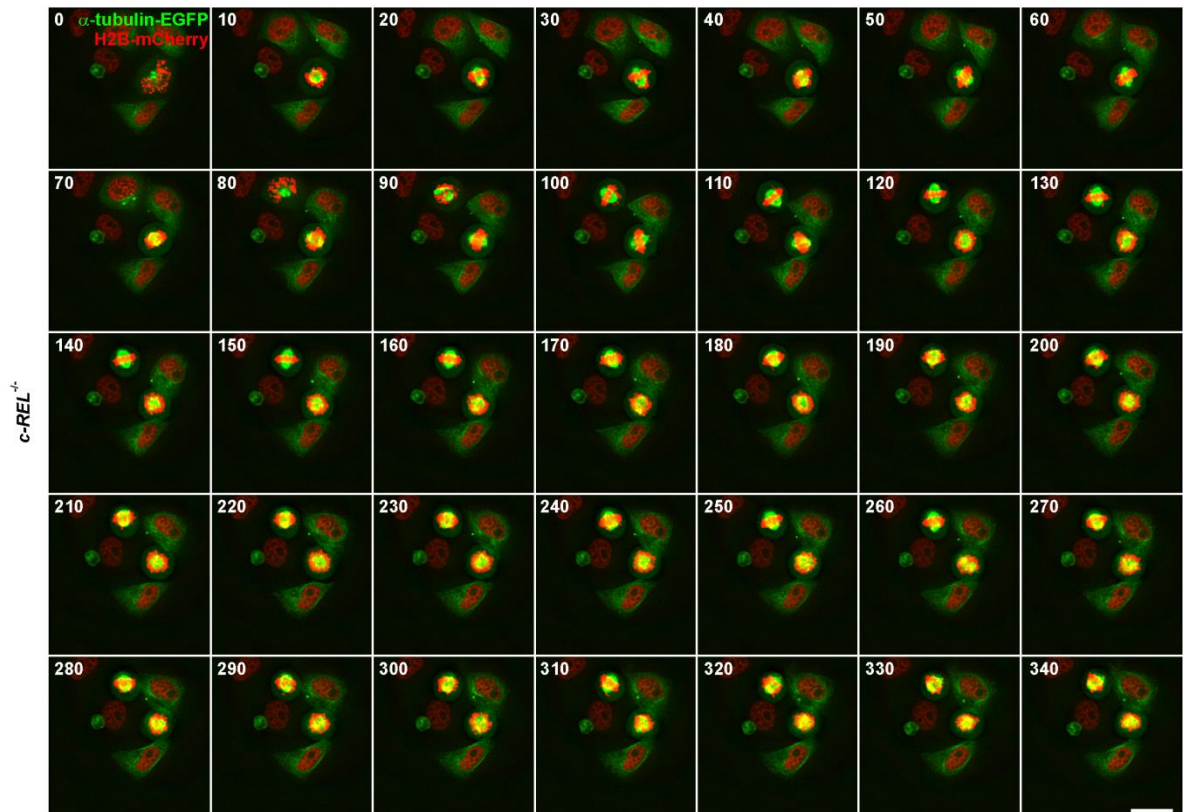
Figure S3
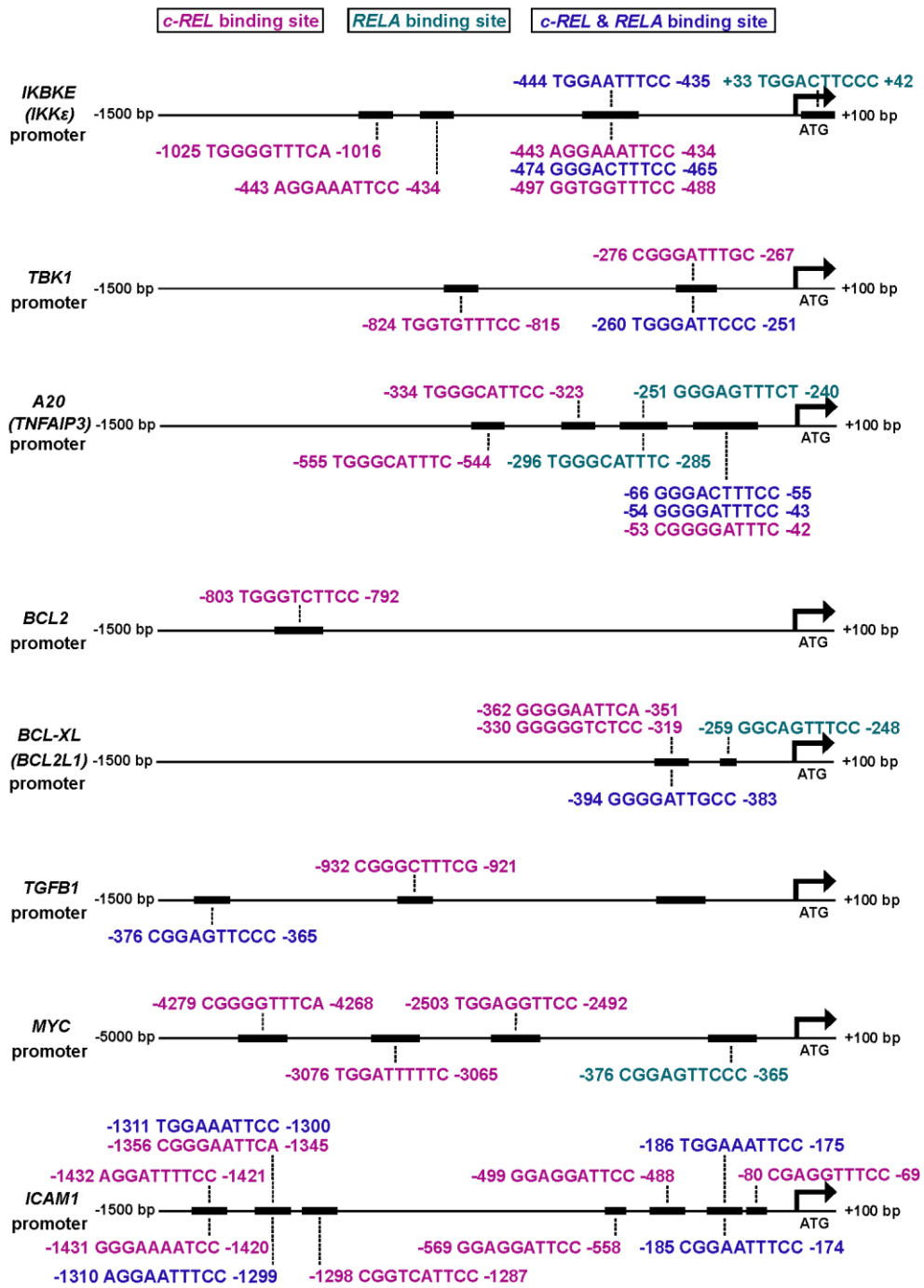
CRISPR/Cas9-mediated deficiency of human *IKBK1/IKBK2* leads to TNFα-induced programmed cell death in an NF-κB-independent manner

Carsten Slotta[1,2], Jonathan Storm[1], Nina Pfisterer[1], Svenja Kleinwächter[1], Maren Pieper[1],

Lucia M Ruiz-Perera[2], Elena Henkel[1], Johannes FW Greiner[1], Barbara Kaltschmidt[1,2*],

Christian Kaltschmidt[1*#]

[1] Department of Cell Biology, University of Bielefeld, Universitaetsstr. 25, 33501 Bielefeld, Germany

[2] Molecular Neurobiology, University of Bielefeld, Universitaetsstr. 25, 33501 Bielefeld, Germany

* These authors contributed equally to this work

Corresponding Author:

Christian Kaltschmidt, Department of Cell Biology, University of Bielefeld, Universitaetsstr. 25, 33501 Bielefeld, Germany,

Tel.: + 49 521 106 5625; Fax: + 49 521 106 5654; E-Mail: c.kaltschmidt@uni-bielefeld.de

Abstract

20 TNF signaling is directly linked to cancer development and progression. A broad range of

21 tumor cells is able to evade cell death induced by TNF impairing the potential anti-cancer

22 value of TNF in therapy. Although sensitizing cells to TNF-induced death therefore has great

23 clinical implications, detailed mechanistic insights into TNF-mediated human cell death still

24 remain unknown. Here, we analyzed human cells by applying CRISPR/Cas9n to generate cells

25 deficient of IKK1, IKK2, IKK1/2 and RELA. Despite stimulation with TNF resulted in impaired

26 NF-κB activation in all genotypes compared to wildtype cells, increased cell death was

27 observable only in IKK1/2-double-deficient cells. Cell death could be detected by Caspase-3

28 activation and binding of Annexin V. TNF-induced programmed cell death in IKK1/2$^{-/-}$ cells

29 was further shown to be mediated via RIPK1 in a predominantly apoptotic manner. Our

30 findings demonstrate the IKK complex to protect from TNF-induced cell death in human cells

31 independently to NF-κB RelA suggesting IKK1/2 to be highly promising targets for cancer

32 therapy.

1

Introduction

The tumor necrosis factor (TNF) is a well-characterized pro-inflammatory cytokine known to activate the canonical NF-κB signaling pathway. A particular important regulatory factor in NF-κB signaling is the IκB kinase (IKK) complex. It consists of the catalytic subunits IKKα (IKK1) and IKKβ (IKK2) and the regulatory subunit NF-kappa-B essential modulator (NEMO; IKKγ). The IKK complex is required for the activation of the transcription factor NF-κB, which ultimately results in the expression of NF-κB target genes involved in cell growth, survival, but also inflammation and cell death (1). Deregulation of NF-κB signaling is strongly associated with diseases, in particular with tumor formation (2, 3).

In the canonical NF-κB signaling pathway binding of TNF to the TNF receptor 1 (TNFR1) results in the formation of the so-called complex I consisting of the TNFR1 associated death domain protein (TRADD), TNF receptor associated factor 2 (TRAF2), cellular inhibitors of apoptosis 1 and 2 (cIAP1/2), linear ubiquitin assembly complex (LUBAC) and Receptor-interacting serine/threonine-protein kinase 1 (RIPK1) (4). Ubiquitination of RIPK1 leads to the recruitment of the IKK complex by binding of NEMO to M1-linked ubiquitin chains on the one hand and of the TAK1/TAB2/3 complex via K63-linked chains on the other hand (5, 6). Being phosphorylated by TAK1, IKK2 in turn phosphorylates IκBα at Ser32/36. Phosphorylated IκBα will be polyubiquitinated by SCF$^{\beta\text{-TrCP}}$ E3 ubiquitin ligases leading to its proteasomal degradation (7). This results in the unmasking of the nuclear localization sequence of NF-κB, in canonical signaling mostly comprised of a p65/p50 dimer, whereby p65 is the transactivating subunit (8). Due to the unmasked NLS, NF-κB is no longer retained in the cytoplasm and can enter the nucleus leading to the expression of target genes (9). Tight regulation of the specificity of this process is achieved by a broad range of post-

56   translational modifications (PMTs) potentially resulting in conformational changes of NF-κB

57   and by this specifying the subset of target genes being expressed (10, 11).

58   Although TNFR1 belongs to the death receptor family (12), under physiological conditions

59   TNF signaling will not induce cell death in a broad range of cell types, since TNF-mediated

60   activation of NF-κB will result in the expression of anti-apoptotic genes such as c-FLIP, cIAP-

61   1,cIAP-2 and Bcl-2 (13-16). However, genetic or pharmacological inhibition of NF-κB is known

62   to increase sensitivity to TNF-induced apoptosis (17). Here, cell death is mediated via the so-

63   called complex IIa comprised of TRADD, Fas-associated protein with death domain (FADD)

64   and caspase-8, which only assembles upon NF-κB inhibition (18, 19). However, programmed

65   cell death induced by TNF signaling can also be mediated via an NF-κB – independent

66   manner (20). In this context, cell death occurs via the complex IIb (20). In contrast to

67   complex IIa, FADD and caspase-8 are recruited by RIPK1 in complex IIb. Upon inhibition of

68   caspase-8, NF-κB – independent cell death via TNFR1 can also be necroptotic. Necroptosis is

69   a more recently described way of programmed cell death, which is independent on caspase-

70   8 activation and induced by RIPK3 and the pseudokinase mixed lineage kinase like (MLKL)

71   (21-23).

72   Most studies regarding TNF-induced cell death were performed using mouse models, in

73   which members of the NF-κB signaling pathway were genetically depleted. Many of these

74   genetic knockouts are resulting in lethality during embryonic development, e.g. in RelA- and

75   Ikk2-deficient mice (24-26). In both cases, embryonic lethality is caused by TNFα-induced

76   death of hepatocytes and subsequent liver degeneration, which can be rescued by additional

77   depletion of TNFR1 (25, 27). In contrast to this, a frameshift mutation within the human

78   *IKBKB* gene, which was found in patients suffering from severe combined immunodeficiency

79   (SCID), had no effect on embryonic survival or liver constitution (28). These findings suggest

3

80   the presence of potential differences in the regulation of TNFα-induced cell death between

81   mouse and human. Since TNF signaling is highly elevated in a broad range of cancer cells,

82   which are resistant to cell death induced by TNF (29), sensitizing these cells to TNF-induced

83   cell death appears to be a promising approach for cancer therapy. Despite this clinical

84   relevance, the detailed molecular mechanisms of TNF-induced cell death in human cells still

85   remain unknown.

86   Facing this challenge, we made use of the CRISPR/Cas9 system to generate genomic

87   knockouts of several members of the NF-κB signaling pathway in human cells. Originally

88   discovered as part of the bacterial adaptive immune system (30, 31), the clustered regularly

89   interspaced short palindromic repeats (CRISPR) system has become a state-of-the-art tool

90   broadly applied for efficient genome editing (32, 33). In this study, a nickase mutant of the *S.*

91   *pyogenes* Cas9 (D10A; Cas9n) has been used minimizing potential off-target effects and by

92   this increasing the specificity of genome editing (34). We successfully generated cells

93   deficient for IKK1, IKK2, IKK1/2 and RelA and demonstrate that TNFα-induced cell death in

94   human cells is mediated predominantly via RIPK1 and independently of NF-κB. Targeting the

95   IKK complex in tumor cells genetically or pharmacologically therefore appears promising to

96   increase sensitivity to TNF-induced cell death with direct implications for potential

97   therapeutic approaches.

Results

99 **Knockout of IKK1 and IKK2 leads to strongly impaired NF-κB activation**

100 To assess clinical implications of IKK1 and IKK2 knockouts, we first analyzed levels of

101 overexpression in human cancer with database mining using COSMIC (35). Here, particularly

102 *IKBKB* (IKK2) was found to be profoundly overexpressed in a variety of tissues including

103 breast, endometrium, large intestine and skin (Fig. S1).

104 We now aimed to analyze the role of IKK1 and IKK2 in the context of TNF signaling and

105 activation of NF-κB. For this, we utilized the CRISPR/Cas9n system to generate IKK1- and

106 IKK2-deficient cells as well as an IKK1/IKK2 double knockout by inducing two double-strand

107 breaks spanning an intron-exon border (Fig. 1A). Deletions within the *IKBK1* and *IKBK2* gene

108 of clonally grown cells were validated by genomic PCR using primers flanking the deletion

109 (Fig. 1B) and by RT-PCR using primer pairs with one primer set within the deletion (Fig. 1C).

110 Absence of IKK1 and IKK2 protein was finally shown on western blot (Fig. 1D). Notably, we

111 did not observe a strong reduction in the amount of the NF-κB subunit p65 in the knockout

112 clones, which was described earlier for IKK2-deficient human fibroblast (28). Only in *IKK1*-

113 deficient cells, a slight reduction was detected (Fig. S2).

Figure 1
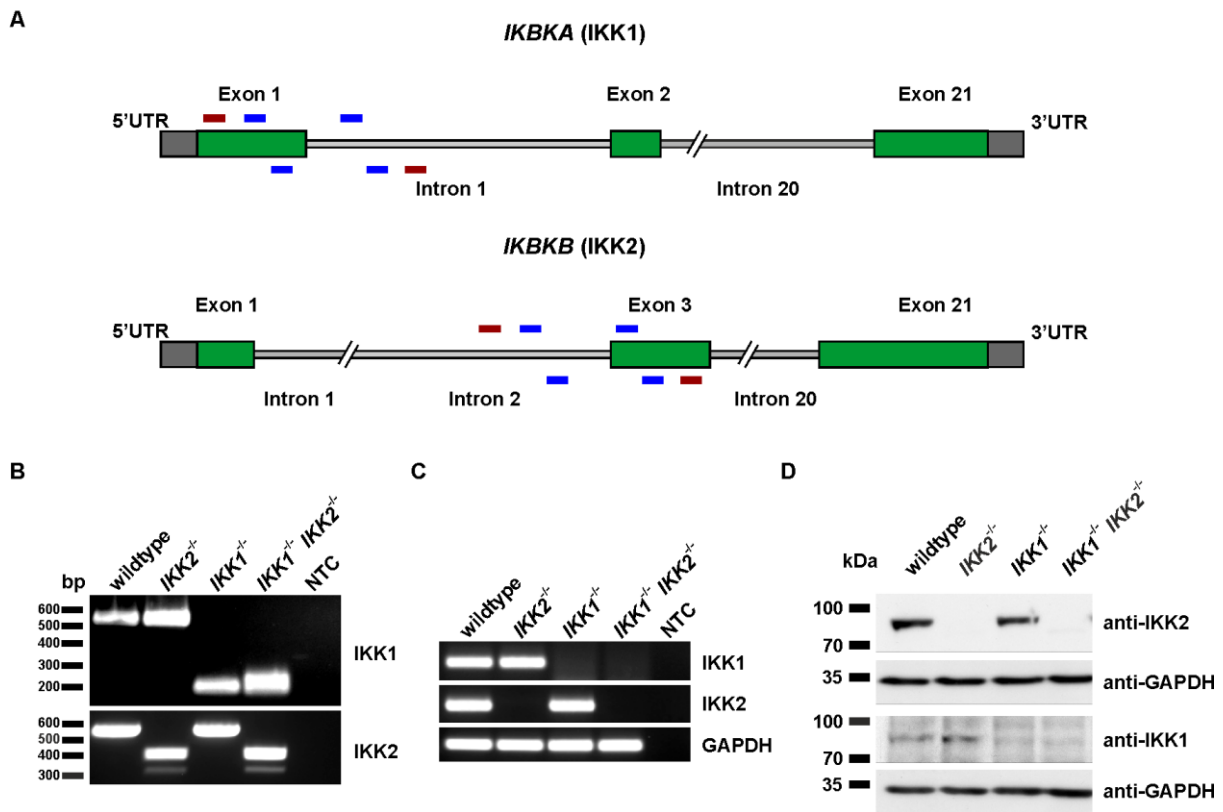
Figure 1. Generation of IKK1, IKK2 and IKK1/2-deficient cells. (A) Target design showing the desired genomic deletion in the *IKBKA* and *IKBKB* gene. Marked in blue are the designed sgRNAs and marked in green are the flanking primers used for genomic PCR. **(B)** Genomic PCR of clonally grown cells demonstrating the desired deletion in the respective genotype. **(C)** RT-PCR using primers designed within the deletion showing no amplification in the respective genotype. **(D)** Western blot analysis revealing lack of IKK2 protein in IKK2-deficient cells, lack of IKK1 protein in IKK1-deficient cells and lack of both in double-deficient cells.

Next, we examined NF-κB activation in all genotypes after stimulation with TNFα. Nuclear translocation of p65 was significantly impaired compared to wildtype cells (Fig. 2A, B). This effect was strongest in the double-deficient cells. In line with this, qPCR analysis of the NF-κB

6

128 target genes IκBα, A20 and IL-8 after TNFα stimulation revealed a significantly reduced

129 expression in all genotypes compared to wildtype cells (Fig. 2D). In IKK1/2-double-deficient

130 cells, no increase in expression upon stimulation was detected at all (Fig. 2D). Moreover, we

131 detected no signs of IκBα degradation upon TNFα treatment in these cells (Fig. 2C).

132 However, degradation of IκBα was reduced in IKK1 and IKK2 single knockouts, although to a

133 lesser extent than in wildtype cells.

134

Figure 2
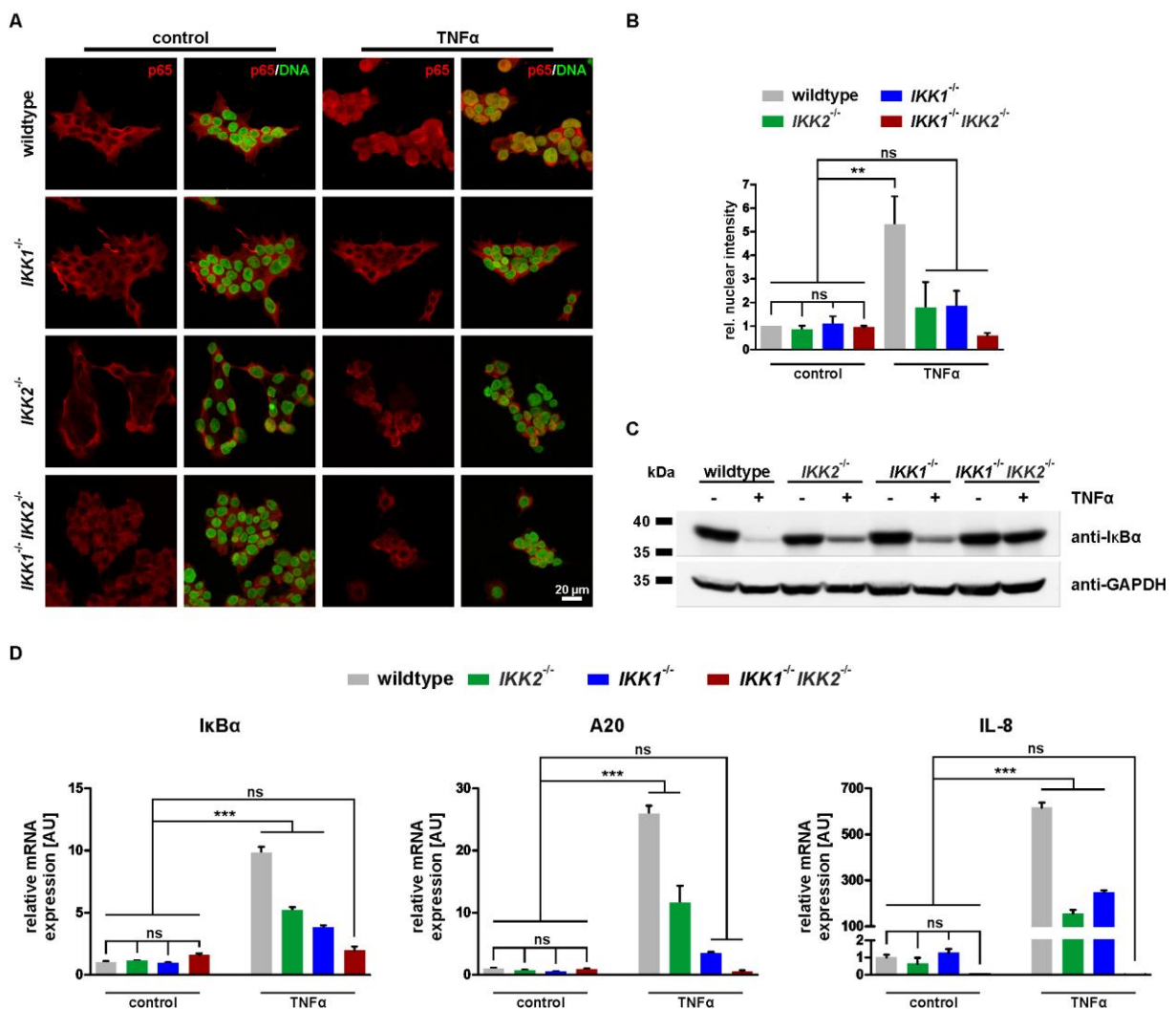
137 **Figure 2. Strongly impaired NF-κB activation in knockout cells. (A)** Immunocytochemical

138 stainings of cells stimulated for 20 min with 10 ng/mL TNFα. Only in wildtype cells a clear

7

139   nuclear translocation of p65 after stimulation is observable. **(B)** Quantification of the nuclear

140   intensity of cells stained against p65 (One-way ANOVA, Bonferroni post-test, n=3). **(C)**

141   Western blot analysis demonstrating degradation of IκBα upon stimulation with 10 ng/mL

142   TNFα for 20 min. While in IKK1- and IKK2-deficient cells a partial degradation is shown

143   compared to wildtype cells, no degradation is visible in the double-deficient cells. **(D)** qPCR

144   analysis of the NF-κB target genes IκBα, A20 and IL-8 revealed reduced expression in the

145   knockout cells after 6 h of TNFα (10 ng/mL) treatment compared to wildtype cells (One-way

146   ANOVA, Bonferroni post-test, n=3).

147

148   **IKK1 and IKK2 double-deficiency results in TNFα-induced cell death**

149   We aimed to analyze TNFα-induced cell death in our newly generated knockout cells. After

150   long-term exposure (24 h) to TNFα, a high number of dead cells was observable only in the

151   double-deficient cells, while there was hardly any difference detectable between the single

152   knockouts and wildtype cells (Fig. 3A). Immunocytochemical staining of TNFα-treated cells

153   also revealed 32.1% of the IKK1/IKK2$^{-/-}$ cells to be positive for activated Caspase-3. In

154   comparison, only 3.0% Caspase-3-positive cells were found in wildtype cells (Fig. 3B).

155   Without TNFα stimulation, in both genotypes less than 0.3% cells were positive (Fig. 3B). We

156   additionally detected the increased cell death in the IKK1/2 double-deficient cells using DNA

157   content measurements (Fig. S3). In the IKK1 and IKK2 single knockout cells, no difference in

158   the amount of apoptotic cells upon TNFα stimulation was observable compared to wildtype

159   cells. However, in IKK1/2-double-deficient cells, this amount was increased from 4.2%

160   (wildtype) to 34.7% (Fig. S3). Furthermore, increased cell death of the IKK1/2$^{-/-}$ cells within

161   24 h of TNFα stimulation could be demonstrated using an Annexin V-based apoptosis assay

162 (Fig. 3C, D). Annexin V-based luminescent signal was strongly elevated in the double-

163 deficient cells (Fig. 3D) in relation to wildtype (Fig. 3C).

164

Figure 3
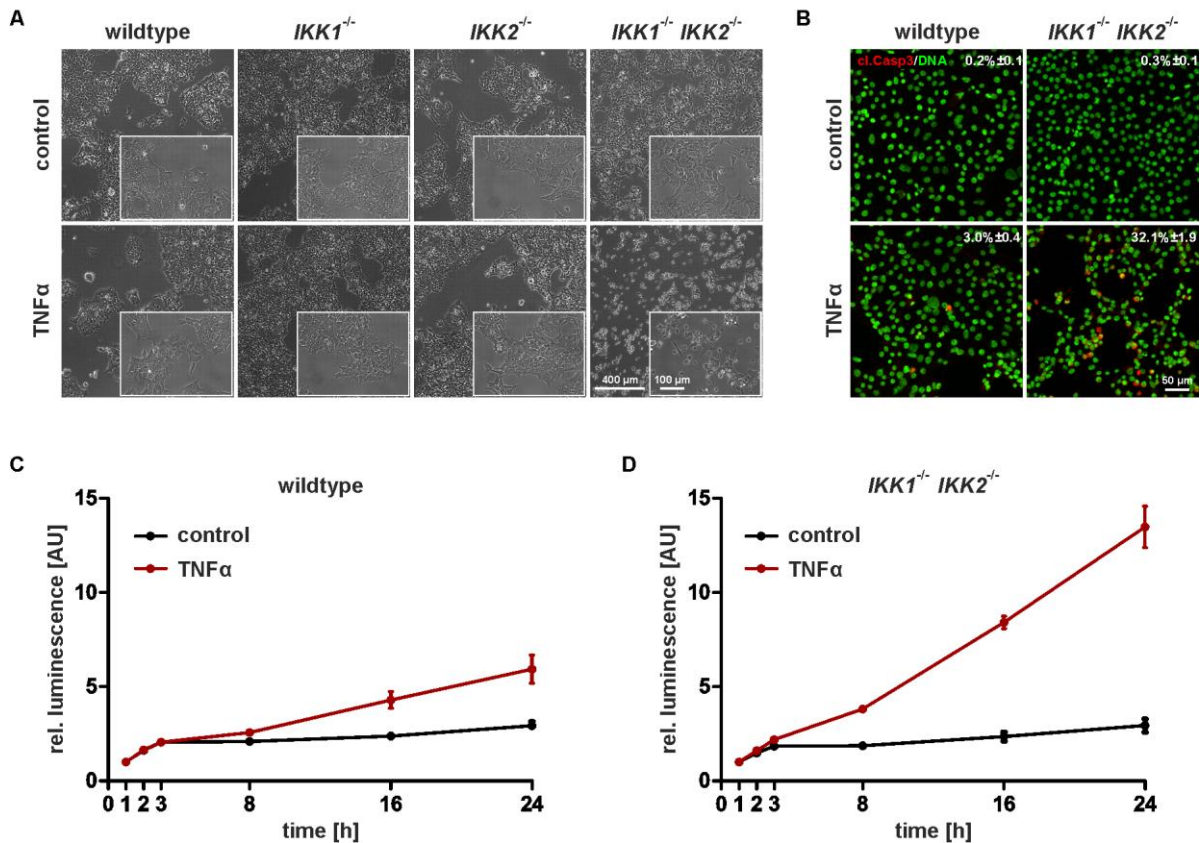
166 **Figure 3. IKK1/2-deficiency results in profound TNFα-induced cell death. (A)** Vastly

167 increased cell death in IKK1/2-double deficient cells upon 24 h exposure to TNFα (20 ng/mL).

168 **(B)** Immunocytochemical stainings of wildtype and IKK1/2$^{-/-}$ cells revealed a huge increase in

169 caspase-3-positive cells in the double knockout after 24 h of TNFα stimulation (20 ng/mL)

170 (n=3; for each genotype and condition more than 2500 cells were analyzed). **(C,D)** RealTime

171 Glo Annexin V apoptosis assay of wildtype (C) and IKK1/2-deficient cells (D). Compared to

172 wildtype cells, a strong increase in apoptotic cells was observed.

173

174   In the presence of Nescrostatin-1s (Nec-1s), a potent inhibitor of RIPK1, cell death was

175   markedly reduced in IKK1/2-deficient cells (Fig. 4A). Stainings against activated caspase-3

176   revealed 12.8% caspase-3-positive cells (Fig. 4B), a strong reduction when compared to the

177   32.8% positive cells, which were stimulated only with TNFα (Fig. 3B). Application of

178   Necrosulfonamide, an inhibitor of MLKL resulted only in slightly reduced amounts of dead

179   cells, when stimulated with TNFα (Fig. 4A, bottom panel). After 24 h, 26.7% of the double-

180   deficient cells were positive for the cleaved caspase-3 (Fig. 4B). However, using the Annexin

181   V-based apoptosis assay, cell death was reduced to similar extents with both inhibitors used

182   (Fig. 4C, D). No protective effects of Nec-1s or Necrosulfonamide were observed on wildtype

183   cells (Fig. 4A, B; Fig. 3B).

Figure 4
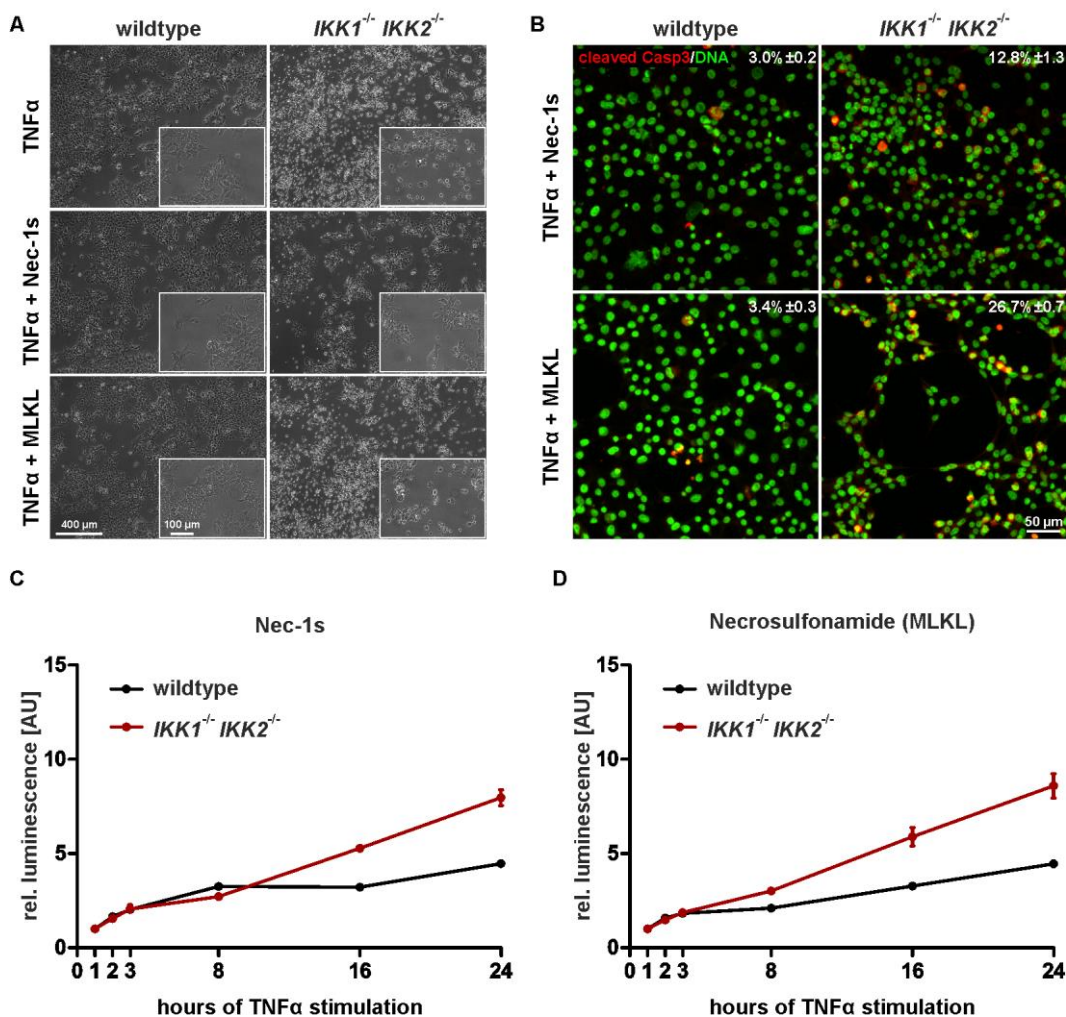
184

185 **Figure 4. TNFα-induced cell death is mediated via RIPK1. (A)** Stimulation of IKK1/2-deficient

186 cells with 20 ng/mL TNFα and the RIPK1 inhibitor Nec-1s (10 μM; middle panel) or the

187 inhibitor of the MLKL necroptosis complex necrosulfonamide (1 μM; bottom panel) resulted

188 in a profound protection from TNFα-induced cell death for Nec1s and a small for

189 necrosulfonamide. **(B)** Upon TNFα treatment immunocytochemistry revealed 12.8% caspase-

190 3-positive cells in the presence of Nec-1s and 26.7% in the presence of necrosulfonamide

191 (n=3; for each genotype and condition more than 2500 cells were analyzed). (C,D) RealTime

192 Glo Annexin V apoptosis assay of TNFα-stimulated wildtype and IKK1/2-deficient cells in the

193 presence of Nec-1s (C) or the MLKL inhibitor Necrosulfonamide (D).

194

195 **TNFα does not induce programmed cell death upon RelA deficiency**

196 Since cells deficient for either IKK1 or IKK2 also showed strongly impaired NF-κB activation,

197 we speculated an NF-κB-independent mechanism might lead the cell death observed. To

198 further analyze this, we generated cells deficient for the NF-κB-subunit RelA (p65) (Fig. 5).

199 Using the same approach, we generated a genomic deletion spanning the intron-exon

200 boundary of exon 2 (Fig. 5A), which is present in all transcript variants listed at ENSEMBL.org.

201 We validated the designed deletion using genomic PCR and qPCR (Fig. 5B, C) and lack of p65

202 protein by immunocytochemistry (Fig. 5D). Analysis of NF-κB activation in these cells was

203 assessed by qPCR of the NF-κB target genes IκBα and A20 showing reduced expression in the

204 RelA$^{-/-}$ cells after stimulation with TNFα compared to wildtype cells (Fig. 5E). This impairment

205 was validated by usage of an NF-κB-driven luciferase reporter demonstrating reduced

206 activation of NF-κB in the knockout cells (Fig. 5F).

207

Figure 5

A

B

C

D

E

F

208
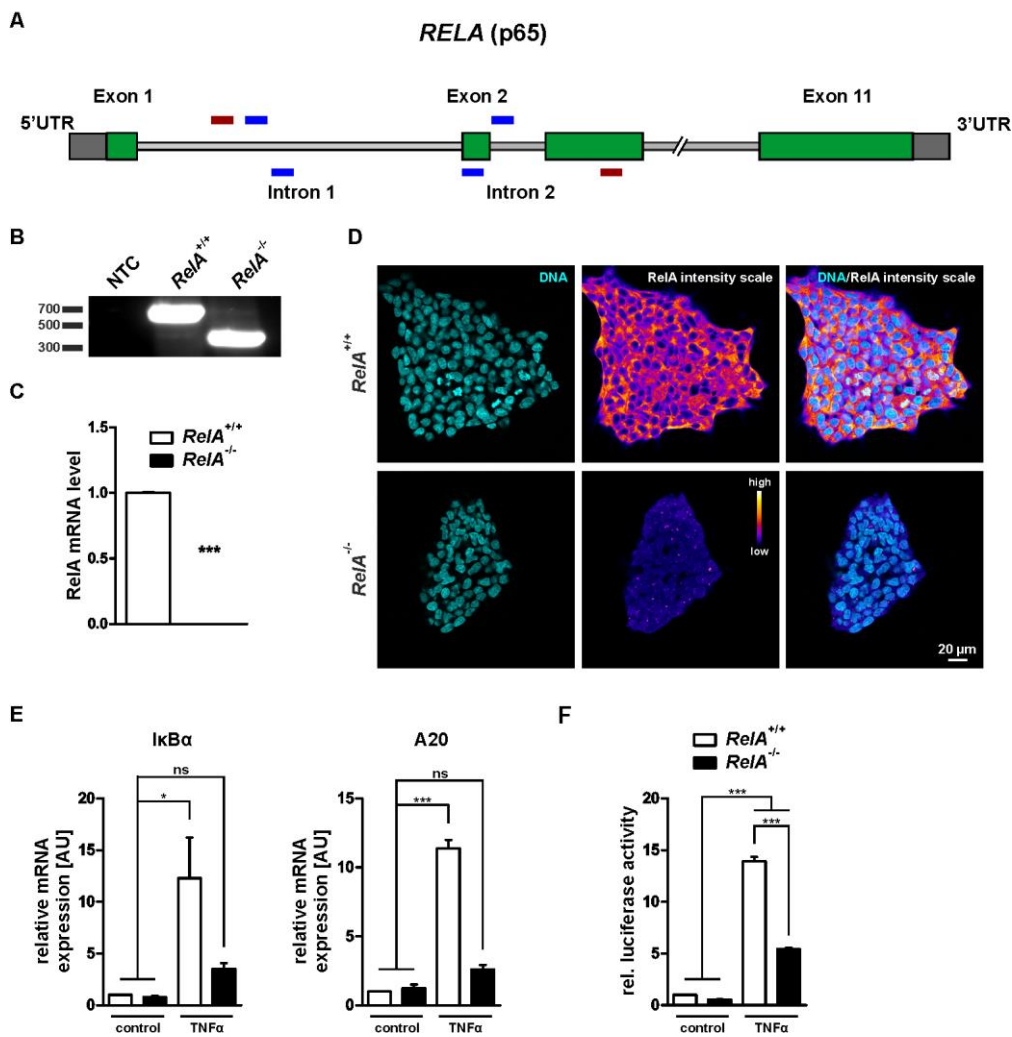
Figure 5. Generation of *RELA*-deficient cells. (A) Target design for the CRISPR/Cas9-mediated knockout of *RELA*. Depicted in blue are the sgRNAs and depicted in red are the flanking primers used for genomic PCR. **(B)** Genomic PCR of clonally grown cells revealed genomic deletion within the *RELA* gene. **(C)** qPCR analysis using a primer set, where one primer is designed within the deletion showed a highly significant downregulation of RelA mRNA (t-test, two-tailed, n=3). **(D)** Immunocytochemical stainings depicted almost complete loss of RelA protein in RelA-deficient cells. **(E)** Expression of the NF-κB target genes IκBα and A20 is markedly reduced in RelA$^{-/-}$ cells after 6 h of TNFα stimulation (10 ng/mL) compared to wildtype cells (One-way ANOVA, Bonferroni post-test, n=3). **(F)** An NF-κB driven luciferase

218 reporter assay revealed a significantly reduced NF-κB activation after 24 h TNFα stimulation

219 in RelA-deficient cells (One-way ANOVA, Bonferroni post-test, n=3).

220

221 Upon long-term exposure to TNFα we detected no increased amount of dead RelA-deficient

222 cells compared to wildtype cells (Fig. 6A). In an immunocytochemical analysis, the amount of

223 cells positive for the activated form of caspase-3 only very mildly increased (Fig. 6B), being

224 even below the values for TNFα-stimulated wildtype cells (Fig. 3B). Signals for Annexin V

225 were hardly elevated in the GloMax Annexin V Apoptosis Assay in RelA$^{-/-}$ cells within 24 h of

226 TNFα treatment (Fig. 6C).

Figure 6
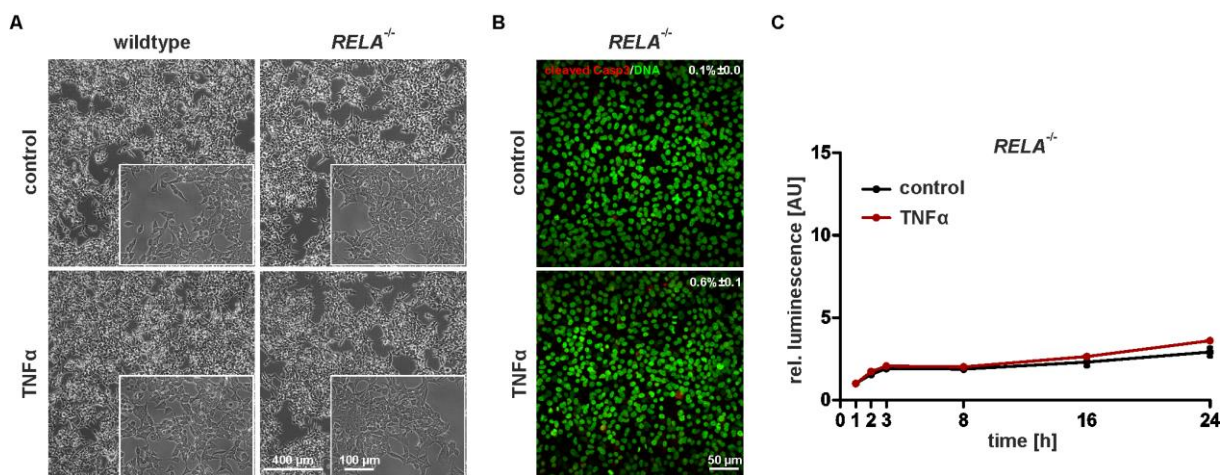
227

228 **Figure 6. No increase in TNFα-induced cell death upon RelA deficiency. (A)** After 24 h of

229 TNFα stimulation (20 ng/mL) no differences in the amount of dead cells between RelA-

230 deficient and wildtype cells was observable. **(B)** Immunocytochemistry revealed only a small

231 increase in Caspase-3-positive cells after TNFα treatment (n=3; for each condition more than

232 5000 cells were analyzed). **(C)** RealTime Glo Annexin V apoptosis assay of TNFα-treated RelA$^-$

233 $^/-$ cells showed no difference in the amount of apoptotic cells compared to untreated cells.

234

Discussion

235

236 In the present study, we successfully generated genomic knockouts for IKK1, IKK2, IKK1/2

237 and RelA in HEK293 cells to initially analyze the role of IKK1 and IKK2 in the context of TNF-

238 induced cell death. HEK293 cells are a broadly used cellular model for TNF-signaling (18).

239 Upon stimulation with TNFα, a vast increase in cell death was observed only in cells deficient

240 for both IKK1 and IKK2. We further partially rescued cell death in these cells using the RIPK1-

241 specific inhibitor Necrostatin-1s indicating RIPK1 activity to be the predominant cause of the

242 cell death observed.

243 Activation of the death receptor TNFR1 does not necessarily lead to death but often results

244 in cell survival or even increased proliferation (36, 37). Downstream of TNFR1 two major

245 pathways – an NF-κB – dependent and an –independent one – have been described to

246 regulate and control cell death (38). The first one is well characterized and demonstrates the

247 activation of NF-κB by TNF-signaling resulting in the expression of anti-apoptotic NF-κB

248 target genes such as cIAP-1, cIAP-2 or c-FLIP (13, 14, 17). In contrast, signaling via TNFR1

249 independently of NF-κB activation is far less well understood and just gained attention in the

250 last years (38, 39). In the present study, we carefully investigated NF-κB activation in

251 response to TNFα in all genotypes we created. While differences between the different

252 knockouts were observable, all cells showed significantly reduced activation when compared

253 to wildtype cells. In contrast, experiments conducted in Ikk1-deficient mice showed no major

254 impairments in canonical NF-κB signaling, although strong developmental aberrations and

255 death shortly after birth were observable (40). Consequently, IKK2 is concluded to be the

256 catalytic subunit needed for canonical NF-kB signaling by directly phosphorylating IκBα.

257 However, in IKK1-deficient cells we observed severely affected NF-κB activation after TNFα

258 stimulation. In fact, most experiments demonstrated impairments within the same range as

259 in IKK2-deficient cells indicating that IKK2 cannot compensate loss of IKK1 in the cells we

260 used. Interestingly, although activation of NF-κB via TNF is associated with cell growth,

261 especially in the context of tumor formation and progression, we detected no signs of

262 reduced proliferation in any of the genotypes created (data not shown). Recently, we

263 generated HeLa cells deficient for the NF-κB subunit c-Rel, which showed a significantly

264 lowered proliferation rate (41). However, although NF-κB activation was significantly

265 impaired in these cells, no increase in cell death was observed after treatment with TNFα

266 already suggesting the presence of an NF-κB-independent mechanism to prevent from TNF-

267 induced cell death in human cells. In 2015, Dondelinger and colleagues described a novel

268 function of both Ikk1 and Ikk2 in mice by demonstrating RIPK1 to be a bona fide target of the

269 Ikk complex (42). By directly phosphorylating RIPK1, Ikk1/2 inactivate RIPK1 and prevent

270 from TNF-induced cell death independently of NF-κB. In this NF-κB independent pathway,

271 RIPK1 will be required to recruit FADD into the so-called complex IIb resulting in apoptosis.

272 Upon caspase-8 inhibition RIPK1 can also be incorporated into the necrosome, which will

273 lead to the activation of RIPK3 and its substrate MLKL leading to necroptotic cell death (20).

274 Interestingly, deficiency of either Ikk1 or Ikk2 was not sufficient to induce cell death upon

275 TNFα. However, in fibroblasts derived from Ikk1/2-double deficient mice, cell death was

276 vastly increased when cells were exposed to TNFα (42). Extending these findings, we

277 observed no strong increase in cell death when either, IKK1 or IKK2 was genetically depleted.

278 Only in cells deficient for both, IKK1 and IKK2, significant increase in cell death was

279 detectable. We hypothesized that cell death predominantly occurred in an NF-κB –

280 independent way mediated via RIPK1. Confirming this, application of the RIPK1-specific

281 inhibitor Nec-1s partially rescued from TNF-induced cell death in the IKK1/2-double deficient

282 cells. Dondelinger and colleagues – as it is done in most studies dealing with the causes of

283   cell death induced by TNFα – applied mouse models to gain their findings. However,

284   differences between humans and mice have been reported in the past in terms of TNF and

285   NF-κB signaling. Mice deficient for either, RelA, Ikk2 or NEMO were reported to die during

286   embryonic development, in each case due to TNF-induced death of hepatocytes resulting in

287   liver degeneration (24-26, 43). In 2013, Panicke and co-workers described a frameshift

288   mutation in the human *IKBKB* gene to be the cause of severe combined immunodeficiency

289   (28). Patients carrying this loss-of-function mutation did not show any signs of liver

290   degeneration indicating potential differences in TNF signaling between humans and mice.

291   This elucidates the necessity to analyze TNF-mediated cell death in human cells, especially

292   when considering that TNF signaling is closely connected to human diseases, in particular

293   with cancer. Several reports describe TNF being involved in all parts of carcinogenesis,

294   namely transformation of healthy cells, survival, proliferation, invasion, angiogenesis and

295   metastasis of tumor cells (reviewed in (29)). In a broad range of tumorigenic tissues or tumor

296   cells, TNF expression is strongly increased (44, 45). Consequently, many types of tumor cells

297   are particularly resistant to TNF-induced cell death (29). A better understanding of the

298   mechanisms, on how tumor cells evade death therefore is a promising approach to increase

299   the anti-cancer value of TNF. Supporting our findings of NF-κB-independent cell death in

300   human cells, Legarda-Addison and co-workers demonstrated in Jurkat cells increased

301   sensitivity to TNF-induced cell death upon NEMO deficiency, which was independent of NF-

302   κB (46). As was observed from Dondelinger, NEMO deficiency in mice also sensitized cells

303   regarding TNF-induced cell death, in a similar manner as Ikk1/2 combined (42).

304   In summary, our findings demonstrate that in human cells IKK1 and IKK2 have an NF-κB –

305   independent function in preventing from TNF-induced cell death. Targeting – genetically or

306   pharmacologically – both catalytic IKKs therefore appears to be a promising approach in

307   cancer therapy, especially for tumor cells resistant to TNF-induced cell death.

Materials and methods

Statistical analysis

All statistical tests were performed using GraphPad Prism 5 (GraphPad Software, La Jolla, USA). Data is presented as the mean of at least three independent experiments ± SEM if not stated otherwise. The statistical test used is mentioned in the respective figure legend. ns, not significant, *p<0.05, **p<0.01, ***p<0.001.

Target design and cloning

Single guide RNAs (sgRNAs) were designed using the online prediction tool from the University of Heidelberg (47). Nicking pairs were chosen as described by Ran and colleagues (34). For efficient gene knockout we designed two nicking pairs creating a deletion spanning an intron-exon border within the respective gene. sgRNAs for IKK1 and IKK2 knockout were cloned into pSpCas9n(BB)-2A-Puro (PX462) V2.0 (Addgene plasmid #62987) essentially as described (48), while sgRNAs for knockout of RELA were cloned into pX335_G2P (modified Addgene plasmid #42335, kindly provided by Boris Greber)

Cell culture and transfection

HEK293 cells were cultivated in Dulbecco's Modified Eagle's Medium (DMEM) (Sigma Aldrich, Taufkirchen, Germany) containing 10% (v/v) heat-inactivated fetal calf serum (FCS) (VWR, Darmstadt, Germany), 2 mM L-glutamine (Sigma Aldrich) and 100 U/ml Penicillin/Streptomycin (P/S) (Sigma Aldrich) at 37°C and 5% CO_2 at saturated humidity. Transfection was performed either using standard calcium-phosphate precipitation or TurboFect transfection reagent (Thermo Fisher Scientific) according to manufacturer's guidelines.

332

Genomic PCR

334 Cells were harvested at 300 g for 5 min and resuspended in cell lysis buffer (0.1 µg/mL

335 Gelatine, 50 mM KCl, 1.5 mM MgCl2, 0.45% NP40, 10 mM TRIS pH 8.3, 0.45 % TWEEN 20,

336 200 µg/mL Protein kinase K). Lysate was incubated for 1 h at 55°C and 5 min at 95°C before

337 being used as template for genomic PCR. The following primers were used: *IKBKA*-fwd 5'-

338 GCCTTGGAACAACTGTGGAAC-3', *IKBKA*-rev 5'-GGACGCACACATTCCCAAAG-3', *IKBKB*-fwd 5'-

339 CCACCTTGTTTGCCTGCTTG-3', *IKBKB*-rev 5'-GTCTCCCCATCCCTCTTCCT-3', *RELA*-fwd 5'-

340 GGAGCAGAGGGAACCTTGAC-3', *RELA*-rev 5'-GTATCTGTGCTCCTCTCGCC-3'.

341

RT-PCR and quantitative real-time PCR

343 Total RNA was isolated using TRI Reagent (Sigmal-Aldrich) according to the manufacturer's

344 protocol. 1 µg of RNA was used for cDNA synthesis. For RT-PCR, 1 µL cDNA was used as

345 template and for quantitative real-time PCR (qPCR), cDNA was diluted 1:100 and 2

346 µL/reaction were used. qPCR was carried out with SYBR Green Master Mix (Thermo Fisher

347 Scientific). The following primers were used: IKK1-fwd 5'-CTTCGGGAACGTCTGTCTGTA-3',

348 IKK1-rev 5'-TTGGCATGGTTCAACTTCTTCAT-3', IKK2-fwd 5'-GCTGACCCACCCCAATGTG-3',

349 IKK2-rev 5'-TAAGCGCAGAGGCAATGTCA-3', RelA-fwd 5'-CTGTTCCCCCTCATCTTCCC-3',

350 RelA-rev 5'- GCCATTGATCTTGATGGTGGG-3', IκBα-fwd 5'-CCCTACACCTTGCCTGTGAG-3',

351 IκBα-rev 5'-TAGACACGTGTGGCCATTGT-3', A20-fwd 5'-CTGAAAACGAACGGTGACGG-3',

352 A20-rev 5'-TCCAGTTGCCAGCGGAATTT-3', IL8-fwd 5'-TCTGTGTGAAGGTGCAGTTTTG-3',

353 IL8-rev 5'-TTTCTGTGTTGGCGCAGTGT-3'. Ct values obtained in qPCR were normalized to the

354 reference genes GAPDH (fwd 5'-CATGAGAAGTATGACAACAGCCT-3'; rev

355 5'-AGTCCTTCCACGATACCAAAGT-3'), eEF2 (fwd 5'-AGGTCGGTTCTACGCCTTTG-3'; rev

356 5'-TTCCCACAAGGCACATCCTC-3') and RPLP0 (fwd 5'-TGGGCAAGAACACCATGATG-3'; rev

357 5'-AGTTTCTCCAGAGCTGGGTTGT-3').

358

359 **Western blotting**

360 Protein extracts were made using RIPA buffer (1 mM EGTA, 150 mM NaCl, 1 mM Na_2EDTA, 1

361 mM Na_3VO_4, 1% (w/v) NP-40, 1 µg/mL leupeptin, 1 % (w/v) sodium deoxycholate, 2.5 mM

362 sodium pyrophosphate, 20 mM Tris-HCl (pH 7,5), 1 mM β-glycerophosphate) and equal

363 amounts of protein were separated by SDS-PAGE and transferred to a PVDF membrane.

364 Membranes were blocked using PBS containing 0.05% Tween 20 and 5% milk powder,

365 followed by probing with primary antibodies (rabbit anti-IKK1 (#7182; Santa-Cruz

366 Biotechnology, Dallas, USA), rabbit anti-IKK2 (#2370; Cell Signaling, Danvers, USA), rabbit

367 anti-p65 (#8242; Cell Signaling), mouse anti-IκBα (#4814; Cell Signaling) overnight at 4°C.

368 Horseradish peroxidase-conjugated secondary antibodies were applied for 1h at room

369 temperature. Blots were developed using enhanced chemiluminescence. GAPDH (#32233;

370 Santa-Cruz Biotechnology) served as loading control.

371

372 **Immunocytochemistry**

373 For immunocytochemical stainings cells were cultivated on coverslips. Fixation was done

374 with 4% paraformaldehyde (PFA) for 10 min at RT. Prior to application of the primary

375 antibodies (rabbit anti-p65 (#8242; Cell Signaling), rabbit anti-cleaved caspase-3 (#9661; Cell

376 Signaling)) cells were permeabilized and blocked using PBS containing 0.02 % Triton X-100

377 and 5 % goat serum. After repetitive washing, secondary fluorochrome-conjugated

378 antibodies (goat anti-rabbit/mouse Alexa Fluor 555, Thermo Fisher Scientific) were applied,

379 followed by nuclear counterstaining with DAPI (1µg/mL) and finally mounting using

380   Mowiol/DABCO. Imaging was done by confocal laser scanning microscopy (LSM 780, Carl

381   Zeiss, Oberkochen, Germany) and image processing was performed using Fiji (49) and Corel

382   Draw (Corel Corporation, Ottawa, Canada).

383

384   **Dual luciferase reporter assay**

385   Cells were transiently transfected with TK (NF-κB)6 LUC vector (50) and pRL-CMV (Promega

386   Cooperation) using TurboFect Transfection Reagent (Thermo Fisher Scientific) according to

387   manufacturer's guidelines. 24h after transfection, cells were stimulated with TNFα or left

388   untreated. The next day, cells were lysed in 1 × Passive Lysis buffer (Promega Corporation)

389   and Luciferase activity was measured using the Dual-Luciferase® Reporter Assay System

390   (Promega Corporation). Signals were normalized as a ratio of Firefly luciferase activity to

391   Renilla luciferase activity.

392

393   **RealTime Glo Annexin V Apoptosis Assay**

394   Apoptosis was analyzed using the RealTime-Glo™ Annexin V Apoptosis Assay (Promega

395   Corporation) according to manufacturer's guidelines. One day prior to stimulation, 10.000

396   cells were seeded in white, tissue culture-treated 96-well multiwell plates (BRAND,

397   Wertheim, Germany). Cells were stimulated as indicated and simultaneously detection

398   reagent – prepared according to the manufacturer's protocol – was added. Annexin V-based

399   luminescence was measured at the times indicated using a GloMax®-Multi Plus Detection

400   System (Promega Corporation). No-cell controls were used for background subtraction.

401

402   **Flow cytometric analysis**

403   DNA content was measured essentially as described (51). Briefly, 1 x 10^6 cells – treated as

404   indicated – were harvested and fixed for 5 min using 70 % (v/v) ethanol. After centrifugation

405   at 300 g cells were stained with staining solution (PBS containing 1 mg/ml glucose (Roth), 50

406   mg/ml propidium iodide (Partec, Sysmex Deutschland GmbH, Bornbarch, Germany) and 100

407   Kunitz units RNaseA (Thermo Fisher Scientific) for 60 min under exclusion of light. PI-staining

408   was analyzed using a Gallios™ 10/3 flow cytometer (Beckman Coulter, Brea, CA, USA). Data

409   analysis was done using FlowJo Software (TreeStar, Olten, Switzerland), doublet

410   discrimination was assured by gating FL3-A- versus FL3-W signals.

411

Acknowledgements

416

Author contributions

418   Conceptualization, C.S., B.K. & C.K.

419   Methodology, C.S., J.S. & L.R.P.

420   Validation, C.S., J.G., B.K. & C.K.

421   Formal analysis, C.S., N.P. & J.G.

422   Investigation, C.S., J.S., N.P., S.K, M.P., E.H. & J.G.

423   Data curation, B.K. & C.K.

424   Writing – Original Draft, C.S.

425   Writing – Review & Editing, C.S., J.S., N.P., S.K., M.P., L.R.P., E.H., J.G., B.K. & C.K.

426   Visualization, C.S.

427   Supervision, B.K. & C.K.

428   Project Administration, B.K. & C.K.

429   Funding Acquisition, C.K.

430

431   **Conflict of interest**

432   The authors declare no conflict of interest.

433

434   **References**

435   1.   **Perkins ND.** 2007. Integrating cell-signalling pathways with NF-kappaB and IKK

436   function. Nat Rev Mol Cell Biol **8:**49-62.

437   2.   **Xia Y, Shen S, Verma IM.** 2014. NF-kappaB, an active player in human cancers.

438   Cancer Immunol Res **2:**823-830.

439   3.   **Ben-Neriah Y, Karin M.** 2011. Inflammation meets cancer, with NF-kappaB as the

440   matchmaker. Nat Immunol **12:**715-723.

441   4.   **Walczak H.** 2011. TNF and ubiquitin at the crossroads of gene activation, cell death,

442   inflammation, and cancer. Immunol Rev **244:**9-28.

443   5.   **Varfolomeev E, Vucic D.** 2016. Intracellular regulation of TNF activity in health and

444   disease. Cytokine doi:10.1016/j.cyto.2016.08.035.

445   6.   **Peltzer N, Darding M, Walczak H.** 2016. Holding RIPK1 on the Ubiquitin Leash in

446   TNFR1 Signaling. Trends Cell Biol **26:**445-461.

447   7.   **Ben-Neriah Y.** 2002. Regulatory functions of ubiquitination in the immune system.

448   Nat Immunol **3:**20-26.

449   8.   **Schmitz ML, Baeuerle PA.** 1991. The p65 subunit is responsible for the strong

450   transcription activating potential of NF-kappa B. EMBO J **10:**3805-3817.

451 9.   **Hayden MS, Ghosh S.** 2008. Shared principles in NF-kappaB signaling. Cell **132:**344-

452   362.

453 10.   **Smale ST.** 2012. Dimer-specific regulatory mechanisms within the NF-kappaB family

454   of transcription factors. Immunol Rev **246:**193-204.

455 11.   **Milanovic M, Kracht M, Schmitz ML.** 2014. The cytokine-induced conformational

456   switch of nuclear factor kappaB p65 is mediated by p65 phosphorylation. Biochem J

457   **457:**401-413.

458 12.   **Schulze-Osthoff K, Ferrari D, Los M, Wesselborg S, Peter ME.** 1998. Apoptosis

459   signaling by death receptors. Eur J Biochem **254:**439-459.

460 13.   **Micheau O, Lens S, Gaide O, Alevizopoulos K, Tschopp J.** 2001. NF-kappaB signals

461   induce the expression of c-FLIP. Mol Cell Biol **21:**5299-5305.

462 14.   **Wang CY, Mayo MW, Korneluk RG, Goeddel DV, Baldwin AS, Jr.** 1998. NF-kappaB

463   antiapoptosis: induction of TRAF1 and TRAF2 and c-IAP1 and c-IAP2 to suppress

464   caspase-8 activation. Science **281:**1680-1683.

465 15.   **Catz SD, Johnson JL.** 2001. Transcriptional regulation of bcl-2 by nuclear factor kappa

466   B and its significance in prostate cancer. Oncogene **20:**7342-7351.

467 16.   **Daniel PT, Schulze-Osthoff K, Belka C, Guner D.** 2003. Guardians of cell death: the

468   Bcl-2 family proteins. Essays Biochem **39:**73-88.

469 17.   **Van Antwerp DJ, Martin SJ, Kafri T, Green DR, Verma IM.** 1996. Suppression of TNF-

470   alpha-induced apoptosis by NF-kappaB. Science **274:**787-789.

471 18.   **Micheau O, Tschopp J.** 2003. Induction of TNF receptor I-mediated apoptosis via two

472   sequential signaling complexes. Cell **114:**181-190.

473 19.   **Ting AT, Bertrand MJ.** 2016. More to Life than NF-kappaB in TNFR1 Signaling. Trends

474   Immunol **37:**535-545.

475   20.   **Kondylis V, Kumari S, Vlantis K, Pasparakis M.** 2017. The interplay of IKK, NF-kappaB

476   and RIPK1 signaling in the regulation of cell death, tissue homeostasis and

477   inflammation. Immunol Rev **277:**113-127.

478   21.   **Cho YS, Challa S, Moquin D, Genga R, Ray TD, Guildford M, Chan FK.** 2009.

479   Phosphorylation-driven assembly of the RIP1-RIP3 complex regulates programmed

480   necrosis and virus-induced inflammation. Cell **137:**1112-1123.

481   22.   **He S, Wang L, Miao L, Wang T, Du F, Zhao L, Wang X.** 2009. Receptor interacting

482   protein kinase-3 determines cellular necrotic response to TNF-alpha. Cell **137:**1100-

483   1111.

484   23.   **Sun L, Wang H, Wang Z, He S, Chen S, Liao D, Wang L, Yan J, Liu W, Lei X, Wang X.**

485   2012. Mixed lineage kinase domain-like protein mediates necrosis signaling

486   downstream of RIP3 kinase. Cell **148:**213-227.

487   24.   **Beg AA, Sha WC, Bronson RT, Ghosh S, Baltimore D.** 1995. Embryonic lethality and

488   liver degeneration in mice lacking the RelA component of NF-kappa B. Nature

489   **376:**167-170.

490   25.   **Li Q, Van Antwerp D, Mercurio F, Lee KF, Verma IM.** 1999. Severe liver degeneration

491   in mice lacking the IkappaB kinase 2 gene. Science **284:**321-325.

492   26.   **Tanaka M, Fuentes ME, Yamaguchi K, Durnin MH, Dalrymple SA, Hardy KL, Goeddel**

493   **DV.** 1999. Embryonic lethality, liver degeneration, and impaired NF-kappa B

494   activation in IKK-beta-deficient mice. Immunity **10:**421-429.

495   27.   **Alcamo E, Mizgerd JP, Horwitz BH, Bronson R, Beg AA, Scott M, Doerschuk CM,**

496   **Hynes RO, Baltimore D.** 2001. Targeted mutation of TNF receptor I rescues the RelA-

497   deficient mouse and reveals a critical role for NF-kappa B in leukocyte recruitment. J

498   Immunol **167:**1592-1600.

499   28.   **Pannicke U, Baumann B, Fuchs S, Henneke P, Rensing-Ehl A, Rizzi M, Janda A, Hese**

500   **K, Schlesier M, Holzmann K, Borte S, Laux C, Rump EM, Rosenberg A, Zelinski T,**

501   **Schrezenmeier H, Wirth T, Ehl S, Schroeder ML, Schwarz K.** 2013. Deficiency of

502   innate and acquired immunity caused by an IKBKB mutation. N Engl J Med **369:**2504-

503   2514.

504   29.   **Wang X, Lin Y.** 2008. Tumor necrosis factor and cancer, buddies or foes? Acta

505   Pharmacol Sin **29:**1275-1288.

506   30.   **Horvath P, Barrangou R.** 2010. CRISPR/Cas, the immune system of bacteria and

507   archaea. Science **327:**167-170.

508   31.   **Makarova KS, Haft DH, Barrangou R, Brouns SJ, Charpentier E, Horvath P, Moineau**

509   **S, Mojica FJ, Wolf YI, Yakunin AF, van der Oost J, Koonin EV.** 2011. Evolution and

510   classification of the CRISPR-Cas systems. Nat Rev Microbiol **9:**467-477.

511   32.   **Cong L, Ran FA, Cox D, Lin S, Barretto R, Habib N, Hsu PD, Wu X, Jiang W, Marraffini**

512   **LA, Zhang F.** 2013. Multiplex genome engineering using CRISPR/Cas systems. Science

513   **339:**819-823.

514   33.   **Mali P, Yang L, Esvelt KM, Aach J, Guell M, DiCarlo JE, Norville JE, Church GM.** 2013.

515   RNA-guided human genome engineering via Cas9. Science **339:**823-826.

516   34.   **Ran FA, Hsu PD, Lin CY, Gootenberg JS, Konermann S, Trevino AE, Scott DA, Inoue A,**

517   **Matoba S, Zhang Y, Zhang F.** 2013. Double nicking by RNA-guided CRISPR Cas9 for

518   enhanced genome editing specificity. Cell **154:**1380-1389.

519   35.   **Forbes SA, Beare D, Gunasekaran P, Leung K, Bindal N, Boutselakis H, Ding M,**

520   **Bamford S, Cole C, Ward S, Kok CY, Jia M, De T, Teague JW, Stratton MR,**

521   **McDermott U, Campbell PJ.** 2015. COSMIC: exploring the world's knowledge of

522   somatic mutations in human cancer. Nucleic Acids Res **43:**D805-811.

523   36.   **Palombella VJ, Vilcek J.** 1989. Mitogenic and cytotoxic actions of tumor necrosis

524   factor in BALB/c 3T3 cells. Role of phospholipase activation. J Biol Chem **264:**18128-

525   18136.

526   37.   **Aggarwal BB.** 2003. Signalling pathways of the TNF superfamily: a double-edged

527   sword. Nat Rev Immunol **3:**745-756.

528   38.   **O'Donnell MA, Ting AT.** 2011. RIP1 comes back to life as a cell death regulator in

529   TNFR1 signaling. FEBS J **278:**877-887.

530   39.   **Wang L, Du F, Wang X.** 2008. TNF-alpha induces two distinct caspase-8 activation

531   pathways. Cell **133:**693-703.

532   40.   **Hu Y, Baud V, Delhase M, Zhang P, Deerinck T, Ellisman M, Johnson R, Karin M.**

533   1999. Abnormal morphogenesis but intact IKK activation in mice lacking the IKKalpha

534   subunit of IkappaB kinase. Science **284:**316-320.

535   41.   **Slotta C, Schluter T, Ruiz-Perera LM, Kadhim HM, Tertel T, Henkel E, Hubner W,**

536   **Greiner JFW, Huser T, Kaltschmidt B, Kaltschmidt C.** 2017. CRISPR/Cas9-mediated

537   knockout of c-REL in HeLa cells results in profound defects of the cell cycle. PLoS One

538   **12:**e0182373.

539   42.   **Dondelinger Y, Jouan-Lanhouet S, Divert T, Theatre E, Bertin J, Gough PJ, Giansanti**

540   **P, Heck AJ, Dejardin E, Vandenabeele P, Bertrand MJ.** 2015. NF-kappaB-Independent

541   Role of IKKalpha/IKKbeta in Preventing RIPK1 Kinase-Dependent Apoptotic and

542   Necroptotic Cell Death during TNF Signaling. Mol Cell **60:**63-76.

543   43.   **Rudolph D, Yeh WC, Wakeham A, Rudolph B, Nallainathan D, Potter J, Elia AJ, Mak**

544   **TW.** 2000. Severe liver degeneration and lack of NF-kappaB activation in

545   NEMO/IKKgamma-deficient mice. Genes Dev **14:**854-862.

546   44.   **Ferrajoli A, Keating MJ, Manshouri T, Giles FJ, Dey A, Estrov Z, Koller CA, Kurzrock R,**

547   **Thomas DA, Faderl S, Lerner S, O'Brien S, Albitar M.** 2002. The clinical significance of

548   tumor necrosis factor-alpha plasma level in patients having chronic lymphocytic

549   leukemia. Blood **100:**1215-1219.

550   45.   **Szlosarek PW, Grimshaw MJ, Kulbe H, Wilson JL, Wilbanks GD, Burke F, Balkwill FR.**

551   2006. Expression and regulation of tumor necrosis factor alpha in normal and

552   malignant ovarian epithelium. Mol Cancer Ther **5:**382-390.

553   46.   **Legarda-Addison D, Hase H, O'Donnell MA, Ting AT.** 2009. NEMO/IKKgamma

554   regulates an early NF-kappaB-independent cell-death checkpoint during TNF

555   signaling. Cell Death Differ **16:**1279-1288.

556   47.   **Stemmer M, Thumberger T, Del Sol Keyer M, Wittbrodt J, Mateo JL.** 2015. CCTop:

557   An Intuitive, Flexible and Reliable CRISPR/Cas9 Target Prediction Tool. PLoS One

558   **10:**e0124633.

559   48.   **Ran FA, Hsu PD, Wright J, Agarwala V, Scott DA, Zhang F.** 2013. Genome engineering

560   using the CRISPR-Cas9 system. Nat Protoc **8:**2281-2308.

561   49.   **Schindelin J, Arganda-Carreras I, Frise E, Kaynig V, Longair M, Pietzsch T, Preibisch S,**

562   **Rueden C, Saalfeld S, Schmid B, Tinevez JY, White DJ, Hartenstein V, Eliceiri K,**

563   **Tomancak P, Cardona A.** 2012. Fiji: an open-source platform for biological-image

564   analysis. Nat Methods **9:**676-682.

565   50.   **Bachelerie F, Alcami J, Arenzana-Seisdedos F, Virelizier JL.** 1991. HIV enhancer

566   activity perpetuated by NF-kappa B induction on infection of monocytes. Nature

567   **350:**709-712.

568   51.   **Kaltschmidt B, Kaltschmidt C, Hehner SP, Droge W, Schmitz ML.** 1999. Repression of

569   NF-kappaB impairs HeLa cell proliferation by functional interference with cell cycle

570   checkpoint regulators. Oncogene **18:**3213-3225.
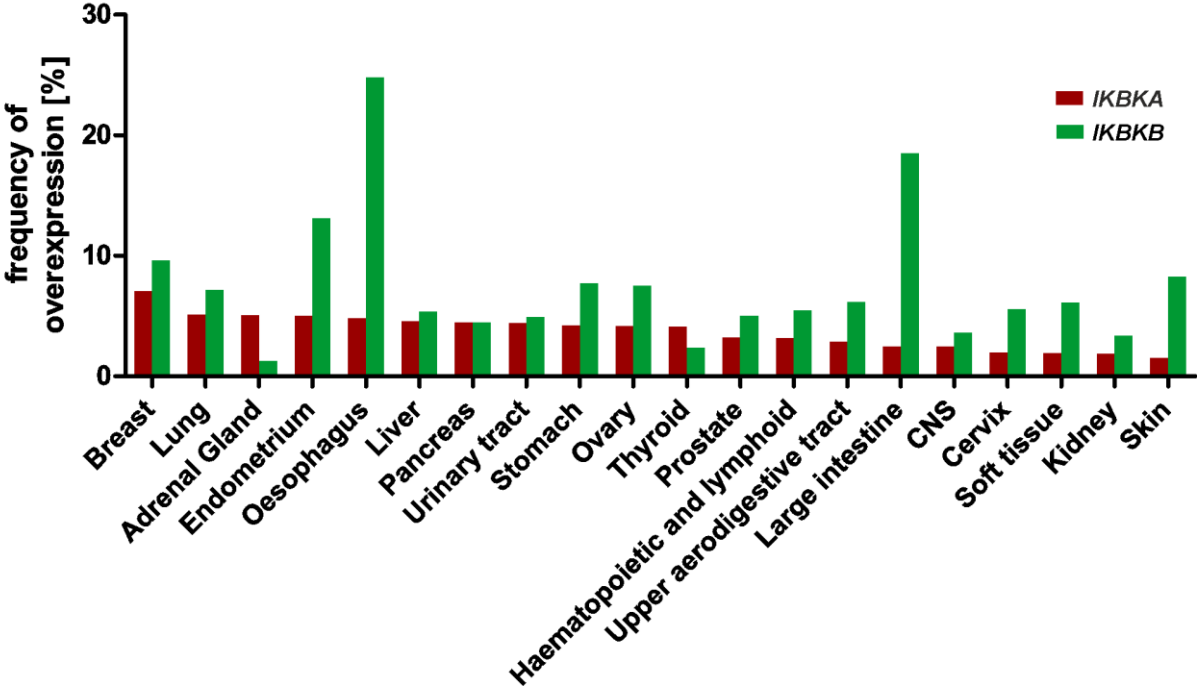
571

572

Figure S1

Figure S1. Database mining using COSMIC for overexpression of *IKBKA* and *IKBKB* in various tissues. cancer.sanger.ac.uk 05-02-2017 13:05
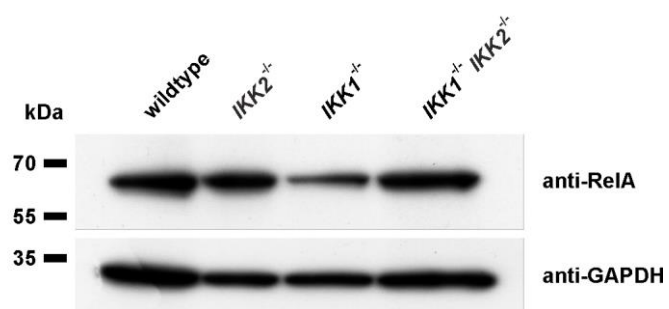
Figure S2

Figure S2. No reduction of RelA protein in IKK-deficient cells. IKK-deficiency did not result in

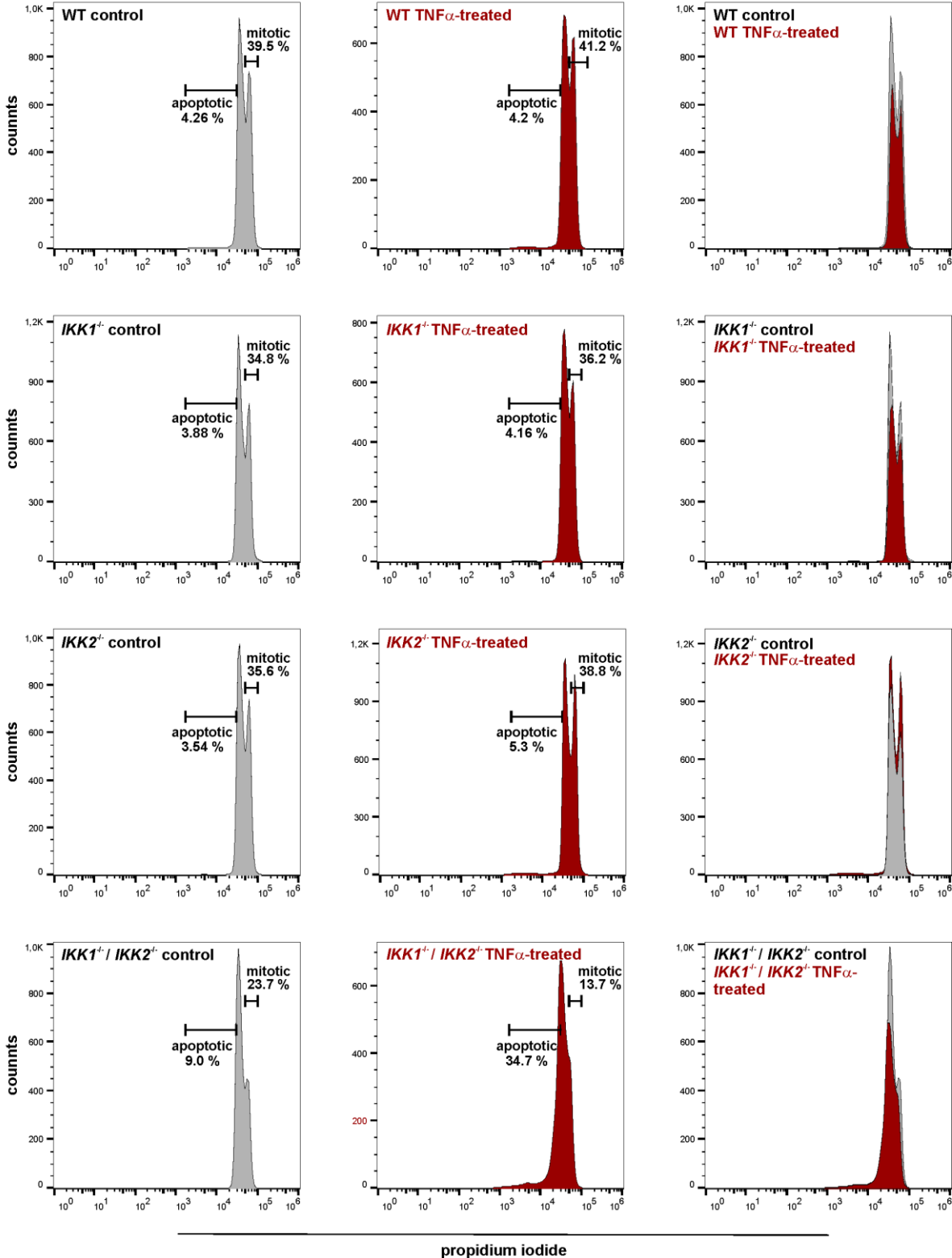prominent downregulation of the NF-κB subunit RelA.

Figure S3

Figure S3. Flow Cytometric analysis revealed TNFα-induced cell death in IKK1/2-deficient cells. DNA content measurement of propidium iodide stained cells showed a strong increase

in the amount of apoptotic cells in IKK1/IKK2-double-deficient cells upon TNFα stimulation (24 h; 20 ng/mL). This effect was not observed in cell deficient for either IKK1 or IKK2.